

BULLETIN OF RUSSIAN STATE MEDICAL UNIVERSITY

BIOMEDICAL JOURNAL OF PIROGOV RUSSIAN NATIONAL
RESEARCH MEDICAL UNIVERSITY

EDITOR-IN-CHIEF Denis Rebrikov, DSc, professor

DEPUTY EDITOR-IN-CHIEF Alexander Oettinger, DSc, professor

EDITORS Valentina Geidebrekht, Nadezda Tikhomirova

TECHNICAL EDITOR Nina Tyurina

TRANSLATORS Ekaterina Tretiyakova, Vyacheslav Vityuk

DESIGN AND LAYOUT Marina Doronina

EDITORIAL BOARD

Averin VI, DSc, professor (Minsk, Belarus)

Alipov NN, DSc, professor (Moscow, Russia)

Belousov VV, DSc, professor (Moscow, Russia)

Bogomilskiy MR, corr. member of RAS, DSc, professor (Moscow, Russia)

Bozhenko VK, DSc, CSc, professor (Moscow, Russia)

Bylova NA, CSc, docent (Moscow, Russia)

Gainetdinov RR, CSc (Saint-Petersburg, Russia)

Gendlin GYe, DSc, professor (Moscow, Russia)

Ginter EK, member of RAS, DSc (Moscow, Russia)

Gorbacheva LR, DSc, professor (Moscow, Russia)

Gordeev IG, DSc, professor (Moscow, Russia)

Gudkov AV, PhD, DSc (Buffalo, USA)

Gulyaeva NV, DSc, professor (Moscow, Russia)

Gusev EI, member of RAS, DSc, professor (Moscow, Russia)

Danilenko VN, DSc, professor (Moscow, Russia)

Zarubina TV, DSc, professor (Moscow, Russia)

Zatevakhin II, member of RAS, DSc, professor (Moscow, Russia)

Kagan VE, professor (Pittsburgh, USA)

Kzyzhkowska YuG, DSc, professor (Heidelberg, Germany)

Kobrinikii BA, DSc, professor (Moscow, Russia)

Kozlov AV, MD PhD, (Vienna, Austria)

Kotelevtsev YuV, CSc (Moscow, Russia)

Lebedev MA, PhD (Darem, USA)

Manturova NE, DSc (Moscow, Russia)

Milushkina OYu, DSc, professor (Moscow, Russia)

Mitupov ZB, DSc, professor (Moscow, Russia)

Moshkovskii SA, DSc, professor (Moscow, Russia)

Munblit DB, MSc, PhD (London, Great Britain)

Negrebetsky VV, DSc, professor (Moscow, Russia)

Novikov AA, DSc (Moscow, Russia)

Pivovarov YuP, member of RAS, DSc, professor (Moscow, Russia)

Platonova AG, DSc (Kiev, Ukraine)

Polunina NV, corr. member of RAS, DSc, professor (Moscow, Russia)

Poryadin GV, corr. member of RAS, DSc, professor (Moscow, Russia)

Razumovskii AYU, corr. member of RAS, DSc, professor (Moscow, Russia)

Rebrova OYu, DSc (Moscow, Russia)

Rudoy AS, DSc, professor (Minsk, Belarus)

Rylova AK, DSc, professor (Moscow, Russia)

Savelieva GM, member of RAS, DSc, professor (Moscow, Russia)

Semiglazov VF, corr. member of RAS, DSc, professor (Saint-Petersburg, Russia)

Skoblina NA, DSc, professor (Moscow, Russia)

Slavyanskaya TA, DSc, professor (Moscow, Russia)

Smirnov VM, DSc, professor (Moscow, Russia)

Spallone A, DSc, professor (Rome, Italy)

Starodubov VI, member of RAS, DSc, professor (Moscow, Russia)

Stepanov VA, corr. member of RAS, DSc, professor (Tomsk, Russia)

Suchkov SV, DSc, professor (Moscow, Russia)

Takhchidi KhP, member of RAS, DSc, professor (Moscow, Russia)

Trufanov GE, DSc, professor (Saint-Petersburg, Russia)

Favorova OO, DSc, professor (Moscow, Russia)

Filipenko ML, CSc, leading researcher (Novosibirsk, Russia)

Khazipov RN, DSc (Marsel, France)

Chundukova MA, DSc, professor (Moscow, Russia)

Shimanovskii NL, corr. member of RAS, DSc, professor (Moscow, Russia)

Shishkina LN, DSc, senior researcher (Novosibirsk, Russia)

Yakubovskaya RI, DSc, professor (Moscow, Russia)

SUBMISSION <http://vestnikrgmu.ru/login?lang=en>

CORRESPONDENCE editor@vestnikrgmu.ru

COLLABORATION manager@vestnikrgmu.ru

ADDRESS ul. Ostrovityanova, d. 1, Moscow, Russia, 117997

Indexed in Scopus. CiteScore 2018: 0.20

Scopus[®]

Indexed in RSCI. IF 2018: 0,321

**НАУЧНАЯ ЭЛЕКТРОННАЯ
БИБЛИОТЕКА
LIBRARY.RU**

Indexed in WoS. JCR 2018: 0.21

WEB OF SCIENCE[™]

Listed in HAC 31.01.2020 (№ 507)



**ВЫСШАЯ
АТТЕСТАЦИОННАЯ
КОМИССИЯ (ВАК)**

Five-year h-index is 6

**Google
scholar**

Open access to archive

CYBERLENINKA

Issue DOI: 10.24075/brsmu.2020-04

The mass media registration certificate no. 012769 issued on July 29, 1994

Founder and publisher is Pirogov Russian National Research Medical University (Moscow, Russia)

The journal is distributed under the terms of Creative Commons Attribution 4.0 International License www.creativecommons.org



Approved for print 31.08.2020
Circulation: 100 copies. Printed by Print.Formula
www.print-formula.ru

ВЕСТНИК РОССИЙСКОГО ГОСУДАРСТВЕННОГО МЕДИЦИНСКОГО УНИВЕРСИТЕТА

НАУЧНЫЙ МЕДИЦИНСКИЙ ЖУРНАЛ РНИМУ ИМ. Н. И. ПИРОГОВА

ГЛАВНЫЙ РЕДАКТОР Денис Ребриков, д. б. н., профессор

ЗАМЕСТИТЕЛЬ ГЛАВНОГО РЕДАКТОРА Александр Эттингер, д. м. н., профессор

РЕДАКТОРЫ Валентина Гейдебрект, Надежда Тихомирова

ТЕХНИЧЕСКИЙ РЕДАКТОР Нина Тюрина

ПЕРЕВОДЧИКИ Екатерина Третьякова, Вячеслав Виток

ДИЗАЙН И ВЕРСТКА Марины Дорониной

РЕДАКЦИОННАЯ КОЛЛЕГИЯ

В. И. Аверин, д. м. н., профессор (Минск, Белоруссия)

Н. Н. Алипов, д. м. н., профессор (Москва, Россия)

В. В. Белоусов, д. б. н., профессор (Москва, Россия)

М. Р. Богомилский, член-корр. РАН, д. м. н., профессор (Москва, Россия)

В. К. Боженко, д. м. н., к. б. н., профессор (Москва, Россия)

Н. А. Былова, к. м. н., доцент (Москва, Россия)

Р. Р. Гайнетдинов, к. м. н. (Санкт-Петербург, Россия)

Г. Е. Гендлин, д. м. н., профессор (Москва, Россия)

Е. К. Гинтер, академик РАН, д. б. н. (Москва, Россия)

Л. Р. Горбачева, д. б. н., профессор (Москва, Россия)

И. Г. Гордеев, д. м. н., профессор (Москва, Россия)

А. В. Гудков, PhD, DSc (Буффало, США)

Н. В. Гуляева, д. б. н., профессор (Москва, Россия)

Е. И. Гусев, академик РАН, д. м. н., профессор (Москва, Россия)

В. Н. Даниленко, д. б. н., профессор (Москва, Россия)

Т. В. Зарубина, д. м. н., профессор (Москва, Россия)

И. И. Затевахин, академик РАН, д. м. н., профессор (Москва, Россия)

В. Е. Каган, профессор (Питтсбург, США)

Ю. Г. Кжышковска, д. б. н., профессор (Гейдельберг, Германия)

Б. А. Кобринский, д. м. н., профессор (Москва, Россия)

А. В. Козлов, MD PhD (Вена, Австрия)

Ю. В. Котелевцев, к. х. н. (Москва, Россия)

М. А. Лебедев, PhD (Дарем, США)

Н. Е. Мантурова, д. м. н. (Москва, Россия)

О. Ю. Милушкина, д. м. н., доцент (Москва, Россия)

З. Б. Митупов, д. м. н., профессор (Москва, Россия)

С. А. Мошковский, д. б. н., профессор (Москва, Россия)

Д. Б. Мунблит, MSc, PhD (Лондон, Великобритания)

В. В. Негребецкий, д. х. н., профессор (Москва, Россия)

А. А. Новиков, д. б. н. (Москва, Россия)

Ю. П. Пивоваров, д. м. н., академик РАН, профессор (Москва, Россия)

А. Г. Платонова, д. м. н. (Киев, Украина)

Н. В. Полунина, член-корр. РАН, д. м. н., профессор (Москва, Россия)

Г. В. Порядин, член-корр. РАН, д. м. н., профессор (Москва, Россия)

А. Ю. Разумовский, член-корр., профессор (Москва, Россия)

О. Ю. Реброва, д. м. н. (Москва, Россия)

А. С. Рудой, д. м. н., профессор (Минск, Белоруссия)

А. К. Рылова, д. м. н., профессор (Москва, Россия)

Г. М. Савельева, академик РАН, д. м. н., профессор (Москва, Россия)

В. Ф. Семглазов, член-корр. РАН, д. м. н., профессор (Санкт-Петербург, Россия)

Н. А. Скоблина, д. м. н., профессор (Москва, Россия)

Т. А. Славянская, д. м. н., профессор (Москва, Россия)

В. М. Смирнов, д. б. н., профессор (Москва, Россия)

А. Спаллоне, д. м. н., профессор (Рим, Италия)

В. И. Стародубов, академик РАН, д. м. н., профессор (Москва, Россия)

В. А. Степанов, член-корр. РАН, д. б. н., профессор (Томск, Россия)

С. В. Сучков, д. м. н., профессор (Москва, Россия)

Х.П.Тахчиди, академик РАН, д. м. н., профессор (Москва, Россия)

Г. Е. Труфанов, д. м. н., профессор (Санкт-Петербург, Россия)

О. О. Фаворова, д. б. н., профессор (Москва, Россия)

М. Л. Филипенко, к. б. н. (Новосибирск, Россия)

Р. Н. Хазипов, д. м. н. (Марсель, Франция)

М. А. Чундокова, д. м. н., профессор (Москва, Россия)

Н. Л. Шимановский, член-корр. РАН, д. м. н., профессор (Москва, Россия)

Л. Н. Шишкина, д. б. н. (Новосибирск, Россия)

Р. И. Якубовская, д. б. н., профессор (Москва, Россия)

ПОДАЧА РУКОПИСЕЙ <http://vestnikrgmu.ru/login>

ПЕРЕПИСКА С РЕДАКЦИЕЙ editor@vestnikrgmu.ru

СОТРУДНИЧЕСТВО manager@vestnikrgmu.ru

АДРЕС РЕДАКЦИИ ул. Островитянова, д. 1, г. Москва, 117997

Журнал включен в Scopus. CiteScore 2018: 0,20

Журнал включен в WoS. JCR 2018: 0,21

Индекс Хирша (h²) журнала по оценке Google Scholar: 6

Scopus[®]

WEB OF SCIENCE[™]

Google
scholar

Журнал включен в РИНЦ. IF 2018: 0,321

Журнал включен в Перечень 31.01.2020 (№ 507)

Здесь находится открытый архив журнала

**НАУЧНАЯ ЭЛЕКТРОННАЯ
БИБЛИОТЕКА
LIBRARY.RU**



**ВЫСШАЯ
АТТЕСТАЦИОННАЯ
КОМИССИЯ (ВАК)**

CYBERLENINKA

DOI выпуска: 10.24075/vrgmu.2020-04

Свидетельство о регистрации средства массовой информации № 012769 от 29 июля 1994 г.

Учредитель и издатель — Российский национальный исследовательский медицинский университет имени Н. И. Пирогова (Москва, Россия)

Журнал распространяется по лицензии Creative Commons Attribution 4.0 International www.creativecommons.org



Подписано в печать 31.08.2020

Тираж 100 экз. Отпечатано в типографии Print.Formula
www.print-formula.ru

REVIEW	5
MicroRNA and vascular pathology of the eye Moshetova LK, Usharova SA, Turkina KI, Sychev DA, Saburina IN	
МикроРНК и сосудистая патология глаза Л. К. Мошетова, С. А. Ушарова, К. И. Туркина, Д. А. Съчев, И. Н. Сабурина	
METHOD	10
New <i>in vitro</i> model to evaluate kinetics of antimycobacterial drug release from bioresorbable polymeric carriers Andreevskaya SN, Smirnova TG, Antonov EN, Chernousova LN, Bogorodsky SE, Larionova EE, Popov VK, Ergeshov AE	
Новая модель <i>in vitro</i> для оценки высвобождения противотуберкулезных препаратов из биорезорбируемых полимерных носителей С. Н. Андреевская, Т. Г. Смирнова, Е. Н. Антонов, Л. Н. Черноусова, С. Э. Богородский, Е. Е. Ларионова, В. К. Попов, А. Э. Эргешов	
ORIGINAL RESEARCH	16
Gut microbiota assessment in Moscow long-livers using next generation sequencing Kashtanova DA, Klimenko NS, Strazhesko ID, Tkacheva ON, Starikova EV, Glushchenko OE, Gudkov DA, Ilna EN	
Анализ микробиоты долгожителей Москвы с использованием высокопроизводительного секвенирования Д. А. Каштанова, Н. С. Клименко, И. Д. Стражеско, О. Н. Ткачева, Е. В. Старикова, О. Е. Глущенко, Д. А. Гудков, Е. Н. Ильина	
ORIGINAL RESEARCH	21
Spread of variants with gene N hot spot mutations in Russian SARS-CoV-2 isolates Kiryayov SA, Levina TA, Kirillov MYu	
Распространение вариантов с частыми мутациями в гене капсидного белка N в российских изолятах SARS-CoV-2 С. А. Кирьянов, Т. А. Левина, М. Ю. Кириллов	
ORIGINAL RESEARCH	27
Predictive monitoring of secondary epidemic waves of COVID-19 in Iran, Russia and other countries Kovriguine DA, Nikitenkova SP	
Прогнозный мониторинг вторых волн эпидемии COVID-19 в Иране, России и других странах Д. А. Ковригин, С. П. Никитенкова	
ORIGINAL RESEARCH	33
Rehabilitation of patients with cerebral palsy using hand exoskeleton controlled by brain-computer interface Bobrov PD, Biryukova EV, Polyayev BA, Lajsheva OA, Usachjova EL, Sokolova AV, Mihailova DI, Dement'eva KN, Fedotova IR	
Реабилитация больных с детским церебральным параличом с помощью экзоскелета кисти, управляемого интерфейсом «мозг-компьютер» П. Д. Бобров, Е. В. Бирюкова, Б. А. Поляев, О. А. Лайшева, Е. Л. Усачёва, А. В. Соколова, Д. И. Михайлова, К. Н. Дементьева, И. Р. Федотова	
ORIGINAL RESEARCH	41
Changes in EEG patterns in the α-frequency band following BCI-based therapy in children with cerebral palsy Larina NV, Nacharova MA, Korsunskaya LL, Vlasenko SV, Pavlenko VB	
Изменение ЭЭГ в частотном диапазоне α-ритма у детей с детским церебральным параличом при применении роботизированной терапии Н. В. Ларина, М. А. Начарова, Л. Л. Корсунская, С. В. Власенко, В. Б. Павленко	
ORIGINAL RESEARCH	47
Thrombogenicity in patients with ischemic stroke and pre-existing polycythemia vera Tanashyan MM, Shabalina AA, Roitman EV, Vavilova TV, Kuznetsova PI	
Тромбогенность у больных ишемическим инсультом на фоне истинной полицитемии М. М. Танащян, А. А. Шабалина, Е. В. Ройтман, Т. В. Вавилова, П. И. Кузнецова	
ORIGINAL RESEARCH	54
Complexes of fluconazole with alanine, lysine and threonine: mass spectrometry and theoretical modeling Chagovets VV, Starodubtseva NL, Frankevich VE	
Масс-спектрометрическое исследование и теоретическое моделирование комплексов флуконазола с аланином, лизином и треонином В. В. Чаговец, Н. Л. Стародубцева, В. Е. Франкевич	
ORIGINAL RESEARCH	60
Hypoxia enhances transcytosis in intestinal enterocytes Maltseva DV, Shkurnikov MYu, Nersisyan SA, Nikulin SV, Kurnosov AA, Raigorodskaya MP, Osipyants AI, Tonevitsky EA	
Гипоксия усиливает транцитоз в энтероцитах кишечника Д. В. Мальцева, М. Ю. Шкурников, С. А. Нерсисян, С. В. Никулин, А. А. Курносов, М. П. Райгородская, А. И. Осипьянц, Е. А. Тоневецкий	

Stomach wall changes after gastroplication in patients with morbid obesity

Galimov OV, Khanov VO, Ziangirov RA, Galimova ES, Minigalin DM, Galimov DO

Изменения в стенке желудка после гастропликации у пациентов с морбидным ожирением

О. В. Галимов, В. О. Ханов, Р. А. Зиангиров, Е. С. Галимова, Д. М. Минигалин, Д. О. Галимов

Information model of post stroke rehabilitation conception

Rybakova PA, Koroleva Yul, Ivanova GE, Zarubina TV

Концепция информационной модели системы реабилитации больных с острым нарушением мозгового кровообращения

П. А. Рыбакова, Ю. И. Королева, Г. Е. Иванова, Т. В. Зарубина

MICRORNA AND VASCULAR PATHOLOGY OF THE EYE

Moshetova LK, Usharova SA ✉, Turkina KI, Sychev DA, Saburina IN

Russian Medical Academy of Continuous Professional Education, Moscow, Russia

Since the discovery of microRNAs just a few decades ago, our knowledge of these molecules and their potential as diagnostic biomarkers and therapeutic targets has significantly expanded. There is an ongoing discussion in the scientific community about the possibility of using microRNA for the diagnosis of cardiovascular diseases. It has been shown recently that levels of some microRNAs vary in vascular eye disorders, such as age-related macular degeneration and diabetic retinopathy. However, despite serious advances in our understanding of microRNA's role in eye pathology, we still do not know whether it is possible to use microRNA as a biomarker for central retinal vein occlusion. Perhaps, the discovery of such candidate microRNAs will help in making the timely diagnosis and improve the quality of medical care in patients with retinal vein occlusion.

Keywords: retinal vessel occlusion, microRNA, biomarkers, vascular pathology, retinal vessels

Author contribution: Moshetova LK — concept and manuscript preparation; Usharova SA, Turkina KI — literature analysis and manuscript preparation; Sychev DA, Saburina IN — manuscript preparation.

✉ **Correspondence should be addressed:** Svetlana A. Usharova
Barrikadnaya, 2/1, str. 1, Moscow, 125993, svetlalexar@gmail.com

Received: 26.06.2020 **Accepted:** 09.07.2020 **Published online:** 15.07.2020

DOI: 10.24075/brsmu.2020.042

МИКРОРНК И СОСУДИСТАЯ ПАТОЛОГИЯ ГЛАЗА

Л. К. Мошетова, С. А. Ушарова ✉, К. И. Туркина, Д. А. Сычев, И. Н. Сабурина

Российская медицинская академия непрерывного профессионального образования, Москва, Россия

С момента открытия первой микроРНК несколько десятилетий назад представления о данных молекулах как о биомаркерах и потенциальных терапевтических мишенях различных заболеваний значительно расширились. В современном научном обществе активно обсуждают возможность применения микроРНК для диагностики сердечно-сосудистых заболеваний. Более того, ряд недавно проведенных исследований доказывает, что уровни определенных микроРНК варьируют и при сосудистых заболеваниях глаза, включающих возрастную макулярную дегенерацию и диабетическую ретинопатию. Однако, несмотря на прогресс в исследовании роли некоторых микроРНК в диагностике ряда офтальмологических патологий, информации о возможности использования микроРНК в качестве биомаркеров окклюзии центральной вены сетчатки на сегодняшний день нет. Возможно, что поиск и идентификация данных молекул смогут облегчить постановку диагноза и улучшить качество оказываемой медицинской помощи.

Ключевые слова: окклюзия сосудов сетчатки, микроРНК, биомаркеры, сосудистая патология, ретинальные сосуды

Вклад авторов: Л. К. Мошетова — определение концепции рукописи и ее редактирование; С. А. Ушарова, К. И. Туркина — подбор и анализ литературы, подготовка рукописи; Д. А. Сычев, И. Н. Сабурина — редактирование рукописи.

✉ **Для корреспонденции:** Светлана Александровна Ушарова
ул. Баррикадная, д. 2/1, стр. 1, г. Москва, 125993; svetlalexar@gmail.com

Статья получена: 26.06.2020 **Статья принята к печати:** 09.07.2020 **Опубликована онлайн:** 15.07.2020

DOI: 10.24075/vrgmu.2020.042

Making a timely and accurate diagnosis is crucial for effective treatment and positive clinical outcomes. This cannot be any truer for vascular disorders. MicroRNAs (miRNAs) were discovered back in 1993 [1]. They are a class of single-stranded non-coding RNAs constituted by 16 to 27 (an average of 22) nucleotides [2]. Transcription of miRNA precursor genes is regulated by genomic DNA methylation and histone modifications, which, in turn, vary across pathologies [3]. All around the globe, research teams are actively exploring the possibility of using miRNA as a diagnostic biomarker for a broad range of health conditions. Although it is not yet common practice to use miRNAs as biomarkers of eye diseases, such as retinal vessel occlusion, the ongoing research into their role in systemic vascular pathology suggests that they are potent diagnostic tools.

MicroRNA and systemic vascular pathology

There is a huge body of evidence that miRNA expression is changed significantly in systemic and localized vascular pathologies; the amassed data suggest tremendous diagnostic potential for miRNA and, specifically, circulating miRNA [4]. Circulating miRNA levels reflect physiological and pathological changes in the body, including cardiovascular and

neurodegenerative disorders. For example, miR-1, miR-133b, miR-145, miR-208b, miR-499, miR-133a, and miR-208a are diagnostic biomarkers for coronary artery disease [5].

Patients with atherosclerosis have significantly elevated miR-122, miR-21, miR-130a, miR-211c and low miR92a, miR-222, miR-126 in their blood [6]. In addition to their diagnostic potential, these miRNAs and their inhibitors can be used to treat atherosclerosis [7].

Ischemic stroke and myocardial infarction are the most severe complications of atherosclerosis. Multiple studies conducted on animal models and human patients indicate a link between the levels of circulating and tissue microRNAs and ischemic stroke or its effects. In the acute phase of ischemic stroke, miR-124 and miR-21 are elevated whereas miR-221 concentrations decline; elevated miR-145 and miR-210 are predictors of a more favorable outcome [8]. Changes in miRNA levels are also reported in patients with myocardial infarction; specifically, such patients demonstrate a sharp decrease in miR-375 expression [9].

Hypertension is the most prevalent cardiovascular condition. It is a risk factor for many vascular disorders, including eye disorders. A Russian study investigated the profiles of miR-126, miR-155, miR-221, and miR-222 in hypertensive patients and healthy volunteers. Increased dispersion was observed for all

studied miRNA in all hypertensive patients, as compared with healthy individuals. MiR-221 prevailed in hypertensive patients, whereas miR-126, in healthy volunteers [10].

Thus, the levels of some circulating miRNAs change in patients with systemic vascular disorders and therefore might be a potent candidate diagnostic biomarkers. Because systemic vascular disorders and vascular eye disorders have the same pathogenesis, there might be microRNAs that could act as biomarkers for conditions associated with impeded retinal blood flow. So far, no qualitative and quantitative miRNA analysis has been conducted for retinal vessel occlusion but the available data on changes in microRNA profiles accompanying vascular eye disorders suggest this research field holds great promise.

MicroRNA in age-related macular degeneration

Age-related macular degeneration (AMD) is the primary cause of irreversible central vision loss in elderly people. Choroidal neovascularization (CNV) leads to increased vascular permeability, fluid exudation, and irreversible damage to photoreceptor cells, causing vision decline. Being a complex progressive disease, AMD is linked to genetic (including complementary) and environmental factors [11]. Some miRNAs associated with complementary factors were found to change their regulation function in the blood and ocular tissue of patients with AMD. A PCR-based study of 384 miRNAs in the blood plasma of patients with AMD revealed that characteristics of 16 miRNAs were significantly changed in such patients and 10 other microRNAs were expressed only in individuals with exudative AMD [12]. A team of Italian researchers studied the expression profiles of different microRNAs in patients with or without AMD and in rats with experimentally induced retinal pathology. The levels of miR-9, miR-23a, miR-27a, miR-34a, miR-146a, and miR-155 were significantly different between diseased and healthy individuals. The most pronounced differences were observed for miR-27a, miR-146a and miR-155, suggesting they might have potential as biomarkers and therapeutic targets for treating AMD [13].

MicroRNA in diabetic retinopathy

The possibility of using microRNAs as biomarkers is being considered for diabetic retinopathy (DR), another serious visual impairment arising from a vascular disorder. DR is a common microvascular complication of diabetes mellitus (DM), which is currently recognized as a global epidemic. DR results from damage to microvessels following prolonged exposure to hyperglycemia. Progressive retinal ischemia triggers expression

of hypoxia-inducible growth factors, including VEGF, which, in turn, stimulate retinal neovascularization [14]. Consequently, the blood-retinal barrier breaks down, leading to vascular leakage and retinal edema [15]. The analysis of circulating miRNAs isolated from serum and plasma samples of patients with and without DR revealed changes in the expression of many miRNAs in patients of different age, with different DM types, different time of onset, etc. [16]. There were reports of quantitative and qualitative changes in the profiles of miR-126 [17–19], miR-150 [20], miR-155 [21], and miR-200b isolated from patients with DR. Of all those miRNAs, miR-155 and miR-126 had the highest clinical relevance [22]. A research group from China compared serum levels of miR-126 in patients with DR and healthy volunteers by means of real-time PCR and found statistically significant differences in miR-126 expression between the two cohorts. According to the analysis of blood serum samples collected from patients with proliferative (PDT) and non-proliferative (NPDT) diabetic retinopathies, miR-126 levels varied across patients with retinal pathology depending on its severity. MiR-126 concentrations were declining as proliferative retinal pathology was progressing. The researchers were able to determine the diagnostic thresholds for miR-126 that could be used to predict the risk of PDT and NPDT and detect borderline conditions at high risk of transformation into PDT. The researchers pointed out that miR-126 could be used as a biomarker of retinal endothelial damage and early stages of PDT [17].

Using this information, we shortlisted a few microRNA candidates that in our opinion have the best diagnostic and prognostic potential as candidate biomarkers of retinal vein occlusion (Table).

miR-126

MiR-126 is one of the key pro-angiogenic microRNAs that regulate expression of some growth factors, including VEGF and FGF [23, 24]. MicroRNA expression profiles were studied on several animal models of human vascular eye disorders, including oxygen-induced retinopathy (DR-type neovascularization) and laser-induced CNV (wet ARMD). MiR-126 concentrations declined in the choroid of mice with laser-induced CNV [25] and also in the retina and choroid of rodents with oxygen-induced retinopathy [26]. Besides, mice with decreased miR-126 concentrations had signs of damage to the peripheral choroid [27]; stimulated elevation of miR-126 was shown to inhibit retinal neovascularization and breakdown of the blood-retinal barrier in mice with oxygen-induced retinopathy [28]. These findings suggest that miR-126 might be an important biomarker mirroring the condition of

Table 1. Expression of candidate microRNAs in different pathologies

	miR-126	miR-155	miR-21
Vascular disorders			
Atherosclerosis	microRNA expression decreases [6]	[6]*	microRNA expression increases [6]
Ischemic stroke	microRNA expression decreases [36]	[36]*	microRNA expression increases [36]
Hypertension	microRNA expression increases [10]	[10]*	microRNA expression increases [38]
Coronary artery disease	microRNA expression increases [10, 24]	[10, 39]*	microRNA expression increases [38]
Eye disorders			
Diabetic retinopathy	microRNA expression decreases [17–19, 22]	microRNA expression increases [31]	microRNA expression increases [40]
Age-related macular degeneration	microRNA expression decreases [23–25]	microRNA expression increases [13]	microRNA expression increases [35]

Note: *— Changes in microRNA expression depend on the character of the pathology.

the choroid in various pathologies and a potential therapeutic target for developing new approaches to the management of eye disorders.

miR-155

MiR-155 is a proinflammatory microRNA that is specifically expressed in atherosclerotic plaques and proinflammatory M1 macrophages [6]. Retinal miR-155 expression undergoes significant changes in wet ARMD, experimental oxygen-induced retinopathy [29], light-induced retinal degeneration [30], and streptozotocin-induced DR [31]. Its deficit leads to the shrinkage of vascular areas and neovascularization in the rodent model of oxygen-induced retinopathy [29]. Besides, miR-155 was proved to regulate the levels of complement factor H in ARMD [32], maintaining its role in the angiogenesis and inflammation in a range of eye disorders. MiR-155 is an important biomarker that reflects the unfolding of the proinflammatory cascades accompanying the progression of vascular disorders. In addition, this miRNA is being investigated as a potential therapeutic target in eye pathology.

miR-21

MiR-21 is known to be linked to tumor formation and neovascularization [33]. Its expression changes in cardiac pathology [34]. MiR-21 plays a crucial role in the pathogenesis

of ARMD. It participates in the regulation of retinal vessel growth, which can be inferred from high miR-21 expression in retinal endothelial cells. Increased miR-21 expression was detected in the experimental mouse model of laser-induced CNV. In another study, stimulation of miR-21 expression inhibited proliferation and migration of cultured endothelial cells through targeted inhibition of certain proteins that affect the dynamics of actin networks [35]. This indicates the diagnostic and modulating potential of miR-21.

CONCLUSIONS

There is a paucity of research studies looking at the expression profiles of miRNA genes in eye pathology. Nevertheless, the available data suggests that miRNAs might hold great promise as potent diagnostic markers of eye disorders, such as retinal vein occlusion. The comprehensive analysis of their expression will help to conduct minimally invasive screening, provide adequate treatment and take timely prevention measures. It is important to develop microRNA panels and determine their threshold values that signal the risk of complications in patients during or after therapy.

Further basic and clinical research on complex 3D organoid and spheroid models is needed to better understand the role of individual microRNAs or their clusters and to evaluate their diagnostic and therapeutic potential in retinal vascular pathology.

References

- Lee RC, Feinbaum RL, Ambros V. The *C. elegans* heterochronic gene *lin-4* encodes small RNAs with antisense complementarity to *lin-14*. *Cell*. 1993; 75 (5): 843–54. DOI: 10.1016/0092-8674(93)90529-y.
- Fang Z, Du R, Edwards A, Flemington EK, Zhang K. The Sequence Structures of Human MicroRNA Molecules and Their Implications. *PLoS ONE*. 2013; 8 (1): e54215. Available from: <https://doi.org/10.1371/journal.pone.0054215>.
- Kucher AN, Babushkina NP. Role of microRNA, genes involved in their biogenesis and functioning in the development of human disorders. *Medical Genetics*. 2011; 1: 3–13. Russian.
- Pogribny IP. MicroRNAs as biomarkers for clinical studies. *Exp Biol Med (Maywood)*. 2018; 243 (3): 283–90. DOI: 10.1177/1535370217731291.
- Navickas R, Gal D, Laucevičius A, Tapauskaitė A, Zdanytė M, Holvoet P. Identifying circulating microRNAs as biomarkers of cardiovascular disease: a systematic review. *Cardiovasc Res*. 2016; 111 (4): 322–37. DOI: 10.1093/cvr/cvv174.
- Kucher AN, Nazarenko MS. The role of microRNA in atherogenesis. *Kardiologija*. 2017; 57 (9): 65–76. Available from: <https://doi.org/10.18087/cardio.2017.9.10022>. Russian.
- Koroleva IA, Nazarenko MS, Kucher AN. Role of microRNA in development of instability of atherosclerotic plaque. *Biochemistry*. 2018; 83 (1): 34–46. Russian.
- Gareev IF, Beilerly OA. Role of microRNA in ischemic stroke. *Neurologic magazine*. 2018; 23 (4): 166–75. Russian.
- Baulina N, Osmak G, Kiselev I, et al. NGS-identified circulating miR-375 as a potential regulating component of myocardial infarction associated network. *J Mol Cell Cardiol*. 2018; 121: 173–9. DOI: 10.1016/j.yjmcc.2018.07.129.
- Shheglova NE, Kalinkin MN. Kachestvennye harakteristiki miR-126, miR-155, miR-221, miR-222 u bol'nyh gipertonicheskoy bolezni'ju i postinfarktnym kardiosklerozom [dissertacija]. K., 2015. Russian.
- Coleman HR, Chan CC, Ferris FL 3rd, Chew EY. Age-related macular degeneration. *Lancet*. 2008; 372 (9652): 1835–45. DOI: 10.1016/S0140-6736(08)61759-6.
- Ertekin S, Yıldırım O, Dinç E, et al. Evaluation of circulating miRNAs in wet age-related macular degeneration. *Molecular Vision*. 2014; 20: 1057–66.
- Romano GL, Platania CBM, Drago F, et al. Retinal and circulating miRNAs in age-related macular degeneration: an in vivo animal and human study. *Front Pharmacol*. 2017; 8: 168. DOI: 10.3389/fphar.2017.00168.
- Fong DS, Aiello LP, Ferris FL, Klein R. Diabetic retinopathy. *Diabetes Care*. 2004 Oct; 27 (10): 2540–53. Available from: <https://doi.org/10.2337/diacare.27.10.2540>.
- Qazi Y, Maddula S, Ambati BK. Mediators of ocular angiogenesis. *J Genet*. 2009; 88 (4): 495–515. DOI: 10.1007/s12041-009-0068-0.
- Qing S, Yuan S, Yun C, et al. Serum miRNA biomarkers serve as a fingerprint for proliferative diabetic retinopathy. *Cell Physiol Biochem*. 2014; 34 (5): 1733–40. DOI: 10.1159/000366374.
- Qin LL, An MX, Liu YL, Xu HC, Lu ZQ. MicroRNA-126: a promising novel biomarker in peripheral blood for diabetic retinopathy. *Int J Ophthalmol*. 2017; 10 (4): 530–4. DOI: 10.18240/ijo.2017.04.05.
- Barutta F, Bruno G, Matullo G, et al. MicroRNA-126 and micro-/macrovascular complications of type 1 diabetes in the EURODIAB Prospective Complications Study. *Acta Diabetol*. 2017; 54 (2): 133–9. DOI: 10.1007/s00592-016-0915-4.
- Rezk NA, Sabbah NA, Saad MS. Role of MicroRNA 126 in screening, diagnosis, and prognosis of diabetic patients in Egypt. *IUBMB Life*. 2016; 68 (6): 452–8. DOI: 10.1002/iub.1502.
- Mazzeo A, Beltramo E, Lopatina T, Gai C, Trento M, Porta M. Molecular and functional characterization of circulating extracellular vesicles from diabetic patients with and without retinopathy and healthy subjects. *Exp Eye Res*. 2018; 176: 69–77. DOI: 10.1016/j.exer.2018.07.003.
- Yang TT, Song SJ, Xue HB, Shi DF, Liu CM, Liu H. Regulatory T cells in the pathogenesis of type 2 diabetes mellitus retinopathy by miR-155. *Eur Rev Med Pharmacol Sci*. 2015; 19 (11): 2010–5.
- Li EH, Huang QZ, Li GC, Xiang ZY, Zhang X. Effects of miRNA-200b on the development of diabetic retinopathy by targeting VEGFA gene. *Biosci Rep*. 2017; 37 (2): BSR20160572. DOI: 10.1042/BSR20160572.
- Wang S, Aurora AB, Johnson BA, et al. The endothelial-

- specific microRNA miR-126 governs vascular integrity and angiogenesis. *Dev Cell*. 2008; 15 (2): 261–71. DOI: 10.1016/j.devcel.2008.07.002.
24. Fish JE, Santoro MM, Morton SU, et al. miR-126 regulates angiogenic signaling and vascular integrity. *Dev Cell*. 2008; 15 (2): 272–84. DOI: 10.1016/j.devcel.2008.07.008.
 25. Wang L, Lee AY, Wigg JP, Peshavariya H, Liu P, Zhang H. miR-126 Regulation of Angiogenesis in Age-Related Macular Degeneration in CNV Mouse Model. *Int J Mol Sci*. 2016; 17 (6): 895. DOI: 10.3390/ijms17060895.
 26. Desjarlais M, Rivera JC, Lahaie I, Cagnone G, Wirt M, Omri S, et al. MicroRNA expression profile in retina and choroid in oxygen-induced retinopathy model. *PLoS ONE*. 2019; 14 (6): e0218282. Available from: <https://doi.org/10.1371/journal.pone.0218282>
 27. Zhao F, Anderson C, Karnes S, et al. Expression, regulation and function of miR-126 in the mouse choroid vasculature. *Exp Eye Res*. 2018; 170: 169–76. DOI: 10.1016/j.exer.2018.02.026
 28. Bai X, Luo J, Zhang X, et al. MicroRNA-126 Reduces Blood-Retina Barrier Breakdown via the Regulation of VCAM-1 and BCL2L1 in Ischemic Retinopathy. *Ophthalmic Research*. 2017; 57 (3): 173–85. DOI: 10.1159/000454716.
 29. Yan L, Lee S, Lazzaro DR, Aranda J, Grant MB, Chaqour B. Single and Compound Knock-outs of MicroRNA (miRNA)-155 and Its Angiogenic Gene Target CCN1 in Mice Alter Vascular and Neovascular Growth in the Retina via Resident Microglia. *J Biol Chem*. 2015; 290 (38): 23264–81. DOI: 10.1074/jbc.M115.646950.
 30. Pilakka-Kanthikeel S, Raymond A, Atluri VS, et al. Sterile alpha motif and histidine/aspartic acid domain-containing protein 1 (SAMHD1)-facilitated HIV restriction in astrocytes is regulated by miRNA-181a. *J Neuroinflammation*. 2015; 12: 66. DOI: 10.1186/s12974-015-0285-9.
 31. Kovacs B, Lumayag S, Cowan C, Xu S. MicroRNAs in early diabetic retinopathy in streptozotocin-induced diabetic rats. *Invest Ophthalmol Vis Sci*. 2011; 52 (7): 4402–9. DOI: 10.1167/iov.10-6879.
 32. Lukiw WJ, Surjyadipta B, Dua P, Alexandrov PN. Common micro RNAs (miRNAs) target complement factor H (CFH) regulation in Alzheimer's disease (AD) and in age-related macular degeneration (AMD). *Int J Biochem Mol Biol*. 2012; 3 (1): 105–16.
 33. Liu HY, Zhang YY, Zhu BL, et al. miR-21 regulates the proliferation and apoptosis of ovarian cancer cells through PTEN/PI3K/AKT. *Eur Rev Med Pharmacol Sci*. 2019; 23 (10): 4149–55. DOI: 10.26355/eurrev_201905_17917.
 34. Yuan J, Chen H, Ge D, et al. Mir-21 Promotes Cardiac Fibrosis After Myocardial Infarction Via Targeting Smad7. *Cell Physiol Biochem*. 2017; 42 (6): 2207–19. DOI: 10.1159/000479995.
 35. Sabatel C, Malvaux L, Bovy N, et al. MicroRNA-21 exhibits antiangiogenic function by targeting RhoB expression in endothelial cells. *PLoS One*. 2011; 6 (2): e16979. DOI: 10.1371/journal.pone.0016979.
 36. Aitbaev KA, Murkamilov IT, Fomin W, Murkamilova JA, Yusupov FA. MicroRNA in ischemic stroke. *Journal of Neurology and Psychiatry named after S.S. Korsakov. Special Issues*. 2018; 118 (3): 48–56. Available from: <https://doi.org/10.17116/jnevro20181183248-56.Russian>.
 37. Li X, Wei Y, Wang Z. microRNA-21 and hypertension. *Hypertens Res*. 2018; 41: 649–61. Available from: <https://doi.org/10.1038/s41440-018-0071-z>.
 38. Thum T, Gross C, Fiedler J, et al. MicroRNA-21 contributes to myocardial disease by stimulating MAP kinase signalling in fibroblasts. *Nature*. 2008; 456 (7224): 980–4. DOI: 10.1038/nature07511.
 39. Fichtlscherer S, De Rosa S, Fox H, et al. Circulating microRNAs in patients with coronary artery disease. *Circ Res*. 2010; 107 (5): 677–84. DOI: 10.1161/CIRCRESAHA.109.215566.
 40. Chen Q, Qiu F, Zhou K, et al. Pathogenic Role of microRNA-21 in Diabetic Retinopathy Through Downregulation of PPAR α . *Diabetes*. 2017; 66 (6): 1671–82. DOI: 10.2337/db16-1246.

Литература

1. Lee RC, Feinbaum RL, Ambros V. The *C. elegans* heterochronic gene *lin-4* encodes small RNAs with antisense complementarity to *lin-14*. *Cell*. 1993; 75 (5): 843–54. DOI: 10.1016/0092-8674(93)90529-y.
2. Fang Z, Du R, Edwards A, Flemington EK, Zhang K. The Sequence Structures of Human MicroRNA Molecules and Their Implications. *PLoS ONE*. 2013; 8 (1): e54215. Available from: <https://doi.org/10.1371/journal.pone.0054215>.
3. Кучер А. Н., Бабушкина Н. П. Роль микро-РНК, генов, их биогенеза и функционирования в развитии патологических состояний у человека. *Медицинская генетика*. 2011; 1: 3–13.
4. Pogribny IP. MicroRNAs as biomarkers for clinical studies. *Exp Biol Med (Maywood)*. 2018; 243 (3): 283–90. DOI: 10.1177/1535370217731291.
5. Navickas R, Gal D, Laucevičius A, Taparauskaitė A, Zdanytė M, Holvoet P. Identifying circulating microRNAs as biomarkers of cardiovascular disease: a systematic review. *Cardiovasc Res*. 2016; 111 (4): 322–37. DOI: 10.1093/cvr/cvw174.
6. Кучер А. Н., Назаренко М. С. Роль микро-РНК при атерогенезе. *Кардиология*. 2017; 57 (9): 65–76. Available from: <https://doi.org/10.18087/cardio.2017.9.10022>.
7. Королева Ю. А., Назаренко М. С., Кучер А. Н. Роль микроРНК в формировании нестабильных атеросклеротических бляшек. *Биохимия*. 2018; 83 (1): 34–46.
8. Гареев И. Ф., Бейлерли О. А. Роль микро-РНК в ишемическом инсульте. *Неврологический журнал*. 2018; 23 (4), 166–75.
9. Baulina N, Osmak G, Kiselev I, et al. NGS-identified circulating miR-375 as a potential regulating component of myocardial infarction associated network. *J Mol Cell Cardiol*. 2018; 121: 173–9. DOI: 10.1016/j.yjmcc.2018.07.129.
10. Щеглова Н. Е., Калинин М. Н. Качественные характеристики miR-126, miR-155, miR-221, miR-222 у больных гипертонической болезнью и постинфарктным кардиосклерозом [диссертация]. К., 2015.
11. Coleman HR, Chan CC, Ferris FL 3rd, Chew EY. Age-related macular degeneration. *Lancet*. 2008; 372 (9652): 1835–45. DOI: 10.1016/S0140-6736(08)61759-6.
12. Ertekin S, Yıldırım O, Dinç E, et al. Evaluation of circulating miRNAs in wet age-related macular degeneration. *Molecular Vision*. 2014; 20: 1057–66.
13. Romano GL, Platania CBM, Drago F, et al. Retinal and circulating miRNAs in age-related macular degeneration: an in vivo animal and human study. *Front Pharmacol*. 2017; 8: 168. DOI: 10.3389/fphar.2017.00168.
14. Fong DS, Aiello LP, Ferris FL, Klein R. Diabetic retinopathy. *Diabetes Care*. 2004 Oct; 27 (10): 2540–53. Available from: <https://doi.org/10.2337/diacare.27.10.2540>.
15. Qazi Y, Maddala S, Ambati BK. Mediators of ocular angiogenesis. *J Genet*. 2009; 88 (4): 495–515. DOI: 10.1007/s12041-009-0068-0.
16. Qing S, Yuan S, Yun C, et al. Serum miRNA biomarkers serve as a fingerprint for proliferative diabetic retinopathy. *Cell Physiol Biochem*. 2014; 34 (5): 1733–40. DOI: 10.1159/000366374.
17. Qin LL, An MX, Liu YL, Xu HC, Lu ZQ. MicroRNA-126: a promising novel biomarker in peripheral blood for diabetic retinopathy. *Int J Ophthalmol*. 2017; 10 (4): 530–4. DOI: 10.18240/ijo.2017.04.05.
18. Barutta F, Bruno G, Matullo G, et al. MicroRNA-126 and micro-/macrovascular complications of type 1 diabetes in the EURODIAB Prospective Complications Study. *Acta Diabetol*. 2017; 54 (2): 133–9. DOI: 10.1007/s00592-016-0915-4.
19. Rezk NA, Sabbah NA, Saad MS. Role of MicroRNA 126 in screening, diagnosis, and prognosis of diabetic patients in Egypt. *IUBMB Life*. 2016; 68 (6): 452–8. DOI: 10.1002/iub.1502.
20. Mazzeo A, Beltramo E, Lopatina T, Gai C, Trento M, Porta M. Molecular and functional characterization of circulating extracellular vesicles from diabetic patients with and without retinopathy and healthy subjects. *Exp Eye Res*. 2018; 176: 69–77. DOI: 10.1016/j.exer.2018.07.003.
21. Yang TT, Song SJ, Xue HB, Shi DF, Liu CM, Liu H. Regulatory T cells in the pathogenesis of type 2 diabetes mellitus retinopathy

- by miR-155. *Eur Rev Med Pharmacol Sci.* 2015; 19 (11): 2010–5.
22. Li EH, Huang QZ, Li GC, Xiang ZY, Zhang X. Effects of miRNA-200b on the development of diabetic retinopathy by targeting VEGFA gene. *Biosci Rep.* 2017; 37 (2): BSR20160572. DOI: 10.1042/BSR20160572.
 23. Wang S, Aurora AB, Johnson BA, et al. The endothelial-specific microRNA miR-126 governs vascular integrity and angiogenesis. *Dev Cell.* 2008; 15 (2): 261–71. DOI: 10.1016/j.devcel.2008.07.002.
 24. Fish JE, Santoro MM, Morton SU, et al. miR-126 regulates angiogenic signaling and vascular integrity. *Dev Cell.* 2008; 15 (2): 272–84. DOI: 10.1016/j.devcel.2008.07.008.
 25. Wang L, Lee AY, Wigg JP, Peshavariya H, Liu P, Zhang H. miR-126 Regulation of Angiogenesis in Age-Related Macular Degeneration in CNV Mouse Model. *Int J Mol Sci.* 2016; 17 (6): 895. DOI: 10.3390/ijms17060895.
 26. Desjarlais M, Rivera JC, Lahaie I, Cagnone G, Wirt M, Omri S, et al. MicroRNA expression profile in retina and choroid in oxygen-induced retinopathy model. *PLoS ONE.* 2019; 14 (6): e0218282. Available from: <https://doi.org/10.1371/journal.pone.0218282>
 27. Zhao F, Anderson C, Karnes S, et al. Expression, regulation and function of miR-126 in the mouse choroid vasculature. *Exp Eye Res.* 2018; 170: 169–76. DOI: 10.1016/j.exer.2018.02.026
 28. Bai X, Luo J, Zhang X, et al. MicroRNA-126 Reduces Blood-Retina Barrier Breakdown via the Regulation of VCAM-1 and BCL2L1 in Ischemic Retinopathy. *Ophthalmic Research.* 2017; 57 (3): 173–85. DOI: 10.1159/000454716.
 29. Yan L, Lee S, Lazzaro DR, Aranda J, Grant MB, Chaqour B. Single and Compound Knock-outs of MicroRNA (miRNA)-155 and Its Angiogenic Gene Target CCN1 in Mice Alter Vascular and Neovascular Growth in the Retina via Resident Microglia. *J Biol Chem.* 2015; 290 (38): 23264–81. DOI: 10.1074/jbc.M115.646950.
 30. Pilakka-Kanthikeel S, Raymond A, Atluri VS, et al. Sterile alpha motif and histidine/aspartic acid domain-containing protein 1 (SAMHD1)-facilitated HIV restriction in astrocytes is regulated by miRNA-181a. *J Neuroinflammation.* 2015; 12: 66. DOI: 10.1186/s12974-015-0285-9.
 31. Kovacs B, Lumayag S, Cowan C, Xu S. MicroRNAs in early diabetic retinopathy in streptozotocin-induced diabetic rats. *Invest Ophthalmol Vis Sci.* 2011; 52 (7): 4402–9. DOI: 10.1167/iov.10-6879.
 32. Lukiw WJ, Surjyadipta B, Dua P, Alexandrov PN. Common micro RNAs (miRNAs) target complement factor H (CFH) regulation in Alzheimer's disease (AD) and in age-related macular degeneration (AMD). *Int J Biochem Mol Biol.* 2012; 3 (1): 105–16.
 33. Liu HY, Zhang YY, Zhu BL, et al. miR-21 regulates the proliferation and apoptosis of ovarian cancer cells through PTEN/PI3K/AKT. *Eur Rev Med Pharmacol Sci.* 2019; 23 (10): 4149–55. DOI: 10.26355/eurev_201905_17917.
 34. Yuan J, Chen H, Ge D, et al. Mir-21 Promotes Cardiac Fibrosis After Myocardial Infarction Via Targeting Smad7. *Cell Physiol Biochem.* 2017; 42 (6): 2207–19. DOI: 10.1159/000479995.
 35. Sabatel C, Malvaux L, Bovy N, et al. MicroRNA-21 exhibits antiangiogenic function by targeting RhoB expression in endothelial cells. *PLoS One.* 2011; 6 (2): e16979. DOI: 10.1371/journal.pone.0016979.
 36. Айтбаев К. А., Муркамилов И. Т., Фомин В. В., Муркамилова Ж. А., Юсупов Ф. А. МикроРНК при ишемическом инсульте. *Журнал неврологии и психиатрии им. С. С. Корсакова. Спецвыпуски.* 2018; 118 (3): 48–56. Available from: <https://doi.org/10.17116/jnevro20181183248-56>.
 37. Li X, Wei Y, Wang Z. microRNA-21 and hypertension. *Hypertens Res.* 2018; 41: 649–61. Available from: <https://doi.org/10.1038/s41440-018-0071-z>.
 38. Thum T, Gross C, Fiedler J, et al. MicroRNA-21 contributes to myocardial disease by stimulating MAP kinase signalling in fibroblasts. *Nature.* 2008; 456 (7224): 980–4. DOI: 10.1038/nature07511.
 39. Fichtlscherer S, De Rosa S, Fox H, et al. Circulating microRNAs in patients with coronary artery disease. *Circ Res.* 2010; 107 (5): 677–84. DOI: 10.1161/CIRCRESAHA.109.215566.
 40. Chen Q, Qiu F, Zhou K, et al. Pathogenic Role of microRNA-21 in Diabetic Retinopathy Through Downregulation of PPAR α . *Diabetes.* 2017; 66 (6): 1671–82. DOI: 10.2337/db16-1246.

NEW *IN VITRO* MODEL TO EVALUATE KINETICS OF ANTIMYCOBACTERIAL DRUG RELEASE FROM BIORESORBABLE POLYMERIC CARRIERS

Andreevskaya SN¹✉, Smirnova TG¹, Antonov EN², Chernousova LN¹, Bogorodsky SE², Larionova EE¹, Popov VK², Ergeshov AE¹

¹ Central Tuberculosis Research Institute, Moscow, Russia

² Institute of Photon Technologies FSRC 'Crystallography and Photonics' RAS, Moscow, Russia

Sustained-release drugs against tuberculosis are a promising approach to therapy since they positively affect patient compliance with long regimens, especially when it comes to the multidrug-resistant form of the disease. Conventional UV-visible spectroscopy does not work well with multicomponential culture media used for growing *M. tuberculosis*. The aim of this study was to develop a method for evaluating the kinetics of anti-tuberculosis drug released from bioresorbable polymeric carriers suitable for screening a wide range of encapsulated prolonged-release drugs and identifying the best performing candidate. While studying the growth dynamics of the laboratory susceptible strain *M. tuberculosis* H37Rv in the presence of different levofloxacin concentrations (from 0.03 to 0.4 µg/ml), we developed a model, which is essentially a set of 2 parallel experiments evaluating the kinetics of drug release into the culture medium. The results of these 2 experiments conducted on 3 encapsulated forms of levofloxacin loaded onto bioresorbable polymeric PLGA carriers (particles sized 50 µm and 100 µm and the matrix) revealed that release kinetics of the drug largely depended on the type of polymeric carrier. The best encapsulation of the antibiotic and its gradual release into the culture medium was observed for the matrix. All experiments were run in 3 replicates. The obtained data were analyzed using descriptive statistics.

Keywords: *Mycobacterium tuberculosis*, *in vitro* model, levofloxacin, bioresorbable polymeric carrier, sustained-release

Funding: the study was supported by the Russian Ministry of Science and Higher Education and carried out as part of the State Assignment for FSRC "Crystallography and Photonics" RAS (developing an SCF-based method for creating bioactive matrices), as part of the State Assignment № 0515-2019-0015 (Formation of resistance to antimycobacterial drugs in mycobacteria and somatic cells) for the Central Tuberculosis Research Institute (evaluation of the bacteriostatic activity of different levofloxacin concentrations). The study was also supported by the Russian Foundation for Basic Research (Project № 18-29-06062 mk: development of sustained-release therapeutic formulations and an *in vitro* model for the evaluation of their efficacy).

Author contribution: Andreevskaya SN — interpretation of study results, manuscript preparation; Smirnova TG — modeling of conditions for levofloxacin release from its carriers; discussion of study results; Antonov EN — preparation of matrices; Chernousova LN, Ergeshov AE — study design; discussion of study results; Bogorodsky SE — preparation of microparticles; discussion of study results; Larionova EE — literature analysis; discussion of study results; Popov VK — method for antibiotic encapsulation into polymeric carriers; discussion of study results.

Compliance with ethical standards: manipulations with virulent strains of *M. tuberculosis* were conducted in compliance with the safety guidelines for the experiments involving Risk Group III–IV pathogens, infectious agents and utilization of medical waste specified in sanitary regulations 1.3.2322-08, 1.3.2518-09, 1.3.2885-11, and 2.1.7.2790-10.

✉ **Correspondence should be addressed:** Sofia N. Andreevskaya
Yauzskaya alleya, 2, str. 1A., Moscow, 107564; andsofia@mail.ru

Received: 06.08.2020 **Accepted:** 20.08.2020 **Published online:** 30.08.2020

DOI: 10.24075/brsmu.2020.050

НОВАЯ МОДЕЛЬ *IN VITRO* ДЛЯ ОЦЕНКИ ВЫСВОБОЖДЕНИЯ ПРОТИВОТУБЕРКУЛЕЗНЫХ ПРЕПАРАТОВ ИЗ БИОРЕЗОРБИРУЕМЫХ ПОЛИМЕРНЫХ НОСИТЕЛЕЙ

С. Н. Андреевская¹✉, Т. Г. Смирнова¹, Е. Н. Антонов², Л. Н. Черноусова¹, С. Э. Богородский², Е. Е. Ларионова¹, В. К. Попов², А. Э. Эргешов¹

¹ Центральный научно-исследовательский институт туберкулеза, Москва, Россия

² Институт фотонных технологий Федерального научно-исследовательского центра «Кристаллография и фотоника», Москва, Россия

Создание противотуберкулезных препаратов пролонгированного действия крайне перспективно, так как позволяет сохранить приверженность больных к лечению при длительных курсах терапии, особенно при химиотерапии туберкулеза с множественной лекарственной устойчивостью. Традиционно используемый для оценки кинетики выхода препаратов из полимерных носителей метод УФ-спектрофотометрии не подходит для применения в многокомпонентных питательных средах для культивирования микобактерий туберкулеза. Целью исследования было разработать метод оценки высвобождения противотуберкулезных препаратов из биорезорбируемых полимерных носителей, позволяющий проводить скрининг большого числа инкапсулированных пролонгированных форм противотуберкулезных препаратов и отбирать наиболее перспективные композиции. При изучении динамики роста лабораторного чувствительного штамма *M. tuberculosis* H37Rv в присутствии серии концентраций левофлоксацина (от 0,03 до 0,4 мкг/мл) была разработана модель, представляющая собой два параллельно проводимых опыта, позволяющих оценить кинетику высвобождения препарата в культуральную среду. Все эксперименты проводили трехкратно, при оценке использовали методы описательной статистики. Результаты, полученные в этой модели для трех инкапсулированных форм левофлоксацина в биорезорбируемых полимерных носителях из полилактидогликолида (частицы 50 и 100 мкм и матрикс), показали, что кинетика накопления препарата в среде существенно зависит от вида полимерного носителя. Наиболее перспективен из них матрикс, который хорошо включает в себя левофлоксацин и достаточно равномерно высвобождает его при инкубации в питательной среде.

Ключевые слова: микобактерии туберкулеза, модель *in vitro*, левофлоксацин, биорезорбируемые полимерные носители, пролонгированное высвобождение

Финансирование: работа выполнена при поддержке Министерства науки и высшего образования в рамках выполнения работ по Государственному заданию ФНИЦ «Кристаллография и фотоника» РАН в части развития СКФ методов формирования биоактивных матричных структур, в рамках выполнения работ по Государственному заданию ФГБНУ «ЦНИИТ» № 0515-2019-0015 «Формирование лекарственной устойчивости микобактерий и соматических клеток к противотуберкулезным препаратам» в части оценки бактериостатической активности диапазона концентраций левофлоксацина и РФФИ (проект № 18-29-06062 мк) в части разработки лекарственных форм пролонгированного действия и *in vitro* модели оценки их эффективности.

Вклад авторов: С. Н. Андреевская — интерпретация результатов, написание текста рукописи; Т. Г. Смирнова — отработка условий для оценки высвобождения левофлоксацина из носителя, обсуждение результатов; Е. Н. Антонов — формирование матриц, обсуждение результатов; Л. Н. Черноусова, А. Э. Эргешов — разработка дизайна исследования, обсуждение результатов; С. Э. Богородский — формирование микрочастиц, обсуждение результатов; Е. Е. Ларионова — анализ литературы, обсуждение результатов; В. К. Попов — разработка метода включения антибиотика в полимеры, обсуждение результатов.

Соблюдение этических стандартов: работы с вирулентными штаммами *M. tuberculosis* проводили с соблюдением мер безопасности при работе с патогенами III–IV группы патогенности согласно требованиям СП 1.3.2322-08 (с дополнениями СП 1.3.2518-09 и СП 1.3.2885-11) «Безопасность работы с микроорганизмами III–IV групп патогенности (опасности) и возбудителями паразитарных болезней», СанПиН 2.1.7.2790-10 «Санитарно-эпидемиологические требования к обращению с медицинскими отходами».

✉ **Для корреспонденции:** Софья Николаевна Андреевская
Яузская аллея, д. 2, стр. 1А, г. Москва, 107564; andsofia@mail.ru

Статья получена: 06.08.2020 **Статья принята к печати:** 20.08.2020 **Опубликована онлайн:** 30.08.2020

DOI: 10.24075/vrgmu.2020.050

Over the past decade, the global incidence of multidrug-resistant tuberculosis (MDR-TB) has been on the rise [1]. Difficult, lengthy treatment regimens often discourage patients with MDR-TB, undermining their compliance with therapy. A promising solution to this problem would be sustained-release anti-TB drugs (ATBD) encapsulated in bioresorbable polymer microparticles ensuring targeted delivery and controlled release of the active ingredient from the polymeric carrier into surrounding tissues over a prolonged period of 1–4 weeks [2]. The use of supercritical fluid technologies (SCF) can create versatile environmentally friendly micronized systems completely free from organic solvent residues [3]. The release time of the drug from the polymer carrier depends on the properties of the polymer matrix (microcapsule): its composition, dispersion and morphology. In some cases, the active ingredient is concentrated on or immediately below the surface of the carrier, which results in a rapid uncontrolled release of the encapsulated drug. This initial burst release poses a serious problem for the application of polymeric carriers since it can have a toxic effect on the body [4–6].

UV-visible spectroscopy is employed to estimate the kinetics of drug release from polymer microparticles or matrices. This technique can measure drug accumulation in a phosphate buffered saline incubated with a polymeric drug carrier [4]. However, given that many microorganisms and specifically *Mycobacterium tuberculosis* (MTB) are fastidious and require enriched, complex culture media to support their growth [7], which impedes spectral analysis, UV-visible spectroscopy produces only rough estimates and cannot be used to evaluate drug release kinetics under near-natural conditions.

The aim of this study was to design an *in vitro* model for the evaluation of ATBD release kinetics from polymeric carriers in a culture medium suitable for MTB growth.

METHODS

Levofloxacin (LFX), a compulsory component of MDR-TB treatment regimens, was chosen for encapsulation into the bioresorbable carrier.

The plan was to adapt our experimental model for work in an automated BACTEC MGIT 960 system. Advantageously, BACTEC MGIT 960 can be used to work with highly effective standardized and ISO9001-certified reagents and conventional protocols [8]. In BACTEC MGIT 960, culture is performed in special mycobacteria growth indicator tubes (MGIT). At the bottom of the tube, there is a bound fluorophore under a semi-permeable membrane. Fluorophore release and emission of light of a certain wavelength are directly proportional to oxygen consumption by bacterial cells in the tube: the more vigorously dividing cells there are, the more oxygen they consume, causing brighter fluorescence. Time to culture growth in the presence of a tested drug is an important parameter allowing to infer the antimycobacterial effect or the lack of thereof. Significant (over 3 days) growth delay of *M. tuberculosis* cultured in the presence vs. absence of an antimycobacterial drug means partial death of the mycobacterial population induced by the tested drug.

Encapsulated LFX formulations

Bioresorbable carriers for LFX (Sigma-Aldrich; USA) were fabricated from Purasorb PDLG7502 poly(lactic-co-glycolic acid) (PLGA, inherent viscosity: 0.2 dl/g; by CorbionPurac, Netherlands). High-purity oxygen dioxide (99.998%; NiiKm; Russia) was used without additional purification. PLGA was

combined with LFX (10% wt., i.e. 100 mg of LFX per each 900 mg of the polymer), compressed in cylindrical molds, plasticized with supercritical CO₂ and foamed while lowering the actual CO₂ pressure to the atmospheric pressure. The obtained matrices were chilled with dry ice and cryoground in a rotor mill to generate microparticles with an average size of 50 and 100 μm; details are provided in [4].

The precalculated amount of the polymeric microparticles with encapsulated LFX was incubated in a Middlebrook 7H9 broth at 37 °C for 66 days; samples of the broth containing LFX released from the carriers were collected at predefined time points.

MTB culture

The tests were conducted on the susceptible laboratory strain *M. tuberculosis* H37Rv from the collection of the Central Research Institute of Tuberculosis. For our experiments, we used suspensions of well-separated *M. tuberculosis* cells harvested in the log phase for which CFU were counted. To prepare the suspension, the culture grown in a Lowenstein-Jensen medium was passaged at 37 °C in a Dubos broth (Difco; USA) supplemented with 0.5% BSA for two cycles of 14 days each. Then, 20 μl drops of 10-fold serial dilutions of the suspension filtered through a 5 μm pore size filter (Millipore; USA) were transferred to Petri dishes coated with Dubos agar (Difco; USA). The dishes were cultured at 37 °C; the initial suspension was stored at 4 °C. After 3–4 days, mycobacterial colonies were counted under an inverted microscope (Olympus; USA) operated at ×200 magnification. The suspension of mycobacterial cells (500 μl) standardized to CFU was seeded into MGIT tubes containing a Middlebrook 7H9 broth (BD; USA) supplemented with OADC. Automated detection of mycobacterial growth was performed in BACTEC MGIT 960 (BD; USA).

Evaluation of bacteriostatic activity by BACTEC MGIT 960

The bacteriostatic activity of the tested formulation was evaluated based on the presence of mycobacterial growth in a MGIT tube containing the drug. Earlier experiments in a BACTEC MGIT 960 system conducted on MTB cultures with varying CFU numbers had revealed that a reduction in CFU by less than 75% (75% growth inhibition) caused at least a 3-day delay in mycobacterial growth; a reduction by at least 90% caused an 8-day delay; by 99%, a 16-day delay; by 99.9%, a 21-day delay, etc. [9]. The experiment described in this paper was conducted according to the manufacturer's protocol and lasted for 42 days. All grown colonies were subject to species identification. Acid-fastness was tested by means of Ziehl-Neelsen staining. If a positive MGIT tube contained acid-fast bacteria, a rapid immunochromatography assay (BD MGIT TBc Identification test) was performed following the manufacturer's instructions. To monitor the presence of nonspecific bacteria in the BACTEC MGIT 960 system, the bacterial suspension was cultured in blood agar. Microbial growth registered after 24 h of incubation at 37 °C indicated nonspecific bacterial contamination of the studied sample.

Statistical analysis

The obtained data were analyzed using descriptive statistics. All microbiological experiments were conducted in 3 replicates. Statistical analysis was carried out in Microsoft Office Excel 2019 (Microsoft; USA).

Table 1. Growth dynamics of *M. tuberculosis* H37Rv in the presence of levofloxacin

LFX concentration, µg/ml	Growth onset (days), Mean ± SD	Growth delay relative to control, days	Growth inhibition, %
0 (drug-free control)	6.07 ± 0.06	–	–
0.03125	6.08 ± 0.12	no	–
0.0625	6.20 ± 0.27	no	–
0.125	7.69 ± 0.09	1.62	25
0.15	16.92 ± 1.14	10.85	90
0.20	24.76 ± 3.21	18.69	99
0.25	there is no growth of culture		100
0.3	there is no growth of culture		100
0.4	there is no growth of culture		100

RESULTS

Since our plan was to estimate the accumulation of the drug in a culture medium based on the dynamics of MTB growth in a BACTEC MGIT960 system, we decided not to place the polymeric carrier directly into the MGIT tube for a number of reasons. First, the polymer could have impacted fluorophore fluorescence and skewed the results of the experiment. Second, with such experimental design, we would have been able to estimate only final concentrations of the tested formulation after complete drug release, but not its concentrations within the first few hours or days of incubation.

Therefore, the polymeric carrier loaded with the drug was added into a Middlebrook 7H9 broth (the same culture medium as in MGIT tubes). Samples of the broth (100 µl) containing the released antibiotic were collected at equal time intervals. The amount of encapsulated LFX taken for incubation in Middlebrook 7H9 was precalculated to ensure that once the antibiotic was completely released from the carrier, its concentration in 100 µl of the culture medium equaled its minimal inhibitory concentration (MIC) in an MGIT tube after the addition of the same volume of culture medium into the tube.

LFX loaded into the polymeric carrier can be distributed on its surface or throughout the entire carrier volume. So, we assumed that the superficially localized drug would be easy to remove from the carrier by vigorous washing. The polymeric carrier was washed in Middlebrook 7H9 multiple times. Briefly, the polymeric carrier placed into a centrifuge test tube was immersed in 30 ml of a sterile culture medium, vortex shaken and centrifuged

at 3,000 g for 5 min at room temperature; the supernatant was removed. The washed carrier was ready for further experiments. Considering that the antibiotic could be localized to the surface of the carrier, the amount of the tested drug was doubled in the experiments involving the washed carrier (vs. the unwashed carrier) to ensure the probability of a bacteriostatic effect in cases when some of the antibiotic had been eliminated from the surface of the carrier. In the experiment involving the unwashed carrier, 6.3 mg of the polymer loaded with LFX (0.63 mg) was incubated in 30 ml of the culture medium. For the experiment involving the washed carrier, 12.6 mg of the carrier loaded with LFX (1.26 mg) was incubated in 30 ml of the culture medium.

Thus, the proposed model is essentially a set of 2 experiments run in parallel evaluating LFX release into the culture medium from washed and unwashed polymeric carriers. Drug release kinetics can be elucidated by comparing the results of the 2 experiments. For example, if a rapid bacteriostatic effect is observed in the medium incubated with the unwashed encapsulated LFX formulation but no bacteriostatic effect is observed in the aliquots of the medium incubated with the washed formulation, it means that the drug (or most of the drug) is distributed on the surface of its polymeric carrier. A delayed bacteriostatic effect observed for the washed vs. unwashed encapsulated LFX formulation would suggest that some amount of the drug was evenly distributed throughout the polymer carrier during synthesis, while some amount of it remained on the surface of the carrier. If the unwashed LFX formulation has a delayed bacteriostatic effect on MTB in comparison with the unwashed formulation, the drug is evenly distributed in the polymeric carrier

Table 2. Growth inhibition of *M. tuberculosis* H37Rv exposed to LFX released from a polymeric carrier

Incubation time	Growth inhibition, %*						LFX concentration in the medium **, µg/ml (amount released, %)					
	Particles sized 50 µm		Particles sized 100 µm		Matrix		Particles sized 50 µm		Particles sized 100 µm		Matrix	
	unwashed	washed	unwashed	washed	unwashed	washed	unwashed	washed	unwashed	washed	unwashed	washed
1 h	90	0	90	0	0	0	0.15 (60)	–	0.15 (60)	–	–	–
3 h	90	0	99	0	0	0	0.15 (60)	–	0.20 (80)	–	–	–
1 days	99	0	99	0	0	25	0.20(80)	–	0.20 (80)	–	–	0.125 (25)
3 days	99	0	99	0	0	25	0.20 (80)	–	0.20 (80)	–	–	0.125 (25)
7 days	99	0	99	0	0	90	0.20 (80)	–	0.20 (80)	–	–	0.15 (30)
10 days	99.9	50	99	0	0	90	0.225 (90)	0.135 (67.5***)	0.20 (80)	–	–	0.15 (30)
16 days	99.9	50	99	0	0	99	0.225 (90)	0.135 (67.5)	0.20 (80)	–	–	0.2 (40)
22 days	99.9	50	99	0	0	99	0.225 (90)	0.135 (67.5)	0.20 (80)	–	–	0.2 (40)
29 days	99.99	75	99.99	25	25	99.9	0.235 (94)	0.145 (72.5)	0.235 (94)	0.09 (90)	0.125 (50)	0.225 (45)
45 days	99.99	75	99.99	25	90	100	0.235 (94)	0.145 (72.5)	0.235 (94)	0.09 (90)	0.15 (60)	0.25 (50)
66 days	99.99	75	99.99	25	99	100	0.235 (94)	0.145 (72.5)	0.235 (94)	0.09 (90)	0.2 (80)	0.25 (>50)

Note: * — calculated based on the growth delay relative to the control drug-free culture; ** — determined from the dose-response curve (see Figure); *** — hereinafter (in the experiments involving matrix washing): accounts for the drug amount washed from the carrier surface (% of the washed formulation = % of the unwashed drug released into the medium within 3 h); unwashed — indicates the experiment without carrier washing, washed — indicates the experiment involving carrier washing; – — the amount of released LFX is not enough to achieve the desired bacteriostatic effect (< 0.125 µg/ml).

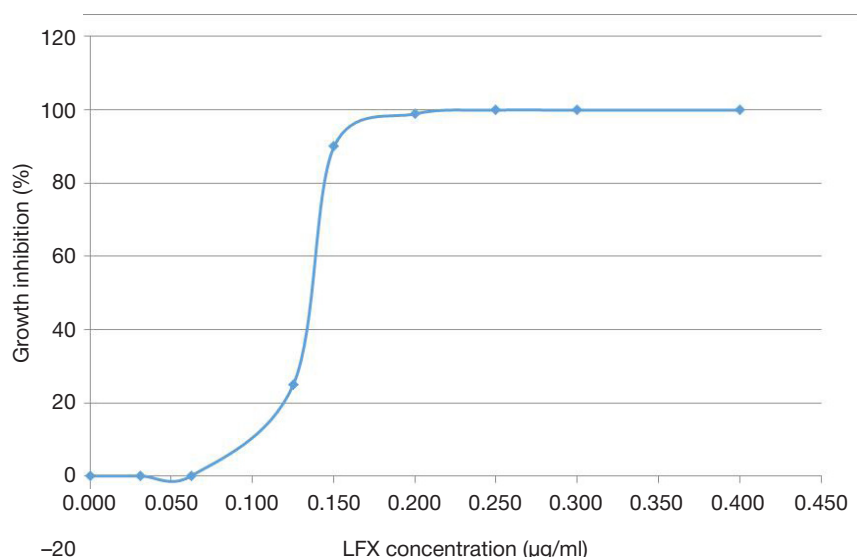


Figure. An LFX dose-response curve for the susceptible H37Rv strain of *M. tuberculosis*

and released gradually (bear in mind that the amount of the washed LFX formulation was doubled in comparison with the unwashed, so the bacteriostatic effect was faster).

Effects of different LFX concentrations on the growth dynamics of *M. tuberculosis* H37Rv

To determine the amount of encapsulated LFX formulation necessary for exploring the kinetics of drug release into a culture medium, we studied the effects of different LFX concentrations on the growth of an MTB laboratory strain. Briefly, after CFU were counted, the mycobacterial culture was incubated with LFX taken at a range of different concentrations from 0.031 to 0.4 µg/ml in a BACTEC MGIT 960 system. A drug-free MTB culture was used as a control (Table 1). For the strain used in our experiment, LFX MIC was 0.25 µg/ml. Based on the obtained data, we constructed a dose-response curve (Figure) subsequently used to determine the amount of LFX released from the polymeric carrier into the culture medium.

Evaluation of kinetics of LFX release from bioresorbable polymers into culture medium based on growth dynamics of *M. tuberculosis* H37Rv

Following the procedures described above, we studied 3 encapsulated LFX formulations differing in the carrier type: a PLGA matrix and particles sized 50 µm and 100 µm. A drug-free MTB culture and a MTB culture containing samples of the medium incubated with the intact PLGA matrix (without LFX) were used as controls. The results are provided in Table 2.

An immediate bacteriostatic effect was observed for PLGA particles sized 50 and 100 µm in the experiments involving the unwashed formulation; the bacteriostatic effect was delayed in the experiment involving the washed polymeric carrier. This suggests that at least 60% of the antibiotic was concentrated on the polymer surface: after 3 h of incubation, the unwashed carrier released 0.15–0.20 µg/ml of LFX into the culture medium, which was enough to inhibit the growth of 90% of the mycobacterial population.

By contrast, LFX encapsulated into the PLGA matrix had a delayed bacteriostatic effect on the mycobacterial population in the experiment without carrier washing (with carrier washing on day 1 and without carrier washing on day 29); this suggests that LFX was evenly distributed throughout the matrix and was released gradually. Besides, the experiment with the washed

matrix shows that some amount of the drug was concentrated just below the surface: 25% of LFX was released on day 1, causing inhibition of 25% of mycobacterial cells; then the drug was gradually released until 50% of it was present in the medium on day 45; complete inhibition of mycobacterial growth was observed for LFX concentrations of 0.25 µg/ml (MIC).

No differences were observed between the growth of cultures with added aliquots of the medium incubated with the drug-free matrix and the growth of untreated cultures, indicating adequacy of the proposed model.

DISCUSSION

The proposed model and the experiments described in this study can be used to evaluate the release kinetics of anti-TB agents in a culture medium *in vitro* based on the inhibition of *M. tuberculosis* growth. Previous *in vitro* studies of antimycobacterial activity looked at the kinetics of liposomal formulations that were not meant for gradual drug release but merely facilitated delivery of the tested drug to the target. Those experiments relied on a classic *in vitro* design and aimed at evaluating the efficacy of encapsulated formulations vs. pure active substance and assessing the immediate toxic effect of the liposome on mycobacterial cells [10–12]. *In vitro* models were also exploited to study sustained-release drugs against bacteria other than members of the *Mycobacterium* genus, such as *Staphylococcus aureus*; they involved constructing time-response curves for cultures grown in the presence of a polymer carrier with an encapsulated antibiotic [13].

The antimicrobial effect of encapsulated anti-TB drugs was mainly studied in *in vivo* models. Experiments on mice and rabbits demonstrated high anti-TB activity, prolonged effect and reduced toxicity (as compared to traditional therapeutic formulations) for PLGA-based microparticles loaded with rifampin [14], isoniazid [15, 16], ethionamide [17], rifampin + isoniazid [18], and rifampin + cycloserine [19]. Using experimental animals for testing long-acting encapsulated formulations makes the laboratory part and data analysis much easier, because in this way the pharmacokinetics of the drug can be studied under natural conditions. On the other hand, *in vivo* models are costly and, for ethical reasons, cannot be employed for screening studies involving a wide range of carriers and active ingredients. Developing a model for evaluating the growth of *M. tuberculosis* at different time points in the presence of the drug released into the medium is a promising approach since such a

model would allow testing more than one combination of carriers and encapsulated drugs and identifying the best-performing candidate for future *in vivo* experiments.

The analysis of the obtained data offers an answer to the question of whether the drug-loaded carrier should be prepared for the experiment (washed before the experiment to remove the active substance localized to its surface) and allows determining the amount of the drug needed for the *in vivo* experiment, given the preparatory washing and the release kinetics.

CONCLUSION

The proposed *in vitro* model allows conducting screening studies of encapsulated, sustained-release formulations of

anti-TB drugs. This approach helps to select the most promising formulation with smaller amounts of the drug concentrated on the carrier surface and ensuring its gradual release through the experiment.

Tests of 3 different formulations of LFX encapsulated in bioresorbable PLGA carriers revealed that release kinetics of the tested drug largely depended on the type of polymeric carrier. The best encapsulation of the antibiotic and its gradual release into the medium was observed for the matrix.

The proposed model can be used in screening studies investigating the antimycobacterial activity of encapsulated LFX or other encapsulated drugs. Such screening conducted before an *in vivo* experiment will reduce its costs and offer a solution to some ethical issues.

References

- World Health Organization. Global tuberculosis report 2019. Geneva: World Health Organization, 2019.
- Bogorodskii SE, Krotova LI, Mironov AV, Popov VK. Fabrication of highly porous bioresorbable polymer matrices Using Supercritical Carbon Dioxide. *Russian Journal of Physical Chemistry B*. 2013; 7 (8): 916–23.
- Alsens J, Kansy M. High throughput solubility measurement in drug discovery and development *Adv Drug Del Rev*. 2007; 59: 546.
- Antonov EN, Bogorodskiy SE, Dunayev AG, Krotova LI, Mariyanats AO, Syachina MA, i dr. Razrabotka komponentov antibakterial'nykh lekarstvennykh form prolongirovannogo deystviya s ispol'zovaniyem SKF-tekhnologiy. *Sverkhkriticheskiye flyuidy: teoriya i praktika*. 2020; 15 (1): 124–35. Russian.
- Yehia SA, Elshafeey AH, Elsayed I. A novel injectable in situ forming poly-DL-lactide and DL-lactide/glycolide implant containing lipospheres for controlled drug delivery. *J Liposome Res*. 2012; 22 (2): 128–38.
- Ahmed T. Review: approaches to develop PLGA based in situ gelling system with low initial burst. *Pak J Pharm Sci*. 2015; 28 (2): 657–65.
- Ergeshov AE, editor. *Tuberkulez organov dykhaniya. Rukovodstvo dlya vrachev*. M.: Galleya-Print, 2017; 524 s. Russian.
- Chemousova LN, Sevastyanova EV, Larionova EE, Smirnova TG, Andreyevskaya SN, i dr. Federal'nyye klinicheskiye rekomendatsii po organizatsii i provedeniyu mikrobiologicheskoy i molekulyarnogeneticheskoy diagnostiki tuberkuleza. *Tver': Triada*, 2014; 29 s.
- Matyugina E, Khandazhinskaya A, Chemousova L, Andreevskaya S, Smirnova T, Chizhov A, et al. The synthesis and antituberculosis activity of 50-nor carbocyclic uracil derivatives. *Bioorganic and Medicinal Chemistry*. 2012; 20: 6680–86.
- Bhardwaj A, Kumar L, Narang RK, Murthy RS. Development and characterization of ligand-appended liposomes for multiple drug therapy for pulmonary tuberculosis. *Artif Cells Nanomed Biotechnol*. 2013; 41 (1): 52–9.
- Sorokoumova GM, Yasin YaOH, Mikulovich YuL, Smirnova TG, Andreyevskaya SN, Selishcheva AA, i dr. Sozdaniye i izucheniye svoystv liposomal'noy formy levofloksatsina. *Tonkiye khimicheskiye tekhnologii*. 2013; 8 (5): 72–6. Russian.
- Andreevskaya SN, Smirnova TG, Zhogina YA, Smirnova DI, Mikulovich YL, Sorokoumova GM, et al. Effect of exogenous cardiolipin on the growth and viability of *Mycobacterium tuberculosis* H37Rv *in vitro*. *Dokl Biol Sci*. 2010; 434: 371–4.
- Qiao Z, Yuan Z, Zhang W, Wei D, Hu N. Preparation, *in vitro* release and antibacterial activity evaluation of rifampicin and moxifloxacin-loaded poly(D,L-lactide-co-glycolide) microspheres. *Artif Cells Nanomed Biotechnol*. 2019; 47 (1): 790–8.
- Quenelle DC, Staas JK, Winchester GA, Barrow EL, Barrow WW. Efficacy of microencapsulated rifampin in *Mycobacterium tuberculosis*-infected mice. *Antimicrob Agents Chemother*. 1999; 43 (5): 1144–51.
- Kailasam S, Daneluzzi D, Gangadharam PR. Maintenance of therapeutically active levels of isoniazid for prolonged periods in rabbits after a single implant of biodegradable polymer. *Tuber Lung Dis*. 1994; 75 (5): 361–5.
- Gangadharam PR, Kailasam S, Srinivasan S, Wise DL. Experimental chemotherapy of tuberculosis using single dose treatment with isoniazid in biodegradable polymers. *J Antimicrob Chemother*. 1994; 33 (2): 265–71.
- Kumar G, Malhotra S, Shafiq N, Pandhi P, Khuller GK, Sharma S. *In vitro* physicochemical characterization and short term *in vivo* tolerability study of ethionamide loaded PLGA nanoparticles: potentially effective agent for multidrug resistant tuberculosis. *J Microencapsul*. 2011; 28 (8): 717–28.
- Dutt M, Khuller GK. Therapeutic efficacy of Poly(DL-lactide-Co-Glycolide)-encapsulated antitubercular drugs against *Mycobacterium tuberculosis* infection induced in mice. *Antimicrob Agents Chemother*. 2001; 45 (1): 363–6.
- Naydenova AA, Sukoyan GV, Vorontsov EA, Kuznetsov SL, Gukasova NV, Ryabtseva MS, i dr. Razrabotka nanosomal'nykh kompozitsiy rifampitsina i D-tsikloserina na osnove polilaktidglikolidov i issledovaniye ikh protivotuberkuleznoy aktivnosti. *Nanotekhnologii i okhrana zdorov'ya*. 2012; 3 (12): 23–30. Russian.

Литература

- World Health Organization. Global tuberculosis report 2019. Geneva: World Health Organization, 2019.
- Bogorodskii SE, Krotova LI, Mironov AV, Popov VK. Fabrication of highly porous bioresorbable polymer matrices Using Supercritical Carbon Dioxide. *Russian Journal of Physical Chemistry B*. 2013; 7 (8): 916–23.
- Alsens J, Kansy M. High throughput solubility measurement in drug discovery and development *Adv Drug Del Rev*. 2007; 59: 546.
- Антонов Е. Н., Богородский С. Э., Дунаев А. Г., Кротова Л. И., Мариянац А. О., Сячина М. А., и др. Разработка компонентов антибактериальных лекарственных форм пролонгированного действия с использованием СКФ-технологий. *Сверхкритические флюиды: теория и практика*. 2020; 15 (1): 124–35.
- Yehia SA, Elshafeey AH, Elsayed I. A novel injectable in situ forming poly-DL-lactide and DL-lactide/glycolide implant containing lipospheres for controlled drug delivery. *J Liposome Res*. 2012; 22 (2): 128–38.
- Ahmed T. Review: approaches to develop PLGA based in situ gelling system with low initial burst. *Pak J Pharm Sci*. 2015; 28 (2): 657–65.
- Эргешов А. Э., редактор. *Туберкулез органов дыхания*.

- Руководство для врачей. М.: Галлея-Принт, 2017; 524 с.
8. Черноусова Л. Н., Севастьянова Э. В., Ларионова Е. Е., Смирнова Т. Г., Андреевская С. Н., Попов С. А. и др. Федеральные клинические рекомендации по организации и проведению микробиологической и молекулярно-генетической диагностики туберкулеза. Тверь: Триада, 2014; 29 с.
 9. Matyugina E, Khandzhinskaya A, Chernousova L, Andreevskaya S, Smirnova T, Chizhov A, et al. The synthesis and antituberculosis activity of 50-nor carbocyclic uracil derivatives. *Bioorganic and Medicinal Chemistry*. 2012; 20: 6680–86.
 10. Bhardwaj A, Kumar L, Narang RK, Murthy RS. Development and characterization of ligand-appended liposomes for multiple drug therapy for pulmonary tuberculosis. *Artif Cells Nanomed Biotechnol*. 2013; 41 (1): 52–9.
 11. Сорокоумова Г. М., Ясин Я. О. Х., Миколович Ю. Л., Смирнова Т. Г., Андреевская С. Н., Селищева А. А., и др. Создание и изучение свойств липосомальной формы левофлоксацина. Тонкие химические технологии. 2013; 8 (5): 72–6.
 12. Andreevskaya SN, Smirnova TG, Zhogina YA, Smirnova DI, Mikulovich YL, Sorokoumova GM, et al. Effect of exogenous cardiolipin on the growth and viability of *Mycobacterium tuberculosis* H37Rv in vitro. *Dokl Biol Sci*. 2010; 434: 371–4.
 13. Qiao Z, Yuan Z, Zhang W, Wei D, Hu N. Preparation, in vitro release and antibacterial activity evaluation of rifampicin and moxifloxacin-loaded poly(D,L-lactide-co-glycolide) microspheres. *Artif Cells Nanomed Biotechnol*. 2019; 47 (1): 790–8.
 14. Quenelle DC, Staas JK, Winchester GA, Barrow EL, Barrow WW. Efficacy of microencapsulated rifampin in *Mycobacterium tuberculosis*-infected mice. *Antimicrob Agents Chemother*. 1999; 43 (5): 1144–51.
 15. Kailasam S, Daneluzzi D, Gangadharam PR. Maintenance of therapeutically active levels of isoniazid for prolonged periods in rabbits after a single implant of biodegradable polymer. *Tuber Lung Dis*. 1994; 75 (5): 361–5.
 16. Gangadharam PR, Kailasam S, Srinivasan S, Wise DL. Experimental chemotherapy of tuberculosis using single dose treatment with isoniazid in biodegradable polymers. *J Antimicrob Chemother*. 1994; 33 (2): 265–71.
 17. Kumar G, Malhotra S, Shafiq N, Pandhi P, Khuller GK, Sharma S. In vitro physicochemical characterization and short term in vivo tolerability study of ethionamide loaded PLGA nanoparticles: potentially effective agent for multidrug resistant tuberculosis. *J Microencapsul*. 2011; 28 (8): 717–28.
 18. Dutt M, Khuller GK. Therapeutic efficacy of Poly(DL-lactide-Co-Glycolide)-encapsulated antitubercular drugs against *Mycobacterium tuberculosis* infection induced in mice. *Antimicrob Agents Chemother*. 2001; 45 (1): 363–6.
 19. Найденова А. А., Сукоян Г. В., Воронцов Е. А., Кузнецов С. Л., Гукасова Н.В., Рябцева М. С. и др. Разработка наносомальных композиций рифампицина и D-циклосерина на основе полилактидгликолидов и исследование их противотуберкулезной активности. *Нанотехнологии и охрана здоровья*. 2012; 3 (12): 23–30.

GUT MICROBIOTA ASSESSMENT IN MOSCOW LONG-LIVERS USING NEXT GENERATION SEQUENCING

Kashtanova DA^{1,2} ✉, Klimenko NS³, Strazhesko ID¹, Tkacheva ON¹, Starikova EV⁴, Glushchenko OE⁴, Gudkov DA⁴, Ilina EN⁴¹ Pirogov Russian National Research Medical University, Moscow, Russia² Center for Strategic Planning of FMBA, Moscow, Russia³ Institute of Gene Biology, Moscow, Russia⁴ Federal Research and Clinical Centre of Physical-Chemical Medicine, Moscow, Russia

Demographic aging poses a challenge to the medical community, pressing for research into the biological factors promoting longevity and its features. Below, we look at the gut microbiota as one of such factors. The aim of this non-longitudinal study was to profile the gut microbiota of centenarians and to compare it with that of relatively healthy, younger Moscow residents. The study recruited 20 people aged 97–100 years (mean age 98 ± 1 year); the control group consisted of 92 individuals aged 53 ± 13 years. For each stool sample, the variable V3–V4 regions of the microbial 16S rRNA gene were sequenced. Primary analysis, read filtering and taxonomic identification were conducted in the QIIME 1.9 environment; reconstruction of metabolic pathways was aided by PICRUSt. Statistical analysis was performed by means of Python v. 3.2. A few differences were detected between the gut microbiota of centenarians and younger individuals: *Bifidobacterium* ($p = 0.026$) and *Coprococcus eutactus* ($p = 0.026$) were more abundant in centenarians, whereas *Bacteroides* ($p = 0.003$) and *Prevotella* ($p = 0.002$) were better represented in younger participants. The potential for butyric acid synthesis was higher in the group of centenarians ($p = 0.048$). Surprisingly, the gut microbiota of centenarians was more diverse and surprisingly beneficial for advanced age. Besides, the gut microbiota of centenarians might have more pronounced anti-inflammatory potential due to its ability to better synthesize butyric acid.

Keywords: gut microbiota, longevity, butyric acid, aging, systemic low-grade inflammation

Funding: the study was supported by the Russian Foundation for Basic Research (Grant 19-34-80033).

Author contribution: Kashtanova DA — study design, participant recruitment, data interpretation, manuscript preparation; Klimenko NS — bioinformatic analysis, data interpretation, manuscript preparation; Strazhesko ID — study concept, manuscript revision; Tkacheva ON — study concept and design; Starikova EV — gut microbiota profiling, manuscript revision; Glushchenko OE, Gudkov DA — gut microbiota profiling; Ilina EN — final revision of the manuscript.

Compliance with ethical standards: the study was approved by the Ethics Committee of Pirogov Russian National Research Medical University (Protocol № 2 dated March 18, 2016). Informed consent was obtained from all study participants.

✉ **Correspondence should be addressed:** Daria A. Kashtanova
1-ya Leonova, 16, Moscow, 129226; dr.kashtanova@gmail.com

Received: 01.07.2020 **Accepted:** 15.07.2020 **Published online:** 26.07.2020

DOI: 10.24075/brsmu.2020.044

АНАЛИЗ МИКРОБИОТЫ ДОЛГОЖИТЕЛЕЙ МОСКВЫ С ИСПОЛЬЗОВАНИЕМ ВЫСОКОПРОИЗВОДИТЕЛЬНОГО СЕКВЕНИРОВАНИЯ

Д. А. Каштанова^{1,2} ✉, Н. С. Клименко³, И. Д. Стражеско¹, О. Н. Ткачева¹, Е. В. Старикова⁴, О. Е. Глуценко⁴, Д. А. Гудков⁴, Е. Н. Ильина⁴¹ Российский национальный исследовательский медицинский университет имени Н. И. Пирогова, Москва, Россия² Центр стратегического планирования Федерального медико-биологического агентства России, Москва, Россия³ Институт биологии гена, Москва, Россия⁴ Федеральный научно-клинический центр физико-химической медицины Федерального медико-биологического агентства России, Москва, Россия

Старение населения ставит перед медицинским обществом задачу изучения здорового долголетия, предрасполагающих к нему биомаркеров и характерных особенностей. В настоящей работе рассмотрен один из таких факторов — микробиота кишечника. Целью исследования было изучить состав микробиоты кишечника долгожителей и провести сравнительный анализ с группой относительно здоровых более молодых лиц, проживающих на территории г. Москвы. В одномоментное исследование были включены 20 человек в возрасте 97–100 лет, средний возраст 98 ± 1 год, в качестве группы сравнения была выбрана группа из 92 человек 53 ± 13 лет. Для участников исследования обеих групп проводили секвенирование V3–V4 переменных участков гена 16S рРНК микробиоты кишечника. Для первичного анализа, фильтрации ридов и идентификации операционных таксономических единиц использовали QIIME 1.9, для реконструкции метаболических путей — алгоритм PICRUSt. Статистический анализ проводили с использованием языка Python v. 3.2. При межгрупповом сравнении были обнаружены значимые различия в микробиоте долгожителей и относительно здоровых лиц: в составе микробиоты первых были достоверно более представлены *Bifidobacterium* ($p = 0,026$) и *Coprococcus eutactus* ($p = 0,026$), в то время как у относительно здоровых лиц выявлено больше *Bacteroides* ($p = 0,003$) и *Prevotella* ($p = 0,002$). Потенциал синтеза масляной кислоты был выше в группе долгожителей ($p = 0,048$). Состав микробиоты кишечника долгожителей оказался неожиданно благополучным, с большей представленностью полезных бактерий. Кроме того, можно говорить о возможном наличии у долгожителей более выраженного «противовоспалительного» потенциала микробиоты кишечника ввиду лучшей способности микробиоты синтезировать масляную кислоту.

Ключевые слова: микробиота кишечника, долголетие, масляная кислота, старение, системное вялотекущее воспаление

Финансирование: работа выполнена при поддержке гранта Российского фонда фундаментальных исследований 19-34-80033

Вклад авторов: Д. А. Каштанова — дизайн исследования, набор пациентов, интерпретация данных, написание статьи; Н. С. Клименко — биоинформатический анализ, интерпретация данных, написание статьи; И. Д. Стражеско — концептуализация исследования, редактирование статьи; О. Н. Ткачева — концептуализация и дизайн исследования; Е. В. Старикова — анализ микробиоты кишечника, редактирование статьи; О. Е. Глуценко, Д. А. Гудков — анализ микробиоты кишечника; Е. Н. Ильина — финальное редактирование статьи.

Соблюдение этических стандартов: исследование одобрено этическим комитетом РНИМУ им. Н. И. Пирогова (протокол № 2 от 18 марта 2016 г.). Все участники подписали информированное добровольное согласие на участие в исследовании.

✉ **Для корреспонденции:** Дарья Андреевна Каштанова
ул. 1-я Леонова, д. 16, г. Москва, 129226; dr.kashtanova@gmail.com

Статья получена: 01.07.2020 **Статья принята к печати:** 15.07.2020 **Опубликована онлайн:** 26.07.2020

DOI: 10.24075/vrgmu.2020.044

The gut microbiota plays a crucial role in human health and disease. It is thought to be involved in the processes associated with aging. For example, it affects glucose metabolism [1], atherogenesis and cardiovascular health [2]. A link has been established between the gut microbiota and negative aging outcomes, such as frailty and other geriatric conditions [3]. It is hypothesized that the gut microbiota “ages” together with its host. As the host progresses into senescence, the diversity of microbial community inhabiting the gut declines, the abundance of opportunistic pathogens (*Clostridium difficile*, *C. perfringens*, and *Escherichia coli*) increases, whereas the number of beneficial microbes, including *Lactobacillus*, *Bifidobacterium*, and butyrate-producing bacteria essential in reducing inflammation, drops [4]. With age, endotoxins rise, whereas the levels of butyric acid decline [5]. Thus, the aging microbiota can drive low-grade inflammation underlying age-associated diseases.

Longevity is a unique model of aging. Long-lived individuals, who effectively realize their biological potential, have a delayed onset of age-related pathologies. Their gut microbiota is quite diverse and contains high levels of beneficial bacteria [6, 7]. In spite of advanced age, they manage to retain the pro- and anti-inflammatory potential of their microbiota. This might be the anti-risk factor for aging that the modern science is still searching for. Until recently, no research studies were conducted in Russia exploring the composition of the gut microbiota in long-lived individuals. The aim of this paper was to study the composition of the gut microbiota in such individuals and to compare it with that of younger Moscow residents without chronic conditions and of centenarians from other countries.

METHODS

Twenty participants were recruited for the study. The only inclusion criterion was age of 97–100 years (mean age 98 ± 1 year). Exclusion criteria were as follows: antibacterial therapy, chemotherapy or probiotic therapy within 3 months before stool collection. All participants underwent a physical examination and a geriatric assessment; complete medical histories were taken. The Mini Nutritional Assessment (MNA) was used to identify malnourished individuals. The control group consisted of 92 individuals aged 25 to 76 years with no severe somatic pathology at the time of the examination. The demographics and clinical characteristics of the control group are described in [8].

For each stool sample, the variable V3–V4 regions of the microbial 16S rRNA gene were sequenced using a MiSeq Illumina sequencer (Illumina; USA) following the manufacturer's protocol. Libraries were prepared using a Nextera XT Index Kit (Illumina) and the 16S Metagenomic Sequencing Library Preparation protocol provided by the manufacturer. Metagenomic data analysis was carried out in the Knomics-Biota system [9]. Primary analysis, read filtering and taxonomic identification were conducted in the QIIME 1.9 environment [10]; reconstruction of metabolic pathways was aided by PICRUSt [11]. Statistical analysis was done with Python v. 3.2. In the group of long-lived individuals, the results were adjusted for multiple comparisons and sex using MaAsLin [12]; for intergroup analysis, adjustments were made for multiple comparisons, age and sex. All samples ($n = 112$) met the quality criteria for the number of mapped species > 70%.

RESULTS

Composition of gut microbiota in long-livers

Symbiotic bacteria were the most abundant microorganisms in the gut microbiota of centenarians; many of them were

butyrate-producing bacteria from the *Christensenellaceae* and *Ruminococcaceae* families and the *Ruminococcus* genus. All samples were close to the enterotype *Ruminococcus* [13]. They can be arbitrarily divided into clusters with low silhouette width. In terms of composition, all samples in this group were relatively similar to each other. The mean alpha-diversity value (the Shannon index) was 6.3 ± 0.59 . The phylum distribution of bacteria looked interesting. In the group of centenarians, the *Bacteroidetes* phylum was lowly abundant, amounting to 7.8% of the gut microbiota, whereas *Firmicutes* made up 78.7% (Fig. 1). Clinical characteristics of the studied cohort of centenarians are provided in Table 1.

Comparison of gut microbiota composition in centenarians and younger individuals

The composition of the gut microbiota in relatively healthy younger participants was not out of the ordinary typically observed in healthy individuals. According to QIIME 1.9, *Bacteroidetes* made up an average of 20.23% of the gut microbiota, *Firmicutes* amounted to 73.4% (Fig. 1). Differences in the abundance of *Bacteroidetes* were significant between the groups (*adj. p* < 0.002; MaAsLin).

In younger participants, the Shannon index was 7.56 ± 0.49 , which was higher than in the group of centenarians; however, the difference was insignificant (*p* = 0.10).

The intergroup comparison at the genus and species levels produced a few remarkable findings. According to PCoA (Principal Coordinate Analysis), the samples collected from centenarians and healthy younger participants were different (Fig. 2).

A more thorough analysis allowed us to identify the differences in the gut microbiota of centenarians and other study participants. There were significantly more beneficial bacteria, including *Bifidobacterium* and *Coprococcus*, in the samples obtained from centenarians (Table 2).

The differences show on the MDS plot were confirmed by the MaAsLin analysis. The microbiota composition of healthy younger participants abounded with the bacteria representing 2 enterotypes: *Bacteroides* and *Prevotella* (Table 3).

Reconstruction of metabolic pathways

The analysis of metabolic pathways revealed that in long-lived participants, butyric acid synthesis through acetyl coenzyme A conversion was more prevalent than in younger individuals (*adj. p* = 0.048; *lda* = 3.35); other butyrate synthesis pathways did not differ significantly between the groups (Fig. 3).

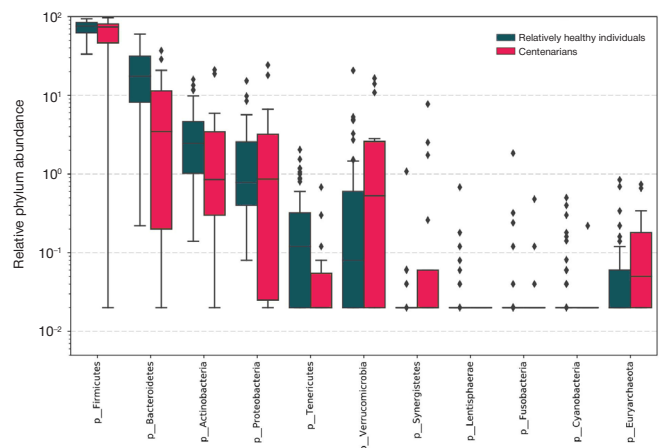


Fig. 1. Phylum distribution of gut microorganisms in the groups of centenarians and relatively healthy younger participants

Table 1. Clinical characteristics of the centenarian group

Factor	Median	IQR
Body mass index, kg/m ²	25.10	5.66
“Age is no barrier” local scale (0–7 points)	3.00	1.25
Systolic blood pressure, mmHg	155.00	32.50
Diastolic blood pressure, mmHg	78.00	9.00
Heart rate, beats/min	69.00	9.00
Geriatric depression scale	6.00	7.25
IADL	16.00	9.25
MNA	22.75	7.00
CIMT, mm	1.31	0.25
Glycated hemoglobin, %	5.79	0.50
HSCRP, mg/L	2.06	3.91
Triglycerides, mmol/L	1.04	0.34
High-density lipoproteins, mmol/L	1.43	0.48
Low-density lipoproteins, mmol/L	3.55	1.18
Hand grip strength, kg	17.00	6.38
MOCA	11.50	18.00
MMSE	23.00	25.00

Note: HSCRP — high-sensitivity C-reactive protein; CIMT — carotid intima-media thickness; IQR — interquartile range; IADL — Instrumental Activities of Daily Living; MMSE — Mini-Mental State Examination; MNA — Mini Nutritional Assessment; MOCA — Montreal Cognitive Assessment.

A possible association between a healthy diet and the microbiota composition/the potential for metabolite synthesis was analyzed in the group of centenarians. The analysis established an association with the prevalence of metabolic pathways. The MNA score was associated with the potential synthesis of a few types of vitamin B, especially B12. The higher was the score, the higher was the potential activity of some metabolic pathways, as demonstrated by MaAsLin (Table 4).

Thus, we have described a few characteristic features of the gut microbiota in centenarians and discovered that their microbiota was able to effectively synthesize butyrate through acetyl coenzyme A conversion.

DISCUSSION

The tremendous role of microorganisms inhabiting the human body is indisputable. Still, our knowledge of these inhabitants

is very limited. The majority of currently known microbes were discovered not so long ago owing to the advances in next generation sequencing. The possible mechanisms underlying their effects on the human body remain understudied. Studies in humans are still scarce and mostly non-longitudinal. However, understanding the unique features of the gut microbiota in centenarians might be helpful in preventing conditions associated with its disturbances, including age-related diseases. The most important outcome of our study is the obtained profile of the gut microbiota of centenarians; its composition was found to be very beneficial for advanced age. Most studies looking into the “aging” gut microbiota demonstrate that the number of pathobionts increases with advancing age, while the number of beneficial bacteria declines [4]. This pattern, however, was not confirmed for healthily aging individuals.

Until recently, such studies were conducted abroad. One of them reported high levels of *Bifidobacterium* in a group of

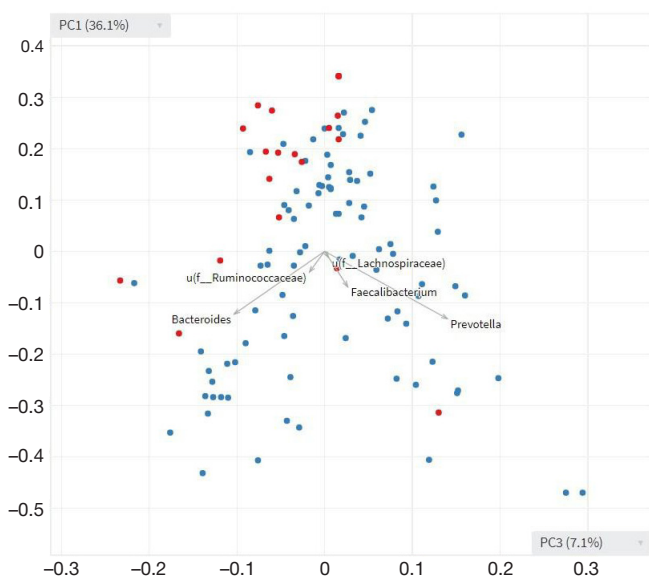


Fig. 2. A multidimensional scaling plot of gut microbiota samples obtained from centenarians (red dots) and relatively healthy individuals (blue dots).

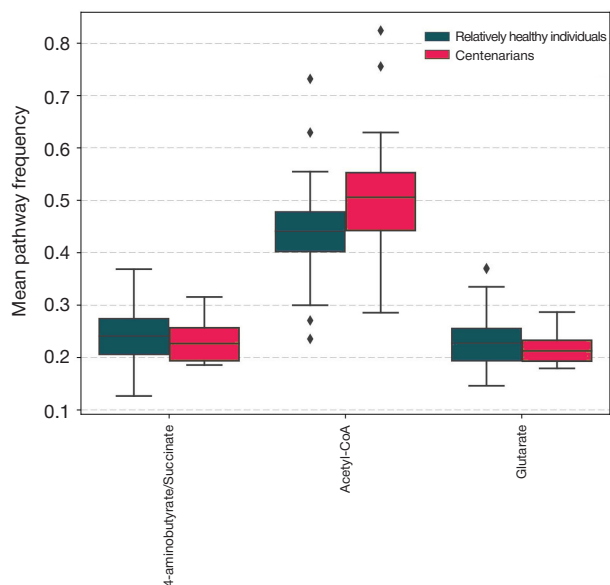


Fig. 3. Metabolic pathways for butyric acid synthesis in the groups (the mean prevalence of the pathways is plotted on the Y axis)

Table 2. Microorganisms found to be more abundant in the gut microbiota of centenarians

	Relatively healthy M, %	Relatively healthy IQR	Centenarians M, %	Centenarians IQR	<i>p</i>	<i>adj. p</i>
<i>Bifidobacterium</i>	1.904	2.598	2.278	4.724	0.013	0.026
<i>Bifidobacterium longum</i>	0.472	0.887	0.779	2.041	0.021	0.043
<i>Coprococcus eutactus</i>	0.211	0.326	0.610	1.457	0.012	0.026

Table 3. Microorganisms found to be more abundant in the gut microbiota of relatively healthy participants

	Relatively healthy M, %	Relatively healthy IQR	Centenarians M, %	Centenarians IQR	<i>p</i>	<i>adj. p</i>
<i>Bacteroides</i>	9.917	10.418	3.999	6.011	0.001	0.003
<i>Prevotella</i>	6.505	10.129	1.811	6.352	0.001	0.002
<i>Dialister</i>	2.104	3.066	0.129	0.392	< 0.001	0.001

Table 4. Associations between MNA scores and the prevalence of metabolic pathways for vitamin synthesis by the gut microbiota

Vitamin synthesis pathway	Coefficient	<i>adj. p</i>	<i>p</i>
B ₁₂	0.002048	0.009	0.001
B ₇	0.000681	0.043	0.015
B ₁	0.000588	0.048	0.024

centenarians over 105 years of age, in comparison with middle-aged individuals; this trend was observed in supercentenarians but not in their younger peers [6]. Interestingly, according to the same study *Akkermansia* and *Christensenellaceae* were also more abundant in centenarians. This sparked the hypothesis that maintaining a healthy microbiota might contribute to longevity.

In our study, pathogens and opportunistic pathogens were poorly represented in the gut microbiota; no difference in their abundance was observed between the group of long-lived individuals and younger participants. Moreover, *Bacteroides* and the *Bacteroidetes* phylum in general were poorly represented in the microbiota of centenarians. By contrast, a Japanese study [7] reports that the level of these bacteria increases in very old people.

In addition to having a beneficial composition, the gut microbiota of centenarians seems to affect the rate of aging; using the advanced tools for metabolism reconstruction, we were able to identify a few possible mechanisms underlying this effect. One interesting finding was discovery of high potential for butyrate synthesis in the gut microbiota of centenarians. Butyric acid is an anti-inflammatory agent [14, 15]; the ability of the gut microbiota to maintain its synthesis might slow down aging. In a recent experiment, butyric acid was administered to mice, leading to an increase in fibroblast growth factor

21 (the pleiotropic hormone); this elevation was found to correlate with the activation of AMPK and SIRT-1 and decreased activity of the mTOR signaling pathway [16], i.e. had a “rejuvenating” effect. We hope that further studies will be more conclusive and establish the cause and effect relationships. That said, we think that our finding reflects the main trends of healthy aging. High metabolic activity of the gut microbiota (vitamin synthesis) observed in centenarians who scored highly on the diet assessment scale should be interpreted with caution. Although vitamin transporters were detected in the colon [17], it is still unclear how critical is vitamin synthesis by the gut microbiota to maintaining sufficient levels of vitamins in blood.

CONCLUSIONS

Next generation sequencing gives us a chance to expand our knowledge of the microbial communities inhabiting the human body. This study shows that healthy old individuals over 97 years retain normal profiles of their gut microbiota. Maintaining healthy levels of symbiotic bacteria and high potential for butyrate synthesis might contribute to longevity by keeping the balance between pro- and anti-inflammatory potential of the gut microbiota.

References

- Tilg H, Moschen AR. Microbiota and diabetes: an evolving relationship. *Gut*. 2014; 63: 1513–21.
- Tang WH, Kitai T, Hazen SL. Gut Microbiota in Cardiovascular Health and Disease. *Circ Res*. 2017; 120 (7): 1183–96.
- Gemikonakli G, Mach J, Hilmer SN. Interactions between the aging gut microbiome and common geriatric giants: polypharmacy, frailty and dementia. *J Gerontol A Biol Sci Med Sci*. 2020; Feb 17: glaa047. DOI: 10.1093/gerona/glaa047. Epub ahead of print. PMID: 32064521.
- Nagpal R, Mainali R, Ahmadi S, Wang S, Singh R, Kavanagh K, et al. Gut microbiome and aging: Physiological and mechanistic insights. *Nutr Healthy Aging*. 2018; 4 (4): 267–85.
- Aleman FDD, Valenzano DR. Microbiome evolution during host aging. *PLoS Pathog*. 2019 Jul 25; 15 (7): e1007727.
- Biagi E, Franceschi C, Rampelli S, Severgnini M, Ostan R, Turroni S, et al. Gut Microbiota and Extreme Longevity. *Curr Biol*. 2016; 26 (11): 1480–5.
- Odamaki T, Kato K, Sugahara H, Hashikura N, Takahashi S, Xiao JZ, et al. Age-related changes in gut microbiota composition from newborn to centenarian: a cross-sectional study. *BMC Microbiol*. 2016; 16: 90.
- Kashtanova DA, Tkacheva ON, Doudinskaya EN, Strazhesko ID, Kotovskaya YV, Popenko AS, et al. Gut Microbiota in Patients with Different Metabolic Statuses: Moscow Study. *Microorganisms*. 2018; 6 (4): 98.
- Efimova D, Tyakht A, Popenko A, Vasilyev A, Altukhov I, Dovidchenko N, et al. Knomics-Biota — a system for exploratory analysis of human gut microbiota data. *BioData Min*. 2018; 11: 25.
- Caporaso JG, Kuczynski J, Stombaugh J, Bittinger K, Bushman FD, Costello EK, et al. QIIME allows analysis of high-throughput community sequencing data. *Nature methods*. 2010; 7 (5): 335–6.
- Langille MG, Zaneveld J, Caporaso JG, McDonald D, Knights D,

- Reyes JA, et al. Predictive functional profiling of microbial communities using 16S rRNA marker gene sequences. *Nature biotechnology*. 2013; 31 (9): 814–21.
12. Mallick H, Ma S, Franzosa EA, Vatanen T, Morgan XC, Huttenhower C. Experimental design and quantitative analysis of microbial community multiomics. *Genome Biol*. 2017; 18 (1): 228.
 13. Arumugam M, Raes J, Pelletier E, Le Paslier D, Yamada T, Mende DR, et al. Enterotypes of the human gut microbiome. *Nature*. 2011; 473 (7346): 174–80.
 14. Mishiro T, Kusunoki R, Otani A, Ansary MM, Tongu M, Harashima N, et al. Butyric acid attenuates intestinal inflammation in murine DSS-induced colitis model via milk fat globule-EGF factor 8. *Lab Invest*. 2013; 93 (7): 834–43.
 15. Ohira H, Tsutsui W, Fujioka Y. Are Short Chain Fatty Acids in Gut Microbiota Defensive Players for Inflammation and Atherosclerosis? *J Atheroscler Thromb*. 2017; 24 (7): 660–72.
 16. Kundu P, Lee HU, Garcia-Perez I, Tay EXY, Kim H, Faylon LE, et al. Neurogenesis and longevity signaling in young germ-free mice transplanted with the gut microbiota of old mice. *Sci Transl Med*. 2019; 11 (518): eaau4760.
 17. Said HM. Intestinal absorption of water-soluble vitamins in health and disease. *Biochem J*. 2011; 437 (3): 357–72.

Литература

1. Tilg H, Moschen AR. Microbiota and diabetes: an evolving relationship. *Gut*. 2014; 63: 1513–21.
2. Tang WH, Kitai T, Hazen SL. Gut Microbiota in Cardiovascular Health and Disease. *Circ Res*. 2017; 120 (7): 1183–96.
3. Gemikonakii G, Mach J, Hilmer SN. Interactions between the aging gut microbiome and common geriatric giants: polypharmacy, frailty and dementia. *J Gerontol A Biol Sci Med Sci*. 2020; Feb 17: glaa047. DOI: 10.1093/gerona/glaa047. Epub ahead of print. PMID: 32064521.
4. Nagpal R, Mainali R, Ahmadi S, Wang S, Singh R, Kavanagh K, et al. Gut microbiome and aging: Physiological and mechanistic insights. *Nutr Healthy Aging*. 2018; 4 (4): 267–85.
5. Aleman FDD, Valenzano DR. Microbiome evolution during host aging. *PLoS Pathog*. 2019 Jul 25; 15 (7): e1007727.
6. Biagi E, Franceschi C, Rampelli S, Severgnini M, Ostan R, Turroni S, et al. Gut Microbiota and Extreme Longevity. *Curr Biol*. 2016; 26 (11): 1480–5.
7. Odamak T, Kato K, Sugahara H, Hashikura N, Takahashi S, Xiao JZ, et al. Age-related changes in gut microbiota composition from newborn to centenarian: a cross-sectional study. *BMC Microbiol*. 2016; 16: 90.
8. Kashtanova DA, Tkacheva ON, Doudinskaya EN, Strazhesko ID, Kotovskaya YV, Popenko AS, et al. Gut Microbiota in Patients with Different Metabolic Statuses: Moscow Study. *Microorganisms*. 2018; 6 (4): 98.
9. Efimova D, Tyakht A, Popenko A, Vasilyev A, Altukhov I, Dovidchenko N, et al. Knomics-Biota — a system for exploratory analysis of human gut microbiota data. *BioData Min*. 2018; 11: 25.
10. Caporaso JG, Kuczynski J, Stombaugh J, Bittinger K, Bushman FD, Costello EK, et al. QIIME allows analysis of high-throughput community sequencing data. *Nature methods*. 2010; 7 (5): 335–6.
11. Langille MG, Zaneveld J, Caporaso JG, McDonald D, Knights D, Reyes JA, et al. Predictive functional profiling of microbial communities using 16S rRNA marker gene sequences. *Nature biotechnology*. 2013; 31 (9): 814–21.
12. Mallick H, Ma S, Franzosa EA, Vatanen T, Morgan XC, Huttenhower C. Experimental design and quantitative analysis of microbial community multiomics. *Genome Biol*. 2017; 18 (1): 228.
13. Arumugam M, Raes J, Pelletier E, Le Paslier D, Yamada T, Mende DR, et al. Enterotypes of the human gut microbiome. *Nature*. 2011; 473 (7346): 174–80.
14. Mishiro T, Kusunoki R, Otani A, Ansary MM, Tongu M, Harashima N, et al. Butyric acid attenuates intestinal inflammation in murine DSS-induced colitis model via milk fat globule-EGF factor 8. *Lab Invest*. 2013; 93 (7): 834–43.
15. Ohira H, Tsutsui W, Fujioka Y. Are Short Chain Fatty Acids in Gut Microbiota Defensive Players for Inflammation and Atherosclerosis? *J Atheroscler Thromb*. 2017; 24 (7): 660–72.
16. Kundu P, Lee HU, Garcia-Perez I, Tay EXY, Kim H, Faylon LE, et al. Neurogenesis and longevity signaling in young germ-free mice transplanted with the gut microbiota of old mice. *Sci Transl Med*. 2019; 11 (518): eaau4760.
17. Said HM. Intestinal absorption of water-soluble vitamins in health and disease. *Biochem J*. 2011; 437 (3): 357–72.

SPREAD OF VARIANTS WITH GENE N HOT SPOT MUTATIONS IN RUSSIAN SARS-COV-2 ISOLATES

Kiryanov SA ✉, Levina TA, Kirillov MYu

"DNA-Technology", Moscow, Russia

SARS-CoV-2 is a RNA coronavirus of the β -CoVs family responsible for the pandemic of the severe acute respiratory syndrome (COVID-19). It is hypothesized that the viral genome of the contemporary predominant founder clones is likely to be evolving in geographic-dependent manner. Thus, strains of different origin may be characterized by different mutation patterns. The study was aimed to perform the mutational and phylogenetic analysis of the Russian SARS-CoV-2 genomes at different time periods and in various regions, as well as to characterize the mutational profiles of isolates using the bioinformatics approaches. The mutation accumulation was compared in 86 SARS-CoV-2 whole-genome sequences from Russia and 220 from Europe and North America in order to reveal the characteristic gene variations, the possible positive selection patterns. Along with the known mutation variants in the structural proteins genes, typical for isolates of European origin, several additional mutations including the synonymous mutation in gene *M* (C26750T) characteristic for Russian isolates were revealed. Double mutation R203K and G204R in the nucleocapsid gene which previously emerged in Europe began spreading and rapidly (within a month) became the dominant form in Russia. The results obtained indicate that the viral genome of most Russian isolates evolves with accumulation of new mutations associated with increased viral transmission. Data on the SARS-CoV-2 genome specific mutation patterns might be used for the detection of the virus, as well as for tracking and controlling of its spread.

Keywords: SARS-CoV-2, COVID-19, genome, coronavirus, mutations, Russian isolates

Author contribution: the authors contributed to the manuscript equally.

✉ **Correspondence should be addressed:** Sergei A. Kiryanov
PO Box 181, Moscow, 117587; kiryanov@dna-technology.ru

Received: 26.06.2020 **Accepted:** 10.07.2020 **Published online:** 27.07.2020

DOI: 10.24075/brsmu.2020.045

РАСПРОСТРАНЕНИЕ ВАРИАНТОВ С ЧАСТЫМИ МУТАЦИЯМИ В ГЕНЕ КАПСИДНОГО БЕЛКА N В РОССИЙСКИХ ИЗОЛЯТАХ SARS-COV-2

С. А. Кирьянов ✉, Т. А. Левина, М. Ю. Кириллов

ООО «ДНК-Технология», Москва, Россия

SARS-CoV-2 представляет собой РНК-вирус семейства β -коронавирусов, вызвавший пандемию тяжелого острого респираторного синдрома (COVID-19). Предполагают, что эволюционные изменения генома ныне преобладающих исходных клонов могут быть обусловлены географическими особенностями, поэтому для штаммов разного происхождения могут быть характерны различные паттерны мутаций. Целью исследования было провести мутационный и филогенетический анализы геномов SARS-CoV-2 российского происхождения в разные периоды и в разных регионах, а также охарактеризовать мутационные профили изолятов, используя подходы биоинформатики. Проведено сравнение накопления мутаций в 86 полногеномных последовательностях SARS-CoV-2 из России и 220 из Европы и Северной Америки для выявления характерных генных вариаций, возможных паттернов селективного отбора. Помимо известных мутаций в генах структурных белков, типичных для изолятов европейского происхождения, выявлены дополнительные синонимичные мутации российского происхождения, в том числе в гене *M* (C26750T). Двойная мутация R203K и G204R в гене нуклеокапсида, ранее появившаяся в Европе, распространилась и быстро (в течение месяца) стала доминирующим вариантом в России. Полученные результаты свидетельствуют о том, что геном значительной части изолятов SARS-CoV-2 из России эволюционирует с накоплением новых мутаций, способствующих повышению трансмиссивности вируса. Данные о специфичных мутационных паттернах генома SARS-CoV-2 могут быть использованы для выявления вируса, отслеживания и контроля его распространенности.

Ключевые слова: SARS-CoV-2, COVID-19, геном, коронавирус, мутации, российские изоляты

Вклад авторов: авторы внесли равный вклад в написание статьи.

✉ **Для корреспонденции:** Сергей Альбертович Кирьянов
а/я 181, г. Москва, 117587; kiryanov@dna-technology.ru

Статья получена: 26.06.2020 **Статья принята к печати:** 10.07.2020 **Опубликована онлайн:** 27.07.2020

DOI: 10.24075/vrgmu.2020.045

COVID-19 pandemic is characterized by rapid spread of the virus in many (over 187) countries of the world [1]. The prevalence, mortality and severity of the disease vary significantly between geographic regions, countries, and among the age groups of infected people [2–4].

The differences can be explained by geographic-dependent pattern of SARS-CoV-2 genome evolution and differentiation (due to quarantine measures and physical distancing), and by formation of several types from the ancestral Wuhan type (Hubei province, China) [5, 6]. RNA viruses appear to be characterized by high mutation rate. The emerging non-adaptive mutations lead to elimination of the strain from the population. The emerging adaptive mutations can be expected to provide the strain with a selective advantage usually in the form of high mutation rate and, consequently, of higher transmission rate.

The rapid spread of SARS-CoV-2 raises questions whether its evolution is driven by adaptive mutations and, if so, by which mutations in which genes.

The coronavirus genome is comprised of approximately 29,900 nucleotides. It encodes the extended open reading frame 1ab (ORF1ab) polyprotein, functioning as replicase and polymerase complex, and four structural proteins: membrane (M) protein, spike (S) glycoprotein, envelope (E) protein and nucleocapsid (N) phosphoprotein (the same as in all other β -CoVs) [7].

SARS-CoV-2 genome is being intensively studied aimed to diagnose the infection, to assess its pathogenic potential, and to track the evolution. To date, the GISAID database comprises over 25,000 viral genomic sequences collected in a few dozen countries. Previously, the mutation patterns of *ORF1ab* gene,

S glycoprotein gene and the non-structural proteins nsp6 and nsp8 genes were used for the SARS-CoV-2 genome evolution tracking [8–10]. Thus, the hot spot mutations C241T, C3037T and C14408T in the *ORF1ab* gene encoding the replication complex proteins were detected in the SARS-CoV-2 genomes isolated in Western Europe, together with the hot spot mutation A23403G in the S gene, the products of which interact with the ACE2 receptor. In Western European patients, the course of COVID-19 infection was more severe than in patients from other geographic regions [11]. The listed co-mutations combination determined the clade 20A (formerly known as clade G) is likely to be responsible for the enhanced transmission of the variant and for its being a dominant form in Europe.

The SARS-CoV-2 genome evolution record remains incomplete since the current reports cover mainly isolates retrieved in the USA, European countries, China, and some other countries. Particularly, there is a lack of data about SARS-CoV-2 genome mutational profiles retrieved in Russia. This study is of special relevance in connection with the observed contrast between the rapid viral expansion and low lethality rate in Russia.

The study was aimed to perform the mutational and phylogenetic analysis of the Russian SARS-CoV-2 genomes at different time periods and in various regions, as well as to characterize the mutational profiles of isolates using the bioinformatics approaches.

METHODS

From March 1 to April 29, 2020, subset of 86 SARS-CoV-2 nucleotide sequences isolated from Russian patients and 220 sequences collected in Europe and the USA were selected for analysis (were downloaded from the NCBI and GISAID databases). Inclusion criteria: full-length sequence of 26,000–30,000 nucleotides, sequences annotated as SARS-CoV-2. Exclusion criteria: re-submitted sequences, sequences containing too many undefined nucleotides. The multiple sequences alignment was performed using Clustal Omega (EMBL-EBI; Great Britain) and Blast (NCBI; USA). The MT233519 sequence, SARS-CoV-2/human/ESP/Valencia5/2020B, was considered a reference sequence for the analysis of isolates sampled in Russia.

Nextstrain (<https://nextstrain.org/>) was used for the SARS-CoV-2 sequences phylogenetic analysis, temporal dating of

ancestral nodes, as well as for discrete traits, frequency and anchor mutations emergence dates reconstruction across the tree [12].

The B-cell epitopes were predicted based on the analysis results with the algorithm previously proposed for SARS-CoV by a group of researchers [13]. The following prediction tools were used for the primary N phosphoprotein amino acid sequence: BepiPred-2.0 (DTU; Denmark) for the linear B-cell epitopes prediction [14], and DiscoTope 2.0 (DTU; Denmark) for the conformational B-cell epitopes prediction [15]. Both tools were provided by the IEDB Immunobrowser resource (NIAID; USA).

When attempting to predict the linear B-cell epitopes with BepiPred-2.0 (DTU; Denmark) [14], the maximum threshold value was set at 0.75, the specificity was >0.85, and the sensitivity was <0.40. The sequences of more than 7 amino acid residues were analyzed. When predicting the conformational B-cell epitopes with DiscoTope 2.0 (DTU; Denmark) [15], the predictive positive value (PPV) was >–3.7, the specificity was ≥ 0.75, and the sensitivity was <0.40.

RESULTS

The total of 86 SARS-CoV-2 whole-genome sequences isolated from Russian patients in March–April 2020 was analyzed. Of those, 38 isolates (44%) were collected in March, and 56 (66%) were isolated by the end of April 2020. The SARS-CoV-2 genome nucleotide sequences were aligned and compared with those isolated from 220 Europeans and Americans (selected randomly from the GISAID global database). Phylogenetic analysis of the selected nucleotide sequences of Russian and European ancestry showed that all Russian isolates except one belonged to clade 20A (previously known as G) (Fig. 1). All other sequences except one sample from the Kabardino-Balkarian Republic identified in March carried the mutation A23403G with the substitution D614G in the S glycoprotein gene, and mutation C14408T with the substitution P314L in the gene encoding the ORF1b protein, along with the synonymous mutations C241T and C3037T. In Europe the listed mutations had been previously detected in the isolate of German ancestry (Germany/BavPat1/2020), and later in isolates from Italy retrieved in February. All the observed mutations are likely to define the stable haplotype currently dominant in European isolates, isolates from the East Coast of the USA, and in Russian isolates.

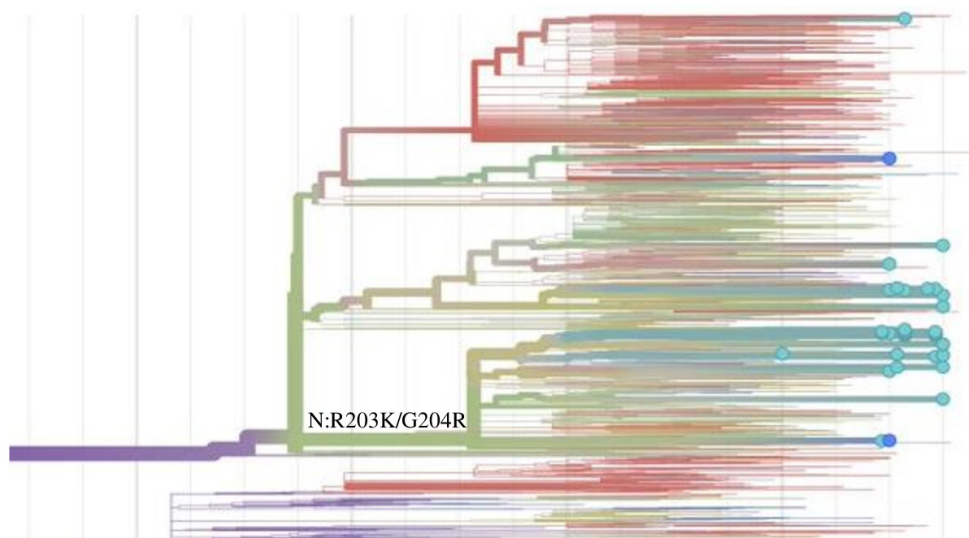


Fig. 1. Phylogenetic analysis of Russian, European, and American SARS-CoV-2 sequences, distinguished by the double mutation R203K and G204R in gene *N*. Russian isolates are highlighted in blue, European isolates in green and dark green, and American isolates in dark red

Table 1. Subclusters and characteristic mutations identified in the SARS-CoV-2 isolates from Russia

Subclusters: mutations in gene <i>N</i>	* <i>ORF1ab</i> mutations	**Other genes mutations	***Additional mutations	Possible origin	Emergence time	Region of Russia and number of isolates
AP1 - R203K G204R		M: c26750t	ORF1a: P959S - 7 ORF1a: P309L 8	Italy Italy	02.03.2020 16.04.2020	Saint-Petersburg (40) Yakutia, Buryatia (5)
AP2 - R203K G204R	ORF1a: G3278S (g10097a) S: c23731t	ORF1a: A364S	ORF1b: M1499I	England	09–16.03.2020	Moscow (2) Yakutia (2)
		ORF1a: T1246I L3606F	ORF7a: L5F	England	02.03.2020	Moscow (4)
AP3 - R203K G204R		M: T175M	ORF1a: P892S, ORF1b: I1887V N: A152S	Italy	01–10.03.2020 14.03.2020	Lipetsk (2) Krasnodar (1) Moscow (3)
R203 G204	a20268g		N: N140T 8 N: N140K, T205I; ORF8: R101L	Spain	04–08.03.2020	Saint-Petersburg (14) Pskov (1) Omsk (1)
R203 G204	ORF1a: T265I (c1059t)	ORF3a: Q57H (g25563t)	ORF1a: P3395L S: G261V, ORF1a: L3606F c29200t	France Austria	04–16.03.2020 08–15.03.2020	Orenburg (2) Sakhalin (1) Chelyabinsk (1) Moscow (2)
R203 G204		M: D3G (a26530g)	G4255T ORF1a: L890F; ORF1b: Q348H, M1156I; ORF1b: L1701F, V1615I	England	04–05.03.2020 11.03.2020	Moscow (2) Moscow (2)

Note: * mutations in the *ORF1ab* gene defining the subgroup of the isolate; ** mutations in other genes defining the subgroup of the isolate; *** other frequent mutations identified in the isolates.

By the presence or lack of a triple mutation G28881A, G28882A, and G28883C in the *N* gene causing double nonsynonymous mutation R203K and G204R, genome sequences of SARS-CoV-2 isolates from Russia can be divided into two unequal groups of 59 and 26 sequences, respectively. Phylogenetic analysis of isolates retrieved in Russia, Europe and the USA reveals that the double mutation R203K and G204R previously discovered in the isolate from Valencia, Spain (MT233522, March 2, 2020) also forms a distinct subclade 20B (Fig.1). It should be noted that in contrast to Russian isolates the most European and American isolates form clades with lack of the triple mutation G28881A, G28882A and G28883C.

The subclade of Russian isolates defined by the double mutation R203K and G204R is subdivided into three unequal groups. The most numerous group is the group named AP1, comprising more than 40 isolates mainly from Saint-Petersburg and, apparently, of Italian origin. This group diverged from its predecessor is defined by the synonymous mutation C26750T in gene *M*, specific substitution only for these Russian isolates. The time of emergence of this mutation is not later than early March. The group is also characterized by the microclonality effect, defined by the accumulation of mostly synonymous mutations in the 5' region of the gene *ORF1ab*, and divided genome variants into additional subpopulations. Detailed information about defined subgroups and mutations is presented in Table 1.

The group AP2 comprising six isolates from Moscow and two from Yakutia is defined by the mutations in gene *ORF1a* (G3278S, T1246I, L3606F) and the synonymous mutation C23731T in gene *S*. The subgroup of four isolates from Moscow and Yakutia subsequently diverged from the ancestor with accumulation the mutation A364S and an additional mutation M1499I in the gene *ORF1ab*. The latter is exclusively found in isolates of Russian origin till now, it emerged before the middle of March.

Another group AP3 (six isolates from Moscow, Lipetsk and Krasnodar) probably originated from Italy has a characteristic mutation T175M in gene *M*. Further these isolates also differ

by mutations in gene *ORF1ab* (P892S, I1887V). The less numerous group of three isolates (Moscow) is defined by the additional mutation A152S in gene *N*. This mutation is probably of Russian origin, and identified no later than the middle of March.

In the group of 26 isolates without mutation 203K and G204R in gene *N*, the accumulation of mutations also occurs mainly in the gene *ORF1ab*. The most common differentiating mutation is a synonymous mutation at the position A20268G of Spanish origin (found in 16 isolates, mostly from Saint-Petersburg). The presence of nonsynonymous mutations in the gene *ORF1ab* (T265I, P3395L, etc.), as well as in the genes *ORF3a* (Q57H) and *M* (D3G) allowed to identify several subgroups with insignificant the number of isolates (4–6). For information on the isolates' origin and additional mutations see Table 1. Only three isolates of 26 were found to carry additional nonsynonymous mutations in gene *N*: double mutation N140K and T205I, as well as N140T and A397V.

Thus, regardless of their origin, the SARS-CoV-2 variants with double mutation R203K and G204R in the gene *N* are a dominant form in various regions of Russia.

To determine the time of appearance and distribution double mutations R203K and G204R in Russia the analysis of most abundant viral genomes obtained from patients from Moscow and Saint-Petersburg in March–April 2020 classified according to the sampling date (available from GISAIID) was performed. Four time-period subgroups according to the emergence date were identified as follows: March 10–12, 2020 (genomes collected from eight patients), March 19–21, 2020 (genomes from nine patients), April 1–3, 2020 (genomes from 16 patients), April 10–12, 2020 (genomes from 29 patients). The number of other accumulated mutations (mainly in the gene *ORF1ab*) changed during each time period: was 2, 4 and 4 in the group of genomes with double mutation R203K and G204R, and 2, 3 and 3 in the group of genomes with no the mutation. The latter group included two isolates with additional mutations in gene *N*: double mutation N140K and T205I, and N140T. Divergence of other genes did not affect the distribution of variants with double mutation R203K and G204R in gene *N*. In late March

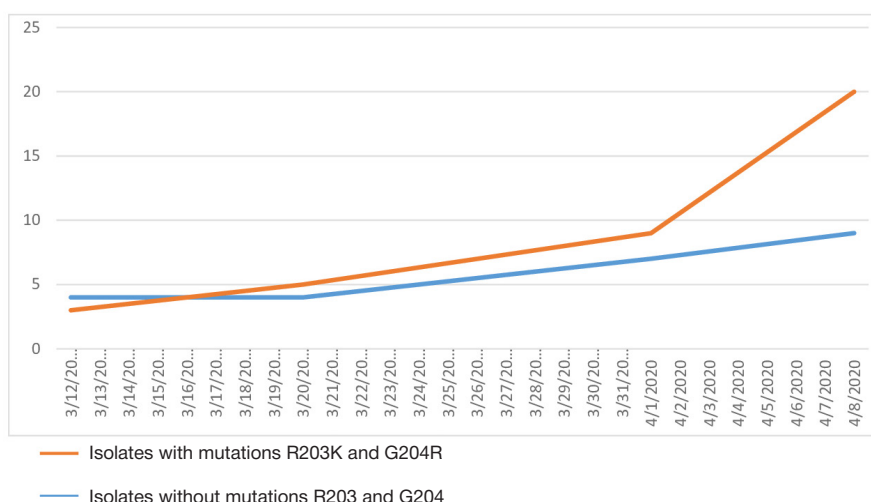


Fig. 2. Abundance of SARS-CoV-2 isolates carrying mutations R203K and G204R in gene *N* (Russia, March–April 2020)

and early April the proportion of isolates with double mutation R203K and G204R was more than doubled, by the middle of April it was more than 69.5% (Fig. 2).

The overall distribution and abundance mutation patterns in the *N* gene s in the nucleotide sequences of isolates from Europe and the United States deposited in the GISAID and NCBI databases was verified. It is worth noting that in European populations the abundance of subclade with double mutation R203K and G204R in gene *N* was significantly lower than in Russia, and presented in 32.6 % (1068 genomes out of 3241). In the USA the abundance of the same subclade was even lower (13.3%, 464 genomes out of 3479). The distribution of nonsynonymous mutations in gene *N* turned out to be uneven: 58.7% of mutations were located within the $N_{179-217}$ region. Using the linear B-cell epitope prediction tool, two possible linear B-cell epitope variants were predicted in the *N* protein at the positions of 23–36 and 178–207 respectively with the maximum threshold value at >0.758 , (Table 2). Using the appropriate tool the conformational B-cell epitopes in the *N* gene with the threshold value >-0.37 and specificity 0.75 were predicted in about the same positions (26–36 and 193–207). The flanking positions R203, G204 and T205 within predicted B-cell epitope peptide were also noted (no data reported). However, about 25% of amino acid residues may be predicted as a part of the B-cell epitope incorrectly due to specificity of 0.75.

DISCUSSION

The data reported indicate that the SARS-CoV-2 genome is evolves forming several types clustered in distinct groups in geographic-dependent manner [16]. The mutation analysis of geographic-dependent isolates provides an insight into the hot spot mutation patterns responsible for high transmissibility of the virus. It has been reported, that at least five major mutations (C241T, C3037T, T28144C, C14408T, A23403G) turned out to be the most abundant in the Western European SARS-CoV-2 isolates [11]. The listed co-mutations, probably formed clade 20A, are likely to be responsible for the increased transmission of the virus and for its being a dominant form in Europe. According to mutational and phylogenetic analysis of SARS-CoV-2 genomes

isolated in Russia in March–April 2020, clade 20A appears to be one of the most widespread, which indicates European origin of Russian isolates. However, in Russia, unlike Western Europe, the subclade 20B characterized by the triple mutation G28881A, G28882A and G28883C which results in double substitution R203K and G204R in the *N* protein has spread and has become a dominant form. Thus, in Russia at the end of April the abundance of genomes with the double mutation R203K and G204R was over 69.5%, while in Europe it was 32.6 %. In the USA the number of genomes belonging to the same subclade defined by mutations R203K and G204R was even lower and accounted for 13.3%. The observed variant was likely to start circulating in Russia in early to mid-March 2020. The further expansion of the variant was accompanied by the formation of new subtypes with accumulation characteristic mutations in gene *M* (C26750T) or *ORF1b* (M1499I or G17964T), following subsequent divergence due to new single (mostly synonymous) mutations in the gene *ORF1ab*. Rapid spread of the variant with double mutation R203K and G204R in gene *N* may be indicative of its adaptability and ability to increase the transmission rate rather than modulate the virulence.

The functional effect of the mutant AAACGA motif in the nucleocapsid gene remains uncertain. The *N* protein appears to be responsible for the formation of the helical nucleocapsid during the virion assembly, and also plays a key role in replication and transcription. The protein is able to elicit the immune response and therefore may become a potential target for vaccine development [17]. The localization of potential B-cell and T-cell epitopes in the *S* glycoprotein, membrane *M* protein and capsid phosphoprotein *N*, predicted using the homologous regions of the SARS-CoV viral genome has been previously reported [18]. Our attempt at mapping the predicted $N_{179-207}$ B-cell epitope peptide amino acid sequence of the protein *N* allows suggesting that the positions R_{203} and G_{204} are located within the epitope. Mutations R203K and G204R result in two strong positively charged amino acid residues in close positions, in contrast to one positively charged residue in the wild type genotype, which may contribute to a decreased conformational entropy compared to the initial genotype. Currently, the bioinformatics methods without experimental data support do

Table 2. SARS-CoV2 B-cell epitope variants predicted in the nucleocapsid *N* protein

Epitope type	Position in the <i>N</i> protein	Mutation position	Epitope amino acid sequence
B-cell	178–207	R203K G204R T205I	GGSQASSRSSSRNRSSRNSTPGSSRGTSF
B- cell	23–36		STGSNQNGERSGAR

not allow us to assess the biological significance of these mutations. Moreover, there is no reason to link the prevalence of these mutations of the SARS-CoV-2 in Russia with the viral pathogenicity. Further study of the SARS-CoV-2 viral genome evolution will allow the researchers not only to monitor the current epidemiological processes, but also optimize the existing RT-PCR diagnostic tests and search for new targets for vaccine development.

CONCLUSION

The current data indicate that the vast majority of SARS-CoV-2 isolates from Russia is of European origin. The viral genome of

the most Russian isolates evolves with the accumulation the new mutations associated with increased viral transmission. The double mutation R203K and G204R in the nucleocapsid gene has begun spreading and has rapidly become the dominant form in Russia.

Identification of the SARS-CoV-2 genome variants characteristic to the Russian population provides an insight into their further adaptive evolution. Data on the SARS-CoV-2 genome characteristic mutation patterns including the mutation patterns of the genes for structural proteins N and M might be used for the detection of the virus, as well as for tracking and controlling of its spread.

References

- Zhou P, Yang X-L, Wang X-G, Hu B, Zhang L, Zhang W, et al. A pneumonia outbreak associated with a new coronavirus of probable bat origin. *Nature*. 2020; 579 (7798): 270–3. PubMed PMID: 32015507.
- Verity R, Okell LC, Dorigatti I, Winskill P, Whittaker C, Imai N, et al. Estimates of the severity of coronavirus disease 2019: a model-based analysis. *Lancet Infect Dis*. 2020; 20 (6): 669–7. PubMed PMID: 32240634.
- Spychalski P, Błażyńska-Spychalska A, Kobiela J. Estimating case fatality rates of COVID-19. *Lancet Infect Dis*. 2020; 20 (7): 774–5. PubMed PMID: 32243815.
- Khafaie MA, Rahim F. Cross-country comparison of case fatality rates of Covid-19/SARS-CoV-2. *Osong Public Heal Res Perspect*. 2020; 11 (2): 74–80. PubMed PMID: 32257772.
- Phan T. Novel coronavirus: from discovery to clinical diagnostics. *Infect Genet Evol*. 2020; 79: 104211. PubMed PMID: 32007627.
- Forster P, Forster L, Renfrew C, Forster M. Phylogenetic network analysis of SARS-CoV-2 genomes. *Proc Natl Acad Sci*. 2020; 117 (17): 9241–3. PubMed PMID: 32269081.
- Boopathi S, Poma A, Kolandaivel P. Novel 2019 coronavirus structure, mechanism of action, antiviral drug promises and rule out against its treatment. *J Biomol Struct Dyn*. 2020: 1–10. PubMed PMID: 32306836.
- Pachetti M, Marini B, Benedetti F, Giudici F, Mauro E, Storici P, et al. Emerging SARS-CoV-2 mutation hot spots include a novel RNA-dependent-RNA polymerase variant. *J Transl Med*. 2020; 18: 179. Available from: <https://doi.org/10.1186/s12967-020-02344-6>.
- Benvenuto D, Angeletti S, Giovanetti M, Bianchi M, Pascarella S, Cauda R, et al. Evolutionary analysis of SARS-CoV-2: how mutation of Non-Structural Protein 6 (NSP6) could affect viral autophagy. *J Infect*. 2020; 81 (1): 24–7. PubMed PMID: 32283146.
- Stefanelli P, Faggioni G, Lo Presti A, Fiore S, Marchi A, Benedetti E, et al. Whole genome and phylogenetic analysis of two SARSCoV-2 strains isolated in Italy in January and February 2020: additional clues on multiple introductions and further circulation in Europe. *Euro Surveill*. 2020; 25 (13): 1–5. PubMed PMID: 2000305.
- Yin C. 2020 Genotyping coronavirus SARS-CoV-2: methods and implications. *Genomics*. 2020; 112 (5): 3588–6. PubMed PMID: 32353474.
- Hadfield J, Megill K, Bell SM, Huddleston J, Potter B, Callender C, et al. Nextstrain: real-time tracking of pathogen evolution. *Bioinformatics*. 2018; 34 (23): 4121–3. PubMed PMID: 29790939.
- Grifoni A, Sidney J, Zhang Y, Scheuermann RH, Peters B, Sette A. A sequence homology and bioinformatic approach can predict candidate targets for immune responses to SARS-CoV-2. *Cell Host Microbe*. 2020; 27 (4): 671–80. PubMed PMID: 32183941.
- Jespersen MC, Peters B, Nielsen M, Marcatili P. BepiPred-2.0: improving sequence-based B-cell epitope prediction using conformational epitopes. *Nucleic Acids Res*. 2017; 45 (1): 24–9. PubMed PMID: 28472356.
- Kringelum JV, Lundegaard C, Lund O, Nielsen M. Reliable B cell epitope predictions: impacts of method development and improved benchmarking. *PLoS Comput Biol*. 2012; 8 (12): e1002829: 1–10. PubMed PMID: 23300419.
- Hahn G, Lee S, Weiss S, and Lange C. Unsupervised cluster analysis of SARS-CoV-2 genomes reflects its geographic progression and identifies distinct genetic subgroups of SARS-CoV-2 virus. *bioRxiv*. Preprint. 2020 Jun 30. Available from: <https://www.biorxiv.org/content/10.1101/2020.05.05.079061v2>
- Zhao P, Cao J, Zhao L-J, Qin Z-L, Ke J-S, Pan W, Ren H, et al. Immune responses against SARS-coronavirus nucleocapsid protein induced by DNA vaccine. *Virology*. 2005; 331 (1): 128–5. PubMed PMID: 15582659.
- Koyama T, Weeraratne D, Snowdon J, and Parida L. Emergence of drift variants that may affect COVID-19 vaccine development and antibody treatment. *Pathogens*. 2020; 9 (5): 324. PubMed PMID: 32357545.

Литература

- Zhou P, Yang X-L, Wang X-G, Hu B, Zhang L, Zhang W, et al. A pneumonia outbreak associated with a new coronavirus of probable bat origin. *Nature*. 2020; 579 (7798): 270–3. PubMed PMID: 32015507.
- Verity R, Okell LC, Dorigatti I, Winskill P, Whittaker C, Imai N, et al. Estimates of the severity of coronavirus disease 2019: a model-based analysis. *Lancet Infect Dis*. 2020; 20 (6): 669–7. PubMed PMID: 32240634.
- Spychalski P, Błażyńska-Spychalska A, Kobiela J. Estimating case fatality rates of COVID-19. *Lancet Infect Dis*. 2020; 20 (7): 774–5. PubMed PMID: 32243815.
- Khafaie MA, Rahim F. Cross-country comparison of case fatality rates of Covid-19/SARS-CoV-2. *Osong Public Heal Res Perspect*. 2020; 11 (2): 74–80. PubMed PMID: 32257772.
- Phan T. Novel coronavirus: from discovery to clinical diagnostics. *Infect Genet Evol*. 2020; 79: 104211. PubMed PMID: 32007627.
- Forster P, Forster L, Renfrew C, Forster M. Phylogenetic network analysis of SARS-CoV-2 genomes. *Proc Natl Acad Sci*. 2020; 117 (17): 9241–3. PubMed PMID: 32269081.
- Boopathi S, Poma A, Kolandaivel P. Novel 2019 coronavirus structure, mechanism of action, antiviral drug promises and rule out against its treatment. *J Biomol Struct Dyn*. 2020: 1–10. PubMed PMID: 32306836.
- Pachetti M, Marini B, Benedetti F, Giudici F, Mauro E, Storici P, et al. Emerging SARS-CoV-2 mutation hot spots include a novel RNA-dependent-RNA polymerase variant. *J Transl Med*. 2020; 18: 179. Available from: <https://doi.org/10.1186/s12967-020-02344-6>.
- Benvenuto D, Angeletti S, Giovanetti M, Bianchi M, Pascarella S, Cauda R, et al. Evolutionary analysis of SARS-CoV-2: how mutation

- of Non-Structural Protein 6 (NSP6) could affect viral autophagy. *J Infect.* 2020; 81 (1): 24–7. PubMed PMID: 32283146.
10. Stefanelli P, Faggioni G, Lo Presti A, Fiore S, Marchi A, Benedetti E, et al. Whole genome and phylogenetic analysis of two SARSCoV-2 strains isolated in Italy in January and February 2020: additional clues on multiple introductions and further circulation in Europe. *Euro Surveill.* 2020; 25 (13): 1–5. PubMed PMID: 2000305.
 11. Yin C. 2020 Genotyping coronavirus SARS-CoV-2: methods and implications. *Genomics.* 2020; 112 (5): 3588–6. PubMed PMID: 32353474.
 12. Hadfield J, Megill K, Bell SM, Huddleston J, Potter B, Callender C, et al. Nextstrain: real-time tracking of pathogen evolution. *Bioinformatics.* 2018; 34 (23): 4121–3. PubMed PMID: 29790939.
 13. Grifoni A, Sidney J, Zhang Y, Scheuermann RH, Peters B, Sette A. A sequence homology and bioinformatic approach can predict candidate targets for immune responses to SARS-CoV-2. *Cell Host Microbe.* 2020; 27 (4): 671–80. PubMed PMID: 32183941.
 14. Jespersen MC, Peters B, Nielsen M, Marcatili P. BepiPred-2.0: improving sequence-based B-cell epitope prediction using conformational epitopes. *Nucleic Acids Res.* 2017; 45 (1): 24–9. PubMed PMID: 28472356.
 15. Kringelum JV, Lundegaard C, Lund O, Nielsen M. Reliable B cell epitope predictions: impacts of method development and improved benchmarking. *PLoS Comput Biol.* 2012; 8 (12): e1002829: 1–10. PubMed PMID: 23300419.
 16. Hahn G, Lee S, Weiss S. and Lange C. Unsupervised cluster analysis of SARS-CoV-2 genomes reflects its geographic progression and identifies distinct genetic subgroups of SARS-CoV-2 virus. *bioRxiv.* Preprint. 2020 Jun 30. Available from: <https://www.biorxiv.org/content/10.1101/2020.05.05.079061v2>
 17. Zhao P, Cao J, Zhao L-J, Qin Z-L, Ke J-S, Pan W, Ren H, et al. Immune responses against SARS-coronavirus nucleocapsid protein induced by DNA vaccine. *Virology.* 2005; 331 (1): 128–5. PubMed PMID: 15582659.
 18. Koyama T, Weeraratne D, Snowdon J, and Parida L. Emergence of drift variants that may affect COVID-19 vaccine development and antibody treatment. *Pathogens.* 2020; 9 (5): 324. PubMed PMID: 32357545.

PREDICTIVE MONITORING OF SECONDARY EPIDEMIC WAVES OF COVID-19 IN IRAN, RUSSIA AND OTHER COUNTRIES

Kovrigin DA¹, Nikitenkova SP² ✉

¹ Nizhny Novgorod State Technical University n.a. R.E. Alekseev, Nizhny Novgorod, Russia

² National Research Lobachevsky State University of Nizhny Novgorod, Nizhny Novgorod, Russia

In the last decade of April 2020, the second coronavirus epidemic wave in Iran has bloomed. The new wave has started in the vicinity of the critical point, marked by approximately 44,000 infections, where the rate of increase of the primary epidemic that appeared in Iran in mid-February 2020 was the highest. Today, this secondary wave almost has doubled the peak of the primary, and, passing the epidemic threshold of about 70,000 total cases in early June, generated the new third epidemic wave developing unpredictably and dynamically. The purpose of this work was to call into use a simple dynamical system represented by the discrete logistic equation with unknown parameters to predict secondary waves using the official statistical data. The mathematical modelling reveals the secondary epidemic waves in Sweden, the United States, Ukraine, Serbia, Romania, Czech Republic, Portugal, Luxembourg, Poland, and Ecuador. Also, the second waves appear in Russia and other countries. Despite many individual differences in the epidemic spread in different countries, we have traced regularity in the rise of secondary waves. The beginning of each new wave, if focusing on the number of total cases, practically coincides with the time of the maximum growth rate of the previous early epidemic. Thus, the passing through the threshold of the current wave should be the most responsible for strict observance of the rules of self-isolation and other sanitary standards.

Keywords: COVID-19, pandemic, monitoring, forecasting, second wave, logistic equation

Author contribution: Kovrigin DA — research planning, literature analysis, data analysis and interpretation, manuscript preparation; Nikitenkova SP — research planning, literature analysis, data analysis and interpretation, manuscript preparation.

✉ **Correspondence should be addressed:** Svetlana P. Nikitenkova
Gagarina, 23, Nizhny Novgorod; 603950; snikitenkova@gmail.com

Received: 13.07.2020 **Accepted:** 02.08.2020 **Published online:** 13.08.2020

DOI: 10.24075/brsmu.2020.046

ПРОГНОЗНЫЙ МОНИТОРИНГ ВТОРЫХ ВОЛН ЭПИДЕМИИ COVID-19 В ИРАНЕ, РОССИИ И ДРУГИХ СТРАНАХ

Д. А. Ковригин¹, С. П. Никитенкова² ✉

¹ Нижегородский государственный технический университет имени П. Е. Алексеева, Нижний Новгород, Россия

² Национальный исследовательский Нижегородский государственный университет имени Н. И. Лобачевского, Нижний Новгород, Россия

В последней декаде апреля 2020 г. в Иране поднялась вторая волна новой эпидемии коронавирусной инфекции. Новая волна возникла в окрестности пороговой точки, отмеченной примерно 44 000 случаев заражения, где скорость нарастания первой волны эпидемии, появившейся в Иране в середине февраля 2020 г., была максимальна. Вторая волна почти вдвое превысила пик первой, и, в свою очередь, в начале июня, преодолев новый порог, составляющий около 70 000 случаев заражения, породила третью волну, развивающуюся динамично и непредсказуемо. Целью работы было провести для выявления вторых волн обработку официальных статистических данных на основе простейшей динамической системы, представленной дискретным логистическим уравнением. Изучение этой математической модели показало, что вторые волны эпидемии уже можно наблюдать в Швеции, США, Украине, Сербии, Румынии, Чехии, Эквадоре, Португалии, Люксембурге, а также в России и других странах. Несмотря на индивидуальные различия в динамике распространения эпидемии в отдельных странах, закономерность подъема вторых волн остается той же: начало новой волны, если ориентироваться по количеству общих случаев заражения, практически совпадает со временем достижения максимальной скорости роста предыдущей эпидемии. Это означает, что в период перехода через критический порог текущей волны необходима наибольшая ответственность с точки зрения неукоснительного соблюдения правил самоизоляции и иных санитарных норм.

Ключевые слова: COVID-19, пандемия, мониторинг, прогнозирование, вторая волна, логистическая модель

Вклад авторов: Д. А. Ковригин — планирование исследования, анализ литературы, анализ и интерпретация данных, подготовка черновика и финального варианта статьи; С. П. Никитенкова — планирование исследования, интерпретация данных, подготовка черновика и финального варианта статьи.

✉ **Для корреспонденции:** Светлана Павловна Никитенкова
пр. Гагарина, д. 23, г. Нижний Новгород, 603950; snikitenkova@gmail.com

Статья получена: 13.07.2020 **Статья принята к печати:** 02.08.2020 **Опубликована онлайн:** 13.08.2020

DOI: 10.24075/vrgmu.2020.046

The first epidemic wave in Iran had attracted the attention of observers and researchers by a relatively high rate of overall infections [1–5]. The processing of official statistics to predict the second waves based on a logistic model showed that the first wave was only a harbinger of the spread of a new, higher wave of the epidemic, which had already swept through this country and gave rise to the third wave in early June. (We interpret an epidemic wave as the process either of transferring and spreading the infection to a new territory with a new population or returning to the old places partially or completely have recovered after the primary epidemic.)

Recently, the secondary waves of the epidemic have started in Sweden, the United States, Ukraine, Serbia, Romania, Czech Republic, Ecuador and some other countries. As yet, there are no rigorous mathematical models to shed light, in particular, on those critical points at which the secondary epidemic appears (we understand a strict theory as axiomatics based on the maximum principle. Any epidemic naturally "strives" to occupy the entire territory and cover the entire "available" population).

Today, there are more and more messages in the media about the expectation of second waves of the epidemic in

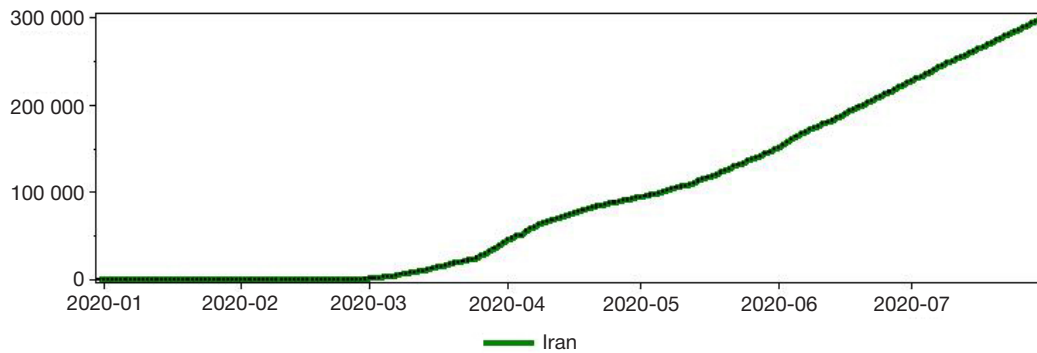


Fig. 1. Epidemic history of Iran. The solid line marks the total officially reported cases by day since the beginning of the epidemic in this country

Russia. However, this acute question remains open without a rigorous analysis of the input data.

The purpose of this work is to describe the secondary epidemic waves mathematically. We have chosen a simple dynamic logistic system with the unknown parameters which are determined by the official data (data source: <https://covid.ourworldindata.org/>). The aim is to identify the most favourable conditions for the occurrence of secondary waves.

METHODS

We use the tabular autocorrelation dependencies $N_{i+1} = f_c(N_i)$, to construct the dynamic system. Here, N_i is the number of total cases, accumulated to the date i , in the country number c . The least-squares method determines the polynomial approximations of tabular functions f_c , denoted as F_c .

Numerical experiments confirm the sufficiency of the quadratic approximation of functions f_s from the argument N_i that provides a logistic model. So, we have got the analytic point mapping having the right-hand side $F_c(N_i) = a_0 + a_1N_i + a_2N_i^2$, where a_j are the parameters determined from the tables (data source: <https://covid.ourworldindata.org/>). The transition time between the states N_i and N_{i+1} takes a day. The logistic mapping approaches the steady-state $N = N^*$, as a positive solution to the equation $N^* = a_0 + a_1N^* + a_2N^{*2}$. The steady-state N^* corresponds to almost zero dynamic increase in disease [6]. At the time of achieving this stable equilibrium, the logistic equation is no longer sufficient to describe the evolution of the disease in a developed human society. The fate of infected people depends on the quality of quarantine measures, medical care, etc.

We suppose that the logistic equation describes the temporal evolution of each wave of the epidemic adequately in countries with high-quality statistics. After processing the

data, we select results using simple criteria and standard Maple software (Maplesoft; Canada).

There is no doubt that, theoretically, the epidemic can develop for the second and third time, etc. in an unpredictable way, if we neglect the appropriate anti-epidemic measures. As calculations show, the second wave of the epidemic, as a rule, rises after passing the critical point, which is the inflexion point of the logistic curve [7–9]. The linear equation $a_1 + 2a_2N = 1$ defines the threshold N .

In the case of secondary epidemic waves, we use the same dynamic system for calculations. The described above procedure calculates the current parameters a_j using a new, appropriately decomposed input data set. We remove the already calculated data, provided by the logistic curve of the first wave, from the old input data set. The computation process continues until the input data will represent a superposition of various individual logistic curves.

There is no doubt that all input is perfect. In case of failure of the specified decomposition of the input data, we decide that the algorithm described above does not work, and omit such input data from the analysis. Note that the idea of such an algorithm is not new — it first appeared in the socio-economic sciences [10].

There are examples of its successful application in mathematical biophysics [11]. In the context of the current pandemic, the work [12] is of interest. The authors take into account the secondary wave to adjust the results of their previous work [13].

RESULTS

Consider an example of the epidemic history of the countries that did not escape the risk of the second wave. Let it be the most vividly manifested country in this respect, Iran, the history of the epidemic of which is shown in Fig. 1.

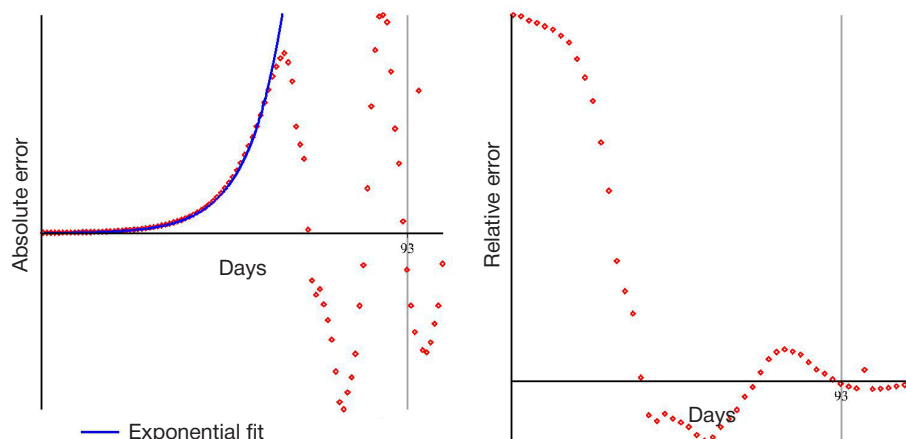


Fig. 2. Absolute and relative errors of forecasting. On the left, the solid line traces the exponential approximation of a discrepancy between actual and forecast data

The graph above shows that around the middle of April, the second wave of the epidemic rose in Iran. The epidemic spread is still very far from complete since the growth of the third wave has been observed from the beginning of June. Notice that the mentioned above algorithm decomposing the secondary waves could not recognize the third wave, and interpreted the data as statistical errors for two or three weeks ago.

Let us now try identifying the first wave of the epidemic in Iran by estimating the absolute and relative errors between the input and forecast data, which are described by the logistic curve. The mean squared error is minimal if the first wave reaches the threshold at 93 days from the start of the epidemic (Fig. 2). Note that the search for the minimum uses a priori dynamic data analysis that should not have to cover the entire history of the epidemic.

Figure 2 on the left displays that the input data, starting from the very beginning of the epidemic and up to the point of the maximum absolute error, obey the exponential dependence shown by the solid line. This fact is not a revelation: the behaviour of real data over time shown in graphs is not a specific feature of the history of the epidemic in Iran only. The authors of some works on the problem of the pandemic have noticed such a pattern, explaining this regular exponential component with useful medical intervention in the early epidemic.

However, it is easier to assume that this unavoidable regular error is due only to the specifics of data monitoring. Moreover, the analytical approximation of the input data set continues further, starting from the point of maximum absolute error up to the inflexion point using the power function [14, 15].

We have studied this regular monitoring error by analyzing the epidemic history in some countries of Western Europe, which had reached the first epidemic peak [16]. Notice that to reach the epidemic peak is necessary to apply a posteriori data analysis that leads to the same results that we obtain in the case of the dynamic a priori analysis. We have analytically revealed the regular component of the monitoring error. This error explained the reason for the failure of a priori mathematical forecasting of probable epidemic events in various countries of the world, undertaken in numerous studies. The statistical data processing of almost all countries that have reached the epidemic peak showed that the regular monitoring error is subject to a simple pattern: the higher the epidemic peak, the greater the time delay of the monitoring data compared to the forecast.

Let us identify the primary epidemic wave in Iran, following a priori approach. Thus, we believe that the discrete logistic equation $N_{i+1} = 1,118N_i - 1,344 \times 10^{-6}N_i^2$ adequately describes the first wave. Notice that the parameters of the first wave no longer change throughout the epidemic when the second wave appears. Figure 3 shows the solution to this equation.

Now we decompose the input data taking into account that the logistic curve shown in the above figure adequately approximates the early history of the epidemic. At the next stage of processing the input data, we identify the second epidemic wave. Calculations are performed recursively in the same way as used above. The discrete logistic equation also adequately describes the second wave, but with a different right-hand side: $N_{i+1} = 1,056N_i - 3,202 \times 10^{-7}N_i^2$. The parameters of this equation slowly change in time until the formation of a sufficient height of the third wave. Figure 4 displays this decomposition graphically.

This figure displays that the residual data, corresponding to the secondary and tertiary waves, can no longer represent a single logistic line. Thus the epidemic in Iran has become a continuous wave cascade, the most unfavourable for

combating the epidemic. In any case, Iran cannot avoid the third epidemic wave.

We can repeat the above arguments and calculations using other data on the epidemic history in other countries, for example, Sweden. The first epidemic wave of in Sweden, compared with Iran, had a relatively small height with the threshold of about 15,000 registered cases reached in 115 days after the start of the epidemic (Fig. 5). Also, this

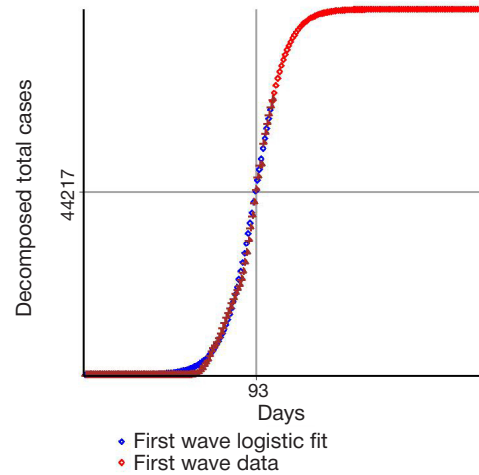


Fig. 3. Profile of the first wave of the epidemic in Iran. The extrapolation points reach the epidemic peak of the first wave

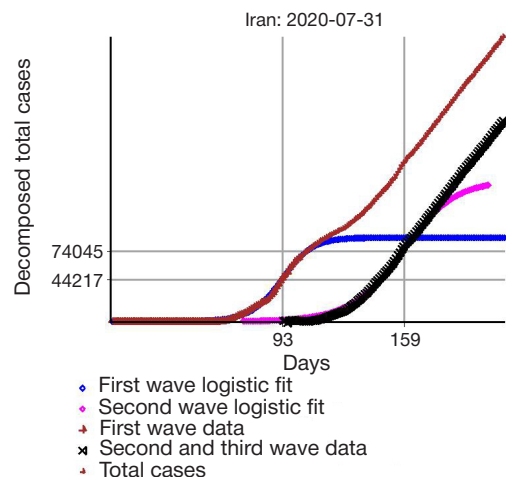


Fig. 4. Superposition of two logistic lines both of the first and second waves. We can observe the beginning of the growth of the tertiary wave

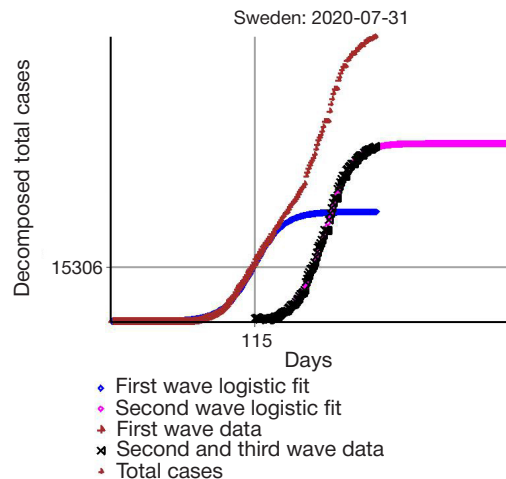


Fig. 5. Decomposition of the full input data by total cases in Sweden as a superposition of two logistic lines of the first and second waves

illustration explains the input-data decomposition for detecting the secondary waves.

Figure 6 shows that a situation similar to that in Iran takes place in Ukraine.

In comparison with the other countries, the secondary epidemic wave in the United States has got a gigantic scale, growing exponentially (Fig. 7).

Today, on the World Wide Web and television, there are more and more messages about the expectation of a second wave of the epidemic in Russia. These reports, as a rule, are based on speculation, which leaves open a burning question: should or not be the second wave of the epidemic in Russia?

Using our mathematical tools, we have found that the second epidemic wave in Russia had already risen in the first half of May. The height of this wave is about half the primary wave. The third wave has started in Russia at the end of June. Figure 8 represents a decomposition of the epidemic history in Russia as a superposition of the primary and secondary waves.

The appearance of the second wave in different countries possesses similar features despite some differences in the epidemic spread. We have admitted regularity in the rise of the second waves. These waves appear when passing through the critical point of the epidemic threshold of the current wave.

Pragmatically, passing through the threshold of a new wave should be the most responsible in terms of strict observance of the rules of self-isolation and other sanitary standards. The secondary waves of the epidemic are insidious in that they do not appear immediately but after a sufficiently long time. For example, in Iran, the second wave significantly showed itself in no less than 60 days.

DISCUSSION

There are several different mechanisms, each of which can generate secondary waves in acute infectious disease. The first two mechanisms are due to the direct viral transmission and a change in its behaviour, which favours the emergence of additional ways of its spread. The third one is associated with the heterogeneity of the population. A new wave either occupies new territories and population or rolls over the previous places again. The fourth item is a mutation in the virus that causes delayed susceptibility to infection in humans. One more mechanism is weakening immunity. There is no problem to take these mechanisms into account in complex mathematical models to simulate secondary waves [17]. We may add that secondary waves are, not least, a consequence of the lax compliance with quarantine and sanitary rules by people who trust rumours and consume unreliable mass information.

In this work, the authors abandoned multivariate models, which, in ideal implementation, are designed to study the impact, for example, of border control at the beginning of an outbreak, predicting the timing of self-isolation, assessing the required amount of available drugs, and others. Indeed, the practice of recent months has shown that the well-tested and widely known mathematical methods, directly used to describe future events of the spread of the epidemic by processing the available statistical data, have demonstrated ineffectiveness.

We know the well-known logistic equation adequately describes the epidemic evolution. However, neither various versions of this mathematical model nor modifications of the logistic equation demonstrate usefulness. In any case, the simulation gives a satisfactory result only on a small-time horizon, within one or two weeks [18].

If so, then we are dealing with not predictive, but with monitoring models, which, for all their value, are still useless

for developing medium-term and strategic action plans to overcome the pandemic [19]. Other promising predictive technologies based on graph theory [20], percolation theory [21], and stochastic processes [22] turned out to be too clumsy or incapable to produce a clear and concrete result on an urgent issue. In other words, the available forecast methods have demonstrated helpless when solving the problem.

There is a paradox. On the one hand, it could seem that everything about the dynamics of the pandemic is known

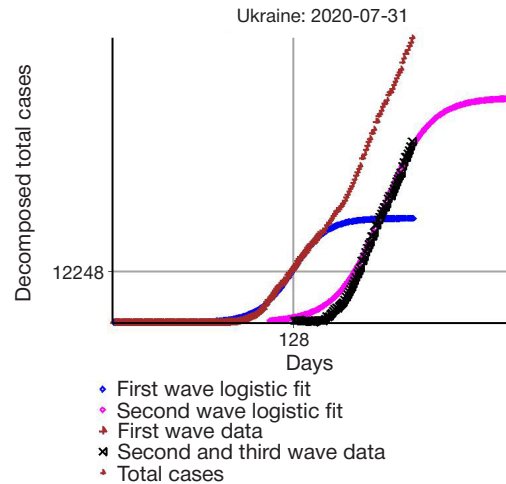


Fig. 6. Decomposition of the input data by total cases in Ukraine

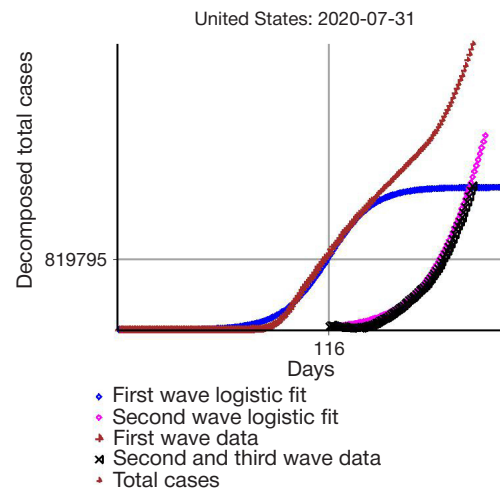


Fig. 7. Secondary epidemic wave in the United States

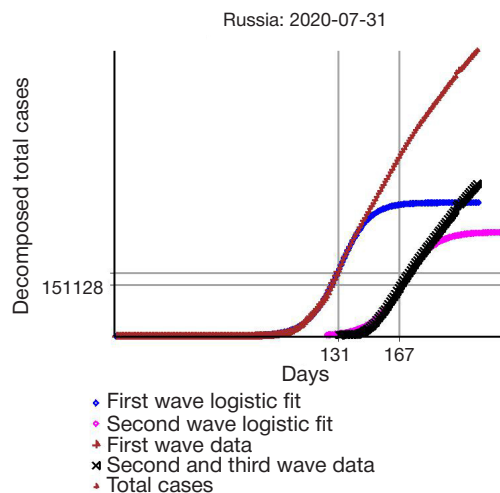


Fig. 8. Sum of two logistic lines of the first and second epidemic waves in Russia

qualitatively in advance. On the other hand, standard methods cannot provide an adequate prediction.

Let us try to shed light on the main reasons for such a failure and try to formulate the principles for overcoming the current situation. First of all, note that, in contrast to the experimental data, say, in physical experiments, data on the epidemic situation cannot be redundant, but only insufficient. Indeed, it is difficult to imagine a situation where redundant data regularly appears in the monitoring fixing the total number of newly detected cases since the case is too delicate to allow such sloppiness. It is natural to expect that the data has a lack of information. Thus, we can postulate that the regular error describes some deficit in the data. Indeed, we can obtain a comprehensive epidemic data only a posteriori. However, a priori analysis requires to identify this regular error using the statistical data of those countries which already have passed the epidemic peak.

We had managed to find the specified regular component of the error inherent in many countries of the world in monitoring the spread of the current pandemic in terms of exponential and power-law approximating functions. This error influences the forecasting of epidemic events critically. However, statistical data of countries have reached an epidemic peak demonstrate the analytical regularity in the virtual time delay. This fact allows us to pose the following question. Is a country that already has passed the threshold close to the peak epidemic or is still far from it?

The regular error of monitoring causes failures of a priori mathematical modelling [16]. We may point out that the predicted and real data, as a rule, practically coincide from the threshold to the peak of the epidemic. The explanation is simple: when crossing the inflexion point, the growth rate of registered infections decreases while the maximum effort is involved in solving the monitoring problem.

Thus, we have decided to limit ourselves to the simplest logistic model in this paper. On the one hand, this model requires a minimum of information to construct it. We need to know the initial number of cases, the final peak number, and the time from the beginning of the epidemic to its peak.

On the other hand, we must understand that the monitoring quality, first of all, determines the reliability of the model, not the number of unknown parameters that we should find out from the input data. In particular, the conservatism of the parameters of the logistic curves for the primary waves confirms the model reliability while the parameters of the current wave slowly change in time because of the indicated natural imperfection of the input data.

CONCLUSION

This text has focused on the appearance of the second epidemic wave in Iran, Sweden and the United States, Ukraine, and Russia. The analysis of the input data by the total cases shows that the most favourable time for the emergence of secondary waves is the critical point in which the rate of the epidemic increase approaches maximum. The pass of the threshold of the new epidemic wave should be the most responsible in terms of strict observance of the rules of self-isolation and other sanitary standards.

The mathematical model allows detecting the secondary waves much earlier than passively observing the epidemic history. An example is the not entirely obvious second wave in Russia, which arose in early May, and which gave rise to the third wave of the epidemic at the end of June. Nonetheless, today, we desire that Russia is still able to avoid the fourth epidemic wave if combating the epidemic. Iran also has such an opportunity.

The algorithm for studying the secondary waves represents a recursive decomposition of the input data to a set of different logistic curves, the parameters of which, unknown in advance, the calculation process determines. At the first step, we check the possibility of adequate approximation of the input data by a single logistic curve. If success, we attempt to identify the second logistic wave, etc.

Logistics decomposition in many features is similar to the well-known Fourier method or wavelet analysis. However, in our case, the decomposition algorithm does not end with a result if the input data is inappropriate.

References

1. Moftakhar L, Mozghan SEIF, Safe MS. Exponentially Increasing Trend of Infected Patients with COVID-19 in Iran: A Comparison of Neural Network and ARIMA Forecasting Models. *Iranian Journal of Public Health*. 2020; 49: 92–100.
2. Tran TT, Pham LT, Ngo QX. Forecasting epidemic spread of SARS-CoV-2 using ARIMA model (Case study: Iran). *Global Journal of Environmental Science and Management*. 2020; 6 (Special Issue (Covid-19)): 1–10.
3. Zareie B, Roshani A, Mansournia MA, Rasouli MA, Moradi G. A model for COVID-19 prediction in Iran based on China parameters. 2020; medRxiv.
4. Ahmadi A, Fadai Y, Shirani M, Rahmani F. Modeling and forecasting trend of COVID-19 epidemic in Iran until May 13, 2020. *Medical Journal of The Islamic Republic of Iran (MJIRI)*. 2020; 34 (1): 183–95.
5. Li L, Yang Z, Dang Z, Meng C, Huang J, Meng H, Wang D, Chen G, Zhang J, Peng H, Shao Y. Propagation analysis and prediction of the COVID-19. *Infectious Disease Modelling*. 2020; 5: 282–92.
6. Nejmark Yul. *Matematicheskie modeli v estestvoznanii i tehnike*. N. Novgorod: Izd-vo Nizhegorodskogo universiteta im. N. I. Lobachevskogo. 2004; 401 s. Russian.
7. Source code Maple-18. Available from: <https://kovrignueda.ucoz.ru/COVID-19/COVID-19-Iran.mw>.
8. Source code Maple-18. Available from: <https://kovrignueda.ucoz.ru/COVID-19/COVID-19-Russia.mw>.
9. Source code Maple-18. Available from: <https://kovrignueda.ucoz.ru/COVID-19/COVID-19-Ukraine.mw>.
10. Meyer P. Bi-logistic growth. *Technological forecasting and social change*. 1994; 47 (1): 89–102.
11. Lavrova AI, Postnikov EB, Manicheva OA, Vishnevsky BI. Bi-logistic model for disease dynamics caused by Mycobacterium tuberculosis in Russia. *Royal Society open science*. 2017; 4 (9): 171033.
12. Dattoli G, et al. On the evolution of covid-19 in Italy: a follow up note. Available from: arXiv preprint arXiv:2003.2020; 12667.
13. Dattoli G, Di Palma E, Licciardi S, Sabia E. A Note on the Evolution of Covid-19 in Italy, arXiv:2003.08684v1 [q-bio.PE], 19 Mar 2020.
14. Bhattacharya S, Islam MM, De A. Search for the trend of COVID-19 infection following Farr's law, IDEA model and power law. medRxiv. 2020; Available from: <https://doi.org/10.1101/2020.05.04.20090233>.
15. Singer HM. The COVID-19 pandemic: growth patterns, power law scaling, and saturation. medRxiv. 2020; Available from: <https://doi.org/10.1101/2020.07.12.20152140>.
16. Nikitenkova SP, Kovrignue DA. It's the very time to learn a pandemic lesson: why have predictive techniques been ineffective when describing long-term events? medRxiv. 2020; Available from: <https://doi.org/10.1101/2020.06.01.20118869>.

17. Mummert A, et al. A perspective on multiple waves of influenza pandemics. *PLoS one*. 2013; 8 (4): e60343.
18. Lakman IA, Agapitov AA, Sadikova LF, Chernenko OV, Novikov SV, Popov DV, i dr. *Vozmozhnosti matematicheskogo prognozirovaniya koronavirusnoj infekcii v Rossijskoj Federacii. Arterial'naja gipertenzija*. 2020; 26 (3): 288–94. Доступно по ссылке: <https://doi.org/10.18705/1607-419X-2020-26-3-288-294>. Russian.
19. Holmdahl I, Buckee C. Wrong but useful — what covid-19 epidemiologic models can and cannot tell us. *N Engl J Med*. 2020 May 15. DOI: 10.1056/NEJMp2016822.
20. Ivannikov YuG, Ogarkov PI. Opyt matematicheskogo komp'yuternogo prognozirovaniya jepidemij grippa dlja bol'shih territorij. *Zhurnal infektologii*. 2012; 4 (3): 101–06. Available from: <https://doi.org/10.22625/2072-6732-2012-4-3-101-106>. Russian.
21. Luo Y, Schaposnik LP. Minimal percolating sets for mutating infectious diseases. *Physical Review Research*. 2020; 2 (2): 023001.
22. de Arruda GF, Petri G, Moreno Y. Social contagion models on hypergraphs. *Physical Review Research*. 2020; 2 (2): 023032.

Литература

1. Moftakhar L, Mozghan SEIF, Safe MS. Exponentially Increasing Trend of Infected Patients with COVID-19 in Iran: A Comparison of Neural Network and ARIMA Forecasting Models. *Iranian Journal of Public Health*. 2020; 49: 92–100.
2. Tran TT, Pham LT, Ngo QX. Forecasting epidemic spread of SARS-CoV-2 using ARIMA model (Case study: Iran). *Global Journal of Environmental Science and Management*. 2020; 6 (Special Issue (Covid-19)): 1–10.
3. Zareie B, Roshani A, Mansournia MA, Rasouli MA, Moradi G. A model for COVID-19 prediction in Iran based on China parameters. 2020; medRxiv.
4. Ahmadi A, Fadaei Y, Shirani M, Rahmani F. Modeling and forecasting trend of COVID-19 epidemic in Iran until May 13, 2020. *Medical Journal of The Islamic Republic of Iran (MJIRI)*. 2020; 34 (1): 183–95.
5. Li L, Yang Z, Dang Z, Meng C, Huang J, Meng H, Wang D, Chen G, Zhang J, Peng H, Shao Y. Propagation analysis and prediction of the COVID-19. *Infectious Disease Modelling*. 2020; 5: 282–92.
6. Неймарк Ю. И. Математические модели в естествознании и технике. Н. Новгород: Изд-во Нижегородского университета им. Н. И. Лобачевского, 2004; 401 с.
7. Код Maple-18. Доступно по ссылке: <https://kovrigineda.ucoz.ru/COVID-19/COVID-19-Iran.mw>.
8. Код Maple-18. Доступно по ссылке: <https://kovrigineda.ucoz.ru/COVID-19/COVID-19-Russia.mw>.
9. Код Maple-18. Доступно по ссылке: <https://kovrigineda.ucoz.ru/COVID-19/COVID-19-Ukraine.mw>.
10. Meyer P. Bi-logistic growth. *Technological forecasting and social change*. 1994; 47 (1): 89–102.
11. Lavrova AI, Postnikov EB, Manicheva OA, Vishnevsky BI. Bi-logistic model for disease dynamics caused by *Mycobacterium tuberculosis* in Russia. *Royal Society open science*. 2017; 4 (9): 171033.
12. Dattoli G, et al. On the evolution of covid-19 in Italy: a follow up note. Available from: [arXiv preprint arXiv:2003.08684](https://arxiv.org/abs/2003.08684). 2020; 12667.
13. Dattoli G, Di Palma E, Licciardi S, Sabia E. A Note on the Evolution of Covid-19 in Italy, [arXiv:2003.08684v1 \[q-bio.PE\]](https://arxiv.org/abs/2003.08684), 19 Mar 2020.
14. Bhattacharya S, Islam MM, De A. Search for the trend of COVID-19 infection following Farr's law, IDEA model and power law. medRxiv. 2020; Available from: <https://doi.org/10.1101/2020.05.04.20090233>.
15. Singer HM. The COVID-19 pandemic: growth patterns, power law scaling, and saturation. medRxiv. 2020; Available from: <https://doi.org/10.1101/2020.07.12.20152140>.
16. Nikitenkova SP, Kovrigin DA. It's the very time to learn a pandemic lesson: why have predictive techniques been ineffective when describing long-term events? medRxiv. 2020; Available from: <https://doi.org/10.1101/2020.06.01.20118869>.
17. Mummert A, et al. A perspective on multiple waves of influenza pandemics. *PLoS one*. 2013; 8 (4): e60343.
18. Лакман И. А., Агапитов А. А., Садикова Л. Ф., Черненко О. В., Новиков С. В., Попов Д. В. и др. Возможности математического прогнозирования коронавирусной инфекции в Российской Федерации. *Артериальная гипертензия*. 2020; 26 (3): 288–94. Доступно по ссылке: <https://doi.org/10.18705/1607-419X-2020-26-3-288-294>.
19. Holmdahl I, Buckee C. Wrong but useful — what covid-19 epidemiologic models can and cannot tell us. *N Engl J Med*. 2020 May 15. DOI: 10.1056/NEJMp2016822.
20. Иванников Ю. Г., Огарков П. И. Опыт математического компьютерного прогнозирования эпидемий гриппа для больших территорий. *Журнал инфектологии*. 2012; 4 (3): 101–06. Available from: <https://doi.org/10.22625/2072-6732-2012-4-3-101-106>.
21. Luo Y, Schaposnik LP. Minimal percolating sets for mutating infectious diseases. *Physical Review Research*. 2020; 2 (2): 023001.
22. de Arruda GF, Petri G, Moreno Y. Social contagion models on hypergraphs. *Physical Review Research*. 2020; 2 (2): 023032.

REHABILITATION OF PATIENTS WITH CEREBRAL PALSY USING HAND EXOSKELETON CONTROLLED BY BRAIN-COMPUTER INTERFACE

Bobrov PD^{1,2}✉, Biryukova EV^{1,2}, Polyayev BA¹, Lajsheva OA^{1,3}, Usachjova EL³, Sokolova AV³, Mihailova DI³, Dement'eva KN³, Fedotova IR²

¹ Pirogov Russian National Research Medical University, Moscow, Russia

² Institute of Higher Nervous Activity and Neurophysiology of RAS, Moscow, Russia

³ Russian Children's Clinical Hospital of Pirogov Russian National Research Medical University, Moscow, Russia

Cerebral palsy (CP) is one of the most severe central nervous system diseases in childhood associated with motor impairment. The study was aimed to assess the efficiency of the complex comprising brain-computer interface (BCI) and hand exoskeleton as an instrument for the motor function recovery in patients with CP complementing the essential therapy. The Fugl-Meyer Assessment scale, ARAT test and Jebsen-Taylor function test were used in 14 children and adolescents for the motor function improvement assessment after the therapy complemented by 7–10 BCI-exoskeleton based procedures. The EEG mu-rhythm sources properties during the motor imagery BCI control were studied. After the procedures completion, the significant improvement of the Fugl-Meyer Assessment scale score (7 (2; 11) for hand active movements; 4.5 (1; 6) for proximal arm and 2.5 (0; 5) for hand), ARAT test score (7.5 (1; 31) for total score, 1.5 (0; 12) for grasp movement and 1.5 (0; 8) for grip movement), as well as significantly different from the zero execution time reduction in three out of seven Jebsen-Taylor function test items (–1 (–4; 13; 0.25) for simulated feeding; –1 (–2; 0) for moving light and heavy cans) were identified. The average BCI detection level was 0.51 (0.45; 0.54) (max = 0.70). In most EEG recordings the mu-rhythm sources were detected, both for intact and affected hemispheres. The mu-rhythm desynchronization associated with motor imagery was observed, significantly affecting the BCI accuracy. The results obtained indicate that the use of BCI-exoskeleton complex effectively complements the standard rehabilitation methods for children with CP, and suggest that its clinical effectiveness in individuals with CP may be proven by enrollment of more patients.

Keywords: cerebral palsy, rehabilitation, brain-computer interface, hand exoskeleton, EEG

Funding: the study received public financial support from the Ministry of Science and Higher Education of the Russian Federation (project ID RFMEFI60519X0184).

Author contribution: Bobrov PD — EEG processing and analysis, BCI accuracy estimation, manuscript writing; Biryukova EV — assessment scales scores statistical processing, manuscript writing; Polyayev BA, Lajsheva OA, Usachjova EL — clinical trial design; Usachjova EL — clinical trial management; Lajsheva OA, Sokolova AV, Mihailova DI, Dement'eva KN — development of methods for working with children, clinical data acquisition; Mihailova DI, Dement'eva KN — neuropsychological testing, training; Fedotova IR — literature analysis. All authors contributed to interpretation of the results and discussion.

Compliance with ethical standards: the study was approved by the Ethics Committee of Pirogov Russian National Research Medical University (protocol № 184 dated April 15, 2019). The informed consent was submitted by all patients' parents, adolescents aged over 14 submitted the additional informed consent.

✉ **Correspondence should be addressed:** Pavel D. Bobrov
Ostrovitianova, 1, Moscow, 117997; p-bobrov@yandex.ru

Received: 31.07.2020 **Accepted:** 13.08.2020 **Published online:** 20.08.2020

DOI: 10.24075/brsmu.2020.047

РЕАБИЛИТАЦИЯ БОЛЬНЫХ С ДЕТСКИМ ЦЕРЕБРАЛЬНЫМ ПАРАЛИЧОМ С ПОМОЩЬЮ ЭКЗОСКЕЛЕТА КИСТИ, УПРАВЛЯЕМОГО ИНТЕРФЕЙСОМ «МОЗГ–КОМПЬЮТЕР»

П. Д. Бобров^{1,2}✉, Е. В. Бирюкова^{1,2}, Б. А. Поляев¹, О. А. Лайшева^{1,3}, Е. Л. Усачёва³, А. В. Соколова³, Д. И. Михайлова³, К. Н. Дементьева³, И. Р. Федотова²

¹ Российский национальный исследовательский медицинский университет имени Н. И. Пирогова, Москва, Россия

² Институт высшей нервной деятельности и нейрофизиологии, Москва, Россия

³ Детская клиническая больница Российского национального исследовательского медицинского университета имени Н. И. Пирогова, Москва, Россия

Детский церебральный паралич — одно из тяжелых заболеваний центральной нервной системы у детей, сопровождающееся двигательными нарушениями. Целью работы было определить эффективность применения комплекса, объединяющего интерфейс «мозг–компьютер» (ИМК) и экзоскелет кисти, в качестве средства восстановления двигательной функции у пациентов с ДЦП в дополнении к основной терапии. У 14 детей и подростков по шкалам ARAT, Fugl-Meyer, Jebsen-Taylor оценивали изменение двигательной функции в результате терапии, дополненной 7–10 процедурами с комплексом ИМК–экзоскелет, а также исследовали свойства источников μ -ритма ЭЭГ при воображении движений во время управления ИМК. После процедур были выявлены достоверно положительный прирост баллов по шкалам Fugl-Meyer (7 (2; 11) — для активных движений руки; 4,5 (1; 6) — для проксимальных отделов и 2,5 (0; 5) — для кисти), ARAT (7,5 (1; 31) — для общей суммы баллов, 1,5 (0; 12) — для шарового и 1,5 (0; 8) — для цилиндрического захвата) и достоверно отличное от нуля снижение времени выполнения трех из семи задач теста Jebsen-Taylor (–1 (–4; 13; 0,25) — для имитации кормления; –1 (–2; 0) — для перестановки легких и тяжелых банок). Средняя вероятность правильного распознавания ИМК составила 0,51 (0,45; 0,54) (max = 0,70). В большинстве записей ЭЭГ были выделены источники μ -ритма, как в сохранном, так и в пораженном полушарии. Показано наличие десинхронизации μ -ритма при воображении движений, от степени которой достоверно зависит точность работы ИМК. Результаты показывают, что применение комплекса ИМК–экзоскелет эффективно дополняет стандартную реабилитацию детей с ДЦП, а также дают основания предполагать, что ее клиническая эффективность в случае ДЦП может быть доказана с привлечением большего числа пациентов.

Ключевые слова: ДЦП, реабилитация, интерфейс «мозг–компьютер», экзоскелет кисти, электроэнцефалограмма

Финансирование: работа выполнена при финансовой поддержке государства в лице Минобрнауки России (идентификатор соглашения RFMEFI60519X0184).

Вклад авторов: П. Д. Бобров — обработка и анализ ЭЭГ, оценка точности работы ИМК, написание статьи; Е. В. Бирюкова — статистическая обработка клинических шкал, написание статьи; Б. А. Поляев, О. А. Лайшева, Е. Л. Усачева — дизайн клинического исследования; Е. Л. Усачева — организация клинического исследования; О. А. Лайшева, А. В. Соколова, Д. И. Михайлова, К. Н. Дементьева — разработка методики работы с детьми, сбор клинических данных; Д. И. Михайлова, К. Н. Дементьева — нейропсихологическое обследование, тренинг; И. Р. Федотова — анализ литературы. Все авторы принимали участие в интерпретации результатов и обсуждении текста статьи.

Соблюдение этических стандартов: исследование одобрено этическим комитетом (протокол № 184 от 15 апреля 2019 г.), проведено согласно протоколу клинической апробации 2019-63-6, утвержденному экспертным советом Минздрава России. Родители всех пациентов подписали информированное согласие на участие в исследовании, дети старше 14 лет подписывали информированное согласие дополнительно к подписи родителей.

✉ **Для корреспонденции:** Павел Дмитриевич Бобров
ул. Островитянова, д. 1, г. Москва, 117997; p-bobrov@yandex.ru

Статья получена: 31.07.2020 **Статья принята к печати:** 13.08.2020 **Опубликована онлайн:** 20.08.2020

DOI: 10.24075/vrgmu.2020.047

Cerebral palsy (CP) is one of the most severe central nervous system (CNS) diseases in childhood associated with organic brain lesions. The prevalence of cerebral palsy in the developed world is 2–3 per 1000 live births [1]. CP is not only the most prevalent CNS pathology in childhood, but is also one of the most common causes of disability.

CP is associated with motor impairments of varying degrees found in patients with all common types of the disorder: spastic diplegia — 69.3%, hemiplegic cerebral palsy — 16.3%, atonic-astatic type — 9.2%, hyperkinetic type — 3.3%, double hemiplegia — 1.9% [2]. The traditional physical rehabilitation methods are as follows: massage, exercise therapy, instrumental kinesiotherapy, as well as physical therapy and electrophysiology helping to decrease spasticity. However, spasticity reduction is just the first step towards increasing the patients' functional activity. There is an urgent need in using the goal-directed functional therapy for further rehabilitation. Methods based on the brain plasticity stimulation are considered promising, particularly those using motor imagery [3]. Fundamental is the idea of successful attempt to imagine movement positive reinforcement using visual and proprioceptive feedback provided by brain-computer interface (BCI)-controlled exoskeleton. BCI classifies the acquired electroencephalogram (EEG) parts and in case the required motor imagery is detected turns on the exoskeleton which executes the appropriate movement providing the proprioceptive feedback. EEG classification is possible due to specific motor imagery patterns, especially the mu-rhythm desynchronization in the primary sensorimotor cortex during the limb imaginary movement detected in healthy individuals [4]. Rehabilitation approach based on the BCI-controlled hand exoskeleton use is considered the efficient method of motor function recovery well-proven in the post-stroke patients' rehabilitation [5, 6]. The method implements the principles of modern neurorehabilitation: patient's active involvement, training intensity and regularity, biofeedback. The technique was validated in randomized controlled trials of post-stroke motor function recovery [7–10].

It is to be hoped that rehabilitation using the BCI-exoskeleton complex would be also effective for children with CP, since the specific brain disorders occur during the period of maximum adaptability and brain plasticity, when the projections from the affected areas of the central nervous system have not yet reached their targets. Such disorders can interfere with the neuron maturation processes [11]. High brain plasticity patterns adaptivity typical for early development plays a positive role in healthy individuals contributing to the formation of motor skills. However, in patients with brain disorders the same patterns may provoke the normal development threatening atypical compensatory motor synergies formation, which often occurs in children with CP [12]. The underlying factor is inadequate plasticity, for example when plastic changes in neuronal circuits during the focused use of the intact limb lead to reduced neuronal activation in the remaining cortex (representing the affected limb) [13].

Motor imagery with kinesthetic feedback activates the brain plasticity pattern and thus teaches the child to perform hand flexion, as well as facilitates execution of atypical but functionally significant movements. That is the whole purpose of rehabilitation using the BCI-exoskeleton complex in patients with CP.

According to studies of kinesthetic imagination, in children with CP, motor imagery activates the same brain regions as in post-stroke patients [14]. It has been also shown that in healthy children the motor imagery ability develops between

5 and 12 years of age and contributes to the motor skills improvement [15]. In children with CP, the described ability is relatively preserved, though reduced compared to normal [16]. Moreover, the motor imagery ability does not depend on the lesion lateralization [17].

Thus, the kinesthetic motor imagery training is of high potential for motor function recovery in children with CP [17, 18]. The study was aimed to assess the efficiency of BCI-exoskeleton complex for rehabilitation of patients with CP. The motor imagery ability was assessed based on the the BCI accuracy and the mu-rhythm desynchronization level in the primary sensorimotor cortex of the hemisphere opposite to the hand used during the motor imagery procedure.

METHODS

The study was carried out at the Russian Children's Clinical Hospital of Pirogov Russian National Research Medical University from May 2019 to February 2020. The total of 14 patients underwent the motor imagery based rehabilitation course using the BCI-controlled hand exoskeleton (Table 1).

Inclusion criteria: age 7–19; patients with central paralysis of the upper extremities, including those diagnosed with cerebral palsy, acute cerebrovascular disease, traumatic brain injury; structural brain lesion identified using neuroimaging techniques. Exclusion criteria: inability to perform the procedures during the study; refusal of patient or his legal representative to participate in the study; extreme aphasia preventing understanding the instructions; severe visual impairment making it impossible to follow the instructions on the computer screen; hand spasticity score 5 according to the Modified Ashworth Scale. The withdrawal criteria were as follows: patient's refusal to continue participating in the study; acute or decompensated chronic disorder potentially affecting the research results; prescription of muscle relaxants (changing the dosage after the patient's inclusion to the study); botulinum toxin preparation injected into the paretic hand muscles after the patient's inclusion to the study.

The procedures were carried out using the Exohand-2 robotic hand complex comprising the BCI-controlled hand exoskeletons. The patient was seated in the medical chair. His hands were put in the hand exoskeletons fixed on the armrests of the chair. In front of the patient at a distance of 1–1.5 m a monitor was placed with a circle for gaze fixation and the visual instructions to perform the following mental tasks: either kinesthetic imagination of the left or right hand opening, or sitting still and relaxed. Neuropsychologist was called upon in the following situations: 1) child's lack of motivation to participate in the procedure; 2) difficulty in understanding the instructions to imagine the movement; 3) pronounced attention problems; 4) phobias and/or panic attacks experienced during the procedure. In the described situations the causes of trouble were diagnosed, and the kinesthetic motor imagery training was carried out.

In order to facilitate the difficult kinesthetic motor imagery task and to make it easier to understand, the clues were used that simplified the imaginary motion initiation (Table 2). The age of the child, his interests, as well as the cognitive functions development level were taken into account.

In children with cognitive deficit, it was recommended to use metaphors proposed for the younger age group. In children with pronounced tendency towards absent-mindedness, increased toggling between associations, as well as violation of purposeful activity, the explanations were simplified and reduced as much as possible, using precise language.

Table 1. Study participants' characteristics

Participant	Gender	Age	Diagnosis	Lateralization
1	Female	11	Consequences of traumatic brain injury	Left-sided hemiparesis
2	Female	16	Spastic hemiplegia. Spastic hemiparesis on the right side	Right sided hemiparesis
			Condition after osteoplastic trepanation, functional hemispherotomy on the left side	
3	Male	17	Spastic cerebral palsy, tetraplegia	Left-sided dominant tetraparesis
4	Female	17	Unspecified cerebral palsy	Left-sided hemiparesis
			Spastic hemiplegia	
			Localization-related (focal) (partial) symptomatic epilepsy and epileptic syndromes with complex partial seizures. Focal structural epilepsy, remission	
5	Male	11	Spastic hemiplegia	Left-sided hemiparesis
			Other disorders of psychological development	
			Hypermetropia	
6	Female	10	Spastic hemiplegia	Left-sided hemiparesis
			Unspecified disorder of psychological development	
			Other types of generalized epilepsy and epileptic syndromes, electrical status epilepticus in slow wave sleep	
7	Male	16	Spastic cerebral palsy	Right sided hemiparesis
8	Male	12	Childhood hemiplegia	Right sided hemiparesis
			Focal structural epilepsy, remission. Condition after the left frontal-central-parietal region cortical dysplasia resection performed in 09.2017. Focal cortical dysplasia, type IIb (ILAE).	
			Inherited epilepsy. Intellectual disability	
			Condition after Coleman's surgical procedure on the left side	
9	Male	10	Consequences of traumatic brain injury	Right sided hemiparesis
10	Female	12	Cerebral palsy	Spastic diplegia
11	Male	12	Cerebral palsy	Right sided hemiparesis
			Focal structural epilepsy	
			Regional cortical dysplasia. Condition after functional hemispherotomy on the left side	
			Mild cognitive impairment due to epilepsy	
			Optic nerve atrophy	
12	Female	16	Spastic cerebral palsy	Left-sided hemiparesis
13	Male	13	Cerebral palsy	Spastic diplegia
14	Female	19	Cerebral palsy	Spastic diplegia

During the tasks execution electroencephalogram (EEG) was acquired, which allowed the classifier to detect the currently executed task. Classification result was presented in the form of visual and proprioceptive feedback: if the detected task corresponded to the instructions, then the color of the circle on the monitor screen changed from white to green, and the exoskeleton performed opening of the hand.

EEG acquisition was performed using the NVX52 unit (Medical Computer Systems; Russia) being a part of the Exohand-2 complex. The total of 32 electrodes located at F3, Fz, F4, Fc5, Fc3, Fc1, Fcz, Fc2, Fc4, Fc6, C5, C3, C1, Cz, C2, C4, C6, Cp5, Cp3, Cp1, Cpz, Cp2, Cp4, Cp6, P3, Pz, P4, Po3, Poz, Po4, O1, O2 was used. The signal processing was performed using the Butterworth filter (passband 5–30 Hz), and the notch filter to filter out the mains hum from the 50 Hz power line. The Bayesian classifier based on the EEG signal covariance matrices analysis was used for the currently performed task detection [19].

The motor imagery training had been carried out for 7–10 days (2–3 daily procedures). The duration of the procedure was 6.5 min, which was about 1.5 times shorter than the procedure conducted in adult post-stroke patients [8]. The duration of the breaks between the procedures was 5 min.

The BCI control accuracy was evaluated based on the answers of the system classifier. The answers made it possible to obtain the confusion matrix G for each session. The number of rows and the number of columns in each matrix were equal to the number of detected tasks (three in this study). Element g_{ij} ($i = 1, 2, 3; j = 1, 2, 3$) was used for evaluation of task i detection level in a case when instruction j was presented. The average value of the matrix diagonal elements was an estimate of the average detection level, i.e. the BCI control accuracy.

The filtered EEG recordings were further processed in order to estimate level of the mu-rhythm desynchronization associated with motor imagery. Each recording was analyzed using the Adaptive Mixture Independent Component Analysis (AMICA) [20], which was chosen as the most informative physiologically significant EEG sources search method [21, 22].

For the signal decomposition into independent components two statistical models were used, which made it possible to automatically select the recording parts containing artifacts occurred due to child's moving in the chair. These parts were excluded from the analysis. For the remaining parts, the detected independent components topographic maps were examined in order to select the components corresponding to the mu-rhythm sources in the left and right hemispheres. The

mu-rhythm desynchronization level was calculated using the following formula: $100\% \cdot (v_{base} - v_{act})/v_{base}$, where v_{act} was a component activity variance when imagining the contralateral hand movement, and v_{base} was a component activity variance at rest.

If the mu-rhythm source identification was impossible, the activity evaluated by LCMV beamforming was taken instead of the source activity [23] based on the averaged topographic map obtained during other sessions for the mu-rhythm source of the appropriate localization.

The motor function assessment was performed using the following standard scales: Fugl-Meyer Assessment scale, Action Research Arm Test (ARAT) and Jebsen-Taylor function test. The Fugl-Meyer Assessment scale was used for analysis of total scores needed for assessment of proximal arm and hand motor function, as well as the total score for all active hand movements. The ARAT test was used for analysis of grasp, grip, pinch and gross movements. The Jebsen-Taylor function test was used to analyze the execution time in seven motion tests: writing a simple sentence, cards turning over, picking up small objects, simulated feeding, stacking checkers, moving light cans, moving large weighted cans. All seven items of the Jebsen-Taylor test were executed with both left and right hand.

Goniometer was used for measurement of the maximum angles in hand joints when performing active movements of the wrist joint, as well as of the metacarpophalangeal and interphalangeal joints of all fingers. All patients passed the clinical tests before the start of the procedure and after its completion.

The assessment scales scores statistical analysis included the comparison of values obtained before and after the procedures using the Wilcoxon test, ANOVA, Student's *t*-test, and the comparison of clinical scales score improvement according to the signed-rank test with a zero median.

RESULTS

BCI control

The average imaginary movements and resting state detection level during the session was 0.51 (0.45; 0.54) (max = 0.70). The mu-rhythm sources in the hemisphere opposite to the intact hand were identified during 72.0% (61; 84) of sessions, and the mu-rhythm sources in the hemisphere opposite to paretic hand were detected during 64% (45; 80) of sessions. In patients with biparesis and tetraparesis, the hand with better Jebsen-Taylor test score was considered intact. Fig. 1A and 1B present the mu-rhythm sources topographic maps averaged for all participants and all acquired recordings (those in which the mu-rhythm sources were identified).

The correlation between the BCI control accuracy and the average source occurrence was significant (Fig. 1C). The high proportion of sessions in which the sources of mu-rhythm were

identified was typical for participants most successful in BCI management.

The mu-rhythm suppression value for the hemisphere opposite to the intact hand was 12% (7; 23) (max = 51%), and for the hemisphere opposite to the paretic hand it was 11% (6.5; 17) (max = 31%). The corresponding average values were 18.6% and 13.4%, the difference was significant (ANOVA: $p = 0.0018$; *t*-test: $p < 10^{-4}$). Thus, the imaginary movement of the paretic hand caused the weaker mu-rhythm desynchronization in the contralateral hemisphere.

The significant correlation between the BCI control accuracy and the mu-rhythm desynchronization level was revealed, both for the hemisphere opposite to the intact hand (Fig. 1D), and the hemisphere opposite to the paretic hand (Fig. 1E). The greater was the rhythm suppression associated with imaginary movement of both intact and paretic hands, the higher was the BCI control accuracy.

Motor function improvement

According to the signed-rank test with zero median, the significant increments indicating the motor function improvement after the procedures' completion were obtained for all sections of the Fugl-Meyer Assessment scale, for proximal arm, hand and for the total score for all active movements (Table 3). According to the ARAT test, the significant improvement was observed in the grasp and grip movement tests score, as well as in the total score. In the pinch movement and gross hand movements tests the improvement detected after the procedures completion was not significant (see Table 3).

The Jebsen-Taylor test items execution using the paretic hand was very difficult: before the start of the procedures the execution time exceeded 2 min in all patients. After the procedures completion only two children were able to finish one test, and three children were able to finish two tests out of seven in less than 2 min. All patients successfully executed the tasks by intact hand, after the procedures completion the execution time was reduced in all functional tests, except the "Writing a simple sentence" test. The "Moving light cans", "Moving large weighted cans" and "Simulated feeding" tests execution time reduction after the procedures completion was significantly different from zero according to the signed-rank test (Table 4).

Of all studied paretic hand active movements only the dorsal extension amplitude increased from 30° (25°; 41.25°) to 40° (40°; 58.75°). The amplitude increase turned out to be significantly greater than zero ($p = 0.016$ according to the signed-rank test).

DISCUSSION

The kinesthetic motor imagery methods are considered an effective instrument for the motor function recovery, and

Table 2. Examples of clues simplifying the initiation of motor imagery

Age	7–10 years	10–13 years	13–18 years
Instruction example	Imagine that you are trying to reach for the flower to pick it/want to take a toy car/want to catch a butterfly/want to grasp your favourite toy	Imagine that you control the robot with the power of thought/open the treasure chest/open the jewelry box	Imagine that you are trying to reach for the doorknob to open the door/hold out your hand for someone to shake/pick an apple from the tree
			The use of specific kinesthetic images is accepted: "Your hand is clenched into a fist. Gradually, the fingers begin to come off the palm, feel them straighten, relax and form a straight line"

therefore are increasingly used in clinical practice for regaining movements after a stroke [5, 6]. There are few papers on the motor imagery in children, both healthy and affected by CP. The papers report that the motor imagery ability develops between 5 and 12 years of age and is peculiar not only to children with typical development [15, 24], but also to children with CP [16–18]. Our evidence confirmed these results: the average detection level of the proposed states (opening the right or left hand, rest) by the EEG classifier during the procedure was 0.51, and the maximum value was 0.70, which exceeded 0.33 (the three states detection random expectation value). However, the detection level 0.51 was lower than the average detection level in adults (0.6 according to the study of 37 healthy individuals and 32 post-stroke patients) [8].

The age of children with CP included in the motor imagery study was the same as in our study: 11–16 years [17], 9–14 years [18], or even younger (5–9 years) [16]. The exclusion criteria in the discussed study were much more stringent: patients with severe paresis, dystonia and cognitive impairment were excluded. In our study, the participants demonstrated severe motor function impairment (see Table 1). However, all of them were successful in the BCI management: the mu-rhythm sources in the hemisphere opposite to the intact hand were identified during most sessions. Our results were in line with the previously obtained data on the successful motor imagery in children with left- and right-sided CP [17].

It is important to note that the observed correlation between the BCI control accuracy and the mu-rhythm desynchronization level is not a trivial matter, since the classifier uses the signal covariance matrices and the response may be affected by

various electric activity sources (including artifacts) [25]. The results obtained indicate that BCI-based training really cause the primary sensorimotor cortex activation specific to the task being performed, which is one of the main goals of the procedure.

The significant motor function impairment in children with CP is associated with muscular weakness, increased muscle tone, spasticity, and sensory deficit [26]. Motor imagery training in children with CP aimed at brain plasticity stimulation promotes the motor function recovery both as individual therapy [16, 18] and being combined with other rehabilitation methods [17]. During our study, the Fugl-Meyer Assessment scale and the ARAT test scores improved which indicated the motor function improvement. Despite the patients group heterogeneity according to age, diagnosis, and lesion lateralization (see Table 1) the score improvement in some function tests was significant (see Table 3). Despite the inevitable subjective nature, the Fugl-Meyer Assessment scale and the ARAT test are widely used in clinical practice for the motor function impairment assessment. Their total scores reliability is based on a large number of motion tests that have been developed for adult patients [27]. The observations of the medical specialists who have performed testing of our patients confirm that such testing can be tedious for children with CP, and thus reduce the motor function assessment reliability.

Unlike the Fugl-Meyer Assessment scale and the ARAT test, the Jebsen–Taylor function test is based on the objective task execution time measurement. Severe motor function impairments in the study participants made it impossible for them to execute the ARAT test tasks prior to the procedures.

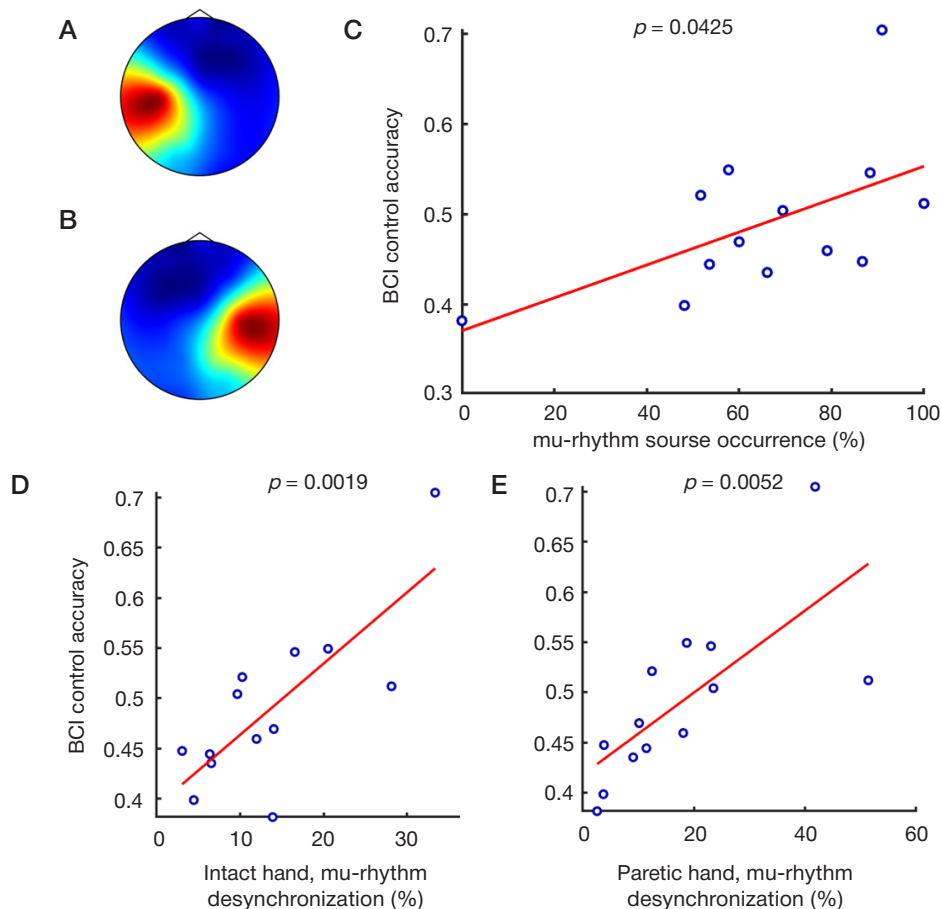


Fig. 1. Topography of mu-rhythm sources and BCI control accuracy. **A.** Average topography of mu-rhythm sources in the left hemisphere. **B.** Average topography of mu-rhythm sources in the right hemisphere. **C.** Correlation between BCI control accuracy and mu-rhythm sources occurrence in all study participants. **D.** Correlation between BCI control accuracy and mu-rhythm desynchronization in the hemisphere opposite to the intact hand. **E.** Correlation between BCI control accuracy and mu-rhythm desynchronization in the hemisphere opposite to the paretic hand

Table 3. Motor function median, quartile and significance level values according to Fugl-Meyer Assessment scale and ARAT test (obtained before and after the procedures)

Scale (motion tests)	Before	After	Difference	p_{wilcoxon}	p_{anova}	p_{diff}
Fugl-Meyer (Proximal arm)	20.5 (15; 25)	26 (22; 27)	4.5 (1; 6)	0.13	0.27	0.032*
Fugl-Meyer (Hand)	6 (2; 12)	9.5 (5; 17)	2.5 (0; 5)	0.24	0.28	0.031*
Fugl-Meyer (Total score for all active movements)	27 (18; 32)	34.5 (26; 43)	7 (2; 11)	0.19	0.25	0.022*
ARAT (Grasp movement)	11 (3; 24)	13 (3; 36)	1.5 (0; 12)	0.62	0.34	0.008*
ARAT (Grip movement)	8 (3; 13)	9.5 (6; 21)	1.5 (0; 8)	0.43	0.34	0.018*
ARAT (Pinch movement)	0.5 (0; 13)	3.5 (0; 18)	0 (0; 3)	0.63	0.56568	0.16
ARAT (Gross hand movement)	7 (4; 16)	9 (4; 16)	0 (0; 1)	0.63	0.63	0.063
ARAT (Total score)	31.5 (12; 76)	42 (15; 110)	7.5 (1; 31)	0.33	0.37	< 10⁻³*

Table 4. Motor function median, quartile (seconds) and significance level values according to Jebsen-Taylor function test (obtained before and after the procedures)

Motion test	Before	After	Difference	p_{wilcoxon}	p_{anova}	p_{diff}
Writing a simple sentence	18 (11.25; 29.75)	24 (14.10; 48.25)	0 (-1.50; 3.70)	0.45	0.41	0.36
Cards turning over	6 (4.00; 8.50)	5 (3.00; 7.75)	0 (-1.25; 0.86)	0.44	0.97	0.40
Picking up small objects	9 (6.00; 11.00)	7 (6.50; 13.75)	-0.06 (-2.00; 1.25)	0.88	1.00	0.90
Simulated feeding	11 (8.50; 15.25)	10 (6.50; 13.00)	-1 (-5.66; 0.00)	0.41	0.27	0.0469*
Stacking checkers	9 (7.75; 16.25)	9 (6.75; 15.75)	-1 (-4.13; 0.25)	0.57	0.91	0.21
Moving light cans	5 (4.50; 9.25)	4 (3.00; 7.25)	-1 (-2.00; 0.00)	0.38	0.44	0.0039*
Moving large weighted cans	6 (4.00; 9.25)	5 (4.00; 7.50)	-1 (-2.00; 0.00)	0.43	0.45	0.0117*

After the procedures completion only five patients out of 14 were able to pass some function tests. However, the execution time for intact hand reduced in all tests except one, and in four tests out of seven the differences were significant (see Table 4). As is known, the motor deficit is typical not only for paretic hand, but also for intact hand [28]. Despite the fact that motor impairment of the intact hand is significantly lower than the motor impairment of the paretic hand, it can significantly limit the patient's functional activity, especially in the case of severe lesions. During the BCI-exoskeleton based training the voluntary activation is observed in both affected and intact hemispheres. The described bilateral activation contributes to the procedures' effectiveness affecting the function of both hands.

For more accurate and fair motor function assessment, the biomechanical analysis of movements registered before and

after rehabilitation is used. The described analysis is widely used in clinical trials for post-stroke patients [29]. In children with CP, the possible movement detection protocols as well as sets of biomechanical parameters for motor function assessment are still being developed [30].

CONCLUSION

BCI-hand exoskeleton procedure is an effective and promising instrument for motor function recovery in children with CP, which may complement the essential therapy. All study participants were successful in the BCI management despite the differences in age, lesion lateralization and motor function impairment severity. It has been shown, that BCI management triggers the specific primary sensorimotor cortex activation, even in the affected hemisphere.

References

- Himmelmann K, Hagberg G, Uvebrant PAP. The changing panorama of cerebral palsy in Sweden. X. Prevalence and origin in the birth-year period 1999–2002. *Acta Paediatrica*. 2010; 99 (9): 1337–43.
- Semenova KA. Vosstanovitel'noe lechenie detej s perinatal'nym porazheniem nervnoj sistemy i detskim cerebral'nym paralichom. M.: Izd-vo «Zakon i porjadok», 2007; 616 s. Russian.
- Frolov AA, Husek D, Biryukova EV, Bobrov PD, Mokienko OA, Alexandrov AV. Principles of motor recovery in post-stroke patients using hand exoskeleton controlled by the brain-computer interface based on motor imagery. *Neural Network World*. 2017; 27 (1): 107–37.
- Pfurtscheller G, Lopes da Silva FH. Event-related EEG/MEG synchronization and desynchronization: basic principles. *Clinical Neurophysiology*. 1999; 110 (11): 1842–57. Epub 1999/11/27. PubMed PMID: 10576479.
- Hétu S, Gregoire M, Sainpont A, Coll M-P, Eugene F, Michon P-E, et al. The neural network of motor imagery: an ALE meta-analysis. *Neuroscience & Biobehavioral Reviews*. 2013; 37 (5): 930–49.
- Monge-Pereira E, Ibañez-Pereda J, Alguacil-Diego I, Serrano J, Spottorno-Rubio M, Molina-Rueda F. Use of Electroencephalography Brain-Computer Interface Systems as a Rehabilitative Approach for Upper Limb Function After a Stroke: A Systematic Review. *PM&R*. 2017; 9 (9): 918–32.
- Ang KK, Chua KSG, Phua KS, Wang C, Chin ZY, Kuah CWK, et al. A randomized controlled trial of EEG-based motor imagery brain-computer interface robotic rehabilitation for stroke. *Clinical EEG and neuroscience*. 2015; 46 (4): 310–20.
- Frolov AA, Mokienko O, Lyukmanov R, Biryukova E, Kotov S, Turbina L, et al. Post-stroke rehabilitation training with a motor-imagery-based brain-computer interface (BCI)-controlled hand exoskeleton: a randomized controlled multicenter trial. *Frontiers in neuroscience*. 2017; 11: 400.
- Ono T, Shindo K, Kawashima K, Ota N, Ito M, Ota T, et al. Brain-computer interface with somatosensory feedback improves functional recovery from severe hemiplegia due to chronic stroke. *Frontiers in neuroengineering*. 2014; 7: 19.
- Ramos-Murguialday A, Broetz D, Rea M, Lärer L, Yılmaz Ö, Brasil FL,

- et al. Brain-machine interface in chronic stroke rehabilitation: a controlled study. *Annals of neurology*. 2013; 74 (1): 100–8.
11. Eyre JA. Corticospinal tract development and its plasticity after perinatal injury. *Neuroscience & Biobehavioral Reviews*. 2007; 31 (8): 1136–49.
 12. Thelen E. Developmental 'movement disorders' and problem solving. In: What are 'normal movements' in atypical populations? *Behavioral and Brain Sciences*. 1996; 19 (1): 55–106.
 13. Allred RP, Jones TA. Maladaptive effects of learning with the less-affected forelimb after focal cortical infarcts in rats. *Experimental Neurology*. 2008; 210 (1): 172–81.
 14. Duarte NAC, Grecco LAC, Zanon N, Galli M, Fregni F, Oliveira CS. Motor cortex plasticity in children with spastic cerebral palsy: a systematic review. *Journal of Motor Behavior*. 2016; 49 (4): 1–10.
 15. Spruijt S, van der Kamp J, Steenbergen B. The ability of 6- to 8-year-old children to use motor imagery in a goal-directed pointing task. *Journal of Experimental Child Psychology*. 2015; 139: 221–33.
 16. Lust JM, Wilson PH, Steenbergen B. Motor imagery difficulties in children with cerebral palsy: A specific or general deficit? *Research in Developmental Disabilities*. 2016; 57: 102–11.
 17. Cabral-Sequeira AS, Coelho DB, Teixeira L. Motor imagery training promotes motor learning in adolescents with cerebral palsy: comparison between left and right hemiparesis. *Experimental Brain Research*. 2016; 234 (6): 1515–24.
 18. Errante A, Bozzetti F, Sghedoni S, Bressi B, Costi S, Crisi G, et al. Explicit motor imagery for grasping actions in children with spastic unilateral cerebral palsy *Frontiers in neurology*. 2019; 10: 837.
 19. Bobrov PD, Korshakov AV, Roshhin VYu, Frolov AA. Bajesovskij podhod k realizacii interfejsa mozg-komp'juter, osnovannogo na predstavlenii dvizhenij. *Zhurnal vysshej nervnoj dejatel'nosti*. 2012; 62 (1): 89–99. Russian.
 20. Palmer JA, Kreutz-Delgado K, Makeig S. AMICA: An adaptive mixture of independent component analyzers with shared components. *Swartz Center for Computational Neuroscience, University of California San Diego, Tech Rep*. 2012.
 21. Delorme A, Palmer J, Onton J, Oostenveld R, Makeig S. Independent EEG sources are dipolar. *PLoS one*. 2012; 7 (2): e30135.
 22. Frolov A, Bobrov P, Biryukova E, Isaev M, Kerechanin Y, Bobrov D, et al. Using Multiple Decomposition Methods and Cluster Analysis to Find and Categorize Typical Patterns of EEG Activity in Motor Imagery Brain-Computer Interface Experiments. *Frontiers in Robotics and AI*. 2020; 7 (88). DOI: 10.3389/frobt.2020.00088.
 23. Van Hoey G, Van de Walle R, Vanrumste B, D'Havse M, Lemahieu I, Boon P. Beamforming techniques applied in EEG source analysis. *Proc ProRISC99*. 1999; 10: 545–9.
 24. Crognier L, Skoura X, Vinter A, Papaxanthis C. Mental representation of arm motion dynamics in children and adolescents. *PLoS one*. 2013; 8: e73042.
 25. Frolov A, Aziatskaya G, Bobrov P, Ljukmanov R, Fedotova I, Gusek D, i dr. Jelektrofiziologicheskaja aktivnost' mozga pri upravlenii interfejsom mozg-komp'juter, osnovannym na voozbrazhenii dvizhenij. *Fiziologija cheloveka*. 2017; 43 (5): 17–28. Russian.
 26. Klingels K, Demeyere I, Jaspers E, De Cock P, Molenaers G, Boyd R, et al. Upper limb impairments and their impact on activity measures in children with unilateral cerebral palsy. *European Journal of Paediatric Neurology*. 2012; 16 (5): 475–84.
 27. Gladstone DJ, Daniells CJ, Black SE. The Fugl-Meyer assessment of motor recovery after stroke: A critical review of its measurement properties. *Neurorehabilitation and Neural Repair*. 2002; 16 (232–240).
 28. Sunderland A. Recovery of ipsilateral dexterity after stroke. *Stroke*. 2000; 31 (2): 430–3.
 29. Alt Murphy MA, Häger CK. Kinematic analysis of the upper extremity after stroke — how far have we reached and what have we grasped? *Physical Therapy Reviews*. 2015; 20: 137–55.
 30. Maillieux L, Simon-Martinez C, Feys H, Jaspers E. Upper extremity movement pathology during functional tasks. In: Müller B, Wolf S, editors. *Handbook of Human Motion*. Cham: Springer International Publishing AG, 2018; p. 1167–1184.

Литература

1. Himmelmann K, Hagberg G, Uvebrant PAP. The changing panorama of cerebral palsy in Sweden. X. Prevalence and origin in the birth-year period 1999–2002. *Acta Paediatrica*. 2010; 99 (9): 1337–43.
2. Семенова К. А. Восстановительное лечение детей с перинатальным поражением нервной системы и детским церебральным параличом. М.: Изд-во «Закон и порядок», 2007; 616 с.
3. Frolov AA, Husek D, Biryukova EV, Bobrov PD, Mokienko OA, Alexandrov AV. Principles of motor recovery in post-stroke patients using hand exoskeleton controlled by the brain-computer interface based on motor imagery. *Neural Network World*. 2017; 27 (1): 107–37.
4. Pfurtscheller G, Lopes da Silva FH. Event-related EEG/MEG synchronization and desynchronization: basic principles. *Clinical Neurophysiology*. 1999; 110 (11): 1842–57. Epub 1999/11/27. PubMed PMID: 10576479.
5. Héту S, Gregoire M, Saimpont A, Coll M-P, Eugene F, Michon P-E, et al. The neural network of motor imagery: an ALE meta-analysis. *Neuroscience & Biobehavioral Reviews*. 2013; 37 (5): 930–49.
6. Monge-Pereira E, Ibañez-Pereda J, Alguacil-Diego I, Serrano J, Spottorno-Rubio M, Molina-Rueda F. Use of Electroencephalography Brain-Computer Interface Systems as a Rehabilitative Approach for Upper Limb Function After a Stroke: A Systematic Review. *PM&R*. 2017; 9 (9): 918–32.
7. Ang KK, Chua KSG, Phua KS, Wang C, Chin ZY, Kuah CWK, et al. A randomized controlled trial of EEG-based motor imagery brain-computer interface robotic rehabilitation for stroke. *Clinical EEG and neuroscience*. 2015; 46 (4): 310–20.
8. Frolov AA, Mokienko O, Ljukmanov R, Biryukova E, Kotov S, Turbina L, et al. Post-stroke rehabilitation training with a motor-imagery-based brain-computer interface (BCI)-controlled hand exoskeleton: a randomized controlled multicenter trial. *Frontiers in neuroscience*. 2017; 11: 400.
9. Ono T, Shindo K, Kawashima K, Ota N, Ito M, Ota T, et al. Brain-computer interface with somatosensory feedback improves functional recovery from severe hemiplegia due to chronic stroke. *Frontiers in neuroengineering*. 2014; 7: 19.
10. Ramos-Murguialday A, Broetz D, Rea M, Lärer L, Yilmaz Ö, Brasil FL, et al. Brain-machine interface in chronic stroke rehabilitation: a controlled study. *Annals of neurology*. 2013; 74 (1): 100–8.
11. Eyre JA. Corticospinal tract development and its plasticity after perinatal injury. *Neuroscience & Biobehavioral Reviews*. 2007; 31 (8): 1136–49.
12. Thelen E. Developmental 'movement disorders' and problem solving. In: What are 'normal movements' in atypical populations? *Behavioral and Brain Sciences*. 1996; 19 (1): 55–106.
13. Allred RP, Jones TA. Maladaptive effects of learning with the less-affected forelimb after focal cortical infarcts in rats. *Experimental Neurology*. 2008; 210 (1): 172–81.
14. Duarte NAC, Grecco LAC, Zanon N, Galli M, Fregni F, Oliveira CS. Motor cortex plasticity in children with spastic cerebral palsy: a systematic review. *Journal of Motor Behavior*. 2016; 49 (4): 1–10.
15. Spruijt S, van der Kamp J, Steenbergen B. The ability of 6- to 8-year-old children to use motor imagery in a goal-directed pointing task. *Journal of Experimental Child Psychology*. 2015; 139: 221–33.
16. Lust JM, Wilson PH, Steenbergen B. Motor imagery difficulties in children with cerebral palsy: A specific or general deficit? *Research in Developmental Disabilities*. 2016; 57: 102–11.
17. Cabral-Sequeira AS, Coelho DB, Teixeira L. Motor imagery training promotes motor learning in adolescents with cerebral palsy: comparison between left and right hemiparesis. *Experimental Brain Research*. 2016; 234 (6): 1515–24.
18. Errante A, Bozzetti F, Sghedoni S, Bressi B, Costi S, Crisi G, et al. Explicit motor imagery for grasping actions in children with spastic unilateral cerebral palsy *Frontiers in neurology*. 2019; 10: 837.

19. Бобров П. Д., Коршаков А. В., Рошин В. Ю., Фролов А. А. Байесовский подход к реализации интерфейса мозг-компьютер, основанного на представлении движений. *Журнал высшей нервной деятельности*. 2012; 62 (1): 89–99.
20. Palmer JA, Kreutz-Delgado K, Makeig S. AMICA: An adaptive mixture of independent component analyzers with shared components. Swartz Center for Computational Neuroscience, University of California San Diego, Tech Rep. 2012.
21. Delorme A, Palmer J, Onton J, Oostenveld R, Makeig S. Independent EEG sources are dipolar. *PloS one*. 2012; 7 (2): e30135.
22. Frolov A, Bobrov P, Biryukova E, Isaev M, Kerechanin Y, Bobrov D, et al. Using Multiple Decomposition Methods and Cluster Analysis to Find and Categorize Typical Patterns of EEG Activity in Motor Imagery Brain-Computer Interface Experiments. *Frontiers in Robotics and AI*. 2020; 7 (88). DOI: 10.3389/frobt.2020.00088.
23. Van Hoey G, Van de Walle R, Vanrumste B, D'Havse M, Lemahieu I, Boon P. Beamforming techniques applied in EEG source analysis. *Proc ProRISC99*. 1999; 10: 545–9.
24. Crognier L, Skoura X, Vinter A, Papaxanthis C. Mental representation of arm motion dynamics in children and adolescents. *PloS one*. 2013; 8: e73042.
25. Фролов А., Азиатская Г., Бобров П., Люкманов Р., Федотова И., Гусек Д., и др. Электрофизиологическая активность мозга при управлении интерфейсом мозг-компьютер, основанным на воображении движений. *Физиология человека*. 2017; 43 (5): 17–28.
26. Klingels K, Demeyere I, Jaspers E, De Cock P, Molenaers G, Boyd R, et al. Upper limb impairments and their impact on activity measures in children with unilateral cerebral palsy. *European Journal of Paediatric Neurology*. 2012; 16 (5): 475–84.
27. Gladstone DJ, Daniells CJ, Black SE. The Fugl-Meyer assessment of motor recovery after stroke: A critical review of its measurement properties. *Neurorehabilitation and Neural Repair*. 2002; 16 (232–240).
28. Sunderland A. Recovery of ipsilateral dexterity after stroke. *Stroke*. 2000; 31 (2): 430–3.
29. Alt Murphy MA, Häger CK. Kinematic analysis of the upper extremity after stroke — how far have we reached and what have we grasped? *Physical Therapy Reviews*. 2015; 20: 137–55.
30. Maillieux L, Simon-Martinez C, Feys H, Jaspers E. Upper extremity movement pathology during functional tasks. In: Müller B, Wolf S, editors. *Handbook of Human Motion*. Cham: Springer International Publishing AG, 2018; p. 1167–1184.

CHANGES IN EEG PATTERNS IN THE α -FREQUENCY BAND FOLLOWING BCI-BASED THERAPY IN CHILDREN WITH CEREBRAL PALSY

Larina NV, Nacharova MA, Korsunskaya LL, Vlasenko SV, Pavlenko VB 

Vernadsky Crimean Federal University, Simferopol, Russia

It was demonstrated previously that neurorehabilitation with the noninvasive BCI-controlled robotic device combined with conventional therapeutic modalities resulted in significant motor improvement in children with cerebral palsy. However, EEG records were not analyzed in the previous study. The aim of this paper was to describe the reactivity patterns of the EEG α -rhythm during a series of 10 BCI-based neurorehabilitation sessions. The study was carried out in 32 boys and girls aged 10 to 18 years with right- or left-side hemiparesis. EEG was recorded from 21 electrodes at rest and during kinesthetic imagery of finger extension. During the first session, patterns of α -rhythm reactivity during motor imagery differed between patients with left- and right-side hemiparesis. The differences were statistically significant at P2 during left hand movement rehearsal ($F_{1,30} = 5.10$; $p < 0.05$). During the final session, the pattern of α -rhythm reactivity was different: synchronization was taken over by desynchronization at some electrode sites, suggesting increased activity of the neocortex. The most conspicuous EEG changes were observed in children with left-side hemiparesis ($F_{20,300} = 1.84$; $p < 0.05$). By the end of the rehabilitation course, the differences between patients with left- and right-side hemiparesis became much less pronounced. Rearrangements in the EEG patterns in the α -frequency band can be regarded as signs of beneficial reorganization of neural circuits responsible for planning and executing complex hand movements.

Keywords: cerebral palsy, EEG, neurorehabilitation, brain-computer interface, motor imagery

Funding: the study was part of the state-funded project RFMEFI60519X0186 on the *Development of a BCI-based hand exoskeleton with biological feedback for the rehabilitation of children with cerebral palsy*. The study was supported by the Ministry of Science and Higher Education of the Russian Federation.

Author contribution: Larina NV, Korsunskaya LL, Vlasenko SV — data acquisition, manuscript preparation; Nacharova MA, Pavlenko VB — data analysis, manuscript preparation.

Compliance with ethical standards: the study was approved by the Ethics Committee of Vernadsky Crimean Federal University (Protocol № 53 dated December 06, 2018). Informed consent was obtained from the patients or their legal representatives.

 **Correspondence should be addressed:** Vladimir B. Pavlenko
Pr. Vernadskogo, 4, Simferopol, 295007; vpav55@gmail.com

Received: 16.06.2020 **Accepted:** 02.07.2020 **Published online:** 16.07.2020

DOI: 10.24075/brsmu.2020.043

ИЗМЕНЕНИЕ ЭЭГ В ЧАСТОТНОМ ДИАПАЗОНЕ α -РИТМА У ДЕТЕЙ С ДЕТСКИМ ЦЕРЕБРАЛЬНЫМ ПАРАЛИЧОМ ПРИ ПРИМЕНЕНИИ РОБОТИЗИРОВАННОЙ ТЕРАПИИ

Н. В. Ларина, М. А. Начарова, Л. Л. Корсунская, С. В. Власенко, В. Б. Павленко 

Крымский федеральный университет имени В. И. Вернадского, Симферополь, Россия

Курс нейрореабилитации с применением комплекса «неинвазивный интерфейс мозг–компьютер и экзоскелет кисти» в сочетании с традиционным курортным лечением приводит у детей с ДЦП к значимому улучшению показателей движений, однако характеристики ЭЭГ не были проанализированы. Целью работы было определить особенности реактивности ЭЭГ пациентов в частотном диапазоне α -ритма при прохождении курса из 10 сеансов роботизированной терапии. ЭЭГ регистрировали в 21 отведении в условиях покоя и кинестетического воображения движений разгибания пальцев рук у 32 детей обоего пола в возрасте 10–18 лет, имеющих диагноз «лево- и правосторонний гемипарез». Во время первого сеанса паттерны реактивности α -ритма при воображении движений у групп детей с лево- и правосторонним гемипарезом различались, причем различия достигали статистической значимости в отведении P2 при воображении движений левой кисти ($F_{1,30} = 5,10$; $p < 0,05$). Паттерн реактивности α -ритма во время десятого сеанса отличался замещением реакций синхронизации в ряде отведений на десинхронизацию, что свидетельствует об увеличении активации неокортекса. Наиболее выраженными были изменения ЭЭГ у детей с левосторонним гемипарезом ($F_{20,300} = 1,84$; $p < 0,05$). По завершении курса степень различия показателей ЭЭГ у пациентов с лево- и правосторонним гемипарезом уменьшилась. Выявленные перестройки паттерна ЭЭГ в частотной полосе α -ритма можно рассматривать как проявление процессов благоприятной реорганизации нейронных цепей, контролирующих планирование и выполнение сложных движений рук.

Ключевые слова: детский церебральный паралич, ЭЭГ, нейрореабилитация, интерфейс мозг–компьютер, воображение движения

Финансирование: исследование выполнено в рамках темы: «Разработка комплекса экзоскелета кисти с внешним программным управлением и биологической обратной связью для процедуры реабилитации детей с синдромом ДЦП» при финансовой поддержке Министерства науки и высшего образования Российской Федерации (RFMEFI60519X0186).

Вклад авторов: Ларина Н. В., Корсунская Л. Л., Власенко С. В. — набор данных, написание статьи; Начарова М. А., Павленко В. Б. — обработка данных, написание статьи.

Соблюдение этических стандартов: исследование одобрено этическим комитетом КФУ им. В. И. Вернадского (протокол № 53 от 06 декабря 2018 г.). Все пациенты или их законные представители подписали добровольное информированное согласие.

 **Для корреспонденции:** Владимир Борисович Павленко
пр. Вернадского, 4, г. Симферополь, 295007; vpav55@gmail.com

Статья получена: 16.06.2020 **Статья принята к печати:** 02.07.2020 **Опубликована онлайн:** 16.07.2020

DOI: 10.24075/vrgmu.2020.043

In most economically developed countries, cerebral palsy (CP) is the leading cause of motor disability in children. CP affects 1 in 500 newborns; globally, there are 17 million people living with CP [1]. CP is an umbrella term for the group of

chronic nonprogressive motor impairments (spastic paresis, hyperkinetic disorder, cerebellar ataxia, pseudobulbar palsy) that stem from brain damage or developmental delay before, during or after birth. In patients with CP, motor dysfunction

usually co-exists with mental retardation, epilepsy, perceptual, learning or communication difficulties [2]. Because clinical manifestations of CP are very diverse, medications and physiotherapy may not always be effective. One of the most promising methods for managing motor dysfunction relies on the use of noninvasive brain-computer interfaces (BCI) and robotic devices with biological feedback [3]. They are capable of recognizing a patient's motor intention from changes in his or her EEG during kinesthetic imagery followed by relevant activation of the robotic device. It is hypothesized [4] that robotic orthoses might significantly improve treatment outcomes: the patient receives feedback about how well the mental task is being performed whereas enhanced sensory input (tactile, proprioceptive or visual) stimulates brain structures that are fully or partially excluded from processing sensory information because of brain damage. This technology has been proved effective for post-stroke patients [5, 6].

Although it is reported that BCI might be a potent rehabilitation tool for children with CP [7, 8], few studies have addressed this possibility so far. It was reported that individuals with CP could benefit from BCI that rely on the analysis of the sensorimotor EEG rhythm [9]. Kinesthetic imagery affected the power of the μ and β EEG rhythms analyzed by a classifier. In another study, a BCI was used to, firstly, explore how the power ratio of the β - to θ -rhythms changed in patients who were mentally rehearsing a wrist extension movement and, secondly, trigger electrical stimulation of wrist extensors [10]. After a series of such BCI-based session, children with CP demonstrated improvement in their hand movement parameters.

In another study, a BCI-controlled robotic hand was tested in children with CP undergoing rehabilitation at a medical health resort [11]. By the end of the neurorehabilitation course, the majority of the participants had achieved a reduction in wrist muscle spasticity, improved muscle strength, expanded the range of wrist movements and the repertoire of daily routines they were able to perform. By contrast, the only positive trend observed in the patients undergoing conventional treatment without BCI-based training consisted in performing more daily tasks, but those improvements were statistically insignificant. At that point, EEG records were not analyzed.

Reactivity of the α - and μ -rhythms is an attractive field for research, especially in the context of analysis of CNS activity in patients with motor impairment undergoing neurorehabilitation. The amplitude of the α - and μ -rhythms can be attenuated or enhanced by physical or mental activity. These phenomena are called event-related desynchronization and synchronization, respectively. A study demonstrated that in healthy volunteers, certain patterns of α -rhythm reactivity indicate involvement of various neocortical regions in processing sensory input from different modalities [12], whereas patterns of μ -rhythm reactivity are indicative of activation in the somatosensory and motor cortex during motor execution and imagery [13, 14]. The μ -rhythm occurs in the alpha frequency range, which has a contribution from the occipital α -rhythm during motor imagery; the occipital α -rhythm is partially retained when the eyes are open and is characterized by high reactivity during cognitive activities [15]. So, the terms "the α -rhythm" or "alpha rhythmic activity" used below will refer to the activity resulting from the α - and μ -rhythms.

It was reported that these rhythms undergo synchronization or desynchronization in poststroke patients during motor imagery [16]. There were changes in the patterns of amplitude attenuation and enhancement following the rehabilitation course with a BCI-controlled robotic hand. The researchers proposed that such reactivity might be indicative of the reorganization of

neural circuits during neurorehabilitation. Today, the patterns of α - and μ -rhythm reactivity in children with CP remain understudied.

The aim of this paper was to describe the reactivity patterns of the EEG α -rhythm during a series of neurorehabilitation sessions with a non-invasive BCI-controlled robotic hand allowing biological feedback in CP-stricken children with a paretic upper limb.

METHODS

Demographics

The study was conducted at the Psychiatry and Neurology Unit of E.P. Glinka Yevpatoria Clinical Sanatorium for Children. The study recruited patients aged 10 to 18 years undergoing neurorehabilitation with a noninvasive BCI-controlled robotic hand (Exohand-2) developed by Android Technics in collaboration with Pirogov Russian National Research Medical University and Institute of Higher Nervous Activity and Neurophysiology (Russia). The following inclusion criteria were applied: CP (according to ICD-10), hemiparesis, GMFCS (Gross Motor Function Classification System for Cerebral Palsy) level III or below. Patients at GMFCS level > III, with plegic upper limbs, aphasia, pharmacologically refractory epilepsy, or visual impairments preventing them from reading instructions on the computer screen, and those with moderate, severe or profound mental retardation (F71–73 according to ICD-10) were excluded from the study.

We shortlisted 32 patients, who were then referred to the medical health resort for rehabilitation. The patients were stratified into 2 groups: those with left-side hemiparesis (16 patients, including 10 boys and 6 girls) and those with right-side hemiparesis (16 children, including 9 boys and 7 girls). Of them, 21 patients were at GMFCS level II and 11 at GMFCS level III. There were 11 children aged 10–12 years, 12 children aged 13–15 years, and 9 patients aged 16–18 years. The mean age was 13.6 ± 2.5 years. The groups did not differ significantly in terms of age.

Rehabilitation, EEG recording and analysis

The device relies on the analysis of EEG patterns during motor imagery by a Bayesian classifier that analyzes covariance matrices of EEG signals [17].

During the sessions, the patients remained seated in armchairs at a 1.5 m distance from the computer screen where visual instructions were displayed. Their hands were inside the "glove" of the robotic hand. A round white fixation mark was displayed in the center of the screen, with 3 arrows around it that changed their color to present a task. The tasks included resting (the top arrow was activated for 10 s) and kinesthetic imagery of right- or left-hand finger extension (the right or left arrows were activated for 10 s). If the task was performed successfully, the fixation mark went green and the robotic hand extended passively. Thus, the patient received both visual and kinesthetic feedback.

Each patient received 10 rehabilitation sessions on alternate days, consisting of 3 8-minute long trials with at least 5-minute breaks. For each hand, the movement was mentally rehearsed 24 times during one session. Apart from BCI sessions, the 21-day-long rehabilitation course included conventional therapy [11], specifically physical exercise, massage of the paretic muscles, peloid therapy, kinesiotherapy in thermal water, electrical stimulation of the antagonists of the paretic muscles.

EEG was recorded in a monopolar fashion using a Neurovisor BMM electroencephalograph (Medical Computer Systems; Russia). Electrodes were placed according to the international 10-10 system over the frontal (Fpz, Fp1, Fp2, Fz, F1, F2, F3, F4), central (Cz, C1, C2, C3, C4), parietal (Pz, P1, P2, P3, P4), and occipital (Oz, O1, O2) lobes. An ear electrode was used as a reference. The cutoff values for high and low frequencies were 5 and 30 Hz, respectively; the sampling rate was 500 Hz.

EEG fragments with an amplitude over 250 μ V or containing a lot of artifacts pertaining to the electrical activity of forehead muscles were excluded from the analysis. EEG fragments recorded during mental rehearsal of the right/left hand movement and the resting stage (eyes open; baseline) that were 10 s long and free of artifacts were selected for further analysis. There were 10 to 15 such fragments for each task per session. These EEG fragments were processed with Fast Fourier transform (epoch time 2.5 s, epoch overlap 50%). The data were tapered using the Blackman window. For each 10-s long EEG fragment, we calculated the mean alpha amplitude for the frequency band of 8 to 13 Hz and the reactivity indices (RI) using the formula: $RI = 100\% \times [(B - A) / A]$, where B is the mean α -rhythm amplitude during the 10-s long motor imagery task and A is the mean α -rhythm amplitude in the resting phase (baseline condition) preceding the motor imagery task. For the right and left hands, mean RI values were calculated separately.

Positive RI values indicated an increase in the α -rhythm amplitude during motor imagery relative to its baseline value (synchronization), whereas negative RI values meant a reduction in the α -rhythm amplitude (desynchronization). RI values from the 1st and 10th sessions were averaged and used in the subsequent analysis.

Statistical analysis

Statistical analysis was carried out in STATISTICA 10.0 (StatSoft Inc.; USA). The Shapiro-Wilk test revealed that the distribution of alpha RI values for all EEG leads was normal. Therefore,

repeated measures ANOVA was applied to the obtained data. Using a $2 \times 2 \times 21$ design, we evaluated the effects of one intersubject factor GROUP (assignment to the group of subjects with right/left hemiparesis) and two intrasubject factors: HAND (mental rehearsal of the right/left hand movement) and LOCUS (position of one of 21 electrodes). Changes in α -rhythm reactivity following rehabilitation were analyzed using ANOVA with 3 intrasubject factors: SESSION (1st and 10th), HAND and LOCUS. To assess RI changes at each of electrode position, a priori contrasts were applied (the F-distribution test). Differences were considered significant at $p < 0.05$, but due to the small sample size, we also kept track of trends ($p < 0.10$).

RESULTS

Previously, we demonstrated that rehabilitation with noninvasive BCI-controlled robotic hand significantly improved motor function of the upper limbs in children with CP [11]. Patients who received only traditional rehabilitation therapy were unable to achieve statistically significant improvements. At that point, no analysis of EEG records was conducted.

Alpha-rhythm reactivity at the beginning of the rehabilitation course

Bidirectional modulations of the α -rhythm amplitude were noted during motor imagery in the first session of BCI-based therapy (Fig. 1, 2, red columns). Event-related synchronization was observed at most electrode sites in both hemispheres. Patterns of α -rhythm modulations were different between children with right-side and left-side hemiparesis. The effect produced by the interaction of GROUP \times HAND \times LOCUS was close to statistically significant ($F_{20, 600} = 1.45$; $p = 0.09$). The a priori contrasts analysis revealed significant differences in α -rhythm reactivity at P2 (the right parietal electrode; $F_{1, 30} = 5.10$; $p < 0.05$) during mental practice of the left-hand movement (Fig. 1) At P2, α -rhythm synchronization was very pronounced in children with left-side hemiparesis (Fig. 1A), whereas children with right-side

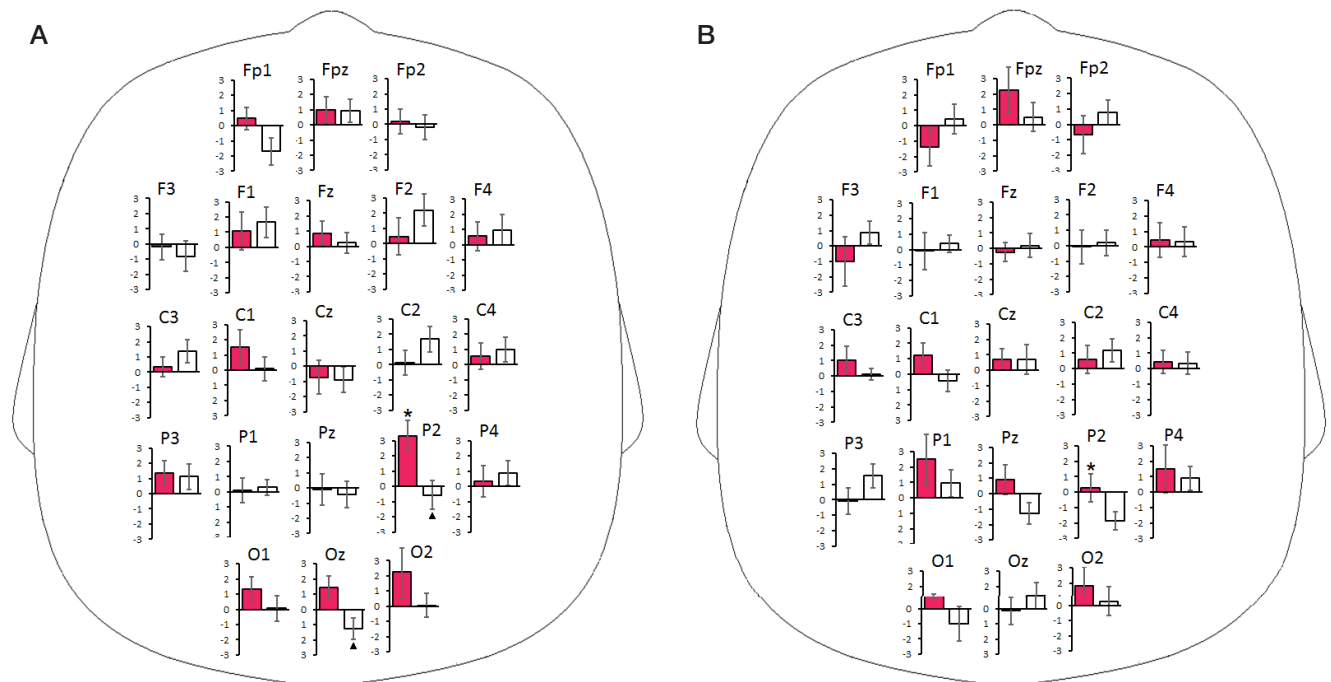


Fig. 1. Reactivity indices of the EEG α -rhythm (%) in children with left-side (A) and right-side (B) hemiparesis during mental rehearsal of the left-hand movement in the first session (red bars) and in the final session (white bars) of the BCI-based rehabilitation course. The figure shows the mean values and standard errors. Differences in RI between the two groups are marked by * ($p < 0.05$) and between the sessions, by ▲ ($p < 0.05$)

hemiparesis demonstrated only a slight change in the α -rhythm amplitude (Fig. 1B).

The a priori contrasts analysis uncovered a tendency to more pronounced α -rhythm synchronization at P2 during right-hand movement imagery in children with right-side hemiparesis ($F_{1,30} = 2.81$; $p = 0.10$), as compared to those with left-side hemiparesis (Fig. 2A, B).

Alpha-rhythm reactivity at the end of the rehabilitation course

The pattern of α -rhythm reactivity observed in our patients during the final session differed from that observed at the beginning of the rehabilitation course.

The impact of the SESSION \times HAND \times LOCUS combination ($F_{20,300} = 1.84$; $p < 0.05$) on α -rhythm reactivity was significant in children with left-side hemiparesis. Synchronization of the α -rhythm during left-hand movement imagery observed at Fp1, Fp2, P2, and Oz at the beginning of the rehabilitation course now gave way to desynchronization (Fig. 1A). Differences in RI values between the 1st and 10th sessions were statistically significant at P2 ($F_{1,15} = 10.02$; $p < 0.01$) and Oz ($F_{1,15} = 7.68$; $p < 0.05$) and close to statistically significant at Fp1 ($F_{1,15} = 3.96$; $p = 0.07$). Significant differences in α -rhythm reactivity were detected at C1 ($F_{1,15} = 6.57$; $p < 0.05$) in children with left-side hemiparesis during mental rehearsal of the right-hand movement. By the end of the rehabilitation course, synchronization had taken over desynchronization (Fig. 2A).

RI values did not differ significantly between the 1st and 10th sessions in children with right-side hemiparesis imagining right- and left-hand movements (Fig. 1B, 2B). The impact of the SESSION \times HAND \times LOCUS combination on α -rhythm reactivity was insignificant ($F_{20,300} = 0.86$; $p = 0.64$).

After the rehabilitation course was over, the differences in α -rhythm reactivity between children with right- and left-side hemiparesis observed during motor imagery became much less pronounced: the impact of the GROUP \times HAND \times LOCUS

combination was now statistically insignificant ($F_{20,600} = 0.88$; $p = 0.61$).

DISCUSSION

This study analyzes changes in EEG signals during BCI-based neurorehabilitation of patients with CP. The EEG amplitude modulations in the alpha frequency band measured in children with CP during motor imagery was surprisingly low. At most electrode sites, RI values did not exceed 3%. To some extent, this can be explained by the atypical modulation of EEG rhythms observed in patients with CP. Event-related μ -rhythm synchronization and desynchronization responses during motor activity were weak in patients with CP, as compared to healthy individuals. Those responses did not have distinct localization in patients with CP: EEG signal changes were observed in different neocortical regions, including the parietal and occipital lobes [18–20]. Besides, although our patients were asked to imagine movements continuously for 10 seconds, changes in α -rhythm amplitude were not always solid. In healthy adults performing motor imagery tasks μ -rhythm changes follow a multiphase pattern characterized by alternating synchronization and desynchronization [14]. The same alternating pattern of the μ - and α -rhythms was observed during motor imagery in adult poststroke patients undergoing rehabilitation with robotic devices [16]. It is possible that in our study event-related synchronization and desynchronization responses appeared smoothed out because we analyzed the EEG amplitude for the entire period of motor imagery.

The pattern of α -rhythm reactivity during motor imagery was bilateral. We saw the amplitude grow and decline not only in the contralateral but also in the ipsilateral hemisphere (relative to the hand the subject was focused on). Such atypical bilateral patterns of motor activity in children with CP were previously reported by other authors [21]. Using functional MRI, the researchers studied activation of CNS structures during motor imagery (grasping a ball) and recorded hand muscle responses to transcranial magnetic stimulation. The authors concluded

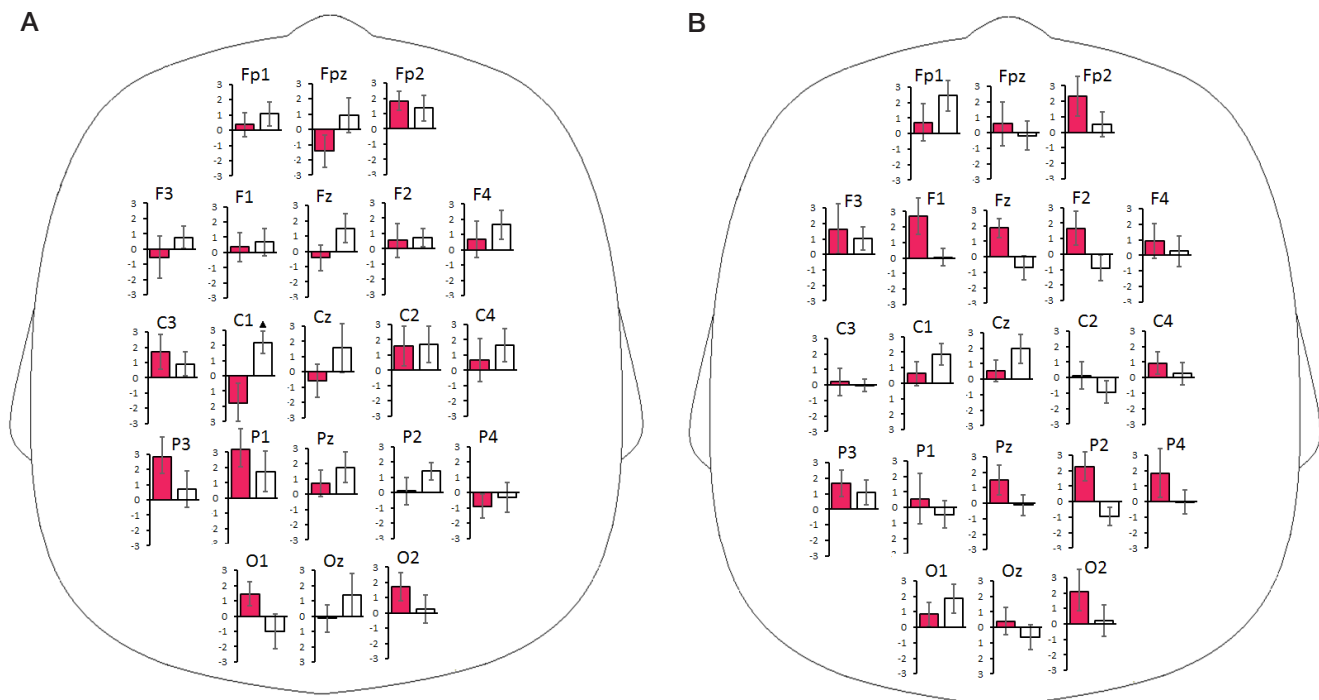


Fig. 2. Reactivity indices of the EEG α -rhythm in children with left-side (A) and right-side (B) hemiparesis during mental rehearsal of the right-hand movement in the first session and in the final session of the BCI-based rehabilitation course. For legend see Fig. 1.

that more than half of children with CP control the paretic hand with either ipsilateral or both hemispheres. Such unusual brain organization is probably compensatory; it develops after brain damage at early age and relies on the plasticity of the nervous system.

Our study was carried out in two groups of patients: with right- and left-side hemiparesis. This allowed us to compare EEG responses to motor imagery in the relatively intact and profoundly damaged hemispheres. At the beginning of the neurorehabilitation course, the patterns of α -rhythm attenuation or enhancement during motor imagery differed between the groups. RI values were significantly different in the parietal lobe of the right hemisphere (P2). After the sessions, differences in the degree of α -rhythm reactivity during motor imagery between children with left- and right-side hemiparesis became much less pronounced, probably indicating positive changes in CNS activity.

These changes are primarily associated with significant EEG reactivity in the alpha frequency band observed in patients with left-side hemiparesis at the end of the rehabilitation course. During the first BCI session, pronounced desynchronization (RI > 0.25%) was observed only at one electrode site (Cz) in this group of children, but during the final session, desynchronization was present in 6 regions of both hemispheres (Fig. 1A). Although changes in EEG reactivity patterns observed at the end of the course in children with right-side hemiparesis were not statistically significant, there still was an increase in α -rhythm attenuation. During the first session, there were no signs of desynchronization at any of the electrode sites when the children were mentally rehearsing the movement of the paretic hand. However, in the final session, desynchronization was recorded at 6 electrode locations, mostly in the ipsilateral hemisphere (Fig. 2B). An increase in event-related α -rhythm desynchronization suggests increased neocortical activation induced by neurorehabilitation [12–14]. An increase in desynchronization at P2 (Fig. 1A, B) is most noteworthy. The EEG signal at this location reflects the activity of the precuneal neural circuits [22]. The precuneus is profoundly involved in performing the broad spectrum of highly integrated tasks, including visuospatial motor imagery and first person perspective taking [23]. Increased activity of this brain region following neurorehabilitation may play a key role in the optimization of planning or executing complex

hand movements and improved performance of daily activities.

Increased desynchronization in some neocortical regions was accompanied by event-related α -rhythm enhancement in other cortical areas. Thus, there was a significant increase in the α -rhythm amplitude in the primary motor (C2, C4) and premotor (F2, F4) cortices in children with left-side hemiparesis as they were imagining the movement of the paretic hand. These changes occurring in the alpha frequency band are evident of active inhibition aimed at preventing the overinvolvement of the damaged contralateral hemisphere in motor activity control.

Because children with CP had significantly improved their motor function by the end of the rehabilitation course [11], the observed changes in EEG patterns in the alpha frequency band can be regarded as mirroring positive reorganization of neural circuits. This study is preliminary in nature. We cannot rule out the impact of factors associated with traditional rehabilitation modalities on the pattern of EEG reactivity. We are planning to conduct a randomized cross-sectional study to evaluate the impact of those factors and to analyze the link between EEG changes and motor improvements in children with CP. We think that this and future studies will help to elaborate new approaches to improving the efficacy of neurorehabilitation.

CONCLUSIONS

Neurorehabilitation of children with CP involving the use of noninvasive BCI-controlled robotic hand significantly improves motor function of the upper limbs and changes the pattern of α -rhythm reactivity during motor imagery. At the beginning of the rehabilitation course, the patterns of α -rhythm reactivity differed significantly between children with left- and right-side hemiparesis. By the end of the course, the differences became much less pronounced, suggesting positive changes in CNS activity. These improvements result from a statistically significant change in EEG reactivity patterns in patients with left-side hemiparesis. On the whole, children with left- and right-side hemiparesis demonstrated an increase in the proportion of α -rhythm desynchronization responses, indicating increased neocortical activity following neurorehabilitation. The observed changes in the EEG patterns in the alpha frequency band reflect increased plasticity of the neural circuits responsible for planning and executing complex hand movements.

References

- Graham HK, Rosenbaum P, Paneth N, Dan B, Lin JP, Damiano DL, et al. Cerebral palsy. *Nat Rev Dis Primers*. 2016; 2: 15082. DOI: 10.1038/nrdp.2015.82.
- Patel DR, Neelakantan M, Pandher K, Merrick J. Cerebral palsy in children: a clinical overview. *Transl Pediatr*. 2020; 9 (Suppl 1): 125–35.
- Frolov AA, Bobrov PD. Interfejs mozg–komp'yuter: nejrofiziologicheskie predposylki i klinicheskoe primenenie. *Zhurnal vysshej nervnoj dejatel'nosti im. I. P. Pavlova*. 2017; 67 (4): 365–76. Russian.
- Chiew M, LaConte S, Graham S. Investigation of fMRI neurofeedback of differential primary motor cortex activity using kinesthetic motor imagery. *NeuroImage*. 2012; 61 (1): 21–31.
- Kotov SV, Turbina LG, Bobrov PD, Frolov AA, Pavlova OG, Kurganskaja ME i dr. Reabilitacija bol'nyh, perenessih insul't, s pomoshh'ju bioinzhenernogo kompleksa «interfejs mozg–komp'yuter + jekzoskelet». *Zhurnal nevrologii i psixiatrii im. C. C. Korsakova*. 2014; 114 (12–2): 66–72. Russian.
- Frolov AA, Mokienko OA, Lyukmanov RKh, Chernikova LA, Kotov SV, Turbina LG et al. Preliminary results of a controlled study of BCI–exoskeleton technology efficacy in patients with poststroke arm paresis. *Bulletin of RSMU*. 2016; 2: 16–23.
- Ponce P, Molina A, Balderas DC, Grammatikou D. Brain Computer Interfaces for Cerebral Palsy. In: E. Suraka, editor. *Cerebral Palsy challenges for the future*. London: IntechOpen, 2014; p. 245–72. DOI: 10.5772/57084.
- Jochumsen M, Shafique M, Hassan A, Niazi IK. Movement intention detection in adolescents with cerebral palsy from single-trial EEG. *J Neural Eng*. 2018; 15 (6): 066030. DOI: 10.1088/1741-2552/aae4b8.
- Daly I, Billinger M, Laparra-Hernández J, Aloise F, Lloria García M, Faller J, et al. On the control of brain-computer interfaces by users with cerebral palsy. *Clin Neurophysiol*. 2013; 124 (9): 1787–97.
- Kim T-W, Lee B-H. Clinical usefulness of brain-computer interface-controlled functional electrical stimulation for improving brain activity in children with spastic cerebral palsy: a pilot randomized controlled trial. *J Phys Ther Sci*. 2016; 28 (9): 2491–4.
- Larina NV, Korsunskaya LL, Vlasenko SV. The “Exo hand-2” complex in the rehabilitation of the upper limb in cerebral palsy using the non-invasive interface “brain-computer”. *Neuromuscular*

- diseases. 2019; 11 (4): 12–20. Russian.
12. Bazanova OM, Vernon D. Interpreting EEG alpha activity. *Neurosci Biobehav Rev.* 2014; 44: 94–110.
 13. Pfurtscheller G, Brunner C, Schlögl A, Lopes da Silva FH. Mu rhythm (de)synchronization and EEG single-trial classification of different motor imagery tasks. *NeuroImage.* 2006; 31 (1): 153–9.
 14. Llanos C, Rodríguez M, Rodríguez-Sabate C, Morales I, Sabate M. Mu-rhythm changes during the planning of motor and motor imagery actions. *Neuropsychologia.* 2013; 51 (6): 1019–26.
 15. Klimesch W. Alpha-band oscillations, attention, and controlled access to stored information. *Trends Cogn Sci.* 2012; 16 (12): 606–17.
 16. Kotov SV, Romanova MV, Kondur AA, Biryukova EV, Frolov AA, Turbina LG i dr. Reorganizacija bioelektricheskoy aktivnosti neokorteksa posle insul'ta v rezul'tate reabilitacii s ispol'zovaniem interfejsa «mozg–komp'yuter», upravljajushhego jekzoskeletom kisti. *Zhurnal vysshej nervnoj dejatel'nosti im. I. P. Pavlova.* 2020; 70 (2): 217–30. Russian.
 17. Bobrov PD, Korshakov AV, Roshhin VYu, Frolov AA. Bajesovskij podhod k realizacii interfejsa mozg–komp'yuter, osnovannogo na predstavlenii dvizhenij. *Zhurnal vysshej nervnoj dejatel'nosti im. I. P. Pavlova.* 2012; 62 (1): 89–99. Russian.
 18. Shin YK, Lee DR, Hwang HJ, You SJ, Im CH. A novel EEG-based brain mapping to determine cortical activation patterns in normal children and children with cerebral palsy during motor imagery tasks. *Neurorehabilitation.* 2012; 31 (4): 349–55.
 19. Inuggi A, Bassolino M, Tacchino C, Pippo V, Bergamaschi V, Campus C, et al. Ipsilesional functional recruitment within lower mu band in children with unilateral cerebral palsy, an event-related desynchronization study. *Exp Brain Res.* 2018; 236 (2): 517–27.
 20. Démas J, Bourguignon M, Périer M, De Tiège X, Dinomais M, Van Bogaert P. Mu rhythm: State of the art with special focus on cerebral palsy. *Annals of Physical and Rehabilitation Medicine [Internet].* 2019 June [cited 2019 July 9]. Available from: <https://doi.org/10.1016/j.rehab.2019.06.007>.
 21. Weinstein M, Green D, Rudisch J, Benthem M, Zielinski IM, Jongsma MLA, et al. Understanding the relationship between brain and upper limb function in children with unilateral motor impairments: A multimodal approach. *Eur J Paediatr Neurol.* 2018; 22 (1): 143–54.
 22. Koessler L, Maillard L, Benhadid A, Vignal JP, Felblinger J, Vespignani H, et al. Automated cortical projection of EEG sensors: Anatomical correlation via the international 10–10 system. *NeuroImage.* 2009; 46 (1): 64–72.
 23. Cavanna AE, Trimble MR. The precuneus: a review of its functional anatomy and behavioural correlates. *Brain.* 2006; 12 (30): 564–83.

Литература

1. Graham HK, Rosenbaum P, Paneth N, Dan B, Lin JP, Damiano DL, et al. Cerebral palsy. *Nat Rev Dis Primers.* 2016; 2: 15082. DOI: 10.1038/nrdp.2015.82.
2. Patel DR, Neelakantan M, Pandher K, Merrick J. Cerebral palsy in children: a clinical overview. *Transl Pediatr.* 2020; 9 (Suppl 1): 125–35.
3. Фролов А. А., Бобров П. Д. Интерфейс мозг–компьютер: нейрофизиологические предпосылки и клиническое применение. *Журнал высшей нервной деятельности им. И.П. Павлова.* 2017; 67 (4): 365–76.
4. Chiew M, LaConte S, Graham S. Investigation of fMRI neurofeedback of differential primary motor cortex activity using kinesthetic motor imagery. *NeuroImage.* 2012; 61 (1): 21–31.
5. Котов С. В., Турбина Л. Г., Бобров П. Д., Фролов А. А., Павлова О. Г., Курганская М. Е. и др. Реабилитация больных, перенесших инсульт, с помощью биоинженерного комплекса «интерфейс мозг–компьютер + экзоскелет». *Журнал неврологии и психиатрии им. С. С. Корсакова.* 2014; 114 (12–2): 66–72.
6. Фролов А. А., Мокиенко О. А., Люкманов Р. Х., Черникова Л. А., Котов С. В., Турбина Л. Г. и др. Предварительные результаты контролируемого исследования эффективности технологии ИМК–экзоскелет при постинсультном парезе руки. *Вестник РГМУ.* 2016; 2: 17–25.
7. Ponce P, Molina A, Balderas DC, Grammatikou D. Brain Computer Interfaces for Cerebral Palsy. In: E. Suraka, editor. *Cerebral Palsy challenges for the future.* London: IntechOpen, 2014; p. 245–72. DOI: 10.5772/57084.
8. Jochumsen M, Shafique M, Hassan A, Niazi IK. Movement intention detection in adolescents with cerebral palsy from single-trial EEG. *J Neural Eng.* 2018; 15 (6): 066030. DOI: 10.1088/1741-2552/aae4b8.
9. Daly I, Billinger M, Laparra-Hernández J, Aloise F, Lloria García M, Faller J, et al. On the control of brain-computer interfaces by users with cerebral palsy. *Clin Neurophysiol.* 2013; 124 (9): 1787–97.
10. Kim T-W, Lee B-H. Clinical usefulness of brain-computer interface-controlled functional electrical stimulation for improving brain activity in children with spastic cerebral palsy: a pilot randomized controlled trial. *J Phys Ther Sci.* 2016; 28 (9): 2491–4.
11. Ларина Н. В., Корсунская Л. Л., Власенко С. В. Комплекс «Экзокисть-2» в реабилитации верхней конечности при детском церебральном параличе с использованием неинвазивного интерфейса «мозг–компьютер». *Нервно-мышечные болезни.* 2019; 11 (4): 12–20.
12. Bazanova OM, Vernon D. Interpreting EEG alpha activity. *Neurosci Biobehav Rev.* 2014; 44: 94–110.
13. Pfurtscheller G, Brunner C, Schlögl A, Lopes da Silva FH. Mu rhythm (de)synchronization and EEG single-trial classification of different motor imagery tasks. *NeuroImage.* 2006; 31 (1): 153–9.
14. Llanos C, Rodríguez M, Rodríguez-Sabate C, Morales I, Sabate M. Mu-rhythm changes during the planning of motor and motor imagery actions. *Neuropsychologia.* 2013; 51 (6): 1019–26.
15. Klimesch W. Alpha-band oscillations, attention, and controlled access to stored information. *Trends Cogn Sci.* 2012; 16 (12): 606–17.
16. Котов С. В., Романова М. В., Кондур А. А., Бирюкова Е. В., Фролов А. А., Турбина Л. Г. и др. Реорганизация биоэлектрической активности неокортекса после инсульта в результате реабилитации с использованием интерфейса «мозг–компьютер», управляющего экзоскелетом кисти. *Журнал высшей нервной деятельности им. И. П. Павлова.* 2020; 70 (2): 217–30.
17. Бобров П. Д., Коршаков А. В., Рощин В. Ю., Фролов А. А. Байесовский подход к реализации интерфейса мозг–компьютер, основанного на представлении движений. *Журнал высшей нервной деятельности им. И. П. Павлова.* 2012; 62 (1): 89–99.
18. Shin YK, Lee DR, Hwang HJ, You SJ, Im CH. A novel EEG-based brain mapping to determine cortical activation patterns in normal children and children with cerebral palsy during motor imagery tasks. *Neurorehabilitation.* 2012; 31 (4): 349–55.
19. Inuggi A, Bassolino M, Tacchino C, Pippo V, Bergamaschi V, Campus C, et al. Ipsilesional functional recruitment within lower mu band in children with unilateral cerebral palsy, an event-related desynchronization study. *Exp Brain Res.* 2018; 236 (2): 517–27.
20. Démas J, Bourguignon M, Périer M, De Tiège X, Dinomais M, Van Bogaert P. Mu rhythm: State of the art with special focus on cerebral palsy. *Annals of Physical and Rehabilitation Medicine [Internet].* 2019 June [cited 2019 July 9]. Available from: <https://doi.org/10.1016/j.rehab.2019.06.007>.
21. Weinstein M, Green D, Rudisch J, Benthem M, Zielinski IM, Jongsma MLA, et al. Understanding the relationship between brain and upper limb function in children with unilateral motor impairments: A multimodal approach. *Eur J Paediatr Neurol.* 2018; 22 (1): 143–54.
22. Koessler L, Maillard L, Benhadid A, Vignal JP, Felblinger J, Vespignani H, et al. Automated cortical projection of EEG sensors: Anatomical correlation via the international 10–10 system. *NeuroImage.* 2009; 46 (1): 64–72.
23. Cavanna AE, Trimble MR. The precuneus: a review of its functional anatomy and behavioural correlates. *Brain.* 2006; 12 (30): 564–83.

THROMBOGENICITY IN PATIENTS WITH ISCHEMIC STROKE AND PRE-EXISTING POLYCYTHEMIA VERA

Tanashyan MM¹, Shabalina AA¹ ✉, Roitman EV¹, Vavilova TV², Kuznetsova PI¹¹ Research Center of Neurology, Moscow, Russia² Almazov National Medical Research Centre, Saint Petersburg, Russia

Thrombogenicity and its causes in patients with ischemic stroke (IS) and pre-existing polycythemia vera (PV) is a significant clinical concern. The aim of this study was to identify the range of factors associated with increased thrombogenicity in patients with IS and pre-existing PV. We performed a physical examination and laboratory tests on 127 patients in the hyperacute stroke stage and 16–18 months after. Of them, 68 patients had PV (the main group) and 59 did not have this condition (the comparison group). Laboratory tests were conducted to evaluate blood rheology, hemostasis, endothelial function, angiogenesis, proinflammatory cytokine levels; we also tested patients for the presence of the V617F mutation in the *JAK2* gene and analyzed the contribution of all studied parameters to the development of thrombotic and hemorrhagic complications. We found that the neurological picture did not differ between the groups: mean NIHSS scores were 12 and 13 points, respectively. Morphological and functional characteristics of red blood cells and platelets, hemostasis and cytokine profiles were compared between patients with IS and pre-existing PV and the comparison group. One of the key elements in potentiating thrombotic complications in patients with IS and PV was *JAK2* V617F allele burden. The obtained data suggest the cumulative effect of the identified factors promoting thrombus formation in post-stroke patients with PV and overpowering the effect of antiplatelet therapy.

Keywords: ischemic stroke, polycythemia vera, thrombosis, blood rheology, hemostasis, angiogenesis

Author contribution: Tanashyan MM — study concept and design; discussion and manuscript preparation; Shabalina AA — literature analysis; data acquisition and statistical analysis; results discussion; Roitman EV, Vavilova TV — literature analysis; results discussion; Kuznetsova PI — patient histories; results discussion.

Compliance with ethical standards: the study was approved by the local Ethics Committee (Protocol № 1–4/18 dated February 7, 2018). Informed consent was obtained from all study participants.

✉ **Correspondence should be addressed:** Alla A. Shabalina
Volokolamskoe shosse, 80/1, Moscow, 125367; shabalina@neurology.ru

Received: 11.08.2020 **Accepted:** 25.08.2020 **Published online:** 31.08.2020

DOI: 10.24075/brsmu.2020.052

ТРОМБОГЕННОСТЬ У БОЛЬНЫХ ИШЕМИЧЕСКИМ ИНСУЛЬТОМ НА ФОНЕ ИСТИННОЙ ПОЛИЦИТЕМИИ

М. М. Танашян¹, А. А. Шабалина¹ ✉, Е. В. Ройтман¹, Т. В. Вавилова², П. И. Кузнецова¹¹ Научный центр неврологии, Москва, Россия² Национальный медицинский исследовательский центр имени В. А. Алмазова, Санкт-Петербург, Россия

Проблема возникновения и возможные причины тромбогенности у пациентов с ишемическим инсультом (ИИ) на фоне истинной полицитемии (ИП) остается актуальной. Целью исследования было определить комплекс факторов, ассоциированных с формированием высокой тромбогенности у пациентов с ИИ на фоне ИП. Проведено комплексное клиничко-лабораторное обследование 127 пациентов в острейшем периоде ИИ и спустя 16–18 месяцев: 68 пациентов с ИИ на фоне истинной полицитемии ИП (основная группа) и 59 пациентов с ИИ без ИП (группа сравнения). Лабораторное обследование включало определение гемореологических параметров, показателей системы гемостаза, функции эндотелия, активности ангиогенеза, цитокинового и воспалительного ряда, молекулярно-генетическое исследование мутации V617F в гене *JAK2* и анализ вклада их изменений в развитие тромбогеморрагических осложнений. Обнаружено, что неврологическая картина в обеих группах была без значимых различий со средней оценкой по шкале NIHSS 12 и 13 баллов соответственно. Отмечены особенности морфофункциональных характеристик эритроцитов и тромбоцитов, а также гемостазиологического и цитокинового профиля у пациентов с ИИ на фоне ИП по сравнению с группой сравнения. Одним из ключевых элементов в потенцировании тромботических осложнений у пациентов с ИИ и ИП стала величина аллельной нагрузки мутации V617F в гене *JAK2*. Полученные данные свидетельствуют о совокупном действии комплекса факторов, формирующих высокую тромбогенность у перенесших ИИ пациентов с ИП и преодолевающих суммарный эффект антитромботической терапии.

Ключевые слова: ишемический инсульт, истинная полицитемия, тромбоз, гемореология, гемостаз, ангиогенез

Вклад авторов: М. М. Танашян — идеология и дизайн исследования, обсуждение результатов и редактирование рукописи; А. А. Шабалина — литературный обзор, сбор и анализ материала, статистическая обработка данных, обсуждение результатов; Е. В. Ройтман, Т. В. Вавилова — литературный обзор, обсуждение результатов; П. И. Кузнецова — описание клинического материала, обсуждение результатов.

Соблюдение этических стандартов: исследование одобрено локальным этическим комитетом (протокол № 1–4/18 от 07 февраля 2018 г.). Все пациенты подписали информированное согласие на проведение обследований.

✉ **Для корреспонденции:** Алла Анатольевна Шабалина
Волоколамское шоссе, д. 80/1, г. Москва, 125367; shabalina@neurology.ru

Статья получена: 11.08.2020 **Статья принята к печати:** 25.08.2020 **Опубликована онлайн:** 31.08.2020

DOI: 10.24075/vrgmu.2020.052

Despite phenotypic heterogeneity, all subtypes of ischemic stroke (IS) share a common underlying mechanism: interruption of micro- and macrovascular blood flow in brain-supplying vessels. Thrombosis develops as a complex multifactorial process involving changes in blood rheology, loss of antithrombotic properties by the endothelium, initiation of systemic inflammatory response, and homeostatic imbalance [1, 2]. Cerebrovascular disorders (CVD) often strike in the

setting of Ph-negative myeloproliferative neoplasms (MPN) [3, 4]. Polycythemia vera (PV) is a Ph-negative MPN that causes severe, frequent thrombohemorrhagic complications, including CVD. PV arises from myeloproliferation of hematopoietic stem cells in the bone marrow followed by successful terminal differentiation of hematopoietic progenitors into mature cells. This results in the sustained elevation of hemoglobin and erythrocyte count in the peripheral blood [5, 6].

PV can be caused by proliferation of 3 myeloid lineages, including erythroid, granulocytic and megakaryocytic. In recent years, the prevalence of erythrocytosis has been on the rise and is now 0.6–2.8 per 100,000 population. The etiology of PV is still vague and largely attributed to the exposure to genome-damaging environmental or other external factors. The 2005 discovery of the V617F mutation in the *Jak2* gene has dramatically expanded our knowledge of PV pathogenesis and biology: V617F occurs in more than 98% of patients with PV and is a diagnostic criterion [7–9].

Being a hematologic disorder, PV is also recognized as a vascular problem fraught with risk of thrombotic, hemorrhagic and cerebral complications. One of the most common manifestations of vascular pathology in patients with PV is arterial hypertension (AH); it affects 60–80% of patients with PV at any stage of the disease, including clinical and hematologic remission [10–12].

Among the most common and dangerous vascular complications of PV are arterial/venous thrombosis, focal or multifocal hemorrhages or bleeding, and disseminated intravascular coagulation. Clinically, they present as strokes, myocardial infarction, deep vein thrombosis, and pulmonary embolism [13]. On average, patients with PV are at two times higher risk of blood vessel occlusion [14]. In such patients, vein thrombosis in the lower extremities is accompanied by inflammation, edema and hyperemia (similarly to thrombophlebitis). Portal vein thrombosis leads to portal hypertension, splenomegaly, esophageal varices, ascites, and Budd–Chiari syndrome [15, 16].

There are a few factors contributing to thrombosis in the setting of PV: high hematocrit, high red blood cell and platelet counts, reduced fibrinolytic activity, leukocyte activation, endothelial damage, platelet-endothelium interactions, the JAK2 V617F mutation, therapy, and increased blood viscosity [17]. The latter is hypothesized to be the leading factor potentiating thrombosis in patients with PV. The available literature on the role of hemostasis, rheological and microcirculatory factors in promoting thrombotic complications in patients with PV leaves unanswered the question of how such complications develop in patients with IS and comorbid PV [18–20]. In light of the aforementioned facts, the aim of this paper was to study factors associated with increased thrombogenic potential in patients with IS and pre-existing PV.

METHODS

We examined 127 patients with first-time IS, including 68 patients with IS and pre-existing PV (group I, or the main group), and 59 patients with IS but without PV (group II, or the comparison group). The groups did not differ in terms of age or sex.

The following inclusion criteria were applied: 1) age of 42–75 years; 2) hyperacute stroke and the follow-up examination 16–18 months after it (median of 17.3 months; 95% CI 16.4–18.3); 3) IS confirmed by neuroimaging; PV diagnosed according to WHO criteria (TOAST subtype: stroke of other determined etiology [21]); 4) cytoreductive therapy for PV (hydroxyurea or IFN- α in combination with antiplatelet drugs, such as aspirin) before stroke; 5) erythrocytapheresis in all patients with PV (2–6 sessions a year).

The studied cohort of patients was dominated by women (64% in group I and 67% in group II). Diabetics and smokers were less prevalent in the main group; dyslipidemia was diagnosed in 25% of patients with isolated IS and only in 3% of main group patients.

Physical examination included general and neurological health assessments with the NIHSS scale, the Barthel index

(on admission) and the modified Rankin scale (1.5 years after stroke). The following laboratory tests were performed:

1) complete blood count on a MEK-7222 analyzer (Nihon Kohden; Japan);

2) evaluation of erythrocyte rheology (aggregation amplitude Amp, a.u.); time to rouleaux formation (Tf, s) and time to 3D aggregation (Ts, s); aggregation index (AI, a.u.); complete disaggregation rate (Y-dis, a.u.), which represents the force needed to break up RBC aggregates and deform RBC (Dlmax, a.u.). The measurements were conducted using a laser-assisted RBC aggregometer (LORRCA, Mechatronics; Netherlands);

3) evaluation of hemostasis and endothelial function (ATP-, adrenaline-induced platelet aggregation (ATP-Adr-PA, %) and ristocetin cofactor test, which measures the functional activity of von Willebrand factor (RCA-VWF, %); the tests were done using an aggregometer (Biola; Russia) and RENAM reagent kits (RENAM; Russia). Besides, we measured fibrinogen concentration (FG, g/L), activated partial thromboplastin time (APTT, s), prothrombin time (s; test results were expressed as the international normalized ratio INR), D-dimer levels (ng/ml), activity of protein C (PC, %), protein S (PS, %), von Willebrand factor (A – VWF, %), plasma coagulation factors V, VII, VIII, XII (%), antithrombin III (AT III, %), plasminogen (PLG, %), alpha2-antiplasmin (PL-IN, %), and von Willebrand factor antigen (VWF, %). The tests were performed using an ACL Elite Pro automatic hemostasis analyzer (Instrumentation Laboratory; USA) and reagents by IL (USA) and RENAM (Russia);

4) measurements of cytokines, inflammation, endothelial function and angiogenesis markers, including vascular endothelial growth factor A (VEGF-A, pg/ml), fibroblast growth factor β (FGF β , pg/ml), transforming growth factor β (TGF β 1, pg/ml), tissue plasminogen activator (t-PA, ng/ml), plasminogen activator inhibitor (PAI-1, ng/ml), tissue factor (TF, pg/ml), metalloproteinase ADAMTS-13 (μ g/ml), soluble thrombomodulin (sTM, ng/ml), soluble intercellular adhesion molecules sICAM and sVCAM, thrombin-activated fibrinolysis inhibitor (TAFI, %), tumor necrosis factor α (TNF α , pg/ml), interleukins IL1 β and IL6 (pg/ml), endothelin-1 (pg/ml), and nitrogen oxide (NO, μ mol/l). The measurements were conducted ELISA assays and reagent kits by eBioscience Bender MedSystems (Austria), Technoclone (Austria), Cloud Clone Corporation (USA, China), R&D Systems (USA, China), Cayman Ataxia (India), Vector-Best (Russia), and Sekisui Diagnostics (American Diagnostica; USA);

5) molecular tests for the V617F mutation in the JAK2 gene; the tests were conducted using assays by GenoTechnology, Russia, and a Real-time DT-Lite PCR thermal cycler (DNA-Technology; Russia).

Statistical analysis was carried out in IBMSPSS 23.0 and R 3.4.3 (IBM Company; USA). Descriptive statistics for categorical data are provided below as frequencies and proportions (%). For normally distributed quantitative data, the results are presented as a mean value (M) and a standard deviation (SD). For non-normal distribution, medians (Md), upper and lower quartiles (Q 25%–75%) were used. For group comparisons, the Kruskal–Wallis test was applied followed by the Mann–Whitney U test for pairwise comparison. Associations between the studied variables were measured using Pearson's correlation analysis. Risks were assessed with the chi square test, contingency tables and OR. Principal component analysis of the correlation matrix was employed for factor extraction, considering weights >1 and the variable loading.

RESULTS

On admission, the neurological picture in both groups was almost the same; mean NIHSS scores were 12 (5.0; 20.0) and 13 points (5.0; 20.0), respectively.

Severe neurological deficit was observed in 16 stroke patients with PV (24%); in patients without PV it was significantly less frequent (11 patients, or 19%). Moderate neurological deficit was observed in 33 patients with PV (50%) and 36 patients without PV (61%), which is significantly more often. Mild deficits manifested as mild sensory disturbances were present in 17 patients with PV (26%) and 12 patients without PV (20%). Barthel index values did not differ significantly between the groups, equaling 70 (59; 76) in group I and 72 (62; 75) in group II.

Pyramidal syndrome was the main neurological symptom of IS in most study participants, presenting as marked hemiparesis or hemiplegia with sensory disturbances in 27% and 29% of patients in groups I and II, respectively.

Speech impairments (total, sensory, motor, or mixed aphasias) and cortical dysarthria were almost equally observed in both groups, affecting 45 (66%) patients in the main group and 38 (60%) patients in the control group. No significant differences were detected between the groups in terms of major neurological symptoms in the acute phase of CVD.

Neurological deficit dynamics were analyzed over the 1.5-year period from the end of the acute IS phase to the follow-up examination. We found that by the time of the follow-up examination, the frequencies of motor, sensory and speech impairments had decreased by 14, 20 and 25%, respectively; patients reported no reduction in the frequency of headaches and only slight improvement in the asthenic syndrome. According to the modified Rankin scale, functional recovery profiles 16–18 months after IS were good (0–1 points) in 18 patients (27%), satisfactory (2–3 points) in 26 patients (38%) and poor (4–5 points) in 24 patients (35%).

Complete blood counts and blood rheology tests performed in the acute phase of IS exposed significantly elevated platelets (613 vs. $271 \times 10^9/L$), RBC count (5.8 vs. $3.8 \times 10^{12}/L$), WBC count (12.6 vs. $8.7 \times 10^9/L$), hemoglobin (174 vs. 119 g/L), and hematocrit (49.5 vs. 38.7%) in patients with PV; their ESR was low (5 vs. 23 mm/h) and all studied morphological and functional erythrocyte characteristics were much worse than in patients without PV. In patients with PV vs. without PV, the aggregation index and the aggregation amplitude (12.8 and 9.3 a.u., respectively; $p = 0.003$), as well as the complete

disaggregation rate, which reflects the density of erythrocyte aggregates (570 and 224 a.u.; $p = 0.000$), were significantly increased in the setting of reduced erythrocyte deformability (0.34 and 0.41 a.u., respectively; $p = 0.000$). We also found that cytokines, FGF β (735.5 vs. 497.1 pg/ml), VEGF-A ($1,257.6$ vs. 568.4 pg/ml), TGF β_1 ($1,824$ vs. 710 pg/ml; $p = 0.000$), and angiogenesis markers were significantly elevated in patients with PV.

Hemostasis profiles of patients with IS with or without pre-existing PV are compared in Fig. 1.

In comparison with patients without PV, individuals with PV had higher concentrations of fibrinogen, p-thrombomodulin, increased TAFI, TF and coagulation factor VII activities, lower concentrations and decreased activity of VWF, ATIII and ADAMTS-13. In the comparison group, coagulation factor VIII exhibited higher activity and D-dimers were also higher, whereas PLG and tPA were decreased and PAI-1 was elevated.

In order to analyze the effect of JAK2 V617F allele burden on the thrombotic potential in the hyperacute phase of IS, we performed dimensionality reduction through factor analysis and identified factors with at least moderate loading (JAK2 V617F allele burden was assumed to be the leading variable with the highest loading). We identified 10 laboratory parameters having the strongest association with JAK2 V617F allele burden (Table 1).

High JAK2 V617F allele burden had the most pronounced effect on the reduction in erythrocyte deformability and the increase in coagulation factor VII activity. High JAK2 V617F allele burden was associated with the activation of pathologic angiogenesis mediated by VEGF-A and TGF β_1 , high platelet count co-occurring with changes in platelet aggregation properties and endothelial dysfunction.

During the follow-up examination (16–18 months after stroke), we estimated the frequency of thrombotic and hemorrhagic complications developed over this period (Table 2).

The number of thrombotic, hemorrhagic and mixed complications in the main group was higher than in the comparison group; one of the key elements in potentiating thrombotic complications in patients with PV (manifested predominantly as recurrent CVD) was JAK2 V617F allele burden (Table 3).

The odds ratio for recurrent ischemic CVD in the long-term period based on JAK2 V617F allele burden in the hyperacute

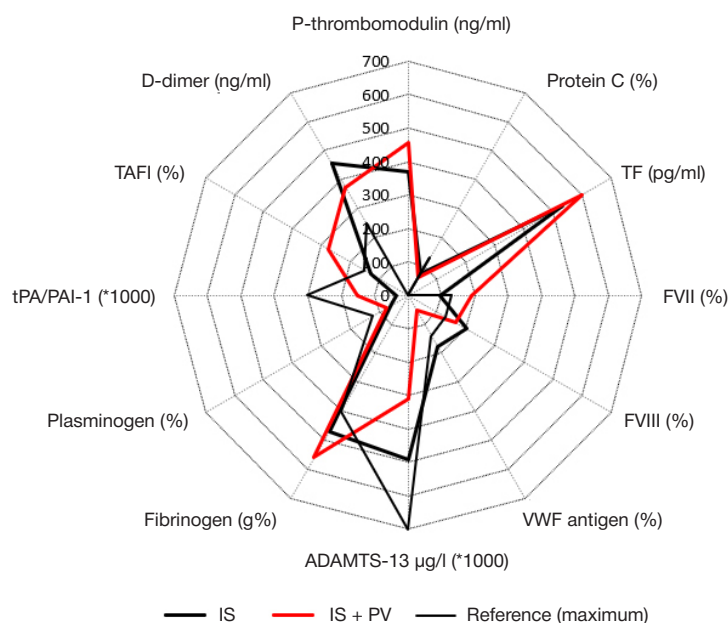


Fig. 1. Hemostasis profiles of patients in the hyperacute IS stage. ADAMTS-13 and fibrinogen concentrations and the tPA/PAI-1 ratio are shown concisely to fit into the overall hemostasis profile picture

Table 1. A correlation matrix showing effects of JAK2 V617F allele burden on the laboratory parameters in patients with PV in the hyperacute stroke phase

	Tested parameters	Component
	JAK2 V617F allele burden	0.722
1	RBC deformability (Dlmax), a.u.	0.492
2	Factor VII, %	0.464
3	VEGF-A, pg/ml	0.425
4	ADAMTS-13, µg/ml	0.412
5	TGF-β ₁ , pg/ml	0.398
6	ATP-PA, %	0.367
7	Platelet count (10 ⁹ /L)	0.354
8	WBC count (10 ⁹ /L)	0.341
9	VWF activity, %	0.323
10	t-PA, ng/ml	0.318

stroke phase with a threshold value of 48% was 2.9 times (95% CI 2.0–3.3).

Among the hemorheological risk factors for recurrent thrombotic complications in the long-term poststroke period were a decline in the complete RBC disaggregation rate (γDis) from 570 to 498 a.u. ($p = 0.017$), elevation of endothelin-1 concentrations from 4.6 to 5.2 pg/ml and elevation of adhesion molecules concentration (sVCAM-1 ($p = 0.008$) and sICAM-1 ($p = 0.007$)). Increasing microcirculation disturbances might have caused or resulted in pronounced inflammatory response reflected in heightened IL6 levels (from 13.5 ± 0.69 pg/ml to 15.2 ± 0.7 pg/ml ($p = 0.034$)).

Almost no differences were observed between the hyperacute stroke phase and the long-term poststroke period in terms of hemostasis profiles of our patients (Fig. 2).

DISCUSSION

Hemostatic homeostasis is regulated by the balance of thrombogenic and antithrombogenic factors. If the balance is shifted towards secretion of procoagulation molecules, thrombosis develops. Therefore, it is important to identify causes, conditions and drivers of first-time and recurrent thrombosis in the affected patients., or, in other words, to timely detect pre-thrombosis or the so-called thrombotic

preparedness [21], which combines clinical signs of pre-thrombosis and laboratory markers of thrombogenic potential. Reinforced by persisting factors of thrombotic risk and high likelihood of such risk, thrombotic preparedness can present as recurrent CVD and variously localized thrombosis.

According to Virchow's triad, changes of blood flow characteristics that can potentially trigger thrombotic complications are among the underlying causes of thrombosis.

It is noteworthy that prior or after stroke, patients with PV were receiving specific cytoreductive therapy (hydroxyurea or IFNα). On the one hand, cytoreductive therapy is an additional risk factor for IS and thrombotic complications in this cohort of patients. On the other hand, given that no significant differences were observed in the effect of cytoreductive therapy on the studied parameters, we can link changes in the studied laboratory parameters to the course and sequelae of IS in patients with pre-existing PV.

Blood counts were significantly elevated in patients going through the hyperacute phase of IS; RBC function and morphology were significantly compromised, which was associated with changes in membrane plasticity, substantial reduction in RBC deformability and increased RBC aggregates.

In general, the hyperacute phase of IS was characterized by multiple signs of vascular wall damage and endotheliopathy accompanied by formation of a prothrombotic endothelial

Table 2. Thrombotic and hemorrhagic complications in patients detected on the follow-up examination 16–18 months after IS

Groups	IS + PV ($n = 68$)	IS ($n = 59$)
Complications		
Thrombotic complications (n)	28	18
– ischemic CVD	16	10
– venous thrombosis of lower extremities	12	8
– Pulmonary embolism	0	0
Г Hemorrhagic syndrome (n)	20	n/a
– nasal, gingival, subcutaneous, hemorrhoidal bleedings	18	n/a
– gastrointestinal bleeding	2	1
Mixed thrombotic and hemorrhagic complications	7	0

Note: n/a — data not available.

Table 3. Coefficients of JAK2 V617F allele burden correlation with long-term thrombotic complications

	Pearson's correlation coefficient
All thrombotic complications, of them:	0.236 ($p < 0.05$)
– ischemic CVD	0.241 ($p < 0.05$)
– venous thrombosis of lower extremities	0.124
– mixed thrombotic and hemorrhagic complications	0.116

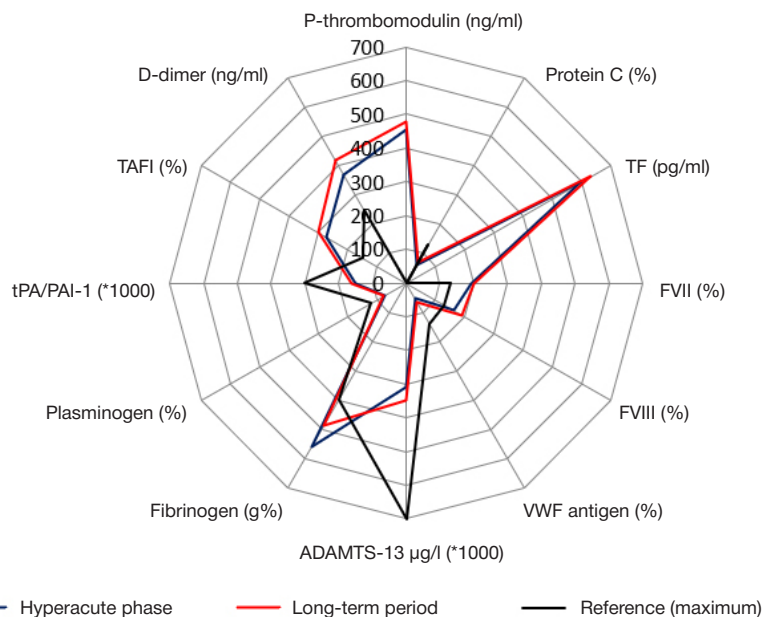


Fig. 2. Hemostasis profiles of main group patients in the hyperacute IS phase and in the long-term stroke period

phenotype. This is indicated by the fact that in both groups of patients with IS, suppressed protein C activity was not compensated by thrombomodulin, which is normally bound to the endothelial cell membrane and is nearly absent in the bloodstream. Its presence in the bloodstream signals significant damage to endothelial cells.

The thrombotic potential of patients with IS and pre-existing PV greatly depended on the tissue factor and coagulation factor VII, whereas for patients with IS the balance between vWF, coagulation factor VIII and ADAMTS-13 were more important contributors to IS. Nevertheless, inflammatory response can be regarded as an initiator of increased thrombotic potential specifically in comorbid patients, as suggested by lower activity of antithrombin III and higher concentrations of fibrinogen, studied cytokines and growth factors. Besides, hypothetically, inflammation might have been promoted by a combination of factors typical to a myeloproliferative process: the presence of neutrophil extracellular traps (NET), circulating free DNA, etc. [22]. Therefore, higher levels of tissue factor and coagulation factor VII in patients with IS and pre-existing PV should be interpreted as secondary signs of endotheliopathy.

Fibrinolysis is traditionally seen as a compensatory mechanism for such condition; in our study, fibrinolytic activity was markedly depressed in both groups, which was manifested as reduced plasminogen reserve, tPA deficit and prevailing activity of fibrinolysis inhibitors. In patients with IS and pre-existing PV, excess generation of thrombin resulting from inflammation also suppressed fibrinolysis through a pronounced increase in TAFI activity.

JAK2 V617F allele burden is a substantial contributor to the development of thrombotic complications (predominantly recurrent CVD). Higher burden is associated with decreased RBC functional properties, activation of pathologic angiogenesis,

increased platelet count, and changes in platelet functional properties in combination with endothelial dysfunction.

Our findings show that the hematologic disorder was the main driver of the thrombotic potential in patients with IS and pre-existing PV. Being a risk factor for thrombosis per se, myeloproliferation was sufficient to trigger thrombotic complications in spite of antithrombotic and cytoreductive therapy received by the patients. Over the 1.5-year followup, pronounced endotheliopathy and the intensity of hemocoagulatory and fibrinolytic activities in patients with IS and pre-existing PV did not undergo any significant changes, and increased systemic thrombotic activity did not attenuate. Considering that arterial or venous thrombosis is a life-threatening situation, it is essential to refine diagnostic and therapeutic methods for vascular ischemia and to prevent the recurrence of vascular events. These facts necessitate 1) further research into the pathogenesis of increased thrombotic potential/ thrombosis in MPN; 2) changes in diagnostic algorithms and standard antithrombotic regimens, including the adoption of personalized approaches to treatment and hemostasis monitoring.

CONCLUSIONS

Our findings suggest that the cumulative effect of all the factors contributing to high thrombotic potential in patients with IS and pre-existing PV overpower the effect of antiplatelet therapy. This happens due to the persistence of almost all prothrombotic conditions promoted by inflammation and manifesting as disturbances in blood rheology, endotheliopathy, thrombinemia and depressed fibrinolysis. This corroborates the postulates about the need for individually tailored and well-reasoned long-term antiplatelet therapy and prophylaxis of recurrent vascular events.

References

1. Suslina ZA, Tanashjan MM, Ionova VG. Ishemicheskij insul't: krov', sosudistaja stenka, antitromboticheskaja terapija. M.: Medicinskaja kniga, 2005; 248 s. Russian.
2. Phipps MS, Cronin CA. Management of acute ischemic stroke. *BMJ*. 2020; 368: l6983. Published 2020 Feb 13. DOI: 10.1136/bmj.l6983.

3. Tanashyan MM, Melikyan AL, Kuznetsova PI, Raskurazhev AA, Shabalina AA, Kononov RN. Brain MRI-findings in Ph-negative myeloproliferative disorders. *Terapevticheskiy Arkhiv*. 2019; 91 (7): 29–34. Russian.
4. Asakura H. Thrombosis in myeloproliferative neoplasms. *The Japanese Journal of Clinical Hematology*. 2018; 59 (8): 1034–41. DOI: 10.11406/rinketsu.59.1034.
5. Tefferi A, Barbui T. Polycythemia vera and essential thrombocythemia: 2017 update on diagnosis, risk-stratification, and management. *Am J Hematol*. 2017; 92 (1): 94–108. DOI: 10.1002/ajh.24607.
6. Barbui T, Thiele J, Gisslinger H, et al. The 2016 WHO classification and diagnostic criteria for myeloproliferative neoplasms: document summary and in-depth discussion. *Blood Cancer J*. 2018; 8 (2): 15. Published 2018 Feb 9. DOI: 10.1038/s41408-018-0054-y.
7. Kaifia A, Kirschner M, Wolf D, Maintz C, Hänel M, Gattermann N, et al. Bleeding, thrombosis, and anticoagulation in myeloproliferative neoplasms (MPN): analysis from the German SAL-MPN-registry. *J Hematol Oncol*. 2016; 9: 18. Available from: <https://doi.org/10.1186/s13045-016-0242-9>.
8. Moulard O, Mehta J, Olivares R, Iqbal U, Mesa RA. Epidemiology of Myelofibrosis (MF), Polycythemia Vera (PV) and Essential Thrombocythemia (ET) in the European Union (EU). *Blood*. 2012; 120 (21): 1744. Available from: <https://doi.org/10.1182/blood.V120.21.1744.1744>.
9. Volkova MA, редактор. *Klinicheskaja onkogematologija: rukovodstvo dlja vrachej*. M.: Medicina, 2007; 1144 s. Russian.
10. Kozlova NS, Baksheev MG, Davydkin IL. Osobennosti narushenij mikrocirkuljacii u bol'nyh istinnoj policitemiej v sochetanii s arterial'noj gipertenziej. *Izvestija Samarskogo nauchnogo centra RAN*. 2015; 17 (2): 319–22. Russian.
11. Davydkin IL, Shhukin YuV, redaktory. *Poliklinicheskaja terapija: uchebnyk*. M.: GJeOTAR-Media, 2013; 688 s. Russian.
12. Rukavicyun OA, редактор. *Gematologija: nacional'noe rukovodstvo*. M.: GJeOTAR-Media, 2015; 776 s. Russian.
13. Kwaan HC, Wang J. Hyperviscosity in polycythemia vera and other red cell abnormalities. *Semin Thromb Hemost*. 2003; 29 (5): 451–8.
14. Fujioka S. Rheological study on vascular occlusion and cellular hyperviscosity syndrome in polycythemia vera. *Nihon Ketsueki Gakkai Zasshi*. 1989; 52 (4): 688–95.
15. Pratesi A, Vella A, Pasini E, Salvi F, Mascalchi M. Parkinsonism in polycythaemia vera probably due to manganism. *Mov Disord*. 2008; 23 (16): 2420–1. DOI: 10.1002/mds.22319.
16. Cerquozzi S, Barraco D, Lasho T, et al. Risk factors for arterial versus venous thrombosis in polycythemia vera: a single center experience in 587 patients. *Blood Cancer J*. 2017; 7 (12): 662. Published 2017 Dec 27. DOI: 10.1038/s41408-017-0035-6.
17. Marchioli R, Finazzi G, Specchia G, Masciulli A, Mennitto MR, Barbui T. The CYTO-PV: A Large-Scale Trial Testing the Intensity of CYTOreductive Therapy to Prevent Cardiovascular Events in Patients with Polycythemia Vera. *Thrombosis*. 2011; 2011 (1): 1–9. DOI: 10.1155/2011/794240.
18. Frederiksen H, Szépligeti S, Bak M, Waleed G, Hasselbalch HC, Christiansen CF. Vascular Diseases In Patients With Chronic Myeloproliferative Neoplasms — Impact Of Comorbidity. *Clinical Epidemiology*. 2019; 11: 955–67. Available from: <https://doi.org/10.2147/CLEP.S216787>, 2019.
19. Tanashjan MM, Kuznetsova PI, Suborceva IN, Shabalina AA, Lagoda OV, Melikjan AL. Hronicheskaja i ostraja cerebrovaskuljarnaja patologija pri ph-negativnyh mieloproliferativnyh zabojevanijah. *Gematologija i transfuziologija*. 2016; 61 (3): 146–50. Russian.
20. Marton I, Pósfai É, Csomor A, Vécsei L, Borbényi Z, Sas K. Cerebrovascular Complications and Polycythaemia Vera. *Pathol Oncol Res*. 2019; 25 (1): 439–42. DOI: 10.1007/s12253-017-0329-9.
21. Adams HP Jr, Bendixen BH, Kappelle LJ, et al. Classification of subtype of acute ischemic stroke. Definitions for use in a multicenter clinical trial. TOAST. Trial of Org 10172 in Acute Stroke Treatment. *Stroke*. 1993; 24 (1): 35–41. DOI: 10.1161/01.str.24.1.35.
22. Momot AP. Problema trombofilii v klinicheskoy praktike. *Rossijskij zhurnal detskoj gematologii i onkologii*. 2015; 1: 37–48.

Литература

1. Суслина З. А., Танашян М. М., Ионова В. Г. Ишемический инсульт: кровь, сосудистая стенка, антитромботическая терапия. М.: Медицинская книга, 2005; 248 с.
2. Phipps MS, Cronin CA. Management of acute ischemic stroke. *BMJ*. 2020; 368: l6983. Published 2020 Feb 13. DOI: 10.1136/bmj.l6983.
3. Танашян М. М., Меликян А. Л., Кузнецова П. И., Раскуражев А. А., Шабалина А. А., Коновалов Р. Н. Изменения вещества головного мозга при Ph-негативных миелолипролиферативных заболеваниях. *Терапевтический архив*. 2019; 91 (7): 29–34.
4. Asakura H. Thrombosis in myeloproliferative neoplasms. *The Japanese Journal of Clinical Hematology*. 2018; 59 (8): 1034–41. DOI: 10.11406/rinketsu.59.1034.
5. Tefferi A, Barbui T. Polycythemia vera and essential thrombocythemia: 2017 update on diagnosis, risk-stratification, and management. *Am J Hematol*. 2017; 92 (1): 94–108. DOI: 10.1002/ajh.24607.
6. Barbui T, Thiele J, Gisslinger H, et al. The 2016 WHO classification and diagnostic criteria for myeloproliferative neoplasms: document summary and in-depth discussion. *Blood Cancer J*. 2018; 8 (2): 15. Published 2018 Feb 9. DOI: 10.1038/s41408-018-0054-y.
7. Kaifia A, Kirschner M, Wolf D, Maintz C, Hänel M, Gattermann N, et al. Bleeding, thrombosis, and anticoagulation in myeloproliferative neoplasms (MPN): analysis from the German SAL-MPN-registry. *J Hematol Oncol*. 2016; 9: 18. Available from: <https://doi.org/10.1186/s13045-016-0242-9>.
8. Moulard O, Mehta J, Olivares R, Iqbal U, Mesa RA. Epidemiology of Myelofibrosis (MF), Polycythemia Vera (PV) and Essential Thrombocythemia (ET) in the European Union (EU). *Blood*. 2012; 120 (21): 1744. Available from: <https://doi.org/10.1182/blood.V120.21.1744.1744>.
9. Волкова М. А., редактор. *Клиническая онкогематология: руководство для врачей*. М.: Медицина, 2007; 1144 с.
10. Козлова Н. С., Бакшеев М. Г., Давыдкин И. Л. Особенности нарушений микроциркуляции у больных истинной полицитемией в сочетании с артериальной гипертензией. *Известия Самарского научного центра РАН*. 2015; 17 (2): 319–322.
11. Давыдкин И. Л., Щукин Ю. В., редакторы. *Поликлиническая терапия: учебник*. М.: ГЭОТАР-Медиа, 2013; 688 с.
12. Руквицын О. А., редактор. *Гематология: национальное руководство*. М.: ГЭОТАР-Медиа, 2015; 776 с.
13. Kwaan HC, Wang J. Hyperviscosity in polycythemia vera and other red cell abnormalities. *Semin Thromb Hemost*. 2003; 29 (5): 451–8.
14. Fujioka S. Rheological study on vascular occlusion and cellular hyperviscosity syndrome in polycythemia vera. *Nihon Ketsueki Gakkai Zasshi*. 1989; 52 (4): 688–95.
15. Pratesi A, Vella A, Pasini E, Salvi F, Mascalchi M. Parkinsonism in polycythaemia vera probably due to manganism. *Mov Disord*. 2008; 23 (16): 2420–1. DOI: 10.1002/mds.22319.
16. Cerquozzi S, Barraco D, Lasho T, et al. Risk factors for arterial versus venous thrombosis in polycythemia vera: a single center experience in 587 patients. *Blood Cancer J*. 2017; 7 (12): 662. Published 2017 Dec 27. DOI: 10.1038/s41408-017-0035-6.
17. Marchioli R, Finazzi G, Specchia G, Masciulli A, Mennitto MR, Barbui T. The CYTO-PV: A Large-Scale Trial Testing the Intensity of CYTOreductive Therapy to Prevent Cardiovascular Events in Patients with Polycythemia Vera. *Thrombosis*. 2011; 2011 (1): 1–9. DOI: 10.1155/2011/794240.
18. Frederiksen H, Szépligeti S, Bak M, Waleed G, Hasselbalch HC,

- Christiansen CF. Vascular Diseases In Patients With Chronic Myeloproliferative Neoplasms — Impact Of Comorbidity. *Clinical Epidemiology*. 2019; 11: 955–67. Available from: <https://doi.org/10.2147/CLEP.S216787>, 2019.
19. Танашян М. М., Кузнецова П. И., Суборцева И. Н., Шабалина А. А., Лагода О. В., Меликян А. Л. Хроническая и острая цереброваскулярная патология при рН-негативных миелопролиферативных заболеваниях. *Гематология и трансфузиология*. 2016; 61 (3): 146–50.
 20. Marton I, Pósfai É, Csomor A, Vécsei L, Borbényi Z, Sas K. Cerebrovascular Complications and Polycythaemia Vera. *Pathol Oncol Res*. 2019; 25 (1): 439–42. DOI: 10.1007/s12253-017-0329-9.
 21. Adams HP Jr, Bendixen BH, Kappelle LJ, et al. Classification of subtype of acute ischemic stroke. Definitions for use in a multicenter clinical trial. TOAST. Trial of Org 10172 in Acute Stroke Treatment. *Stroke*. 1993; 24 (1): 35–41. DOI: 10.1161/01.str.24.1.35.
 22. Момот А. П. Проблема тромбофилии в клинической практике. *Российский журнал детской гематологии и онкологии*. 2015; 1: 37–48.

COMPLEXES OF FLUCONAZOLE WITH ALANINE, LYSINE AND THREONINE: MASS SPECTROMETRY AND THEORETICAL MODELING

Chagovets VV ✉, Starodubtseva NL, Frankevich VE

National Medical Research Center for Obstetrics, Gynecology and Perinatology named after Academician V. I. Kulakov, Moscow, Russia

Investigation of the triazole-derived drugs action mechanisms and understanding of their affinity and specificity molecular basis may contribute to the new drugs development. The study was aimed to investigate the triazoles class representative (fluconazole) complexes with amino acids using mass spectrometry, molecular dynamics and *ab initio* quantum chemistry calculations. During the experimental study, the fluconazole, alanine, lysine and threonine solutions were analyzed by electrospray ionization mass spectrometry and tandem mass spectrometry. The molecular dynamics modeling of the fluconazole–amino acid complexes was performed using the CHARMM force field. The quantum chemistry calculations of the complexes structure and energy parameters were carried out using the density-functional theory by B3LYP calculations (3-21G and 6-311++G** basis sets). Mass spectra indicated that fluconazole formed stable complexes with amino acids in the 1 : 1 stoichiometric ratio. In accordance with the tandem mass spectrometry with varying fluconazole–amino acid associates ion fragmentation energy, the following sequence was obtained: $[\text{Fluc} + \text{Ala} + \text{H}]^+ < [\text{Fluc} + \text{Lys} + \text{H}]^+ < [\text{Fluc} + \text{Thr} + \text{H}]^+$. The fluconazole–amino acid interaction energy values resulting from the quantum chemistry calculations formed the sequence similar to that obtained by experiment. Thus, as seen in the case of fluconazole–amino acid complexes, it is possible to combine the experimental mass spectrometry studies with quantum chemical modeling for the complexes properties assessment.

Keywords: mass spectrometry, molecular dynamics, quantum chemistry, pharmacology, antifungal drugs

Funding: the study was carried out as a part of the convention № 05.604.21.0241, Development of a Technology for Personalized Treatment of Mothers and Newborns With Infectious and Inflammatory Diseases Caused by Multi-resistant Strains of Microorganisms, Based on Genotyping of Pathogens and Therapeutic Drug Monitoring of Antimicrobial Drugs (item 1,2, queue 1), of the Ministry of Science and Higher Education of the Russian Federation. Programme for Research and Development in Priority Areas of Development of the Russian Scientific and Technological Complex for 2014-2020. Project ID: RFMEFI60419X0241.

Author contribution: Chagovets VV, Frankevich VE, Starodubtseva NL — study concept and design, data processing; Chagovets VV — statistical analysis; Chagovets VV, Starodubtseva NL — manuscript writing; Frankevich VE — editing.

Compliance with ethical standards: the study was approved by the Ethics Committee of Ural State Medical University (Protocol № 1451/19 dated September 20, 2019). The patient gave informed consent to participate in the study.

✉ **Correspondence should be addressed:** Vitaliy V. Chagovets
Oparina, 4, Moscow, 117198; vvchagovets@gmail.com

Received: 22.07.2020 **Accepted:** 13.08.2020 **Published online:** 22.08.2020

DOI: 10.24075/brsmu.2020.048

МАСС-СПЕКТРОМЕТРИЧЕСКОЕ ИССЛЕДОВАНИЕ И ТЕОРЕТИЧЕСКОЕ МОДЕЛИРОВАНИЕ КОМПЛЕКСОВ ФЛУКОНАЗОЛА С АЛАНИНОМ, ЛИЗИНОМ И ТРЕОНИНОМ

В. В. Чаговец ✉, Н. Л. Стародубцева, В. Е. Франкевич

Национальный медицинский исследовательский центр акушерства, гинекологии и перинатологии имени В. И. Кулакова, Москва, Россия

Изучение механизмов действия препаратов триазола и понимание молекулярной основы их аффинности и специфичности может быть использовано для рациональной разработки новых лекарственных средств. Целью работы было изучить комплексы представителя класса триазолов флуконазола с аминокислотами с помощью масс-спектрометрии, молекулярной динамики и квантово-химических *ab initio* расчетов. В ходе экспериментального исследования с помощью масс-спектрометрии с электрораспылительной ионизацией и tandemной масс-спектрометрии были проанализированы растворы флуконазола, аланина, лизина и треонина. Молекулярно-динамическое моделирование комплексов флуконазола с аминокислотами проводили с использованием силового поля CHARMM. Квантово-химические расчеты структуры и энергетических параметров комплексов проводили на уровне теории функционала плотности с использованием функций B3LYP с базисом 3-21G и 6-311++G**. Масс-спектры показали, что флуконазол образует стабильные комплексы с аминокислотами в стехиометрическом соотношении 1 : 1. По результатам tandemной масс-спектрометрии с варьированием энергии фрагментации ионов-ассоциатов флуконазола с аминокислотами построен следующий ряд: $[\text{Fluc} + \text{Ala} + \text{H}]^+ < [\text{Fluc} + \text{Lys} + \text{H}]^+ < [\text{Fluc} + \text{Thr} + \text{H}]^+$. Получившиеся в результате квантово-химических расчетов энергии взаимодействия между флуконазолом и аминокислотой образуют ряд, аналогичный полученному по экспериментальным данным. Таким образом, на примере комплексов флуконазола с аминокислотами продемонстрирована возможность комбинирования экспериментальных масс-спектрометрических исследований и квантово-химического моделирования для изучения свойств таких комплексов.

Ключевые слова: масс-спектрометрия, молекулярная динамика, квантовая химия, фармакология, противогрибковые препараты

Финансирование: работа выполнена в рамках соглашения № 05.604.21.0241 «Разработка технологии персонализированного лечения матерей и новорожденных с инфекционно-воспалительными заболеваниями, вызванными мультирезистентными штаммами микроорганизмов, на основании генотипирования возбудителей и терапевтического лекарственного мониторинга антимикробных препаратов» (мероприятие 1,2, очередь 1) Министерства науки и высшего образования РФ. Программа: «Исследование и разработка по приоритетным направлениям развития научно-технологического комплекса России на 2014–2020 годы». Уникальный идентификатор проекта RFMEFI60419X0241.

Вклад авторов: В. В. Чаговец, В. Е. Франкевич, Н. Л. Стародубцева — концепция и дизайн исследования, обработка материала; В. В. Чаговец — статистическая обработка данных; В. В. Чаговец, Н. Л. Стародубцева — написание текста; В. Е. Франкевич — редактирование.

Соблюдение этических стандартов: исследование одобрено этическим комитетом Уральского государственного медицинского университета (протокол № 1451/19 от 20 сентября 2019 г.). Получено добровольное информированное согласие на участие пациента в научном исследовании.

✉ **Для корреспонденции:** Виталий Викторович Чаговец
ул. Академика Опарина, д. 4, г. Москва, 117198; vvchagovets@gmail.com

Статья получена: 22.07.2020 **Статья принята к печати:** 13.08.2020 **Опубликована онлайн:** 22.08.2020

DOI: 10.24075/vrgmu.2020.048

Cytochrome P450 sterol 14 α -demethylase (CYP51), the product of *ERG11* gene, is a target site for triazoles. The CYP51 enzyme converts lanosterol into ergosterol being a part of the fungal cell membrane main component biosynthesis pathway [1]. Ergosterol biosynthesis inhibition slows down the mycelia cells growth due to toxic steroids (such as methylated sterols) accumulation [2–4], violating the membrane integrity, fluidity and permeability [5]. Fluconazole (Fluc) acts as a competitive inhibitor of CYP51. Currently, it is effective for treatment of many fungal infections.

The development of new classes of compounds is necessary for the treatment of mycoses and antifungal drugs resistance. Antifungal drugs are relatively difficult to develop compared to antibacterial drugs due to eukaryotic type of cells. Besides, the triazole derived antifungal agents (such as fluconazole) eventually become insufficient for treatment of many infections. The need to develop new medicinal products is an incentive to the triazole drugs inhibition molecular mechanisms study enabling to understand the molecular basis for the fluconazole affinity and specificity.

Previously, the molecular modeling was used to search for pyrazole analogues. The search was based on the CYP51-Ca protein structure [6, 7]. Furthermore, the molecular modeling made it possible to investigate the features and patterns of various inhibitors interaction with CYP51 [8], as well as the role of mutations in the stability and affinity of enzyme binding [9, 10]. Molecular dynamics also made it possible to study the factors of the fluconazole greater affinity for fungal enzymes rather than mycobacterial and human orthologs [11]. A review of the modeling strategies used to design the P450 binding ligands was recently published [12].

Database analysis revealed a number of conserved amino acids (AA) [13, 14]. Of those, three amino acids playing a vital part in protein–inhibitor binding were selected using the molecular dynamics modeling: threonine (Thr77), alanine (Ala258) and lysine (Lys454) [8].

Although the molecular mechanics studies may help to predict amino acids involved in the protein–inhibitor complex assembly, it is important to have a number of experimental methods allowing one to verify the resulting model. Experimental approach using electrospray ionization mass spectrometry (ESI-MS) may be a powerful means for the host–guest complexation forecasting and complementary theoretical calculation using the molecular mechanical models.

ESI-MS is widely used for studying of noncovalent interactions between proteins and other biomolecules [15–17]. The soft ionization procedure permits the molecular complexes to retain “conformational memory” of their solution state structures in the gas phase [18]. Over the past decades, the rapidly increasing number of papers on the noncovalent interactions assessment using MS indicated that MS had become an important method due to high throughput, sensitivity and small sample volumes [19]. MS was used for the host–guest complexation assessment [20–25].

The noncovalent interactions between fluconazole and amino acids as elementary stages of the protein–inhibitor complex formation have not been previously studied.

The study was aimed to investigate the fluconazole-amino acid complexes in the gas phase using ESI-MS, as well as to assess the complexes structural and energy parameters using molecular dynamics and *ab initio* quantum chemistry methods.

METHODS

Fluconazole (Fluc), alanine (Ala), lysine (Lys), threonine (Thr), and methanol (HPLC grade) were obtained from Merck

(Merck; Germany). Deionized water was prepared using the Milli-Q Reference Water Purification System (Merck; France). Each amino acid and fluconazole stock solution was prepared in methanol at a concentration of 10 mmol/mL. For mass spectrometry of individual compounds, the stock solutions were diluted with water to a concentration of 1 mmol/mL. The samples for the fluconazole-amino acid complexes analysis by tandem mass spectrometry were prepared by mixing the stock solutions of fluconazole and one of the amino acids in the 1 : 1 ratio (v : v). The solutions so obtained were diluted with water to a concentration of 1 mmol/mL for each component and stirred during 30 s. The sample for comparison of the fluconazole–amino acid complexes relative peak intensities was prepared by mixing the equal volumes of fluconazole, alanine, lysine and threonine stock solutions. The resulting solution was diluted with water to a concentration of 1 mmol/mL for each component and stirred during 30 s. All samples were prepared at room temperature.

The experiment was carried out using the MaxisImpact hybrid quadrupole time-of-flight (QTOF) mass spectrometer (BrukerDaltonics; Germany). The following parameters were used in the positive ion mode: mass range (m/z) 50–1000, needle voltage 4.5 kV, nebulizer gas pressure 0.6 bar, drying gas flow rate 5.0 L/min, drying gas temperature 200 °C. The tandem mass spectrometry experiments were carried out using the isolation window 3 m/z and the collision energy variation. The sample was injected directly using the KD Scientific syringe pump (KD Scientific; USA), the flow rate was 3 μ L/min.

The molecular dynamics study of the Fluc + AA complexes was performed using the NAMD software [26]. The force field for the studied complexes modeling was created using the CHARMM General Force-Field (v3.1) basis [27, 28]. The types of atoms and partially the charges of the fluconazole atoms were selected by analogy. The missing parameters of bonds, angles and dihedral angles, as well as the missing charges of the fluconazole atoms were optimized using the Force Field Toolkit (ffTK), the VMD software plugin [26].

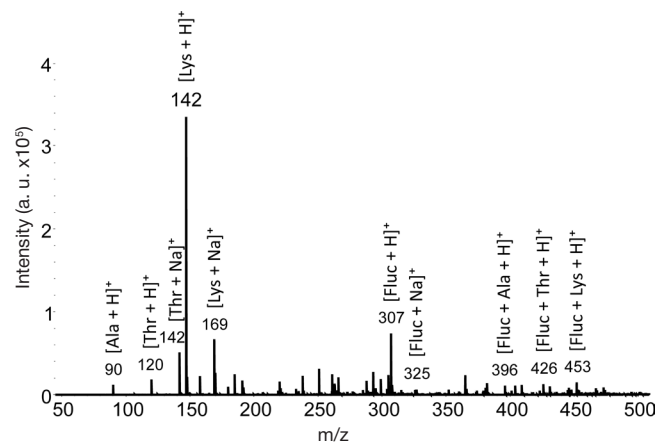


Fig. 1. Positive ion mass spectrum of the sample containing fluconazole, alanine, threonine and lysine

Table 1. Fluconazole–amino acid complexes characteristics

Amino acid	I, a.u. ¹	CE _{50%} , eV ²	B3LYP/6-311++G** IE, kJ/mol ³
Ala	15061	23	–56.8226463
Lys	17540	25	–65.600743
Thr	18325	29	–97.663349

Note: ¹ — mass spectral complex peak intensity, au (Fig. 1); ² — energy needed for the tandem mass spectral precursor ion peak intensity reduction by 50%; ³ — interaction energy calculated by quantum chemical method B3LYP/6-311++G**.

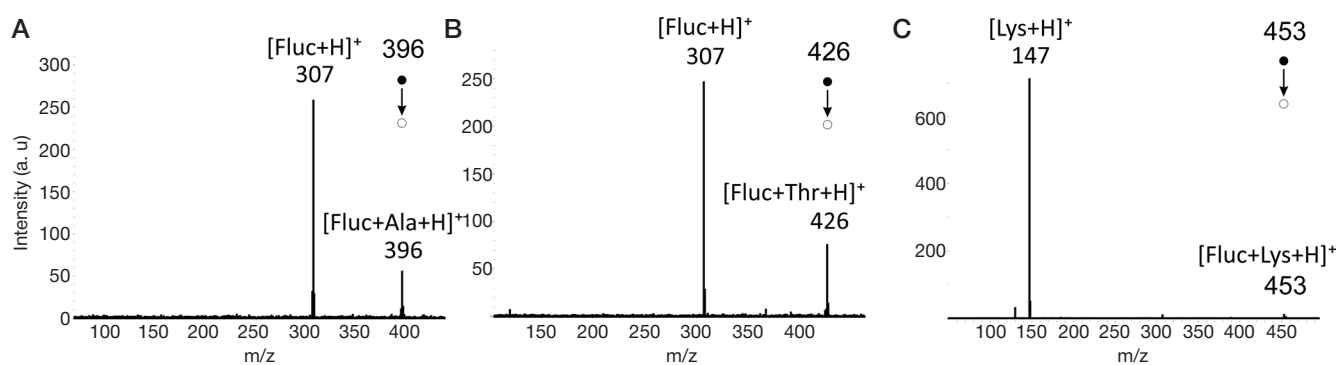


Fig. 2. Tandem mass spectra of fluconazole complexes with alanine (A), threonine (B) and lysine (C) acquired using the positive ion mode

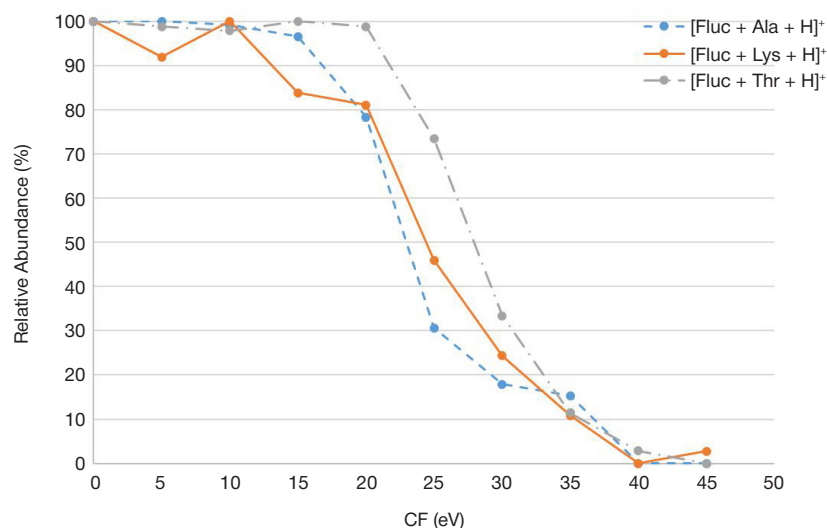


Fig. 3. Correlation between the fluconazole-amino acid complex precursor ion peak relative intensity and the collision energy (CE)

The quantum chemistry calculations of the fluconazole-amino acid complexes structure and energy parameters were performed using the GAMESS software package [29]. The complexes geometry optimization aimed at structural and energy properties study was carried out using the density-functional theory (DFT) by B3LYP calculations (3-21G and 6-311++G** basis sets with diffuse and polarization functions).

RESULTS

During the ESI-MS analysis of individual amino acids, the peaks corresponding to protonated and sodiated amino acids were identified. ESI-MS experiments with aqueous solutions containing both amino acid and fluconazole revealed the associates of amino acid and drug molecules, which indicated the sufficient stability of such complexes in the gas phase.

Fig. 1 provides the positive ion ESI mass spectrum of the aqueous solution containing all three amino acids and fluconazole at equimolar concentrations. The possibility of the associates formation is indicated by the following peaks: $[\text{Fluc} + \text{Ala} + \text{H}]^+$ (m/z 396), $[\text{Fluc} + \text{Lys} + \text{H}]^+$ (m/z 453) and $[\text{Fluc} + \text{Thr} + \text{H}]^+$ (m/z 426). Taking into account the corresponding peaks intensities, the following sequence can be formed (Table 1): $[\text{Fluc} + \text{Ala} + \text{H}]^+ < [\text{Fluc} + \text{Thr} + \text{H}]^+ < [\text{Fluc} + \text{Lys} + \text{H}]^+$. Since the mass spectral peaks intensity is in proportion to the number of corresponding ions reaching the detector, it can be assumed that the described sequence is also valid for the interaction energy of the complex. However, in addition to stability, the intensity of the associate ion is also contributed by its ionization efficiency, stability of individual components of the complex, etc. For the additional experimental assessment of the complexes

stability and interaction energy, the tandem mass spectra obtained as a result of the studied associates collision-induced dissociation have been acquired and analyzed. Fig. 2 provides the complexes $[\text{Fluc} + \text{Ala} + \text{H}]^+$ (Fig. 2A), $[\text{Fluc} + \text{Thr} + \text{H}]^+$ (Fig. 2B) and $[\text{Fluc} + \text{Lys} + \text{H}]^+$ (Fig. 2C) fragmentation mass spectra. The complexes peaks, as well as the complexes fragments peaks resulting from protonated fluconazole (in case of alanine and threonine associates fragmentation) and protonated lysine (in case of fluconazole associate fragmentation) have been identified in the mass spectra. Thus, at this stage, it can be concluded that the studied complexes fragmentation proceeds along two basic lines: either the neutral amino acid, or the neutral fluconazole loss. Apparently, that is due to the described molecules different proton affinity. To quantify the studied complexes stability, the peak intensities of the tandem mass spectra with the collision energy variation have been analyzed. Fig. 3 provides the correlation between the intensity of the precursor ion and the collision energy. The relative stability of fluconazole and various amino acids associates was evaluated by comparison of energy needed for the precursor ion peak intensity reduction by 50%. These values were 23, 25 and 29 eV for the studied complexes containing alanine, lysine and threonine respectively (Table 1).

Thus, in the mass spectra of the fluconazole and alanine, threonine, lysine containing solutions the $[\text{Fluc} + \text{AA} + \text{H}]^+$ clusters were identified. Since the experimental evaluation of the complexes stability was possible, it was of interest to estimate the energy of fluconazole interaction with each of the studied amino acids, which was the subject of the molecular dynamics modeling and quantum chemical calculations described below.

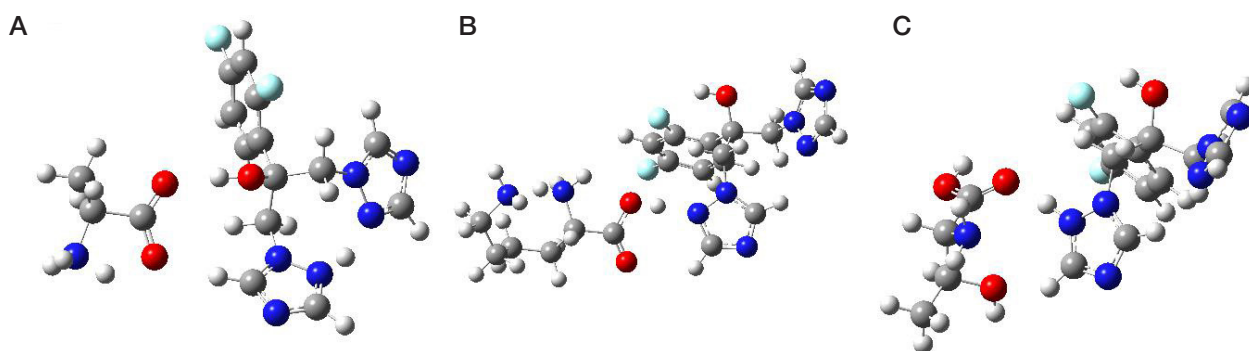


Fig. 4. Structure of fluconazole complexes with alanine (A), lysine (B) and threonine (C) optimized by the B3LYP/6-311++G** method

Table 2. Energy values for complex components and fluconazole-amino acid complexes; interaction energy values obtained by quantum chemical methods B3LYP/3-21 and B3LYP/6-311++G**

Amino acid	$E_{AB}(\text{Fluc} + \text{AA})$, a.u.	$E_A(\text{Fluc})$, a.u.	$E_B(\text{AA})$, a.u.	IE, a.u.	IE, kJ/mol
B3LYP/3-21					
Ala	-1422.2762	-1100.264222	-321.9574674	-0.0544686	-143.007
Lys	-1594.6453	-1100.238944	-494.3018987	-0.1044502	-274.234
Thr	-1536.1547	-1100.238944	-435.8476107	-0.0681227	-178.856
B3LYP/3-311++G**					
Ala	-1430.53104	-1106.65334	-323.85606	-0.02164	-56.82
Lys	-1603.88596	-1106.28645	-497.57453	-0.02499	-65.60
Thr	-1545.09491	-1106.63517	-438.42255	-0.03720	-97.66

The initial structure selection plays a vital part in the molecular geometry optimization by quantum chemistry. Since both amino acids and fluconazole have a large number of degrees of freedom and are conformationally mobile, in our study, the selection of the initial structure for quantum-chemical calculations was carried out using molecular dynamics by simulated annealing. The selection of the molecule (fluconazole or amino acid) being a proton acceptor was performed based on the tandem mass spectra (see Fig. 2). In the $[\text{Fluc} + \text{Ala} + \text{H}]^+$ and $[\text{Fluc} + \text{Thr} + \text{H}]^+$ complexes the fluconazole was protonated. In the $[\text{Fluc} + \text{Lys} + \text{H}]^+$ complex the proton was localized at the lysine. The resulting structures obtained by simulated annealing were optimized using the B3LYP method (first with 3-21G basis set, and then with 6-311++G** basis set). The complex structures obtained by optimization are provided in Fig. 4. In the $[\text{Fluc} + \text{Ala} + \text{H}]^+$ and $[\text{Fluc} + \text{Thr} + \text{H}]^+$ complexes the geometry optimization led to the proton shift towards fluconazole. In the $[\text{Fluc} + \text{Lys} + \text{H}]^+$ complex the proton was localized at the lysine, which was consistent with the hypothesis announced based on the experimental data. Such amino acids behavior might be due to amino acids and fluconazole different proton affinity, as well as to pI value, which was 9.74 for lysine, and 6 and 5.6 for alanine and threonine respectively. Based on the modeling, the complex formation energies were calculated using the formula $\text{IE} = E_{AB} - E_A - E_B$, where E_{AB} was the complex energy, E_A and E_B were the complex components energies. Table 2 provides energy values obtained by quantum chemistry calculations using the B3LYP/3-21 and B3LYP/6-311++G** methods. The interaction energies between the components of the complex calculated using the B3LYP/6-311++G** method matched the sequence experimentally obtained. When using the B3LYP/3-21 method, the energy of fluconazole interaction with lysine was higher than that with threonine. That may indicate the importance of using diffuse and polarization functions when modeling the noncovalent complexes.

DISCUSSION

Previously, the importance of understanding the range of amino acids involved in binding of triazine compounds and the character of interactions determining the stability of the protein–drug complexes was shown [11]. The same paper provided the comparison of fluconazole interactions with various CYP51 enzymes. In such complexes, the interaction energy resulted from the competitive binding of ligand with amino acid residues of the protein, heme and water molecules. The protein–fluconazole binding proved to be more effective in mitochondrial CYP51 due to polar interaction with the arginine residue. However, in fungal enzymes these interactions are substituted by ligand–heme interactions, which compensate for the loss of the polar bond and result in the more energetically favored binding. Therefore, the development of ligand with increased specificity to fungal enzymes should focus on the strengthening the polar ligand–heme interactions. The larger hydrophobic ligands are probably best suited to target the mycobacterial and human enzymes [11]. Such studies demonstrate the importance of understanding and considering the interactions between the drug and the various components of the target. This paper provides the approach, which may be used at the early stages of the new drugs development, making it possible to estimate the drug–amino acid complexes stability both from the experimental and theoretical point of view.

CONCLUSION

ESI-MS and molecular dynamics were used for the study of fluconazole–amino acid interactions, which, according to literary sources, played a vital part in the protein–inhibitor binding. The noncovalent complexes turned out to be stable in the gas phase, which made it possible to identify the corresponding signals in the mass spectra. Tandem mass spectrometry with

varying collision energy was used for the studied complexes stability assessment. The following stability sequence was obtained: [Fluc + Ala + H]⁺ (23 eV) < [Fluc + Lys + H]⁺ (25 eV) < [Fluc + Thr + H]⁺ (29 eV). Molecular dynamics and quantum chemical modeling made it possible to define the complexes structure and interaction energy. The interaction energy values

determined using the B3LYP/6-311++G** method formed the associates stability sequence similar to that obtained by experiment. Such approach combining the experimental mass spectrometry studies and the quantum chemical modeling may be used at the early stages of the new drugs development, and to search for the drug action molecular mechanisms.

References

- Balding PR, Porro CS, McLean KJ, Sutcliffe MJ, Maréchal JD, Munro AW, et al. How do azoles inhibit cytochrome P450 enzymes? A density functional study. *J Phys Chem A*. 2008; 112 (50): 12911–8.
- Lupetti A, Danesi R, Campa M, Tacca M Del, Kelly S. Molecular basis of resistance to azole antifungals. *Trends Mol Med*. 2002; 8 (2): 76–81.
- Marichal P, Gorrens J, Laurijsens L, Vermuyten K, Van Hove C, Le Jeune L, et al. Accumulation of 3-ketosteroids induced by itraconazole in azole-resistant clinical *Candida albicans* isolates. *Antimicrob Agents Chemother*. 1999; 43 (11): 2663–70.
- White TC, Marr KA, Bowden RA. Clinical, cellular, and molecular factors that contribute to antifungal drug resistance. *Clin Microbiol Rev*. 1998; 11 (2): 382–402.
- Shapiro RS, Robbins N, Cowen LE. Regulatory Circuitry Governing Fungal Development, Drug Resistance, and Disease. *Microbiol Mol Biol Rev*. 2011; 75 (2): 213–267.
- Doğan İS, Saraç S, Sari S, Kart D, Eşsiz Gökhan Ş, Vural İ, et al. New azole derivatives showing antimicrobial effects and their mechanism of antifungal activity by molecular modeling studies. *Eur J Med Chem*. 2017; 130: 124–38.
- Jacob K S, Ganguly S, Kumar P, Poddar R, Kumar A. Homology model, molecular dynamics simulation and novel pyrazole analogs design of *Candida albicans* CYP450 lanosterol 14 α -demethylase, a target enzyme for antifungal therapy. *J Biomol Struct Dyn*. 2017; 35 (7): 1446–63.
- Gao P, Cui YL, Wu RL. Molecular dynamic modeling of CYP51B in complex with azole inhibitors. *J Biomol Struct Dyn*. 2018; 36 (6): 1511–9.
- Keighobadi M, Emami S, Lagzian M, Fakhari M, Rafiei A, Valadan R. Molecular modeling and structural stability of wild-type and mutant CYP51 from *Leishmania major*: In vitro and in silico analysis of a laboratory strain. *Molecules*. 2018; 23 (3). DOI: 10.3390/molecules23030696.
- Vijayakumar S, Das P. Structural, molecular motions, and free-energy landscape of *Leishmania* sterol-14 α -demethylase wild type and drug resistant mutant: a comparative molecular dynamics study. *J Biomol Struct Dyn*. 2019; 37 (6): 1477–93.
- Honorato Siqueira T, Martínez L. Molecular simulations of fluconazole-mediated inhibition of sterol biosynthesis. *J Biomol Struct Dyn*. 2020; 38 (6): 1659–69.
- Kontoyianni M, Lacy B. Toward Computational Understanding of Molecular Recognition in the Human Metabolizing Cytochrome P450s. *Curr Med Chem*. 2018; 25 (28): 3353–73.
- Lepesheva GI, Waterman MR. Sterol 14 α -demethylase cytochrome P450 (CYP51), a P450 in all biological kingdoms. *Biochim Biophys Acta — Gen Subj*. 2007; 1770 (3): 467–77.
- Lepesheva GI, Waterman MR. Structural basis for conservation in the CYP51 family. *Biochim Biophys Acta — Proteins Proteomics*. 2011; 1814 (1): 88–93.
- Loo JA. Studying noncovalent protein complexes by electrospray ionization mass spectrometry. *Mass Spectrom Rev*. 1997; 16 (1): 1–23.
- Pramanik BN, Bartner PL, Mirza UA, Liu YH, Ganguly AK. Electrospray ionization mass spectrometry for the study of non-covalent complexes: An emerging technology. *J Mass Spectrom*. 1998; 33 (10): 911–20.
- Loo JA. Electrospray ionization mass spectrometry: A technology for studying noncovalent macromolecular complexes. *Int J Mass Spectrom*. 2000; 200 (1–3): 175–86.
- Ray SS, Singh SK, Balam P. Sulfonate (ANS) Binding to Proteins. *Data Process*. 2001; 0305 (01).
- Zhang S, Van Pelt CK, Wilson DB. Quantitative determination of noncovalent binding interactions using automated nano-electrospray mass spectrometry. *Anal Chem*. 2003; 75 (13): 3010–8.
- Tjernberg A, Camö S, Oliv F, Benkestock K, Edlund PO, Griffiths WJ, et al. Determination of dissociation constants for protein-ligand complexes by electrospray ionization mass spectrometry. *Anal Chem*. 2004; 76 (15): 4325–31.
- Benkestock K. Electrospray Ionization Mass Spectrometry for Determination of Noncovalent Interactions in Drug Discovery. 2008.
- Bligh SWA, Haley T, Lowe PN. Measurement of dissociation constants of inhibitors binding to Src SH2 domain protein by non-covalent electrospray ionization mass spectrometry. *J Mol Recognit*. 2003; 16 (3): 139–48.
- Zhang C, Chen H, Guymon AJ, Wu G, Cooks RG, Ouyang Z. Instrumentation and methods for ion and reaction monitoring using a non-scanning rectilinear ion trap. *Int J Mass Spectrom*. 2006; 255–256 (1–3): 1–10.
- Wu RF, Huang YD, Chu YQ, Liu ZP, Ding CF. Investigation of Non-covalent Interactions of 18-Crown-6 with Amino Acids in Gas Phase by Mass Spectrometry. *Chinese J Anal Chem*. 2018; 46 (2): 273–9.
- Zhang S, Van Pelt CK, Wilson DB. Quantitative determination of noncovalent binding interactions using automated nano-electrospray mass spectrometry. *Anal Chem*. 2003; 75 (13): 3010–8.
- Mayne CG, Saam J, Schulten K, Tajkhorshid E, Gumbart JC. Rapid parameterization of small molecules using the force field toolkit. *J Comput Chem*. 2013; 34 (32): 2757–70.
- Vanommeslaeghe K, Raman EP, MacKerell AD. Automation of the CHARMM General Force Field (CGenFF) II: Assignment of Bonded Parameters and Partial Atomic Charges. *J Chem Inf Model*. 2012; 52 (12): 3155–68.
- Vanommeslaeghe K, Hatcher E, Acharya C, Kundu S, Zhong S, Shim J, et al. CHARMM general force field: A force field for drug-like molecules compatible with the CHARMM all-atom additive biological force fields. *J Comput Chem*. 2010; 31 (4): 671–90.
- Schmidt MW, Baldrige KK, Boatz JA, Elbert ST, Gordon MS, Jensen JH, et al. General atomic and molecular electronic structure system. *J Comput Chem*. 1993; 14 (11): 1347–63.

Литература

- Balding PR, Porro CS, McLean KJ, Sutcliffe MJ, Maréchal JD, Munro AW, et al. How do azoles inhibit cytochrome P450 enzymes? A density functional study. *J Phys Chem A*. 2008; 112 (50): 12911–8.
- Lupetti A, Danesi R, Campa M, Tacca M Del, Kelly S. Molecular basis of resistance to azole antifungals. *Trends Mol Med*. 2002; 8 (2): 76–81.
- Marichal P, Gorrens J, Laurijsens L, Vermuyten K, Van Hove C,

- Le Jeune L, et al. Accumulation of 3-ketosteroids induced by itraconazole in azole-resistant clinical *Candida albicans* isolates. *Antimicrob Agents Chemother*. 1999; 43 (11): 2663–70.
4. White TC, Marr KA, Bowden RA. Clinical, cellular, and molecular factors that contribute to antifungal drug resistance. *Clin Microbiol Rev*. 1998; 11 (2): 382–402.
 5. Shapiro RS, Robbins N, Cowen LE. Regulatory Circuitry Governing Fungal Development, Drug Resistance, and Disease. *Microbiol Mol Biol Rev*. 2011; 75 (2): 213–267.
 6. Doğan İS, Saraç S, Sari S, Kart D, Eşiz Gökhan Ş, Vural İ, et al. New azole derivatives showing antimicrobial effects and their mechanism of antifungal activity by molecular modeling studies. *Eur J Med Chem*. 2017; 130: 124–38.
 7. Jacob K S, Ganguly S, Kumar P, Poddar R, Kumar A. Homology model, molecular dynamics simulation and novel pyrazole analogs design of *Candida albicans* CYP450 lanosterol 14 α -demethylase, a target enzyme for antifungal therapy. *J Biomol Struct Dyn*. 2017; 35 (7): 1446–63.
 8. Gao P, Cui YL, Wu RL. Molecular dynamic modeling of CYP51B in complex with azole inhibitors. *J Biomol Struct Dyn*. 2018; 36 (6): 1511–9.
 9. Keighobadi M, Emami S, Lagzian M, Fakhar M, Rafiei A, Valadan R. Molecular modeling and structural stability of wild-type and mutant CYP51 from *Leishmania major*: In vitro and in silico analysis of a laboratory strain. *Molecules*. 2018; 23 (3). DOI: 10.3390/molecules23030696.
 10. Vijayakumar S, Das P. Structural, molecular motions, and free-energy landscape of *Leishmania* sterol-14 α -demethylase wild type and drug resistant mutant: a comparative molecular dynamics study. *J Biomol Struct Dyn*. 2019; 37 (6): 1477–93.
 11. Honorato Siqueira T, Martínez L. Molecular simulations of fluconazole-mediated inhibition of sterol biosynthesis. *J Biomol Struct Dyn*. 2020; 38 (6): 1659–69.
 12. Kontoyianni M, Lacy B. Toward Computational Understanding of Molecular Recognition in the Human Metabolizing Cytochrome P450s. *Curr Med Chem*. 2018; 25 (28): 3353–73.
 13. Lepesheva GI, Waterman MR. Sterol 14 α -demethylase cytochrome P450 (CYP51), a P450 in all biological kingdoms. *Biochim Biophys Acta — Gen Subj*. 2007; 1770 (3): 467–77.
 14. Lepesheva GI, Waterman MR. Structural basis for conservation in the CYP51 family. *Biochim Biophys Acta — Proteins Proteomics*. 2011; 1814 (1): 88–93.
 15. Loo JA. Studying noncovalent protein complexes by electrospray ionization mass spectrometry. *Mass Spectrom Rev*. 1997; 16 (1): 1–23.
 16. Pramanik BN, Bartner PL, Mirza UA, Liu YH, Ganguly AK. Electrospray ionization mass spectrometry for the study of noncovalent complexes: An emerging technology. *J Mass Spectrom*. 1998; 33 (10): 911–20.
 17. Loo JA. Electrospray ionization mass spectrometry: A technology for studying noncovalent macromolecular complexes. *Int J Mass Spectrom*. 2000; 200 (1–3): 175–86.
 18. Ray SS, Singh SK, Balam P. Sulfonate (ANS) Binding to Proteins. *Data Process*. 2001; 0305 (01).
 19. Zhang S, Van Pelt CK, Wilson DB. Quantitative determination of noncovalent binding interactions using automated nano-electrospray mass spectrometry. *Anal Chem*. 2003; 75 (13): 3010–8.
 20. Tjernberg A, Carnö S, Oliv F, Benkestock K, Edlund PO, Griffiths WJ, et al. Determination of dissociation constants for protein-ligand complexes by electrospray ionization mass spectrometry. *Anal Chem*. 2004; 76 (15): 4325–31.
 21. Benkestock K. Electrospray Ionization Mass Spectrometry for Determination of Noncovalent Interactions in Drug Discovery. 2008.
 22. Bligh SWA, Haley T, Lowe PN. Measurement of dissociation constants of inhibitors binding to Src SH2 domain protein by non-covalent electrospray ionization mass spectrometry. *J Mol Recognit*. 2003; 16 (3): 139–48.
 23. Zhang C, Chen H, Guymon AJ, Wu G, Cooks RG, Ouyang Z. Instrumentation and methods for ion and reaction monitoring using a non-scanning rectilinear ion trap. *Int J Mass Spectrom*. 2006; 255–256 (1–3): 1–10.
 24. Wu RF, Huang YD, Chu YQ, Liu ZP, Ding CF. Investigation of Non-covalent Interactions of 18-Crown-6 with Amino Acids in Gas Phase by Mass Spectrometry. *Chinese J Anal Chem*. 2018; 46 (2): 273–9.
 25. Zhang S, Van Pelt CK, Wilson DB. Quantitative determination of noncovalent binding interactions using automated nano-electrospray mass spectrometry. *Anal Chem*. 2003; 75 (13): 3010–8.
 26. Mayne CG, Saam J, Schulten K, Tajkhorshid E, Gumbart JC. Rapid parameterization of small molecules using the force field toolkit. *J Comput Chem*. 2013; 34 (32): 2757–70.
 27. Vanommeslaeghe K, Raman EP, MacKerell AD. Automation of the CHARMM General Force Field (CGenFF) II: Assignment of Bonded Parameters and Partial Atomic Charges. *J Chem Inf Model*. 2012; 52 (12): 3155–68.
 28. Vanommeslaeghe K, Hatcher E, Acharya C, Kundu S, Zhong S, Shim J, et al. CHARMM general force field: A force field for drug-like molecules compatible with the CHARMM all-atom additive biological force fields. *J Comput Chem*. 2010; 31 (4): 671–90.
 29. Schmidt MW, Baldrige KK, Boatz JA, Elbert ST, Gordon MS, Jensen JH, et al. General atomic and molecular electronic structure system. *J Comput Chem*. 1993; 14 (11): 1347–63.

HYPOXIA ENHANCES TRANSCYTOSIS IN INTESTINAL ENTEROCYTES

Maltseva DV¹ ✉, Shkurnikov MYu^{1,2}, Nersisyan SA¹, Nikulin SV¹, Kurnosov AA¹, Raigorodskaya MP³, Osipyants AI^{2,4}, Tonevitsky EA⁵¹ National Research University Higher School of Economics, Moscow, Russia² Hertsen Moscow Oncology Research Center, Moscow, Russia³ SRC Bioclinicum, Moscow, Russia⁴ Far Eastern Federal University, Vladivostok, Russia⁵ Fund for Development of Innovative Scientific-Technological Center Mendeleev Valley, Moscow, Russia

The integrity of the intestinal epithelial cell lining is crucial for the normal intestinal function. As a rule, intestinal inflammation is associated with additional tissue hypoxia, leading to the loss of epithelial monolayer integrity. However, in the absence of visible damage to the epithelium, there still might be a risk of infection driven by changes in the intracellular transport of bacteria-containing vesicles. The aim of this study was to investigate the effects of hypoxia on transcytosis using a human intestinal enterocyte model. We found that hypoxia enhances transcytosis of the model protein ricin 1.8-fold. The comparative transcriptome and proteome analyses revealed significant changes in the expression of genes involved in intracellular vesicle transport. Specifically, the expression of apoB (the regulator of lipid metabolism) was changed at both protein (6.5-fold) and mRNA (2.1-fold) levels. Further research is needed into the possible mechanism regulating gene expression in intestinal erythrocytes under hypoxic conditions.

Keywords: hypoxia, enterocyte, intestinal epithelium, microRNA, mRNA, proteome, transcriptome, transcytosis, Caco-2

Funding: the study received public financial support from the Ministry of Science and Higher Education of the Russian Federation (project ID RFMEFI60519X0184).

Acknowledgement: the authors thank the Human Proteome Core Facility (Institute of Biomedical Chemistry) for permission to use the Facility's equipment

Author contribution: Maltseva DV — molecular tests, analysis of their results, manuscript preparation; Shkurnikov MYu — analysis of transcriptome and sequencing data, statistical analysis; Nersisyan SA — sequencing data processing, bioinformatic analysis, functional gene analysis; Nikulin SV — cell culture, sample preparation for subsequent proteome analysis, proteomic data analysis; Kurnosov AA — sample preparation for microRNA sequencing, analysis of sequencing data; Raigorodskaya MP — real-time PCR-based analysis of gene expression, transcriptome analysis; Osipyants AI — cell culture, sample preparation for subsequent proteome and transcriptome analyses; Tonevitsky EA — supervision, data analysis, manuscript preparation.

Compliance with ethical standards: the samples were obtained following the principles of the Declaration of Helsinki.

✉ **Correspondence should be addressed:** Diana V. Maltseva
Vavilova, 7, Moscow, 117321; dmaltseva@gmail.com

Received: 08.08.2020 **Accepted:** 21.08.2020 **Published online:** 28.08.2020

DOI: 10.24075/brsmu.2020.049

ГИПОКСИЯ УСИЛИВАЕТ ТРАНСЦИТОЗ В ЭНТЕРОЦИТАХ КИШЕЧНИКА

Д. В. Мальцева¹ ✉, М. Ю. Шкурников^{1,2}, С. А. Нерсисян¹, С. В. Никулин¹, А. А. Курносов¹, М. П. Райгородская³, А. И. Осипьянц^{2,4}, Е. А. Тоневицкий⁵¹ Национальный исследовательский университет «Высшая школа экономики», Москва, Россия² Онкологический институт имени П. А. Герцена (филиал Национального медицинского исследовательского центра радиологии), Москва, Россия³ Научно-технический центр «БиоКлиникум», Москва, Россия⁴ Дальневосточный федеральный университет, Владивосток, Россия⁵ Фонд развития инновационного научно-технологического центра «Долина Менделеева», Москва, Россия

Важнейшее условие нормального функционирования кишечника — сохранение барьерных функций монослоя эпителиальных клеток, выстилающих его поверхность. Воспалительные состояния кишечника, как правило, ассоциированы с дополнительной тканевой гипоксией, что приводит к нарушению целостности эпителия. Однако опасность инфекционных заболеваний может сохраняться и при отсутствии очевидных нарушений монослоя клеток. Возможная причина этого — изменение внутриклеточного транспорта везикул, содержащих бактерии. Целью работы было на модели энтероцитов кишечника человека исследовать влияние гипоксии на процесс транскитоза. Показано, что гипоксия усиливает в 1,8 раза транскитоз модельного белка, растительного лектина рицина. Сравнительное исследование транскриптомов и протеомов выявило достоверное изменение экспрессии генов, вовлеченных во внутриклеточный везикулярный транспорт, в том числе падение экспрессии регулятора метаболизма липидов apoB, как на уровне белка (в 6,5 раза), так и на уровне мРНК (в 2,1 раза). Необходимы работы по изучению возможного механизма регуляции экспрессии генов в энтероцитах кишечника в условиях гипоксии.

Ключевые слова: гипоксия, энтероцит, эпителий кишечника, микроРНК, мРНК, протеом, транскриптом, транскитоз, Caco-2

Финансирование: работа выполнена при финансовой поддержке государства в лице Минобрнауки России (идентификатор соглашения RFMEFI60519X0184).

Благодарности: авторы благодарят Центр коллективного пользования «Протеом человека» (ИБМХ) за возможность использования оборудования.

Вклад авторов: Д. В. Мальцева — молекулярно-биологические исследования, анализ данных, написание статьи; М. Ю. Шкурников — обработка данных транскриптома, секвенирования, статистический анализ; С. А. Нерсисян — обработка данных секвенирования, биоинформатический анализ, функциональный анализ генов; С. В. Никулин — работа с культурой клеток, подготовка образцов для анализа протеома, обработка данных протеома; А. А. Курносов — подготовка образцов для секвенирования микроРНК, анализ данных; М. П. Райгородская — анализ экспрессии генов методом ПЦР-РВ, транскриптомный анализ; А. И. Осипьянц — культуральная работа, подготовка образцов для анализа протеома и транскриптома; Е. А. Тоневицкий — организация исследования, анализ данных, написание статьи.

Соблюдение этических стандартов: все образцы для исследования были получены с соблюдением принципов и правил Хельсинской декларации.

✉ **Для корреспонденции:** Диана Васильевна Мальцева
ул. Вавилова, д. 7, г. Москва, 117321; dmaltseva@gmail.com

Статья получена: 08.08.2020 **Статья принята к печати:** 21.08.2020 **Опубликована онлайн:** 28.08.2020

DOI: 10.24075/vrgmu.2020.049

Protecting the body against infection and creating a proper environment for commensal bacteria inhabiting the intestine are the central functions of the intestinal epithelium. [1, 2]. Bacteria and their antigens are capable of directly interacting with intestinal epithelial cells, including enterocytes [2, 3]. Such interaction can be broken down into a series of events: binding to the cell surface, endocytosis, exocytosis, and transcytosis of bacteria, their fragments or proteins [3]. Proteins, glycolipids and carbohydrates on the enterocyte surface act as receptors for bacterial pathogens [4]. There is a variety of cell lines used to model bacterial adhesion to the intestinal epithelium [5]. Of them, the most popular is the Caco-2 cell line derived from human colon adenocarcinoma cells [6–8]. In a healthy gut lumen, the hypoxic environment is maintained by the metabolic activity of commensal bacteria [5]. Low oxygen levels stabilize hypoxia-inducible factors HIF1 α and HIF2 α , which, in turn, affect the barrier function of the intestinal epithelium [9]. A lot of intestinal disorders are associated with hypoxia [10]. This underscores the importance of researching the interaction between the intestinal microbiota and the intestinal epithelium under low oxygen conditions.

Plant lectins are well-described proteins that are widely used to study intracellular transport and the binding of proteins to the cell surface [11, 12]. Glycosylated proteins and lipids act as receptors for plant lectins, making them a suitable model for studying bacterium-cell interactions. The aim of this work was to investigate the effect of hypoxia on transcytosis in intestinal epithelial cells.

METHODS

Immortalized Caco-2 (colon adenocarcinoma) cells (Institute of Cytology; Saint Petersburg) were cultured in a MEM medium (Gibco; USA) supplemented with 20% fetal bovine serum (FBS; Gibco; USA), 1% (v/v) solution of non-essential amino acids (Gibco; USA), 100 un/ml penicillin, and 100 μ g/ml streptomycin (Gibco; USA). The cells were cultured in 6-well plates (Corning; USA) for 23 days until they differentiated into enterocyte-like cells. The medium was replaced every 2–3 days. To induce hypoxia, 300 mM CoCl₂ (Sigma-Aldrich; USA) was added to the medium; the resultant mixture was incubated for 24 h. Then, the cells were washed in 1 \times DPBS (Gibco; USA) and lysed for the subsequent transcriptome and proteome analysis as previously described in [13, 14].

The effects of hypoxia on the Caco-2 monolayer were evaluated using impedance spectroscopy. Prior to seeding the cells on Transwell[®]-96 permeable supports (Corning; USA), the wells were filled with the culture medium (50 μ l in the upper compartment, 235 μ l in the lower compartment) and incubated for 1 h at 37 °C in a 5% CO₂ atmosphere. Then, about 5,600 cells in 50 μ l medium were seeded in each insert and cultured for 23 days until they differentiated into enterocyte-like cells. The medium was replaced every 2–3 days. To induce hypoxia, CoCl₂ was added to the medium as described above.

Impedance spectra were measured at room temperature in the frequency range of 40 to 20,000 Hz by means of impedance spectrometry (BioClinicum; Russia) using an STX100C96 electrode (World Precision Instruments; USA) [15]. Mean values of cell impedance properties were calculated based on the data obtained from 3 independent inserts. The membrane surface area in each well was 0.143 cm². The data were processed using a graphical user interface for R 3.5 (R-Tools Technology; USA).

The plant lectin ricin was extracted from the seeds of the castor oil plant *Ricinus communis* as described in [16,

17]. Biotinylation, analysis of ricin binding to asialofetuin and cytotoxicity tests on target cells were conducted as described in [18–20].

In order to evaluate transcytosis, differentiated Caco-2 cells were co-incubated with the medium containing biotinylated ricin (1 \times 10⁻⁷ M) in Transwell inserts. The protein was added into the upper compartment onto the apical cell membrane. The colonies were harvested from the lower compartment after 1 and 6 h of incubation for the subsequent immunoassay.

Lectin concentrations in the culture medium were measured using ELISA. Briefly, 100 μ l of anti-ricin RA999 antibodies (10 μ g/ml in 10 mM phosphate buffered saline (PBS) pH 7.4; Sigma-Aldrich; Germany) was immobilized on each well of a 96-well plate (Corning; USA) by passive adsorption. Unbound antibodies were removed by washing the wells in PBS containing 0.05% Tween-20 (PBST). To reduce non-specific binding, the wells were blocked with PBST containing 0.1% bovine serum albumin (BSA) (Diam; Russia). Culture media were diluted 100-fold in PBST supplemented with 50 mM β -lactose (Sigma-Aldrich; Germany) and added into the wells (100 μ l per well) containing the immobilized antibodies. The resultant mixtures were incubated at +37 °C in a thermal shaker. Detection of biotinylated lectin was carried out using HRP-conjugated streptavidin (Intitrogen; Germany). The antibodies were incubated in a 3,3',5,5'-tetramethylbenzidine liquid substrate (Intitrogen; Germany); the reaction was stopped with 1M HCl solution. Absorbance was measured at 450 nm wavelength using a SpectroMax i3 microplate reader (Molecular Devices; USA). Monoclonal antibodies were a gift from Professor Sveshnikov PG (Laboratory of Biotechnology, Russian Research Center for Molecular Diagnostics and Therapy; Russia).

Real-time PCR-based analysis of gene expression was performed as previously described [14]. Transcripts of the *ACTB* and *GAPDH* genes were used as references.

mRNA expression profiles were analyzed using Gene Chip Human Transcriptome Array 2.0 (TermoFisher Scientific-Affymetrix; USA). RNA isolation, quantification and quality control were performed as described in [14]. The RNA integrity number (RIN) was above 9.5 for all studied samples. cDNA was synthesized from 500 ng of isolated total RNA. All stages of sample preparation, hybridization, washing, staining, and microarray scanning were carried out as described in [21]. CEL files generated by the scanner were processed in Transcriptome Analysis Console 2.0 (TermoFisher Scientific-Affymetrix; USA). Unannotated microarray probesets were excluded from the analysis. The microarray intensity signal equal to 6.0 on the Affymetrix log scale was used as a threshold.

MicroRNA expression profiles were analyzed by means of next-generation sequencing (NGS). NGS libraries were prepared from a small RNA fraction using a CATS small RNA-seq kit (Diagenode; Belgium) following the manufacturer's protocol. Upon PCR amplification, the libraries were purified using magnetic AMPPure beads. Final libraries concentrations were measured using a Qubit v2.0 DNA High Sensitivity DNA Kit (TermoFisher Scientific; USA). The pooled libraries were denatured, grouped on 6 Illumina HiSeq2000 V4 flow cell systems (Illumina; USA) and then sequenced. Fifty-one cycles of deep sequencing and 6 index read cycles were run. Sequencing data were exported into a FASTQ file; adapters were trimmed and poly-A-tails were removed from the reads.

Quality control of FASTQ files generated by microRNA sequencing was carried out in FastQC v0.11.9 (Braham Bioinformatics; UK). Adapter sequences were trimmed in Cutadapt v. 2.8 [22]; reads shorter than 18 nucleotides were

removed. MicroRNA expression was quantified in miRDeep2 [23]. Differential expression analysis of the microRNA sequencing data was conducted using the R environment v. 3.6.3 (R-Tools Technology; USA) and the DESeq2 library [24].

For statistical analysis, the raw data from microarrays were normalized in the oligo software package for R (R-Tools Technology; USA). Base 2 logarithm was applied to the normalized data. Differential gene and microRNA expression was analyzed using Student's t test. False Discovery Rate (FDR) and the Benjamini-Hochberg procedure were applied for multiple testing correction.

The functional annotation of genes was performed using DAVID databases and algorithms v. 6.8 (Laboratory of Human Retrovirology and Immunoinformatics; USA). Validated microRNA: gene interactions were exported from the DIANA-TarBase database v. 8 (DIANA Lab; Greece) [25]. microRNA binding sites on 3'-non-translated regions of mRNA targets were predicted using miRWalk [26]. The search for intronic microRNA and their host genes was conducted in the miRIAD database.

Preparation of Caco-2 lysates, total protein extraction, hydrolytic cleavage and subsequent procedures necessary for proteomic analysis were carried out as described in [14]. After tryptic hydrolysis, the supernatant was collected and analyzed in a Q-Exactive HFX mass spectrometer in the positive ion mode using a nano-spray ion (nESI) source (Thermo Fisher Scientific; USA) operated at the emitter voltage of 2.1 kV and the inlet capillary temperature of 240 °C. For the analysis of differentially expressed proteins, primary spectrometry data were processed in MaxQuant 1.6 (the iBAQ algorithm) (Max-

Planck-Institute of Biochemistry; Germany). Further data processing was aided by the Perseus platform and R 3.5 with the integrated RStudio 1.1 development environment (R-Tools Technology; USA). Significance of differences was evaluated using Student's t-test.

RESULTS

Hypoxic culture conditions stimulate transcytosis across intestinal enterocytes and are associated with changed expression of genes involved in vesicle transport

Caco-2 human colon adenocarcinoma cells were cultured under hypoxia-mimicking conditions created by treating the cells with CoCl_2 . According to the impedance spectroscopy data, CoCl_2 did not disrupt the integrity of the Caco-2 monolayer. The transepithelial electrical resistance (TEER) value remained at $2,000 \Omega$, indicating the lack of pronounced cytotoxicity and cell death.

The microarray analysis of mRNA profiles exposed that treating enterocytes with CoCl_2 caused upwards of a twofold increase (FDR < 0.05) in the expression of 165 genes, among which were genes involved in cellular response to hypoxia, such as *DDIT4* (2.4-fold), *EGLN1* (2.7-fold), *LDHA* (twofold), *PFKFB3* (2.1-fold), *SLC2A1* (3.1-fold), *SLC2A3* (3.0-fold), and *VEGFA* (1.4-fold). Changes in the expression profiles of these genes were confirmed by real-time PCR ($p < 0.05$). Besides, the functional annotation of differentially expressed genes assisted by DAVID tools revealed significant enrichment of the

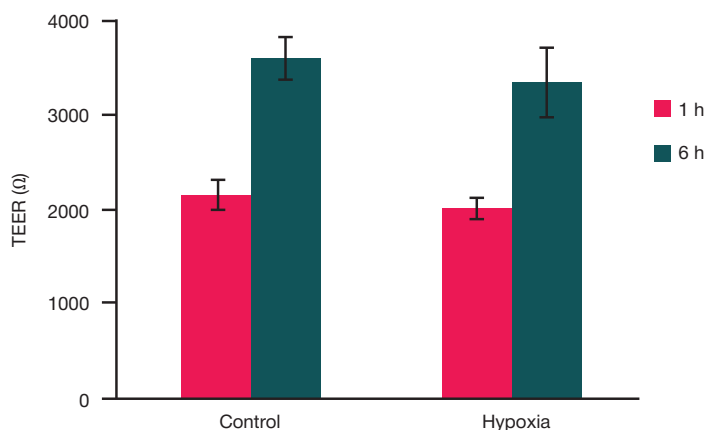


Fig. 1. Transepithelial electrical resistance (TEER) at different time points following the treatment of enterocytes with ricin

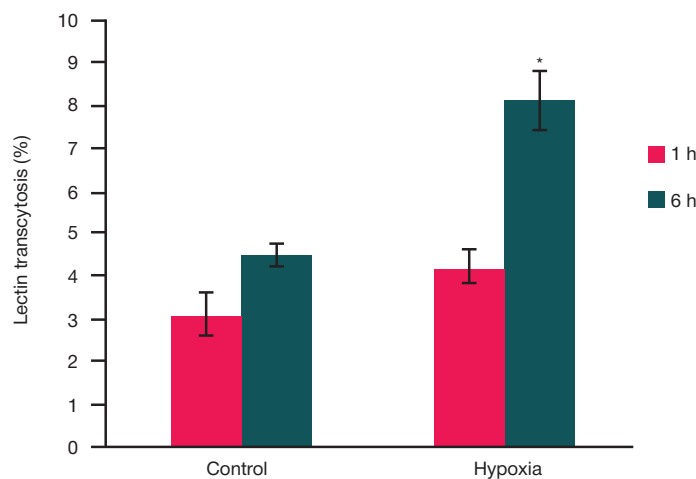


Fig. 2. The amount of biotinylated lectin transcytosed across enterocytes under normoxic conditions (control) and in the hypoxic environment; * — lectin proportion transcytosed after 6 h under hypoxic conditions differs significantly from the control ($p < 0,05$)

HIF-1 signaling pathway, which is known to mediate cellular response to hypoxia (this data is not provided in the present study). Summing up, treatment of enterocytes with CoCl_2 reliably mimics low-oxygen conditions.

To assess the efficacy of transcytosis across the monolayer of enterocytes under normoxic and hypoxic conditions, the apical domain of the differentiated Caco-2 cells grown in Transwell inserts was treated with the culture medium supplemented with biotinylated ricin. In the control wells, where the cells were cultured under normoxic conditions, the medium in the apical compartment was replaced with lectin-free medium. At 1 and 6 hours after the culture medium in the upper compartment was replaced, the medium from the lower compartment was harvested and analyzed for lectin concentrations using ELISA. Cell impedance properties were monitored for 6 h after lectin treatment; impedance spectroscopy data suggested that integrity of the monolayer was retained, which is consistent with earlier findings [27]. Six hours after lectin treatment, the TEER value increased in both control and hypoxic samples (Fig.10). This suggests formation of more intimate contacts between the cells. Thus, we can rule out the possibility of protein molecules being transported from the upper compartment containing the enterocyte monolayer into the lower compartment via paracytosis. Therefore, lectin was transported from the upper compartment to the lower by means of transcytosis.

According to ELISA, lectin undergoes transcytosis across enterocytes under both normoxic and hypoxic conditions. The amount of transcytosed lectin increased 1.8-fold ($p < 0.05$) after 6 h in the hypoxic environment, as compared with normoxic conditions (Fig. 2).

The functional analysis of differentially expressed genes allowed us to identify 16 genes involved in the intracellular vesicular traffic (Table 1).

Gene expression profiles of enterocytes were also analyzed by means of protein mass spectrometry. The total number of reliably detected proteins was 3,361. Levels of 237 proteins differed significantly (\geq two-fold) between the samples cultured under normal and hypoxic conditions. Of all proteins with changed expression profiles (according to microarray data) that were encoded by the genes involved in the intercellular transport of vesicles, only 4 were detected in the proteome: apoB (*APOB*), SorLA-1 (*SORL1*), CAM-PRP (*PPP3CA*), and CEACAM1. A significant (6.5-fold) drop in protein expression was observed for apoB, which is consistent with the results of the transcriptome analysis.

Expression of *APOB*, *SORL1*, *PPP3CA*, and *CEACAM1* genes in intestinal enterocytes can be regulated by miRNA

In order to identify a possible mechanism regulating the expression of genes involved in intracellular transport of

Table 1. Differentially expressed genes involved in intracellular vesicular traffic

Gene	Changes in expression, fold*	p-value	FDR
<i>OLR1</i>	-2.4	0.0003	0.004
<i>ADM</i>	2.1	0.0007	0.006
<i>LRP4</i>	1.5	0.0014	0.008
<i>SORL1</i>	1.9	0.0044	0.019
<i>LDLR</i>	1.9	0.0068	0.019
<i>ABCA1</i>	-2.1	0.0056	0.019
<i>SDCBP</i>	1.7	0.0097	0.024
<i>PPP3CA</i>	-1.6	0.0219	0.029
<i>APOB</i>	-2.1	0.0208	0.029
<i>CEACAM1</i>	1.8	0.0243	0.030
<i>ENPP1</i>	-1.8	0.0142	0.030
<i>ITGA2</i>	3.2	0.0203	0.031
<i>RAB27B</i>	-1.9	0.0201	0.034
<i>FCHSD2</i>	-1.6	0.0193	0.037
<i>SLC9B2</i>	-1.5	0.0381	0.043
<i>KIAA1107</i>	-1.7	0.0434	0.046

Note: * — the ratio of expression levels (arbitrary units) under hypoxic conditions to the expression levels under standard culture conditions. The data were gathered from microarrays. A negative value means that the expression of the studied gene decreased.

Table 2. Differentially expressed miRNAs regulating the expression of genes involved in intracellular vesicle transport

miRNA	Changes in expression, -fold*	mRNA-target
hsa-miR-27a-5p	1.5	<i>APOB</i>
hsa-miR-1303	-2.1	<i>SORL1</i>
hsa-miR-100-5p	-1.8	<i>SORL1</i>
hsa-miR-4521	-1.6	<i>SORL1</i>
hsa-miR-21-3p	1.7	<i>PPP3CA</i>
hsa-miR-32-3p	-1.6	<i>CEACAM1</i>
hsa-miR-148a-5p	-1.5	<i>CEACAM1</i>

Note: * — the ratio of expression levels (arbitrary units) under hypoxic conditions to the expression levels under standard culture conditions; the data were generated by NGS. A negative value means that the expression of the studied miRNA decreased.

vesicles, we analyzed miRNA expression profiles using NGS. Changes in transcript expression were significant (≥ 1.5 -fold, $p \leq 0.05$) for 16 miRNAs. Interestingly, 7 of them were regulatory miRNAs for *APOB*, *SORL1*, *PPP3CA* and *CEACAM1* [25]. For these miRNAs, the direction of changes anticorrelated with the direction of changes in the expression of the corresponding mRNA targets (Table 2).

DISCUSSION

A tremendous amount of evidence has been accrued about the mechanisms underlying the intracellular transport of vesicles by studying how ricin penetrates the cell [11]. The binding of this plant lectin to glycosylated proteins on the cell surface induces endocytosis, and ricin is then carried by the vesicles to the Golgi apparatus and endoplasmic reticulum. Thank to ricin, researchers were able to learn a lot about the apical and basolateral intracellular transport and transcytosis in polarized epithelial cells.

Ever more attention is being paid to the role of hypoxia and hypoxia-inducible signaling pathways in the physiology of the intestine and its disorders. The normal microenvironment of the intestinal epithelium is physiologically hypoxic; additional tissue hypoxia is a sign of active inflammation [10]. The integrity of the epithelial cell lining is key to the normal intestinal function [2]. But even in the absence of visible damage to the epithelial monolayer, there still could be a risk of infection due to transcytosis, e.g. the intracellular transport of vesicles containing bacteria [7, 28]. Our study demonstrates that lectin transcytosis is significantly stimulated in the intact enterocyte monolayer under hypoxic conditions. Comparative transcriptome analysis revealed changes in the expression of genes involved in the intracellular transport of vesicles in the cells cultured in a hypoxic environment. A significant drop in the expression of *APOB* (one of such genes) was subsequently confirmed by the proteomic analysis. Notably, the apoB protein is the key regulator of lipid and cholesterol metabolism in enterocytes [29, 30]. Found predominantly in the endoplasmic reticulum, apoB facilitates

the packaging of lipids and cholesterol adsorbed from the apical lipid domain into prechylomicrons (apoB-containing particles). As these particles are transported inside membrane vesicles to the Golgi apparatus, they mature into chylomicrons and are then secreted from the basolateral enterocyte domain via exocytosis. In a healthy intestinal enterocyte, apoB-containing particles are formed and secreted continuously [29]. Perhaps, the observed significant decrease in apoB expression can activate compensatory mechanisms underlying the secretion of adsorbed and accumulated lipids and cholesterol; one of such possible mechanisms is transcytosis. Importantly, lipids and cholesterol accumulated in the cell are building blocks for cell membranes. Altogether, this might affect membrane transport in enterocytes.

In order to elucidate the mechanism regulating the observed changes, we analyzed miRNA expression profiles. Interestingly, 7 of 16 miRNAs there were found to be differentially expressed in response to hypoxia, were regulators of differentially expressed genes involved in intracellular vesicle transport. Besides, the direction of miRNA expression changes anticorrelated with changes in the expression of the corresponding mRNA-targets. Our findings suggest that enterocyte properties could be altered via a miRNA-dependent mechanism under hypoxic conditions.

CONCLUSION

Using the human intestinal enterocyte model, we demonstrated that hypoxia stimulates transcytosis. This process is accompanied by changes in the expression of genes involved in intracellular vesicle transport. We found that hypoxia is associated with a decrease in the expression of the apoB protein, the key regulator of lipid metabolism at both mRNA and protein levels. The regulatory mechanism underlying changes of cell properties might involve regulation of gene expression by microRNA. Further research into the links between lipid metabolism and transcytosis would help in designing drugs for reducing the risk of intestinal infection promoted by inflammation.

References

1. Chang C-S, Kao C-Y. Current understanding of the gut microbiota shaping mechanisms. *J Biomed Sci.* 2019; 26 (1): 59.
2. Solis AG, Klapholz M, Zhao J, Levy M. The bidirectional nature of microbiome-epithelial cell interactions. *Curr Opin Microbiol.* Elsevier Current Trends. 2020; 56: 45–51.
3. Hu L, Tall BD, Curtis SK, Kopecko DJ. Enhanced microscopic definition of *Campylobacter jejuni* 81-176 adherence to, invasion of, translocation across, and exocytosis from polarized human intestinal Caco-2 cells. *Infect Immun.* American Society for Microbiology Journals. 2008; 76 (11): 5294–304.
4. Blanco LP, DiRita VJ. Bacterial-associated cholera toxin and GM1 binding are required for transcytosis of classical biotype *Vibrio cholerae* through an in vitro M cell model system. *Cell Microbiol.* 2006; 8 (6): 982–98.
5. Bartfeld S. Modeling infectious diseases and host-microbe interactions in gastrointestinal organoids. *Dev Biol Academic Press.* 2016; 420 (2): 262–70.
6. Sakharov D, Maltseva D, Knyazev E, Nikulin S, Poloznikov A, Shilin S, et al. Towards embedding Caco-2 model of gut interface in a microfluidic device to enable multi-organ models for systems biology. *BMC Syst Biol BioMed Central.* 2019; 13 (S1): 19.
7. Panigrahi P, Bamford P, Horvath K, Morris JG, Gewolb IH. *Escherichia coli* transcytosis in a Caco-2 cell model: implications in neonatal necrotizing enterocolitis. *Pediatr Res Nature Publishing Group.* 1996; 40 (3): 415–21.
8. Rubio APD, Martínez J, Palavecino M, Fuentes F, López CMS, Marcilla A, et al. Transcytosis of *Bacillus subtilis* extracellular vesicles through an in vitro intestinal epithelial cell model. *Sci Rep Nature Publishing Group.* 2020; 10 (1): 3120.
9. Kelly CJ, Zheng L, Campbell EL, Saeedi B, Scholz CC, Bayless AJ, et al. Crosstalk between microbiota-derived short-chain fatty acids and intestinal epithelial HIF augments tissue barrier function. *Cell Host Microbe.* 2015; 17 (5): 662–71.
10. Cummins EP, Crean D. Hypoxia and inflammatory bowel disease. *Microbes Infect.* 2017; 19 (3): 210–21.
11. Sandvig K, Torgersen ML, Engedal N, Skotland T, Iversen T-G. Protein toxins from plants and bacteria: Probes for intracellular transport and tools in medicine. *FEBS Lett.* John Wiley & Sons, Ltd. 2010; 584 (12): 2626–34.
12. Moisenovich M, Tonevitsky A, Agapov I, Niwa H, Schewe H, Bereiter-Hahn J. Differences in endocytosis and intracellular sorting of ricin and viscumin in 3T3 cells. *Eur J Cell Biol.* 2002; 81 (10): 529–38.
13. Khaustova NA, Maltseva DV, Oliveira-Ferrer L, Stürken C, Milde-Langosch K, Makarova JA, et al. Selectin-independent adhesion during ovarian cancer metastasis. *Biochimie.* 2017; 142: 197–206.
14. Maltseva D, Raygorodskaya M, Knyazev E, Zgodva V, Tikhonova O, Zaidi S, et al. Knockdown of the $\alpha 5$ laminin chain affects

- differentiation of colorectal cancer cells and their sensitivity to chemotherapy. *Biochimie*. 2020; 174: 107–16.
15. Gerasimenko T, Nikulin S, Zakharova G, Poloznikov A, Petrov V, Baranova A, et al. Impedance spectroscopy as a tool for monitoring performance in 3D models of epithelial tissues. *Front Bioeng Biotechnol*. 2020; 7: 474.
 16. Tonevitsky AG, Agapov II, Shamshiev AT, Temyakov DE, Pohl P, Kirpichnikov MP. Immunotoxins containing A-chain of mistletoe lectin I are more active than immunotoxins with ricin A-chain. *FEBS Lett*. 1996; 392 (2): 166–8.
 17. Moisenovich M, Tonevitsky A, Maljuchenko N, Kozlovskaya N, Agapov I, Volkmandt W, et al. Endosomal ricin transport: involvement of Rab4- and Rab5-positive compartments. *Histochem Cell Biol*. 2004; 121 (6): 429–39.
 18. Agapov II, Tonevitsky AG, Moysenovich MM, Maluchenko NV, Weyhenmeyer R, Kirpichnikov MP. Mistletoe lectin dissociates into catalytic and binding subunits before translocation across the membrane to the cytoplasm. *FEBS Lett*. 1999; 452 (3): 211–4.
 19. Agapov II, Tonevitsky AG, Maluchenko NV, Moisenovich MM, Bulah YS, Kirpichnikov MP. Mistletoe lectin A-chain unfolds during the intracellular transport. *FEBS Lett*. 1999; 464 (1–2): 63–6.
 20. Pohl P, Antonenko YN, Evtodienko VY, Pohl EE, Saparov SM, Agapov II, et al. Membrane fusion mediated by ricin and viscumin. *Biochim Biophys Acta*. 1998; 1371 (1): 11–6.
 21. Kudriaeva A, Galatenko V, Maltseva D, Khaustova N, Kuzina E, Tonevitsky A, et al. The transcriptome of type I murine astrocytes under interferon-Gamma exposure and remyelination stimulus. *Molecules*. 2017; 22 (5): 808.
 22. Martin M. Cutadapt removes adapter sequences from high-throughput sequencing reads. *EMBnet.journal*. 2011; 17 (1): 10.
 23. Friedländer MR, Mackowiak SD, Li N, Chen W, Rajewsky N. miRDeep2 accurately identifies known and hundreds of novel microRNA genes in seven animal clades. *Nucleic Acids Res*. 2012; 40 (1): 37–52.
 24. Love MI, Huber W, Anders S. Moderated estimation of fold change and dispersion for RNA-seq data with DESeq2. *Genome Biol*. 2014; 15 (12): 550.
 25. Karagkouni D, Paraskevopoulou MD, Chatzopoulos S, Vlachos IS, Tastsoglou S, Kanellos I, et al. DIANA-TarBase v8: a decade-long collection of experimentally supported miRNA–gene interactions. *Nucleic Acids Res*. 2018; 46 (D1): D239–45.
 26. Sticht C, De La Torre C, Parveen A, Gretz N. miRWalk: An online resource for prediction of microRNA binding sites. *PLoS One*. 2018; 13 (10): e0206239.
 27. Flora AD, Teel LD, Smith MA, Sinclair JF, Melton-Celsa AR, O'Brien AD. Ricin crosses polarized human intestinal cells and intestines of ricin-gavaged mice without evident damage and then disseminates to mouse kidneys. *PLoS One*. 2013; 8 (7): e69706.
 28. Macutkiewicz C, Carlson G, Clark E, Dobrindt U, Roberts I, Warhurst G. Characterisation of *Escherichia coli* strains involved in transcytosis across gut epithelial cells exposed to metabolic and inflammatory stress. *Microbes Infect*. 2008; 10 (4): 424–31.
 29. Ko C-W, Qu J, Black DD, Tso P. Regulation of intestinal lipid metabolism: current concepts and relevance to disease. *Nat Rev Gastroenterol Hepatol*. 2020; 17 (3): 169–83.
 30. Lo CC, Coschigano KT. ApoB48 as an efficient regulator of intestinal lipid transport. *Front Physiol*. 2020; 11: 796.

Литература

1. Chang C-S, Kao C-Y. Current understanding of the gut microbiota shaping mechanisms. *J Biomed Sci*. 2019; 26 (1): 59.
2. Solis AG, Klapholz M, Zhao J, Levy M. The bidirectional nature of microbiome-epithelial cell interactions. *Curr Opin Microbiol*. Elsevier Current Trends. 2020; 56: 45–51.
3. Hu L, Tall BD, Curtis SK, Kopecko DJ. Enhanced microscopic definition of *Campylobacter jejuni* 81-176 adherence to, invasion of, translocation across, and exocytosis from polarized human intestinal Caco-2 cells. *Infect Immun*. American Society for Microbiology Journals. 2008; 76 (11): 5294–304.
4. Blanco LP, DiRita VJ. Bacterial-associated cholera toxin and GM1 binding are required for transcytosis of classical biotype *Vibrio cholerae* through an in vitro M cell model system. *Cell Microbiol*. 2006; 8 (6): 982–98.
5. Bartfeld S. Modeling infectious diseases and host-microbe interactions in gastrointestinal organoids. *Dev Biol Academic Press*. 2016; 420 (2): 262–70.
6. Sakharov D, Maltseva D, Knyazev E, Nikulin S, Poloznikov A, Shilin S, et al. Towards embedding Caco-2 model of gut interface in a microfluidic device to enable multi-organ models for systems biology. *BMC Syst Biol BioMed Central*. 2019; 13 (S1): 19.
7. Panigrahi P, Bamford P, Horvath K, Morris JG, Gewolb IH. *Escherichia coli* transcytosis in a Caco-2 cell model: implications in neonatal necrotizing enterocolitis. *Pediatr Res Nature Publishing Group*. 1996; 40 (3): 415–21.
8. Rubio APD, Martínez J, Palavecino M, Fuentes F, López CMS, Marcilla A, et al. Transcytosis of *Bacillus subtilis* extracellular vesicles through an in vitro intestinal epithelial cell model. *Sci Rep Nature Publishing Group*. 2020; 10 (1): 3120.
9. Kelly CJ, Zheng L, Campbell EL, Saeedi B, Scholz CC, Bayless AJ, et al. Crosstalk between microbiota-derived short-chain fatty acids and intestinal epithelial HIF augments tissue barrier function. *Cell Host Microbe*. 2015; 17 (5): 662–71.
10. Cummins EP, Crean D. Hypoxia and inflammatory bowel disease. *Microbes Infect*. 2017; 19 (3): 210–21.
11. Sandvig K, Torgersen ML, Engedal N, Skotland T, Iversen T-G. Protein toxins from plants and bacteria: Probes for intracellular transport and tools in medicine. *FEBS Lett*. John Wiley & Sons, Ltd., 2010; 584 (12): 2626–34.
12. Moisenovich M, Tonevitsky A, Agapov I, Niwa H, Schewe H, Bereiter-Hahn J. Differences in endocytosis and intracellular sorting of ricin and viscumin in 3T3 cells. *Eur J Cell Biol*. 2002; 81 (10): 529–38.
13. Khaustova NA, Maltseva DV, Oliveira-Ferrer L, Stürken C, Milde-Langosch K, Makarova JA, et al. Selectin-independent adhesion during ovarian cancer metastasis. *Biochimie*. 2017; 142: 197–206.
14. Maltseva D, Raygorodskaya M, Knyazev E, Zgoda V, Tikhonova O, Zaidi S, et al. Knockdown of the $\alpha 5$ laminin chain affects differentiation of colorectal cancer cells and their sensitivity to chemotherapy. *Biochimie*. 2020; 174: 107–16.
15. Gerasimenko T, Nikulin S, Zakharova G, Poloznikov A, Petrov V, Baranova A, et al. Impedance spectroscopy as a tool for monitoring performance in 3D models of epithelial tissues. *Front Bioeng Biotechnol*. 2020; 7: 474.
16. Tonevitsky AG, Agapov II, Shamshiev AT, Temyakov DE, Pohl P, Kirpichnikov MP. Immunotoxins containing A-chain of mistletoe lectin I are more active than immunotoxins with ricin A-chain. *FEBS Lett*. 1996; 392 (2): 166–8.
17. Moisenovich M, Tonevitsky A, Maljuchenko N, Kozlovskaya N, Agapov I, Volkmandt W, et al. Endosomal ricin transport: involvement of Rab4- and Rab5-positive compartments. *Histochem Cell Biol*. 2004; 121 (6): 429–39.
18. Agapov II, Tonevitsky AG, Moysenovich MM, Maluchenko NV, Weyhenmeyer R, Kirpichnikov MP. Mistletoe lectin dissociates into catalytic and binding subunits before translocation across the membrane to the cytoplasm. *FEBS Lett*. 1999; 452 (3): 211–4.
19. Agapov II, Tonevitsky AG, Maluchenko NV, Moisenovich MM, Bulah YS, Kirpichnikov MP. Mistletoe lectin A-chain unfolds during the intracellular transport. *FEBS Lett*. 1999; 464 (1–2): 63–6.
20. Pohl P, Antonenko YN, Evtodienko VY, Pohl EE, Saparov SM, Agapov II, et al. Membrane fusion mediated by ricin and viscumin. *Biochim Biophys Acta*. 1998; 1371 (1): 11–6.
21. Kudriaeva A, Galatenko V, Maltseva D, Khaustova N, Kuzina E, Tonevitsky A, et al. The transcriptome of type I murine astrocytes under interferon-Gamma exposure and remyelination stimulus. *Molecules*. 2017; 22 (5): 808.
22. Martin M. Cutadapt removes adapter sequences from high-throughput sequencing reads. *EMBnet.journal*. 2011; 17 (1): 10.

23. Friedländer MR, Mackowiak SD, Li N, Chen W, Rajewsky N. miRDeep2 accurately identifies known and hundreds of novel microRNA genes in seven animal clades. *Nucleic Acids Res.* 2012; 40 (1): 37–52.
24. Love MI, Huber W, Anders S. Moderated estimation of fold change and dispersion for RNA-seq data with DESeq2. *Genome Biol.* 2014; 15 (12): 550.
25. Karagkouni D, Paraskevopoulou MD, Chatzopoulos S, Vlachos IS, Tastsoglou S, Kanellos I, et al. DIANA-TarBase v8: a decade-long collection of experimentally supported miRNA–gene interactions. *Nucleic Acids Res.* 2018; 46 (D1): D239–45.
26. Sticht C, De La Torre C, Parveen A, Gretz N. miRWalk: An online resource for prediction of microRNA binding sites. *PLoS One.* 2018; 13 (10): e0206239.
27. Flora AD, Teel LD, Smith MA, Sinclair JF, Melton-Celsa AR, O'Brien AD. Ricin crosses polarized human intestinal cells and intestines of ricin-gavaged mice without evident damage and then disseminates to mouse kidneys. *PLoS One.* 2013; 8 (7): e69706.
28. Macutkiewicz C, Carlson G, Clark E, Dobrindt U, Roberts I, Warhurst G. Characterisation of *Escherichia coli* strains involved in transcytosis across gut epithelial cells exposed to metabolic and inflammatory stress. *Microbes Infect.* 2008; 10 (4): 424–31.
29. Ko C-W, Qu J, Black DD, Tso P. Regulation of intestinal lipid metabolism: current concepts and relevance to disease. *Nat Rev Gastroenterol Hepatol.* 2020; 17 (3): 169–83.
30. Lo CC, Coschigano KT. ApoB48 as an efficient regulator of intestinal lipid transport. *Front Physiol.* 2020; 11: 796.

STOMACH WALL CHANGES AFTER GASTROPLICATION IN PATIENTS WITH MORBID OBESITY

Galimov OV, Khanov VO ✉, Ziangiroy RA, Galimova ES, Minigalin DM, Galimov DO

Bashkir State Medical University, Ufa, Russia

Morbid obesity is a distinct disorder which leads to metabolic disorders and to the development of many severe chronic diseases, therefore, the effective treatment of the disorder is an urgent problem of modern medicine. Currently, morbid obesity and the corresponding disorders are a growing problem associated with a significant risk of morbidity and mortality. The study was aimed to assess the morphological and functional changes in the stomach wall after gastroplication performed by the new method worked out in the Clinic of the Department of Surgical Diseases and New Technologies of the Bashkir State Medical University. Gastroplication was performed in 15 male rabbits of the Gray Giant breed aged 12–16 months weighting 3050–5380 g. The animals were withdrawn from the experiment 3, 6 and 12 months after surgery, followed by histological examination of the stomach wall plicated section. Changes in the mucous membrane and the muscle layer of the stomach wall after gastroplication were adaptive and associated with no severe morphological impairment. That made it possible to use the method in clinical practice in 15 patients with morbid obesity, 9 women and 6 men aged 42 ± 2.1 . In most patients (13 people, 86.7%), a steady decrease in the body weight was achieved during the first 2–12 months. Long-term treatment results had been tracked during two years. It has been confirmed, that the new laparoscopic gastroplication technique does not lead to pathological changes in the stomach wall plicated section, therefore, the simple and cost-effective method may be used in clinical practice for treatment of patients with morbid obesity.

Keywords: bariatric surgery, gastroplication, clinical and experimental studies, operations on rabbits, laparoscopic surgery

Author contribution: Galimov OV, Khanov VO — study concept and design; Khanov VO, Ziangiroy RA, Galimova ES — study planning; Minigalin DM, Galimov DO, Galimova ES — literature analysis; Ziangiroy RA, Minigalin DM, Galimov DO — data acquisition and processing; Galimova ES, Minigalin DM — statistical analysis; Galimov OV, Khanov VO, Minigalin DM — data interpretation; Minigalin DM, Galimov DO — manuscript preparation; O. B. Галимов, В. О. Х. Galimov OV, Khanov VO, Ziangiroy RA — editing.

Compliance with ethical standards: the clinical study was approved by the Ethics Committee of the Bashkir State Medical University Clinic (protocol № 47 dated May 29, 2020). The informed consent was submitted by all patients or their legal representatives. The animals were treated in strict compliance with the Declaration of Helsinki, Directive 2010/63/EU of the European Parliament and the Council (September 22, 2010) on the protection of animals used for scientific purposes, and Good Laboratory Practice guidelines established by the Order 708n of the Ministry of Healthcare of the Russian Federation (August 23, 2010).

✉ **Correspondence should be addressed:** Vladislav O. Khanov
Sultanova, 24-24, Ufa, 450076; khanovv@mail.ru

Received: 12.06.2020 **Accepted:** 26.06.2020 **Published online:** 13.07.2020

DOI: 10.24075/brsmu.2020.041

ИЗМЕНЕНИЯ В СТЕНКЕ ЖЕЛУДКА ПОСЛЕ ГАСТРОПЛИКАЦИИ У ПАЦИЕНТОВ С МОРБИДНЫМ ОЖИРЕНИЕМ

О. В. Галимов, В. О. Ханов ✉, Р. А. Зиангиров, Е. С. Галимова, Д. М. Минигалин, Д. О. Галимов

Башкирский государственный медицинский университет, Уфа, Россия

Морбидное ожирение — самостоятельное заболевание, ведущее к метаболическим нарушениям и развитию многих серьезных хронических заболеваний, поэтому его эффективное лечение является актуальной проблемой современной медицины. На сегодняшний день морбидное ожирение и ассоциированные с ним заболевания представляют собой все возрастающую проблему, связанную со значительным риском заболеваемости и смертности. Целью исследования было изучить морфофункциональные изменения в стенке желудка после выполнения гастропликации в новом варианте, разработанном на базе кафедры хирургических болезней и новых технологий Башкирского государственного медицинского университета. Гастропликацию выполнили 15 кроликам-самцам породы «Серый великан» в возрасте 12–16 месяцев, весившим 3050–5380 г. Животных выводили из эксперимента через 3, 6 и 12 месяцев с последующим гистологическим изучением стенки пликированного участка желудка. Изменения, происходившие в слизистой и мышечном слое стенки желудка после гастропликации, носили адаптивный характер и не сопровождалась серьезными морфологическими нарушениями. Это позволило применить способ в клинической практике у 15 пациентов с морбидным ожирением, 9 женщин и 6 мужчин в возрасте $42 \pm 2,1$ лет. В дальнейшем у большинства (13 пациентов, 86,7%) удалось достичь стойкого снижения массы тела в течение первых 2–12 месяцев. Отдаленные результаты лечения отслеживали в течение двух лет. Было установлено, что разработанная методика лапароскопической гастропликации не вызывает патологических изменений стенки желудка в пликированной ее части, поэтому ее можно применять в клинической практике для лечения пациентов с морбидным ожирением как технически простую и экономически эффективную.

Ключевые слова: бариатрическая хирургия, гастропликация, клиничко-экспериментальная работа, операции на кроликах, лапароскопические вмешательства

Вклад авторов: О. В. Галимов, В. О. Ханов — концепция и дизайн исследования; В. О. Ханов, Р. А. Зиангиров, Е. С. Галимова — планирование исследования; Д. М. Минигалин, Д. О. Галимов, Е. С. Галимова — анализ литературы; Р. А. Зиангиров, Д. М. Минигалин, Д. О. Галимов — сбор и обработка данных; Е. С. Галимова, Д. М. Минигалин — статистическая обработка; О. В. Галимов, В. О. Ханов, Д. М. Минигалин — интерпретация данных; Д. М. Минигалин, Д. О. Галимов — подготовка рукописи; О. В. Галимов, В. О. Ханов, Р. А. Зиангиров — редактирование.

Соблюдение этических стандартов: клиническая работа одобрена этическим комитетом Клиники ФГБОУ ВО БГМУ Минздрава России (протокол № 47 от 29 мая 2020 г.). Добровольное информированное согласие получено от всех участников исследования или их законных представителей. Условия содержания животных и работы с ними соответствовали принципам Хельсинкской декларации о гуманном отношении к животным, директиве Европейского парламента и Совета Европейского союза 2010/63/ЕС от 22 сентября 2010 г. о защите животных, используемых для научных целей, «Правилам лабораторной практики в Российской Федерации», утвержденным приказом Министерства здравоохранения РФ № 708н от 23 августа 2010 г.

✉ **Для корреспонденции:** Владислав Олегович Ханов
ул. Султанова, д. 24, кв. 24, г. Уфа, 450076; khanovv@mail.ru

Статья получена: 12.06.2020 **Статья принята к печати:** 26.06.2020 **Опубликована онлайн:** 13.07.2020

DOI: 10.24075/vrgmu.2020.041

In recent years, in all countries in the doctors of various specialties, there is a growing interest to the problem of metabolic disorders. According to some sources, about 250 million people are obese, representing approximately 7% of the world's adult population. According to WHO, in the developed world, about one third (33.3%) of the population has excess body weight [1, 2]. The consequences of the metabolic syndrome as a complication of obesity are a significant reduction in life expectancy and a decrease in the quality of life. Meanwhile, the risk of severe metabolic disorders, such as type 2 diabetes mellitus, hypertension, coronary heart disease, increases significantly, which leads to an increase in mortality of patients aged under 40 by 12 times. Most modern researchers recognize that that conservative treatment of extreme obesity is an extremely difficult and for 90–95% of patients impossible task [3–5].

Most authors substantiate the need to use a powerful resource of various surgical methods for correction of associated with obesity pathological changes by the rapid increase in the number of obese patients and a significant increase in the cost of their treatment [6, 7]. The use of surgical methods for treating patients with metabolic syndrome is the most effective way to combat morbid obesity, especially in patients with complications. This requires a special approach, both in the pre-operative preparation and in the intra- and postoperative management, which is due to concomitant pathologies of vital organs and systems detected in all patients [8–10].

In bariatric surgery, there is a well known procedure for reducing gastric volume via invagination of the stomach wall section in the lumen (suturing a fold using the corrugated sero-muscular sutures) along the greater curvature [11, 12]. A group of authors has reported the 12-year experience of laparoscopic gastroplication performed in the Laleh and Sina hospitals (Iran) in more than 800 patients [13, 14]. However, currently there are no literature data on the morphological changes in the stomach wall after gastroplication, and therefore the importance of the research is unquestionable [15].

In the Clinic of the Department of Surgical Diseases and New Technologies of the Bashkir State Medical University, the surgical treatment of morbid obesity and metabolic syndrome has been carried out since 2003. For a long period, many generally accepted methods have been used, and the new original methods have been developed. The various invasive bariatric procedures were performed in 165 patients with their

body mass index (BMI) exceeding 35 kg/m². In recent years, the restrictive surgery has been preferred, especially the sleeve gastrectomy performed mainly by laparoscopy.

An alternative to sleeve gastrectomy, aimed at reducing the stomach volume, is the gastric placcation procedure (gastroplication). We have introduced a new method of laparoscopic gastroplication for the surgical treatment of patients with morbid obesity. The method consists of gastric volume reducing due to intraluminal folding (invagination) of the stomach wall section with the help of the specific surgical instrument (suturing a fold using the corrugated sero-muscular sutures) along the greater curvature (Fig. 1). The stomach volume is significantly reduced, and the patient starts feeling full when eating significantly faster than prior to surgery. The technical result is achieved via mobilization of the stomach wall along the greater curvature using the specially designed instrument (intestinal forceps), folding the stomach wall into the tube in the form of a “roll”, and fixation with a non-absorbable filament. The reduction of gastric volume up to 50 ml is achieved using the special calibration tube [16].

Some authors, noting the obvious advantages of gastroplication in the treatment of obesity (simple, cost-effective), draw attention to risks and uncertainties associated with the morphological and physiological state of the gastric wall in the plicated section [7, 12].

The study was aimed to assess the morphological and functional changes in the stomach wall after gastroplication performed by the new method developed in the Clinic of the Department of Surgical Diseases and New Technologies of the Bashkir State Medical University.

METHODS

To assess the histopathological features changes in the invaginated stomach section and to detect the changes capable of causing complications in the postoperative period, the clinical and experimental study was carried out in the veterinary clinic of the Bashkir State Agrarian University in 2017–2020, consisting of performing surgery in 15 rabbits [10]. All rabbits were males of the Gray Giant breed aged 12–16 months. The rabbits' weight varied between 3050–5380 g. Inclusion criteria: age 12–16 months, male, weight 3 kg or above. Exclusion criteria: any disease, history of abdominal surgery, weight below 3 kg, female, participation in any other experiment.

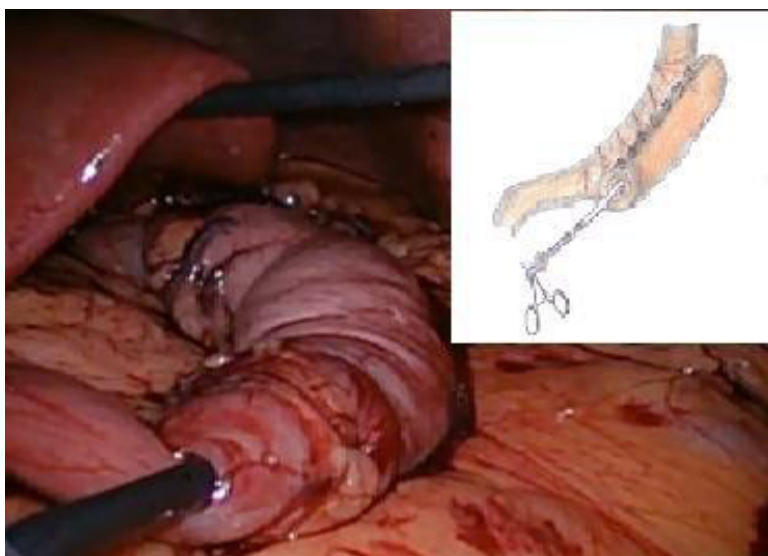


Fig. 1. Gastroplication through folding of the stomach, the new surgical procedure

Two days before surgery, the rabbits were moved to separate cages. The animals received water only for the gastric contents evacuation. All the rabbits underwent gastroplication. The timing of operation was 12–19 min (the average value was 14.5 min). After the three-time preoperative cleansing of the operative field with chlorhexidine alcohol-based solution the upper midline laparotomy was performed under the combined anesthesia (tiletamine–zolazepam–xylazine hydrochloride). The stomach was visualized sized 5.0 x 9.0 cm. It was mobilized along the greater curvature. Then the stomach was fixed in the margin opposite to mesenteric by the intestinal forceps, folded in the “roll”; suturing with sero-muscular sutures, layered closure of the wound.

During the postoperative period, the rabbits were monitored in separate cages, on the day 3 after surgery the animals received grain, on the day 5–6 they received hay and grass. The animals were administered with the solutions of 5% glucose, 0.9% saline in a volume of 20 ml intramuscularly, together with 0.5 ml of B12 vitamin, 0.1 g of biomycin twice a day.

Three and 6 months after surgery, with the appropriate preparation and in similar conditions, a second surgical procedure was performed, the resection of the stomach plicated section. The resected specimen was placed in the 10% formalin for further histological examination. The specimens were also taken 6–12 months after gastroplication.

For histological examination, a piece of tissue sized 1x1 cm, containing all layers of the stomach wall, was taken from the plicated section (from the various stomach regions). The biopsied material was fixed in the 10% formalin, and after the histological wiring, serial sections with a thickness of 7 µm were obtained. The sections were stained with hematoxylin and eosin.

In the clinical practice, the described method was used in 15 patients with morbid obesity and metabolic syndrome. The sample included patients aged over 18 with BMI 35–45 kg/m². There were 9 women and 6 men aged 42 ± 2.1. The patient selection criteria were stringent, gastroplication was chosen for motivated patients able to continuously follow diet control and exercise after surgery.

Inclusion criteria: high BMI (> 35 kg/m²) with comorbidities, age over 18. A number of exclusion criteria were chosen for patients in order to improve homogeneity of the operated patients group. Exclusion criteria: acute exacerbation or decompensation of chronic disorder, history of myocardial infarction or cerebrovascular accident, age under 18, psychological or mental disorders, no weight loss trigger.

Statistical analysis was carried out by standard methods using the Microsoft Excel application (Microsoft; USA).

RESULTS

In the early postoperative period three rabbits had complications: dyspepsia (refused food and water) and apathy. During the further follow-up, on the day 3–4 the animals started drinking water. Then they had slowly begun to eat solid food. No rabbits died during the experiment.

When examining the material taken 3 months after surgery, the macroscopic investigation revealed no obvious pathological changes. Slight cicatricial and sclerotic changes in the folded stomach section were noted, which did not obstruct unfolding the plicated section when removing the sutural material. Microscopic examination of sections and comparison with the unchanged stomach section (Fig. 2) revealed slight dystrophic changes of the gastric superficial-foveolar epithelium (single-layered prismatic glandular epithelium) in the plicated section of the stomach. Small gastric pits, rims evenly smoothed; slightly

atrophic glands; mild glands epithelium dystrophy; moderate interstitial edema in the stroma; small mild sclerosis foci; low focal lymphoid infiltration; vessels with uneven blood filling, sclerotic changes in some vessel walls; some erythrocytes in the vessel lumens; edema and focal perivascular hemorrhages in the submucosa and muscle layer; fragments of sutural material found in single sections; serous membrane thickened due to uneven sclerotic changes and low focal lymphoid infiltration (Fig. 3).

When examining specimens taken 6 months after surgery, the macroscopic investigation revealed pronounced cicatricial changes, it was impossible to unfold the invaginated part of the stomach without damaging or dissecting the tissues. Microscopic examination of sections and comparison with the section which had been obtained 3 months before revealed pronounced dystrophic changes of the superficial-foveolar epithelium in the plicated stomach section. Gastric pits and rims evenly smoothed; moderate gland atrophy; moderate gland epithelium dystrophy; decreased interstitial edema of stroma; sclerosis foci dissemination in the mucosa subepithelial sections and vessel walls; low focal lymphoid infiltration; some erythrocytes in the vessel lumens; decreased edema in the submucosa and muscle layer, uneven sclerotic foci; no

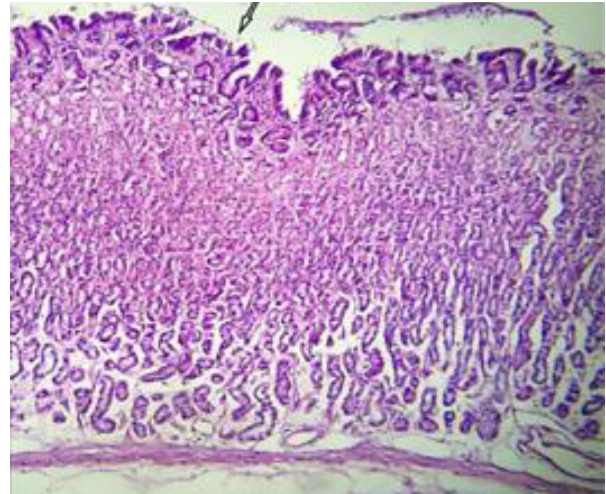


Fig. 2. Unchanged gastric mucosa (hematoxylin and eosin stain, magnification 40x–64x)

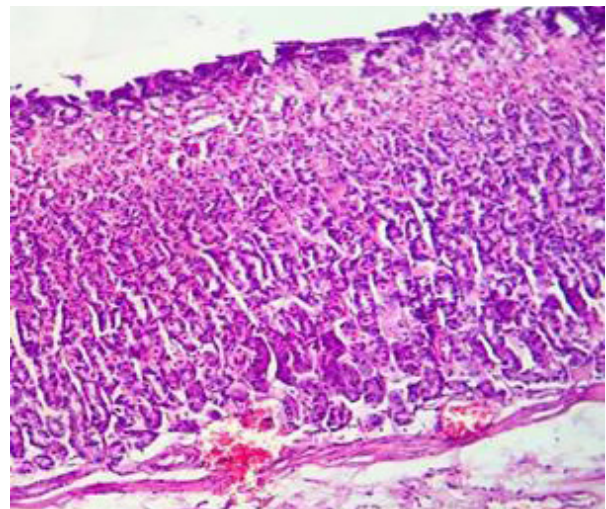


Fig. 3. Gastric mucosa from the plicated section obtained 3 months after surgery (hematoxylin and eosin stain, magnification 40x–64x). Dystrophic changes of the gastric superficial-foveolar epithelium (single-layered prismatic glandular epithelium)

fragments of sutural material; serous membrane thickened due to proliferating fibrous connective tissue (Fig. 4).

The first results of surgical procedures performed at the Clinic by the proposed method demonstrated that in the early postoperative period no complications were observed in the studied group of patients. Later in most patients (13 people, 86.7%) a steady decrease in the body weight was achieved during the first 2–12 months. It should be noted that two patients (13.3%) failed to achieve a consistent result. After the 3 months weight loss, the negative dynamics were noted, patients began to gain weight again. The long-term results were tracked in five patients (33.3%) for 24 months. In two patients, the weight loss and its stabilization at acceptable level occurred. In three patients, the weight loss was followed by weight gain subject to correction by therapeutic methods. Upon the follow-up appointment, the patients underwent additional instrumental examinations aimed to control the formed gastric tube condition (fibrogastroduodenoscopy, contrast radiography, and computed tomography, if necessary). No abnormalities in the operated stomach region or complications associated with the digestive system functioning were noted.

DISCUSSION

According to some authors [13, 14], laparoscopic gastroplication is no less effective than other restrictive methods aimed at weight loss. Moreover, the discussed method has a number of advantages: it is significantly cheaper, less complications (0.6%), over the past 12 years only 31% of cases with repeated weight gain have been recorded, simple rehabilitation. The method may be reversible, if necessary. It also makes it possible to use the additional malabsorptive procedures (second-step surgery) in patients with insufficient weight loss [14]. However, currently there are no published data on morphological changes in the gastric wall after gastroplication. The study demonstrated that the changes found in the mucous membrane and the muscle layer of the stomach wall after gastroplication were adaptive and associated with no severe morphological impairment.

When choosing the type of surgical procedure, it should be considered that patients need a potential trigger for weight loss, such as gastroplication. Our observations demonstrate that gastroplication is effective in preserving the diet during several years. In the postoperative period, within one year, eight

operated patients (53.3%) were subjected to comprehensive examination including fibrogastroduodenoscopy, contrast radiography of stomach and duodenum, abdominal computed tomography. According to the examination results, the plicated stomach had volume less than prior to surgery. No food passage and digestion impairment or associated with surgery abdominal cavity organs pathological changes were observed.

Small sample size and short observation period make it impossible to report the significant treatment results. However, the study is of practical interest due to the low cost and technical simplicity of one of the acknowledged surgical intervention types used in metabolic surgery in patients with morbid obesity.

CONCLUSIONS

In patients with morbid obesity, the weight loss is achieved due to bariatric surgery. Experimental study results demonstrate that the stomach wall changes after gastroplication are adaptive and associated with no severe morphological impairment. The study of the discussed method usage clinical evidence allows us to consider the method quite effective, simple, and enabling to improve the outcome of treatment in patients with overweight and obesity.

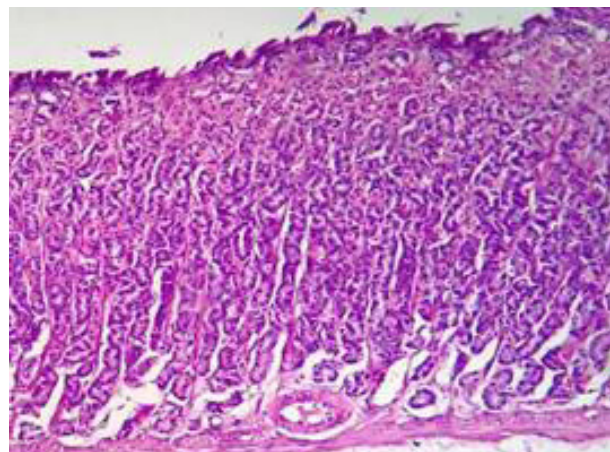


Fig. 4. Gastric mucosa from the plicated section obtained 6 months after surgery (hematoxylin and eosin stain, magnification 40x–64x). Pronounced dystrophic changes of the superficial-foveolar epithelium, gastric pits and rims evenly smoothed; moderate gland atrophy

References

- Fried M, Yumuk V, Oppert JM, et al. Interdisciplinary European guidelines on metabolic and bariatric surgery. *Obes Surg.* 2014; 24 (1): 42–55. DOI: 10.1007/s11695-013-1079-8.
- Borz C, Bara TJ, Bara T, et al. Laparoscopic gastric plication for the treatment of morbid obesity by using real-time imaging of the stomach pouch. *Ann Ital Chir.* 2017; 6: 392–8. PMID: 29197192.
- Fedenko VV, Evdoshenko VV, Kurganov IA, Emeljanov SI, Matveev NL, Bogdanov DJu, Mazikina LN. Sravnitel'nyj analiz jeffektivnosti laparoskopicheskoj rukavnoj rezekcii zheludka i laparoskopicheskogo zheludochnogo shuntirovanija u bol'nyh s sahnym diabetom 2-go tipa i narusheniem tolerantnosti k gljukoze. *Jendoskopicheskaja hirurgija.* 2016; 2: 21–31. Russian.
- Jashkov Jul, Lucevich OJe, Bordan NS, Ivleva OV. Jefferektivnost' laparoskopicheskoj prodol'noj rezekcii zheludka u bol'nyh ozhirenijem. *Ozhirenije i metabolizm.* 2015; 12 (1): 20–8. Russian.
- Zerrweck C, Rodríguez JG, Aramburo E, et al. Revisional surgery following laparoscopic gastric plication. *Obes Surg.* 2017; 27 (1): 38–43. DOI: 10.1007/s11695-016-2242-9.
- Anishhenko VV, Semenov SA, Halzov AV. Vybor metoda operacii pri ozhireнии. *Al'manah Instituta hirurgii im. A.V. Vishnevskogo.* 2012; 7 (1): 130–1. Russian.
- Brethauer SA, Harris JL, Kroh M, Schauer PR: Laparoscopic gastric plication for treatment of severe obesity. *Surg Obes Relat Dis.* 2011; 7: 15–22.
- Galimov OV, Hanov VO, Gabdulsabirova ZR. Rezul'taty hirurgicheskijh operacij i kachestva zhizni pacientov posle razlichnyh variantov bariatricheskijh vmeshatel'stv. *Kreativnaja hirurgija i onkologija.* 2011; 1: 39–44. Russian.
- Pujol Gebelli J, Garcia Ruiz de Gordejuela A, Casajoana Badia A, Secanella Medayo L, Vicens Morton A, Masdevall Noguera C. Laparoscopic Gastric Plication: a new surgery for the treatment of morbid obesity. *Cir Esp.* 2011; 89 (6): 356–61.
- Skovorodin EN, Vehnovskaja EG. *Rukovodstvo k laboratornym zanjatijam po patologicheskoj anatomii zhivotnyh.* Ufa: Bashkirskij gosudarstvennyj agrarnyj universitet, 2015 (3-e izdanie,

- переработанное и дополненное); 258 pp. Russian.
11. Askerhanov RG, Hatkov IE, Bodunova NA, Fejdorov IJu, Petrova AL, Sadyki MN. Pervyj opyt laparoskopicheskoj gastroplikacii u pacientov s morbidnym ozhireniem. Jendoskopicheskaja hirurgija. 2017; 1: 6–9. Russian.
 12. Perivoliotis K, Sioka E, Katsogridaki G, Zacharoulis D. Laparoscopic gastric plication versus laparoscopic sleeve gastrectomy: an up-to-date systematic review and meta-analysis. J Obes. 2018; 9: 3617458. DOI: 10.1155/2018/3617458.
 13. Heidari R, Talebpour M, Soleyman-Jahi S, Zeinoddini A, Sanjari Moghaddam A, Talebpour A. Outcomes of reoperation after laparoscopic gastric plication failure. Obes Surg. 2019; 29 (2): 376–86. DOI: 10.1007/s11695-018-3522-3.
 14. Talebpour, et al. Twelve year experience of laparoscopic gastric plication in morbid obesity: development of the technique and patient outcomes. Annals of Surgical Innovation and Research. 2012; 6: 7. Available from: <http://www.asir-journal.com/content/6/1/7>.
 15. Khidir N, Al Dhaheri M, El Ansari W, Al Kuwari M, Sargsyan D, Bashah M. Outcomes of laparoscopic gastric greater curvature plication in morbidly obese patients. J Obes. 2017; 2017: 7989714. DOI: 10.1155/2017/7989714.
 16. Galimov OV, Hanov VO, Sagitdinov RR, Sajfullin RR, et al. Method of surgical treatment of overweight and obesity. Russian Federation patent № RU 2654572 C1. 21.05.2018.

Литература

1. Fried M, Yumuk V, Oppert JM, et al. Interdisciplinary European guidelines on metabolic and bariatric surgery. Obes Surg. 2014; 24 (1): 42–55. DOI: 10.1007/s11695-013-1079-8.
2. Borz C, Bara TJ, Bara T, et al. Laparoscopic gastric plication for the treatment of morbid obesity by using real-time imaging of the stomach pouch. Ann Ital Chir. 2017; 6: 392–8. PMID: 29197192.
3. Феденко В. В., Евдошенко В. В., Курганов И. А., Емельянов С. И., Матвеев Н. Л., Богданов Д. Ю., Мазикина Л. Н. Сравнительный анализ эффективности лапароскопической рукавной резекции желудка и лапароскопического желудочного шунтирования у больных с сахарным диабетом 2-го типа и нарушением толерантности к глюкозе. Эндоскопическая хирургия. 2016; 2: 21–31.
4. Яшков Ю. И., Луцевич О. Э., Бордан Н. С., Ивлева О. В. Эффективность лапароскопической продольной резекции желудка у больных ожирением. Ожирение и метаболизм. 2015; 12 (1): 20–8.
5. Zerrweck C, Rodríguez JG, Aramburo E, et al. Revisional surgery following laparoscopic gastric plication. Obes Surg. 2017; 27 (1): 38–43. DOI: 10.1007/s11695-016-2242-9.
6. Анищенко В. В., Семенов С. А., Хальзов А. В. Выбор метода операции при ожирении. Альманах Института хирургии им. А. В. Вишневского. 2012; 7 (1): 130–1.
7. Brethauer SA, Harris JL, Kroh M, Schauer PR: Laparoscopic gastric plication for treatment of severe obesity. Surg Obes Relat Dis. 2011; 7: 15–22.
8. Галимов О. В., Ханов В. О., Габдулсабирова З. Р. Результаты хирургических операций и качества жизни пациентов после различных вариантов бариатрических вмешательств. Креативная хирургия и онкология. 2011; 1: 39–44.
9. Pujol Gebelli J, Garcia Ruiz de Gordejuela A, Casajoana Badia A, Secanella Medayo L, Vicens Morton A, Masdevall Noguera C. Laparoscopic Gastric Plication: a new surgery for the treatment of morbid obesity. Cir Esp. 2011; 89 (6): 356–61.
10. Сковородин Е. Н., Вехновская Е. Г. Руководство к лабораторным занятиям по патологической анатомии животных. Уфа: Башкирский государственный аграрный университет, 2015 (3-е издание, переработанное и дополненное); 258 с.
11. Аскерханов Р. Г., Хатьков И. Е., Бодунова Н. А., Фейдоров И. Ю., Петрова А. Л., Садыки М. Н. Первый опыт лапароскопической гастропликации у пациентов с морбидным ожирением. Эндоскопическая хирургия. 2017; 1: 6–9.
12. Perivoliotis K, Sioka E, Katsogridaki G, Zacharoulis D. Laparoscopic gastric plication versus laparoscopic sleeve gastrectomy: an up-to-date systematic review and meta-analysis. J Obes. 2018; 9: 3617458. DOI: 10.1155/2018/3617458.
13. Heidari R, Talebpour M, Soleyman-Jahi S, Zeinoddini A, Sanjari Moghaddam A, Talebpour A. Outcomes of reoperation after laparoscopic gastric plication failure. Obes Surg. 2019; 29 (2): 376–86. DOI: 10.1007/s11695-018-3522-3.
14. Talebpour, et al. Twelve year experience of laparoscopic gastric plication in morbid obesity: development of the technique and patient outcomes. Annals of Surgical Innovation and Research. 2012; 6: 7. Available from: <http://www.asir-journal.com/content/6/1/7>.
15. Khidir N, Al Dhaheri M, El Ansari W, Al Kuwari M, Sargsyan D, Bashah M. Outcomes of laparoscopic gastric greater curvature plication in morbidly obese patients. J Obes. 2017; 2017: 7989714. DOI: 10.1155/2017/7989714.
16. Галимов О. В., Ханов В. О., Сагитдинов Р. Р., Сайфуллин Р. Р. и др. Способ хирургического лечения избыточной массы тела и ожирения. Патент РФ № RU 2654572 C1. 21.05.2018.

INFORMATION MODEL OF POST STROKE REHABILITATION CONCEPTION

Rybakova PA¹ ✉, Koroleva Yul¹, Ivanova GE², Zarubina TV¹¹ Pirogov Russian National Research Medical University, Moscow, Russia² Federal Center of Brain Research and Neurotechnologies of the Federal Medical Biological Agency, Moscow, Russia

Currently, the new model of stroke care is actively implemented. There is a number of problems thereby related to digitalization. The study was aimed to work up the information model of the post-stroke rehabilitation at the first stage. The following basic objects of the rehabilitation system information model were identified and described using system analysis and business process modelling, based on studying laws, regulatory and legal acts, clinical guidelines, the "Development of the System of Medical Rehabilitation in Russia" pilot project protocol, and the problem area experts' findings: patient, health information system (HIS) of a healthcare organization, document management. The objects' properties and interaction are discussed, the information model is been constructed, main directions are described.

Keywords: information model, healthcare digitalization, medical rehabilitation, acute stroke, electronic document management

Acknowledgements: to Maria A. Bulatova, head of the Department of Patients With Central Nervous System Disorders Medical Rehabilitation of the Federal Center of Brain Research and Neurotechnologies of the Federal Medical Biological Agency, for counseling and strong support.

Author contribution: Rybakova PA — literature analysis, analysis of the results, drawing conclusions, manuscript writing; Koroleva Yul — analysis of the results, drawing conclusions; Ivanova GE — counseling, manuscript writing; Zarubina TV — manuscript writing.

✉ **Correspondence should be addressed:** Polina A. Rybakova
Ostrovitianova, 1, Moscow, 117997; polina240895@rambler.ru

Received: 25.07.2020 **Accepted:** 22.08.2020 **Published online:** 31.08.2020

DOI: 10.24075/brsmu.2020.051

КОНЦЕПЦИЯ ИНФОРМАЦИОННОЙ МОДЕЛИ СИСТЕМЫ РЕАБИЛИТАЦИИ БОЛЬНЫХ С ОСТРЫМ НАРУШЕНИЕМ МОЗГОВОГО КРОВООБРАЩЕНИЯ

П. А. Рыбакова¹ ✉, Ю. И. Королева¹, Г. Е. Иванова², Т. В. Зарубина¹¹ Российский национальный исследовательский медицинский университет имени Н. И. Пирогова, Москва, Россия² «Федеральный центр мозга и нейротехнологий» Федерального медико-биологического агентства России, Москва, Россия

В настоящее время происходит активное внедрение новой модели оказания помощи больному с острым нарушением мозгового кровообращения (ОНМК). В связи с этим стоит множество задач, касающихся цифровизации этого процесса. Целью исследования было разработать информационную модель системы реабилитации пациентов с ОНМК на первом этапе оказания помощи. С помощью методов системного анализа, моделирования бизнес-процессов и на основании изучения нормативно-правовых актов, клинических рекомендаций, протокола пилотного проекта «Развитие медицинской реабилитации в РФ» и результатов работы экспертов проблемной области выделены и проанализированы основные объекты информационной модели системы реабилитации: пациент, МИС МО, документооборот, описаны их свойства и взаимоотношения, построена информационная модель и обозначено направление ее развития.

Ключевые слова: информационная модель, цифровизация здравоохранения, медицинская реабилитация, острое нарушение мозгового кровообращения, электронный документооборот

Благодарности: заведующей отделением медицинской реабилитации пациентов с нарушением функции центральной нервной системы ФГБУ «Федеральный центр мозга и нейротехнологий» ФМБА России Марии Анатольевне Булатовой за консультацию и активное участие в работе.

Вклад авторов: П. А. Рыбакова — работа с литературой, анализ результатов, формулировка выводов, оформление рукописи; Ю. И. Королева — анализ результатов, формулировка выводов; Г. Е. Иванова — консультация, подготовка рукописи; Т. В. Зарубина — подготовка рукописи.

✉ **Для корреспонденции:** Полина Алексеевна Рыбакова
ул. Островитянова, д. 1, г. Москва, polina240895@rambler.ru

Статья получена: 25.07.2020 **Статья принята к печати:** 22.08.2020 **Опубликована онлайн:** 31.08.2020

DOI: 10.24075/vrgmu.2020.051

One of the ways to improve the quality of post-stroke patients care is the informatization (digitalization) of healthcare system: the complex of measures aimed at providing timely and full information (processed and transformed in certain way) to specialists involved in the diagnosis and treatment process [1].

On January 1, 2019, the "Digital Healthcare Framework" federal project was launched as part of the National project "Healthcare". [2]. The Federal project was focused on the implementation and development of the healthcare information systems and electronic document management in all healthcare organizations and health authorities. The "Development of National Medical Research Centers Network and Introduction of Innovative Medical Technologies" federal project was also partially focused on problems related to healthcare digitalization.

The four vertical integrated systems were designed as part of the project according to the following profiles: oncology, cardiovascular disorders, obstetrics and gynecology (together with neonatology), preventive healthcare. Those should provide continuity of care, patient routing, monitoring of care provision to patients with certain disorders.

The important stage of all four profiles is medical rehabilitation. Until recently, the developments of medical rehabilitation digitalization were localized, whereas the federal level information system development required the comprehensive analysis of the subject area and the step-by-step information model construction.

The study was aimed to analyze the model of post-stroke care through describing the information model basic objects. The future goals and opportunities are mentioned.

METHODS

The main documents regulating the existing medical care provision are the Ministry of Health of the Russian Federation orders No. 928н (“On Approval of the Procedure for Medical Care to Patients with Acute Stroke”, dated November 15, 2012) and № 1705н (“On the Procedure of Medical Rehabilitation”, dated December 29, 2012). To explore the new model of post stroke medical care, the description of the “Development of the System of Medical Rehabilitation in Russia” pilot project (2015–2016) was used. The Russian and foreign guidelines contain the more detailed description of care measures [3–11]. The WHO documents [12–15] were used to study the International Classification of Functioning, Disability and Health (ICF). The algorithms based on the patient’s route and description of the information model objects were designed using the specialized software: MS VISIO 2010 (Microsoft; USA), Axure RP 9 (Axure; USA), draw.io (Voodoo; France); methods of system analysis (problem analysis, system goals and functions setting, modelling), and business process modelling (use case diagram).

RESULTS

Subject area

The first stage of the information model constructing is the definition of subject area, i.e. the post-stroke medical rehabilitation description. It includes the patient’s condition assessment, rehabilitation goals setting and the formulation of procedure program, drug and non-drug therapy, efficiency of rehabilitation evaluation and prognosis. The updated stroke care model includes three phases [16]. The first phase begins with the patient’s admission to the intensive care unit (ICU) of the specialized vascular department and no later than 24 hours from the admission, i. e. during the acute period of the disease [16, 17]. The patient undergoes the clinical, laboratory and instrumental examinations aimed at identifying the stroke type and subtype, thrombolytic therapy and surgery assignment (if necessary). The intensivist follows the patient’s vital parameters and, if necessary, guides him to other specialists. The medical rehabilitation with multidisciplinary rehabilitation team participation is started at the ICU: correction of dysphagia and

nutritional deficit, immobilization syndrome prevention (passive or active-passive verticalization, early mobilization). Patient is transferred to neurology department after the stabilization, where the attending neurologist continues the treatment and diagnostic process and organizes the patient’s medical rehabilitation with the multidisciplinary team (MDT). The transfer summary report contains the patient’s score according to the Rehabilitation Routing Scale (RRS) which is a selection criterion for patient’s routing. It’s also a selection criteria for clinical and statistical group for medical rehabilitation during all subsequent phases [18, 19]. So the first phase of rehabilitation includes the medical care in the ICU and neurology department.

Depending on the treatment functional result in vascular department the patient may be routed for further rehabilitation to the second phase in-patient clinic (RSS 4–5), or to the day hospital (RSS 3) and the third phase outpatient clinic (RSS 2). The second and third phases are implemented during the early and late recovery periods and apply to patients with residual symptoms or chronic (non-acute) disease. The patient may carry out the medical rehabilitation third stage activities at home under the guidance of a responsible specialist using telemedicine technology.

The initial medical care phase is the most important and difficult as it requires immediate action. The dynamics of the patient’s condition depends on the measures taken at this phase. It is known that the earlier rehabilitation increases medical care effectiveness [20], therefore, the first phase has been chosen as starting point for the information model constructing.

Information model objects

Currently, the updated model of post-stroke care is actively implemented in Russia [18]. Its algorithm is based on the Federal Centre of Cerebrovascular Pathology and Stroke experts’ recommendations (Fig. 1).

The main differences between the new model and the traditional model are the patient-centered care, diagnostics both according to the International Classification of Diseases (ICD) and the International Classification of Functioning, Disability, and Health (ICF), the multidisciplinary team participation. The MDT activity may be presented as a rehabilitation cycle [21]. Representing the new model in this way makes possible to

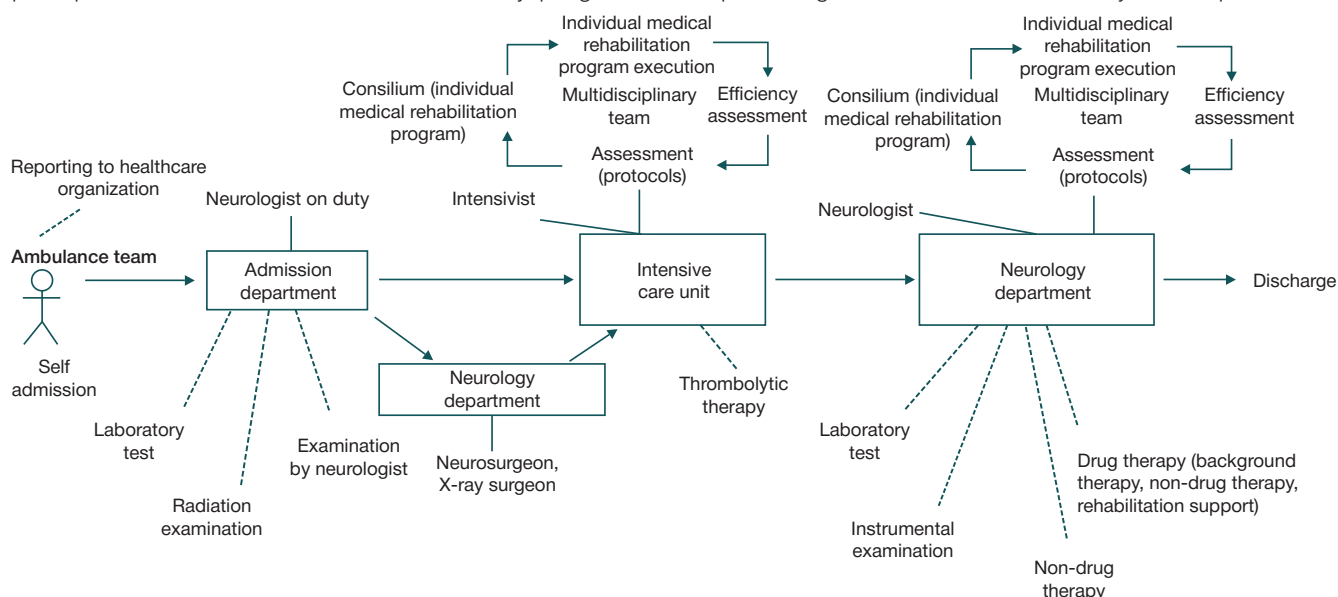


Fig. 1. Post-stroke care algorithm, updated model

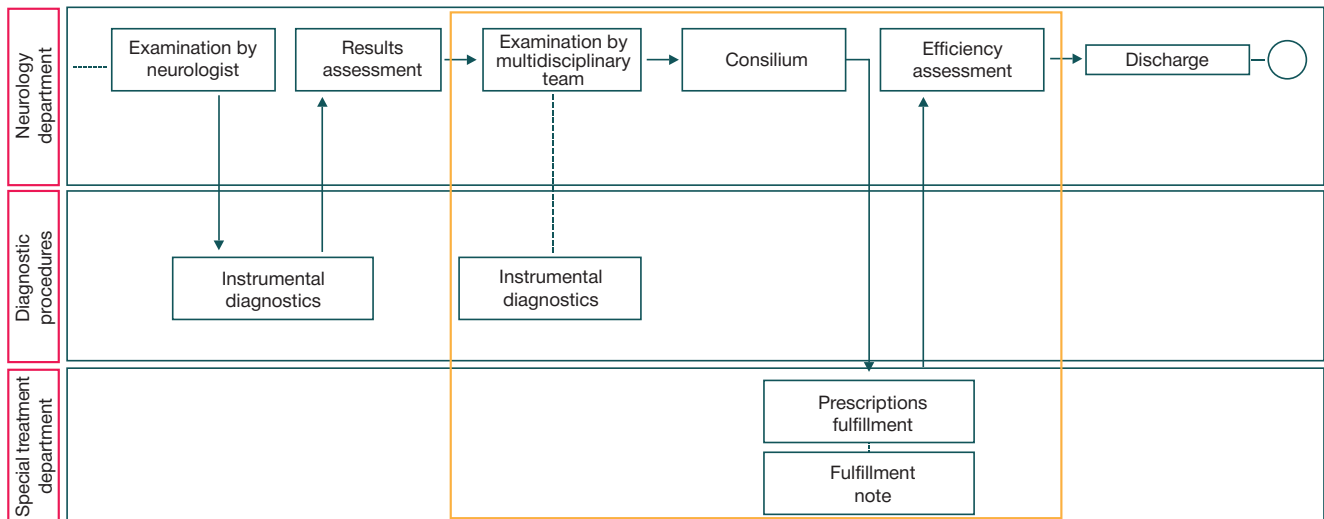


Fig. 2. Fragment of patient's route inside the neurology department

evaluate the time of appearance and actions of each participant of diagnosis and treatment process.

For description and analysis of the object ("Patient") the business process diagram (BPD) was used. It contains details of the patient's route inside the hospital department. The small fragment is presented in Fig. 2. On this diagram the healthcare organization units and the blocks (actions) with the key points of the route are shown as horizontal paths.

After transfer to neurology department the patient is examined by the attending neurologist and all the specialists of the multidisciplinary team, later he undergoes the instrumental and additional laboratory examination with interpretation of the

results. The rehabilitation cycle is highlighted with rectangle in Fig. 2.

The other important object of the information model is the health information system (HIS) of a healthcare organization. The system includes multiple integrated subsystems and basic Practice Management Software (PMS). However, the basic HIS does not satisfy the neurology hospital requirements arising from the new model of post acute care. Therefore, it is necessary to expand its functionality. The development of new PMS is required, it concerns the PMS used by specialists of the multidisciplinary team (physical medicine and rehabilitation (PM&R) physician, intensivist, physical rehabilitation specialist,

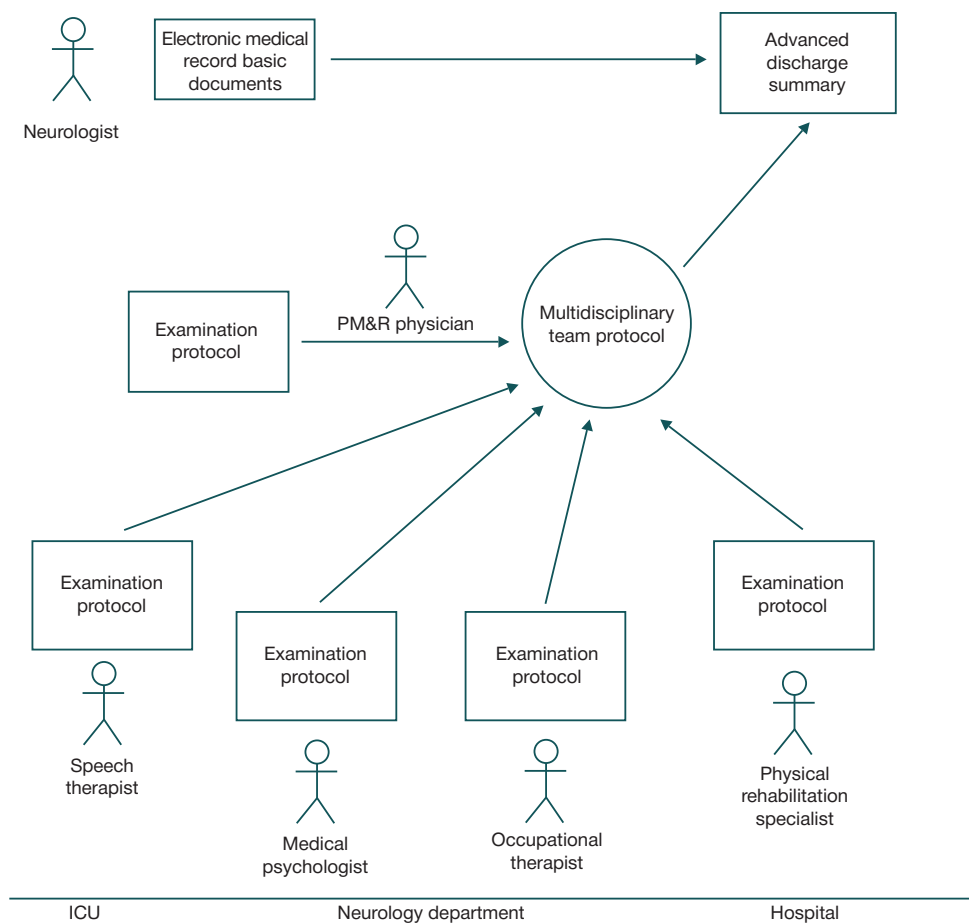


Fig. 3. Medical records registration at the neurology department

Multidisciplinary team protocol № 10

08.05.2019

Healthcare organization: FCCPS of the Ministry of Health of the Russian Federation
Department: Medical and Social Rehabilitation
Patient: Alexey M. Voskresensky
 History №: 35268

Rehabilitation potential:

Rehabilitation Routing Scale Score: 4

Rehabilitation goals:
 Long-term: after 3 months the patient will require the outpatient care
 Short-term: the patient will be able to walk on his own
 Current phase goal: autonomous verticalization

Rehabilitation diagnosis:

Functions and structures

Domain	Description
b134.2	Sleep functions
b28012.2	Pain in stomach or abdomen
b7301.3	Power of muscles of one limb
b7401.4	Endurance of muscle groups
b7603.3	Supportive functions of arm or leg
b820.4	Repair functions of the skin
s810.0	Structure of skin

Activities and Participation

Domain	Description
d410.31	Changing basic body position
d510.43	Washing oneself
d520.32	Caring for body parts
d530.31	Toileting
d540.32	Dressing
d550.21	Eating
d560.20	Drinking

Environmental factors

Domain	Description
e260.3	Air quality
e310+3	Immediate family
e540.1	Transportation services, systems and policies

Personal factors

Domain	Description	
PF	Acceptance of disease	-
PF	Understanding the need for rehabilitation	+

Limiting factors of the rehabilitation program execution

Rehabilitation plan

Рис. 4. Design fragment of the profile document (multidisciplinary team protocol) medical psychologist, speech therapist, occupational therapist [18]), as well as for the PMS used by nursing staff.

Electronic document management

One of the basic PMS functions is the electronic document management, the electronic medical record and profile documents creation. The following is a fragment of the electronic document management at the first phase of rehabilitation based on the care provision algorithm (Fig. 3).

Each multidisciplinary team specialist creates the first profile document, the examination protocol, after the patient's examination. Once a week or more often the multidisciplinary

team specialists hold a consilium, where they discuss and combine the results. After that the physical medicine and rehabilitation (PM&R) physician makes the rehabilitation diagnosis, sets the long-term and short-term goals of medical rehabilitation, forms the individual rehabilitation plan, defines the executives and sets the rehabilitation schedule. This information is included in the multidisciplinary team general protocol, the second profile document, the fragment is provided in Fig. 4.

The patient's condition assessment (according to ICF, expressed in points) obtained from various MDT specialists is included in the rehabilitation diagnosis.

The third profile document (advanced discharge summary report) is finalized by the attending physician after the first

Table. Algorithm fragment of NIHSS to ICF translation

	NIHSS	ICF
1	Motor leg	B740 — Muscle endurance functions B7401 — Endurance of muscle groups
	0 = No drift	0 B7401.0
	1 = Drift: leg drifts down but does not hit bed	1 B7401.1
	2 = Leg falls to bed by 5 seconds but has some effort against gravity	2 B7401.2
	3 = Leg falls immediately	3 B7401.3
	4 = No movement	4 B7401.4
	UN = Assessment is impossible	UN B7401.8
2	Dysarthria	Voice and language functions B320 — Articulation functions
	0 = Normal	0 B320.0
	1 = Mild-to-moderate dysarthria	1 B320.1- B320.2
	2 = Severe dysarthria or mute/anarthric patient	2 B320.3- B320.4
	UN = Assessment is impossible	UN B320.8
3	Sensory (pinprick and touch)	Additional sensory functions (b250-279) B270 — Sensory functions related to temperature and other stimuli
	0 = Normal	0 B270.0
	1 = Partial loss	1 B270.1
	2 = Severe loss	2 B270.3
		B2702 — Sensitivity to pressure
		B2703 — Sensitivity to a noxious stimulus

phase of rehabilitation. The document comprises basic clinical data from the electronic medical record, and data from the MDT protocols that describe the activities results and the patient dynamics during treatment.

According to the new post acute care model, the multidisciplinary team specialists assess the patient's state not only using the traditional scales, but also using the ICF domains. Such kind of rehabilitation diagnosis allows the specialists to distinguish between the measures aimed at the patient's survival (diagnosis and treatment process) and the measures aimed at preservation and restoration of vital functions. It is extremely important for the future rehabilitation arrangement.

It should be noted that if patient has undergone surgery for the underlying disease, the additional scales should be used.

Automated rehabilitation diagnosis procedure

The manual assessment, both using the clinical scales and the required ICF domains, is time-consuming. Therefore, the decision support system element has been developed as an algorithm for converting the NIHSS and other clinical evaluation tools [5] to ICF score. The algorithm fragment is provided in Table.

The algorithm is a matching of the stroke severity scale items scores with the corresponding ICF domains. There is no one-to-one matching in some cases because ICF is a more detailed tool than clinical scales. For example, the item № 2 of ICF (see Table 1) includes more gradations for articulation disorders, and the NIHSS score 1 may correspond to B320.1 or B320.2 items of ICF. The even more ambiguous situation is observed in the item № 3: the NIHSS Sensory section corresponds to several domains of ICF ("Sensory functions related to stimuli", "Sensitivity to pressure", "Sensitivity to a noxious stimulus"). The algorithm

does not offer an unambiguous answer in such "controversial" situations and requires correction by the physician.

DISCUSSION

The study provides a systematic approach to the post-stroke care informatization. The subject area boundaries had been defined, the information model objects (patient, healthcare organization, HIS of a healthcare organization, electronic document management) and their links and relationships analysis has been performed. Only one study of the discussed topic has been found in literature [22]. It describes the software product in which the patient's clinical data entry and the rehabilitation scales for patient state assessment are partially implemented. The diagnosis is supported using ICF, but the conversion algorithm is not transparent so the algorithm implementation in other systems is impossible.

The approach proposed in this paper may become the ideological and algorithmic basis for the post-stroke patients' management information systems (from hospital to state level).

The obtained results make it possible to determine the further strategy of the rehabilitation system information model development and to define the following priorities:

1) development of technical specifications for the electronic medical record profile documents creation: examination protocol by MDT specialists, general MDT protocol, advanced medical discharge (post-mortem) summary. The development of the standardized electronic medical documents for patient transfer to the second and third phases of rehabilitation and higher HIS levels (regional, federal) is required for the discharge documents and the corresponding implementation guidelines;

2) defining the list of the federal medical references for formalization of the clinical data contained in the profile

documents: examination protocol by MDT specialist, multidisciplinary team protocol, medical discharge summary;

3) role model development describing the access rights of all process participants of the hospital units;

4) PMS development for specialists taking part in the rehabilitation process: PM&R physician, physical rehabilitation specialist, neuropsychologist, speech therapist, occupational therapist, massage therapist, physiologist, healthcare assistant;

5) creation of medical decision-support system elements making automated diagnosis according to ICF.

The future development directions are the following: creation of the administrative PMS, analytical and reference modules, patient's account, PMS modules expansion depending on the stroke type and care provided, integration with external systems.

CONCLUSION

Currently, the new post-stroke care model described in the "Development of the System of Medical Rehabilitation in Russia" pilot project protocol is actively implemented both in Russia and foreign countries. According to the model, rehabilitation is carried out by the new diagnosis and treatment process component — the multidisciplinary team using ICF for the patient's condition assessment. This issue should be considered when developing an information system.

The basic information model objects are analyzed, the differences between existing and new models of post-stroke care are identified at this paper. The functions expansion of HIS based on the differences revealed is proposed. The main directions of the rehabilitation system information model are covered: development of profile papers, national references, PMS and HIS additional modules.

References

- Zarubina TV, Kobrinskij BA. Medicinskaja informatika. M.: GJeOTAR-Media, 2016; 512 s. Russian.
- Pasport federal'nogo proekta «Sozdanie edinogo cifrovogo kontura v zdavoohranenii na osnove edinoj gosudarstvennoj informacionnoj sistemy v sfere zdavoohranenija (EGISZ)» (utv. prezidiumom Soveta pri Prezidente Rossijskoj Federacii po strategicheskomu razvitiju i nacional'nym proektam, protokol # 16 ot 24 dekabrja 2018 g.). Available from: <https://minzdrav.gov.ru/poleznye-resursy/natsproektzdravoohranenie/tsifra>. Russian.
- Gusev EI, Geht AB. Klinicheskie rekomendacii po provedeniju tromboliticheskoj terapii pri ishemieskom insul'te. M.: GJeOTAR-Media, 2015; s. 11–14, 16. Russian.
- Denisov IN, Kandyba DV, Kuznecova OYu. Diagnostic and tactics of stroke care in general medical practice, including primary and secondary prevention. Clinical guidelines approved on the IV All-Russian Congress of general practitioners (family doctors) of Russian Federation. 2013; 15: 13–24. Russian.
- Ivanova GE, redaktor. Prakticheskoe primenenie ocenocnyh shkal v medicinskoj reabilitacii. Metodicheskie rekomendacii dlja Pilotnogo proekta «Razvitie sistemy medicinskoj reabilitacii v Rossijskoj Federacii». 2016; s. 4–7. Russian.
- Melnikova EV, Bujlova TV, Bodrova RA, Shmonin AA, Maltseva MN, Ivanova GE. International Classification of Functioning, Disability and Health (ICF) in out-patient and in-patient medical rehabilitation: instruction for specialists. Journal of Restorative Medicine. 2017; 6 (82): 1219–28. Russian.
- Casaubon LK, et al. Canadian stroke best practice recommendations: hyperacute stroke care guidelines, update 2015. International Journal of Stroke. 2016; 10 (6): 924–40.
- Gutenbrunner C, Ward AB, Chamberlain MA. White book on physical and rehabilitation medicine in Europe. European Journal of Physical and Rehabilitation Medicine. 2006; 42 (4): 295.
- Hebert D, et al. Canadian stroke best practice recommendations: stroke rehabilitation practice guidelines, update 2015. International Journal of Stroke. 2016; 11 (4): 459–84.
- Powers WJ, et al. 2018 guidelines for the early management of patients with acute ischemic stroke: a guideline for healthcare professionals from the American Heart Association. American Stroke Association. 2018; 49 (3): 46–99.
- Steiner T, et al. European Stroke Organisation (ESO) guidelines for the management of spontaneous intracerebral hemorrhage. International Journal of stroke. 2014; 9 (7): 840–55.
- ICF Research Branch in cooperation with the World Health Organization Collaborating Centre for the Family of International Classifications (WHO-FIC) in Germany (at DIMDI). Available from: www.icf-research-branch.org.
- Organisation mondiale de la santé, World Health Organization, World Health Organization Staff. International classification of functioning, disability and health: ICF. World Health Organization, 2001; 299 p.
- Gimigliano F, Negrini S. The World Health Organization «rehabilitation 2030—a call for action». Eur J Phys Rehabil Med. 2017; 53 (2): 155–168.
- World Health Organization. WHO global disability action plan 2014–2021: Better health for all people with disability. 2015; 25 p. Available from: <https://extranet.who.int/iris/restricted/handle/10665/199544>.
- Prikaz Ministerstva zdavoohranenija Rossijskoj Federacii # 1705n ot 29.12.2012 «O porjadke organizacii medicinskoj reabilitacii». Available from: <https://base.garant.ru/70330294/>. Russian.
- Prikaz Ministerstva zdavoohranenija Rossijskoj Federacii # 928n ot 15.11.2012 «Porjadok okazanija medicinskoj pomoshhi bol'nym s ostrymi narushenijami mozgovogo krovoobrashhenija». Available from: <https://base.garant.ru/70334856/>. Russian.
- Ivanova GE, Belkin AA, Belyaev AF, Bodrova RA, Bujlova TV, Melnikova EV, et al. Pilot project «Development of medical rehabilitation system in the Russian Federation». General Principles and Protocol. Journal of the Ivanovsky Medical Academy. 2016; (1): 6–11. Russian.
- Ivanova GE, Melnikova EV, Shmonin AA, Aronov DM, Belkin AA, Belyaev AF, et al. Pilot project «Development of medical rehabilitation system in the Russian Federation». Protocol of the second phase of the project. Scientific notes of PSPbGMU. 2016; (2): 27–34. Russian.
- Kadomcev DV, Pasechnikova EA, Zanin SA, Kocharjan VYe, Plotnikova VV, Vinogradov IO. Thrombolytic therapy in ischemic stroke care. Current status. Current status of science and education. 2016; (4): 40. Russian.
- Steiner WA, et al. Use of the ICF model as a clinical problem-solving tool in physical therapy and rehabilitation medicine. Physical therapy. Oxford University Press. 2002; 82 (11): 1098–07.
- Shmonin AA, Nikiforov VV, Maltseva MN, Melnikova EV, Ivanova GE. Electronic monitoring of rehabilitation efficacy system in pilot project «Development of medical rehabilitation system in the Russian Federation» — «ICF-reader» program. Journal of the Ivanovsky Medical Academy. 2016; 21 (1): 66–70. Russian.

Литература

1. Зарубина Т. В., Кобринский Б. А. Медицинская информатика. М.: ГЭОТАР-Медиа, 2016; 512 с.
2. Паспорт федерального проекта «Создание единого цифрового контура в здравоохранении на основе единой государственной информационной системы в сфере здравоохранения (ЕГИСЗ)» (утв. президиумом Совета при Президенте Российской Федерации по стратегическому развитию и национальным проектам, протокол № 16 от 24 декабря 2018 г.). Доступно по ссылке: <https://minzdrav.gov.ru/poleznye-resursy/natsproektzdravooхранenie/tsifra>.
3. Гусев Е. И., Гехт А. Б. Клинические рекомендации по проведению тромболитической терапии при ишемическом инсульте. М.: ГЭОТАР-Медиа, 2015; с. 11–14, 16.
4. Денисов И. Н., Кандыба Д. В., Кузнецова О. Ю. Диагностика и тактика при инсульте в условиях общей врачебной практики, включая первичную и вторичную профилактику. Клинические рекомендации утверждены на IV Всероссийском съезде врачей общей практики (семейных врачей) Российской Федерации. 2013; 15: 13–24.
5. Иванова Г. Е., редактор. Практическое применение оценочных шкал в медицинской реабилитации. Методические рекомендации для Пилотного проекта «Развитие системы медицинской реабилитации в Российской Федерации». 2016; с. 4–7.
6. Мельникова Е. В., Буйлова Т. В., Бодрова Р. А., Шмонин А. А., Мальцева М. Н., Иванова Г. Е. Использование международной классификации функционирования (МКФ) в амбулаторной и стационарной медицинской реабилитации: инструкция для специалистов. Вестник восстановительной медицины. 2017; 6 (82): 1219–28.
7. Casaubon LK, et al. Canadian stroke best practice recommendations: hyperacute stroke care guidelines, update 2015. *International Journal of Stroke*. 2016; 10 (6): 924–40.
8. Gutenbrunner C, Ward AB, Chamberlain MA. White book on physical and rehabilitation medicine in Europe. *European Journal of Physical and Rehabilitation Medicine*. 2006; 42 (4): 295.
9. Hebert D, et al. Canadian stroke best practice recommendations: stroke rehabilitation practice guidelines, update 2015. *International Journal of Stroke*. 2016; 11 (4): 459–84.
10. Powers WJ, et al. 2018 guidelines for the early management of patients with acute ischemic stroke: a guideline for healthcare professionals from the American Heart Association. *American Stroke Association*. 2018; 49 (3): 46–99.
11. Steiner T, et al. European Stroke Organisation (ESO) guidelines for the management of spontaneous intracerebral hemorrhage. *International Journal of stroke*. 2014; 9 (7): 840–55.
12. ICF Research Branch in cooperation with the World Health Organization Collaborating Centre for the Family of International Classifications (WHO-FIC) in Germany (at DIMDI). Available from: www.icf-research-branch.org.
13. Organisation mondiale de la santé, World Health Organization, World Health Organization Staff. *International classification of functioning, disability and health: ICF*. World Health Organization, 2001; 299 p.
14. Gimigliano F, Negrini S. The World Health Organization «rehabilitation 2030—a call for action». *Eur J Phys Rehabil Med*. 2017; 53 (2): 155–168.
15. World Health Organization. WHO global disability action plan 2014–2021: Better health for all people with disability. 2015; 25 p. Available from: <https://extranet.who.int/iris/restricted/handle/10665/199544>.
16. Приказ Министерства здравоохранения Российской Федерации № 1705н от 29.12.2012 «О порядке организации медицинской реабилитации». Доступно по ссылке: <https://base.garant.ru/70330294/>.
17. Приказ Министерства здравоохранения Российской Федерации № 928н от 15.11.2012 «Порядок оказания медицинской помощи больным с острыми нарушениями мозгового кровообращения». Доступно по ссылке: <https://base.garant.ru/70334856/>.
18. Иванова Г. Е., Белкин А. А., Беляев А. Ф., Бодрова Р. А., Буйлова Т. В., Мельникова Е. В. и др. Пилотный проект «Развитие системы медицинской реабилитации в Российской Федерации». Общие принципы и протокол. Вестник ИвГМА. 2016; (1): 6–11.
19. Иванова Г. Е., Мельникова Е. В., Шмонин А. А., Аронов Д. М., Белкин А. А., Беляев А. Ф. и др. Пилотный проект «Развитие системы медицинской реабилитации в Российской Федерации». Протокол второй фазы проекта. Ученые записки ПСПбГМУ им. акад. И. П. Павлова. 2016; (2): 27–34.
20. Кадомцев Д. В., Пасечникова Е. А., Занин С. А., Кочарян В. Э., Плотникова В. В., Виноградов И. О. Тромболитическая терапия при ишемическом инсульте. Современное состояние проблемы. *Современные проблемы науки и образования*. 2016; (4): 40.
21. Steiner WA, et al. Use of the ICF model as a clinical problem-solving tool in physical therapy and rehabilitation medicine. *Physical therapy*. Oxford University Press. 2002; 82 (11): 1098–07.
22. Шмонин А. А., Никифоров В. В., Мальцева М. Н., Мельникова Е. В., Иванова Г. Е. Электронная система мониторинга эффективности реабилитации в пилотном проекте «Развитие системы медицинской реабилитации в Российской Федерации» — программа «ICF-reader». Вестник Ивановской медицинской академии. 2016; 21 (1): 66–70.